CRANFIELD UNIVERSITY

Jibrin Sule

Application of Local Mechanical Tensioning and Laser Processing to Improve Structural Integrity of Multi-pass Welds

School of Aerospace, Transport and Manufacturing

Welding Engineering

PhD Thesis

Academic Year: 2014 - 2015

Supervisor: Supriyo Ganguly

July 2015

CRANFIELD UNIVERSITY

School of Aerospace, Transport and Manufacturing

Welding Engineering

PhD Thesis

Academic Year 2014 - 2015

Jibrin Sule

Application of Local Mechanical Tensioning and Laser Processing to Improve Structural Integrity of Multi-pass Welds

Supervisor: Supriyo Ganguly

July 2015

This thesis is submitted in partial fulfilment of the requirements for the degree of Doctorate of Philosophy

DEDICATION

To my late parents

Mr and Mrs Sule Shaho Sa'ada

And

To my beloved wife Mrs Fatima Jibrin Sule, my beloved daughters; Aminatu and Maryam.

EXECUTIVE SUMMARY

Multi-pass fusion welding by a filler wire (welding electrode) is normally carried out to join thick steel sections used in most engineering applications. Welded joints in an installation, is the area of critical importance, since they are likely to contain a higher density of defects than the parent metal and their physical properties can differ significantly from the parent metal. Fusion arc welding process relies on intense local heating at a joint where a certain amount of the parent metal is melted and fused with additional metal from the filler wire. The intense local heating causes severe transient thermal gradients in the welded component and the resulting uneven cooling that follows produces a variably distributed residual stress field. In multi-pass welds, multiple thermal cycles resulted in a variably distribution of residual stress field across the weld and through the thickness.

These complex thermal stresses generated in welds are undesirable but inevitable during fusion welding. Presence of such tensile residual stresses can be detrimental to the service integrity of a welded structure. In addition to a complex distribution of residual stress state, multi-pass welds also forms dendritic grain structure, which are repeatedly heated, resulting in segregation of alloying elements. Dendritic grain structure is weaker and segregation of alloying elements would result in formation of corrosion microcells as well as reduction in overall corrosion prevention due to depletion of alloying elements.

In this research, redistribution of residual stress magnitude and profile and the microstructural characterisation were studied and compared in three multi-pass welded structural alloys. These three alloys are; API 5L X100 pipeline steel (20 mm thick), S275JR structural steel (12 mm thick) and 304L austenitic stainless steel (12 mm thick).

The main objective of this study is to apply a novel processing to redistribute the harmful tensile residual stress field and minimise the effect of dendritic grain structure. This research aims at understanding the suitability of a novel

processing to create a stress free weldment with recrystallized grain structure in the weld metal.

In order to achieve the objectives in this research, the experiment was carried out in two phases. The first phase of the experiment involved three steps; welding was carried out by Tandem GMAW DC process, the post weld cold rolling was performed using an in-house rolling device and finally, the post weld cold rolling was followed by laser processing using 8 kW (peak power) CW fibre laser. The laser processing in the first phase was in transient heating mode using a laser power of 3 kW with a travel speed of 0.3 m min^{-1} and laser spot dimension (beam diameter) of 20 mm.

The residual stress was determined non-destructively by neutron diffraction, using the SALSA strain scanner at the reactor neutron source at ILL, Grenoble in France. The redistribution of the as-welded residual stress state was achieved by cold rolling which was followed by laser processing to induce recrystallization of the cold rolled grains. The stress measurements were supplemented with mechanical properties (hardness and tensile strength) evolutions in the welded structures after the three processing conditions.

In residual stress analysis, the result indicated that, in all the structural alloys studied, the stress variation in as-welded state, showed diminishing longitudinal peak stress magnitude through the thickness from cap to root pass.

Post weld cold rolling was effective in redistributing the stress field. Up to 4 mm below the capping pass in API 5L x100 grade, modifies the stress state from tensile to compressive across the weld centre line. While in 304L austenitic stainless steel, post weld cold rolling was effective in modifying the residual stress distribution throughout the entire thickness.

Post weld cold rolling followed by laser processing in transient heating mode in all the cases reinstated the as-welded residual stress magnitude and distribution while, microstructural characterization showed minor grain refinement near the capping pass for all the structural alloys.

With respect to mechanical properties, in the post weld cold rolling condition, hardness distribution in all the structural alloys showed a significant evidence of plastic deformation at the cap pass of the weld metal. However, for the ferritic steel (API X100 pipeline steel, S275JR structural steel) the effect of cold working was observed up to about 7 mm below the weld cap. Up to about 4 mm below the weld cap, the effect is more pronounced while after that, from 4 to 7 mm the effect is gradually diminishing. While in austenitic steel (304L stainless steel), the effect of cold working was observed throughout the entire thickness of the material. Laser processing after the localised plastic deformation of all the structural alloys resulted in softening of the weld metal.

The post weld cold rolling resulted in an increase in ultimate tensile strength and proof strength with corresponding reduction in elongation in the fusion zone of all the alloys. Laser processing after cold rolling reverted back the as-welded conditions with reduction of the ultimate tensile strength and proof strength and corresponding increase in elongation.

The second phase of the experiment, was based on the observation made in the first phase of the experiment, that; post weld cold rolling followed by laser processing reinstated as-welded residual stress state profile with even higher magnitude of peak stress and also resulted in minimal refinement of microstructure. This indicated that the re-crystallisation is not complete because the transient thermal cycle is not sufficient to supply enough energy to sustain the entire recrystallization kinetics. Based on this observation, a new laser processing was adopted.

The new laser processing involves applying thermal energy for a prolonged period which would ensure full recrystallization of the grain structure and formation of new set of strain free grains. In order to understand the time-temperature cycle required for full recrystallization, an experiment using reheating furnace was carried out on post weld cold rolled samples.

The furnace experimental result showed that recrystallized grains was formed after heating the API X100 pipeline steel to 900^{o}C, while in austenitic stainless steel, recrystallized grains was observed when heated to 800^{o}C. Based on this

observation, the laser processing in the second phase of the experiment was designed.

In this phase the same CW laser was used as in the first phase, but instead of transient heating mode the post weld cold rolled samples were gradually heated by controlling the laser power at a large beam diameter of 110 mm. The ferritic steel was heated up to 900^{o}C, while, the austenitic steel was heated to 800^{o}C using identical laser parameters.

In order to overcome the problem of restoration of residual stress after laser processing of the post weld cold rolling samples as observed in the first phase of the experiment, a second cold rolling was applied. This cold rolling after laser processing is to redistribute and eliminate the tensile residual stress state which would have formed during laser processing.

The result showed that, the modified laser processing followed by cold rolling resulted in generation of complete recrystallized microstructure with compressive residual stress state. Generation of this compressive stress state is beneficial in improving the structural integrity of a component as most of the in-service deterioration starts with a surface flaw. The generation of the recrystallized microstructure with large proportion of high angle grain boundaries would increase the strength and toughness of the material which is lower in as-welded dendritic grain structure state.

In conclusion, this novel processing clearly demonstrates the improvement of structural features that can be obtained in traditional welded structural alloys. However, optimisation of the post weld cold rolling and laser processing would be required for different alloy systems. In order to optimise such processing, it would be advisable to consider the material's work hardening characteristics, to understand the necessary effects of local tensioning on constitutive properties, and metallurgical characteristic if post weld cold rolling is to be applied.

Keywords: structural steel alloys; multi-pass welds; microstructures; mechanical properties; residual stress; neutron diffraction; rolling; laser processing.

ACKNOWLEDGEMENTS

I wish to express my profound gratitude to Allah (SWT) for his grace and mercy granted to me right form birth to date, "Alhamdulillah."

My profound gratitude goes to my supervisor, Dr. Supriyo Ganguly for his constant support, guidance, encouragement and inspiration throughout my PhD duration.

I would also like to thank the Federal Government of Nigeria through Petroleum Trust Development Trust Fund (PTDF) for funding my studies in Cranfield University.

I will also like to show my appreciation to our technical staffs that have helped me through the practical work, especially Mr Brian Brooks, Flemming Nielsen and Dr. Xianwei Liu for his support during SEM analysis.

My profound gratitude also goes to my review chair Professor Jane Rickson, and my subject adviser Professor Stewart Williams for their care, concern and support during the course of my research.

I am also indebted to Professor O.I. Oloyede, Aruwa Atampa, Mohammed Yahaya Akoresu, Isa Ubam, Adamu M. Bako, Tanimu Adalkhali, DR. Ubam B. Yahaya, Clare Humphries, Engr. (Chief) Otunba Victor Raydon, Keith Hurley and to all my friends and well-wishers for their support and advice.

Finally, my sincere thanks to my family especially my beloved wife for her prayer, understanding, support and encouragement, without which this work would not have been possible.

LIST OF PUBLICATIONS

The following journal articles were published and in process form the research work performed in this thesis. A list of these article is given below and in each of the article, the candidate (Jibrin Sule) contributed principally to all aspects of the work described therein.

- Jibrin Sule, Supriyo Ganguly, Harry Coules, Thilo Pirling
  Comparative Study of Evolution of Residual Stress State by Local Mechanical Tensioning and Laser Processing of Ferritic and Austenitic Structural Steel Welds. *Journal of Mechanical Engineering and Automation*, 5 (1): 33 – 42, 2015

- Jibrin Sule, Supriyo Ganguly,
  Application of local mechanical tensioning and laser processing to modify the residual stress state and microstructural features of multi-pass HSLA steel welds. *SAE International Journal of Materials and Manufacturing*, 8 (2): 494 – 502, 2015.

- Jibrin Sule, Supriyo Ganguly Harry Coules, Thilo Pirling
  Application of Local Mechanical Tensioning and Laser Processing to Refine Microstructure and Modify Residual Stress State of a Multi-pass 304L Austenitic Steels Welds. *Journal of Manufacturing Processes*, 18: 141 – 150, 2015.

- Jibrin Sule, Supriyo Ganguly, Thilo Pirling, Suder Wojciech J.
  Effect of high pressure rolling followed by laser processing on residual stress distribution in multi-pass welds of 304L steel.
  *Journal of Materials Processing Technology (*submitted).

TABLE OF CONTENTS

LIST OF FIGURES

LIST OF TABLES

LIST OF EQUATIONS

LIST OF NOMENCLATURES

Al	Aluminium
Ar	Argon
C	Carbon
CO_2	Carbon dioxide
C_r	Chromium
E	Modulus of elasticity
He	Helium
Hv	Vickers hardness
K	Kelvin
Mn	Manganese
MPa	Mega Pascal
Ni	Nickel
S	Sulphur
T	Titanium
O_2	Oxygen
Si	Silicon
d_0	Stress-free lattice spacing
A	Welding current
V	Arc voltage
^oC	Degrees Celsius
%EL	Percentage elongation
Å	Armstrong
Ɛ	Strain
ʎ	Lamda
σ_{XX}	Longitudinal stress
p_{cm}	Compositional parameters
υ	Poisson's ratio

LIST OF ABBREVIATIONS

AF	Acicular Ferrite
AISI	American Iron and Steel Institute
API	American Petroleum Institute
ASTM	American Society for Testing and Materials
BCC	Body Centered Cubic
CE	Carbon Equivalent
CSP	Controlled Shot Peening
CTOD	Crack Tip Opening Displacement
CTWD	Contact Tip to Workpiece Distance
CW	Continuous Wave
EBSD	Electron Back-Scatter Diffraction
EDM	Electrical Discharge Machining
F	Ferrite
FCA	Flux Cored Arc
FCC	Face- Centered Cubic
FWMH	Full Width at Half Maximum.
GBF	Grain Boundary Ferrite
GMA	Gas metal Arc
GMAW	Gas metal Arc Welding
GMT	Global Mechanical Tensioning
HAZ	Heat Affected Zone
HSLA	High Strength Low Alloy Steel
ILL	Institut Laue Langevin
IRCG	Intercritically Reheated Coarse Grain
LAMP	Large Array Manipulation Program
LNG	Liquefied Natural Gas
LZB	Local Brittle Zone
MIG	Metal-inert Gas
NGW	Narrow Gap Welding
P	Pearlite
PGMAW	Pulse Gas Metal Arc Welding
PM	Parent Metal
PS	Proof Strength
PSD	Position Sensitive Detector
PWHT	Post-Weld Heat Treatment
SALSA	Strain Analyser for Large and Small scale engineering Applications
SCC	Stress Corrosion Cracking

SEM	Scanning Electron Microscopy
SFE	Stacking- Fault Energy
SMYS	Specified Minimum Yield Strength
SPF	Sideplate Ferrite
SRCG	Subcritical Reheated Coarse Grain
SRFG	Supercritical Reheated Fine Grain
TEM	Transmission electron microscopy
TMCP	Thermo-Mechanically Controlled Processed
UTS	Ultimate Tensile Strength
VSR	Vibratory Stress Relief
XRD	X-ray Diffraction
WFS	Wire Feed Speed
WM	Weld Metal

1 Introduction

This chapter of the thesis presents an overview of the background, motivation for the research, research questions and hypothesis, the aim and the objectives of the research. It also describes the thesis structure.

1.1 Background

The need to have a reliable and efficient source of energy has been on increase for the past 100 years. This effort is more pronounced in the recent time [1]. Fossil fuel for example, has been one of the most widely used natural resources. This fuel is been used for the generation of electricity, power plants and for domestic uses in the world today [2]. A number of researches [3],[4],[5], have explained the use of this natural gas. Coupled with its abundance in nature, this natural gas is been consumed by industry as a source of energy.

This natural gas has also been considered as a most reliable and clean transportation fuel. It has been used for powering urban mass transportation systems. Increase in demand for this commodities in European, North American and Asian countries, has called for the development of safe and cost effective transportation of this natural gas (gas fields) which are mostly located in remote area. In fact, in some cases, this gas fields are located 5000-6000km away from the regions where it is used and often located offshore in harsh environments [3].

These fossil fuel and large reserves of natural gas that are located remotely are required to be conveyed from the source to many other countries across the border, for consumption. To transport this large gas volumes under high pressure, the use of high strength steels is considered as the most efficient, safe and the best economical means of transportation for final consumers [5].

1.1.1 Material: Steel

Steel is useful material which has a very wide range of attractive properties, and can be manufactured at a low cost. Steel is generally defined as a ferrous alloy containing less than 2.0 wt. %C [6]. Complexity of steel arises with the introduction of further alloying elements into the iron – carbon alloy system which

lead to different categories of steels. High-strength low-alloy steel (HSLA) types of steels for example, provides good mechanical properties or better corrosion resistance than carbon steel. This type of steels (HSLA) are made to meet a specific mechanical properties. Hence, they differs from other type of steels.

Of course, steel of different varieties (such as ferritic, austenitic and martensitic) are used in a number of applications across a range of different industries. In oil and gas industries for instance, pipelines steel are used to transport hydrocarbon product from one point to another. These pipelines are sometime laid over a long distance. These distance may be across border which may be either on onshore or offshore. The overriding principle and critical activities in maintaining safe, secure and reliable pipeline must be the implementation of an extremely robust pipeline management programme [7]. AISI 304L stainless steel is another form of steel which is extensively used in industries. This structural alloy is been used because of its superior low temperature toughness as well as good corrosion resistance. Application of this types of steels include storing and transportation of liquefied natural gas (LNG). The boiling point of LNG is -162°C under 1 atmosphere [8]. S275JR steel is also another form steel which is common among the low carbon steel grade. This structural alloys is suitable for many general engineering and structural applications especially in construction, maintenance and manufacturing industries.

1.1.2 Welding

In most of these applications mentioned above, it is vital to have a good joints which can allow transfer of load from one steel component to another. In most cases welding is generally the most common method of joining. The welding method reduced the corrosion problems often associated with fasteners. This process (welding) create most robust joint to the application.

The most common and widely used welding processes are those which employ fusion. Fusion arc welding process relies on intense local heating at a joint where a certain amount of the parent metal is melted and fused with additional metal from the filler wire. This fusion arc welding is extensively been used in a number of construction industries, offshore structures and among others.

The main benefits of welding, as joining processes are: creation of robust joint, flexibility in terms of setting up the equipment and low fabrication costs. Disadvantage of this process is that, the mechanical properties of the structural alloy are been alter as result of welding. This process also cause distortion and residual stresses in the welded structure, which to a large extend depends on the welding process.

1.1.2.1 Welding Methods

It is a structural requirement that the weld metal has over–matching strength in comparison to the parent material in most cases, so as to avoid design limitations. These requirements are possible to achieve under well controlled conditions using for example single wire mechanised gas metal arc welding (GMAW). Gas metal arc welding was and still the dominant pipeline welding technique [2]. The development of tandem GMAW in a narrow groove with two tandem torches in a single welding head has offers welding productivity three to four times higher than conventional single wire GMAW technique [2].

Depending upon the applications, plates of different thicknesses are used for the fabrication of components. In most of the applications, the plates are welded by using multi-pass welding methods. This technique creates a significant change in the microstructure and mechanical properties of the weld metal and heat affected zone as a result of the multiple thermal cycles introduced by successive pass. This also creates a variable distribution of residual stress field across the weld and through the material thickness.

1.1.2.2 Weld Residual Stresses

Stresses developed during welding are thermal stresses. These stresses are primarily cooling stresses with possibly superimposed transformation stresses [9]. These transformation stresses are formed due to transformation strains which occur during austenite to ferrite transformation. Of course, mechanically constrained thermal expansion and contraction leads to generation of residual stresses in the weld, with significant tensile residual stresses in and around the welded region. These residual stresses have a large tensile component in the longitudinal direction of the weld; whereas further away from the weld metal, the

stresses are slightly compressive balancing the tensile stresses that formed across the weld metal [10], [11].

The development of welding residual stresses is therefore influenced by many factors, which include material properties e.g. thermal expansion and contraction co-efficient. The effect of residual stresses in a welded structure includes distortion and amplification of the stress state which could affect the fatigue strength of the welded joint. Evaluation of residual stress is essential for process and quality control, design assessment and failure analysis since these stresses can impact on the performance of engineering components. The presence of tensile residual stresses have been reported to influence stress corrosion cracking and fatigue crack growth rates [10],[11],[12] [13].

Compressive residual stresses on the other hand, could be beneficial for structural integrity. For example, compressive stresses are sometimes intentionally introduced to enhance the performance of a weld component [14]. It was also reported that tensile stress in multi-pass weld of austenitic stainless steel can be minimised by water-shower cooling during the final welding pass. [15]

The in-built or “locked-in” character of residual stresses makes them challenging to measure. However, owning to wide range of applications of residual stresses measurement techniques in research and industry, a number of residual stress measurement techniques are found in literature [16]. Some of these measurement techniques are destructive (“relaxation”) while others are non-destructive methods [17].

One of the good ways of determining residual stress fields non-destructively, is by using diffraction method. In this study, neutron diffraction was used to measure residual strain and analyse residual stress state. The main advantages of neutron diffraction over others is it high penetration depth. Neutron diffraction penetrate deep into all common polycrystalline engineering materials. The high penetration characteristic of neutron diffraction is useful for structural alloys of high average atomic number [18]. Majority of neutron strain-scanning instruments use a nuclear reactor as the neutron source, which produces a continuous flux of

neutrons over a range of wavelengths. Current examples of constant flux instruments include SALSA [19]. In this research, SALSA neutron diffractometer at the Institut Laue Langevin in France was used to measure the residual elastic strain, and then analysed them to understand the 3-dimensional residual stress state.

Different techniques in the literature have been used to mitigate the effects of residual stress. These includes; post weld heat treatment, shot peening, modification of the structural configuration and the implementation of the thermal tensioning techniques [20],[21],[22]. Other method is vibratory stress relief (VSR) process. It has been reported that this method (VSR) reduce and redistribute the internal residual stresses of welded stainless steel structures by means of post-weld mechanical vibration [23], [24]. The application of rolling to reduce weld residual stress and distortion for a thin plate has been in practice for years [25], [26], [27]. Recent research by Coules et al [28] and Altenkirch et al [29] has demonstrate that the post weld rolling methods was effective in reducing residual stresses in single pass welds. However, application of rolling on multi-pass welds has not yet been reported.

1.1.2.3 Microstructure of Multi-pass Welds

Multi-pass welds exhibit substantial heterogeneity in microstructure and significant differences in mechanical properties through the material thickness. This can be attributed to the complex nature of thermal cycling experienced by each pass as subsequent passes are deposited. Multi-pass welds also forms dendritic grain structure, which are repeatedly heated, resulting in segregation of alloying elements. Dendritic grain structure is weaker and segregation of alloying elements would result in formation of corrosion microcells as well as reduction in overall corrosion prevention due to depletion of alloying elements.

It has also been reported that the dendrite growth (that is columnar or equiaxed growth) in a multi-pass weld has influence on mechanical properties of the weld [30] and microstructural features such as micro-segregation in the weld [31]. Creation of a refined and recrystallized microstructure was attempted in this research by applying post weld rolling followed by laser processing. It is expected

that refining of grains would improve the strength and toughness in the weld metal.

There are no reported works in the literature concerning the application of post weld rolling followed by laser processing to mitigate residual stresses and create a refined and recrystallized microstructure. This research is therefore, a novel approach of applying post weld cold rolling method (local mechanical tensioning) followed by laser processing (application of thermal energy) in a multi-pass weld to modify the residual stress state as well as create a recrystallized grain structure.

1.2 Motivation for the Research Project

A number of investigations have been undertaken on how to mitigate weld residual stress [15], [22], [32] [33]. In aerospace industry for example, rolling between-roller (that is, passing the welded sample between two roller) techniques has been successful in reducing residual stress in single pass welds [34]. In multi-pass welds, no attempt has been made to apply rolling methods. The main motivation for this research is therefore, to apply post weld cold rolling method at the cap (final pass) as a means of stress mitigation and post weld cold rolling followed by laser processing as means to induce recrystallization of the cold rolled grains. Generation of this compressive stress state is beneficial in improving the structural integrity of a component as most of the in-service deterioration starts with a surface flaw. The generation of the recrystallized microstructure with large proportion of high angle grain boundaries would increase the strength and toughness of the material which is lower in as-welded dendritic grain structure state.

1.3 Research Question and Hypothesis

The primary research questions to be addressed here are:

- ❖ Optimised loading to induce sufficient strain to redistribute residual stress state.
- ❖ Application of thermal energy to nucleate stress free grains, however, care should be exercised to ensure that the residual stress field is not reinstated.

This proposed research is based on the theory that post weld cold rolling will significantly help in redistributing the residual stress state of the welded structure. The post weld cold rolling process will also induce strain in the weld metal which will create dislocations in the weldment. Post weld cold rolling followed by laser processing carried out will induce recrystallization of the cold rolled grains. Thus overall the microstructural characteristics and mechanical properties of the structural alloys will improve with the elimination of residual stress state.

1.4 Aim and Objectives

The aim of this research is to apply a novel technique of local mechanical tensioning (post weld cold rolling) followed by laser processing to improve structural integrity of multi-pass welds.

In order to achieve the objectives in this research, two basic crystallised structures BCC and FCC were studied. In this studies, experiment was carried out and this involved three steps; welding was carried out by using Tandem GMAW DC process, the post weld cold rolling was performed using an in-house rolling device and finally, the post weld cold rolling was followed by laser processing using 8 kW (peak power) CW fibre laser. This aims at understanding the suitability of a novel processing to create a stress free weldment with recrystallized grain structure in the weld metal.

1.5 Thesis Structure

In this work, after the post weld cold rolling of the samples, laser processing was carried out in two phases. The laser processing in the first phase was in transient heating mode while the second phase of the laser processing, was based on the observation made in the first phase of the experiment.

It is therefore, based on this two separate experimental programme that the thesis structure was developed. With exception of the first two chapters (Introduction and Literature review), chapter three and four contains both phases of the experiment which are largely based on articles which have been, or intended to be published elsewhere. Chapter five contain only the second phase of the experiment based on the observation made in the two structural alloys. Chapter six contains the comparison studied of the three structural alloys. Chapter seven contains the conclusion and recommendation for future work.

Therefore, this thesis structure is organised in 7 chapters and appendices as detail below.

Chapter 1: Contains the background of the research, motivation for the research, the aim and objectives of the research and the thesis structure of the research.

Chapter 2: Contains the literature review, which was focused on the main areas of this research which include the development of multi-pass weld, the microstructural changes and residual stress developed as a result of complex nature of thermal cycling experienced by each pass as subsequent passes are deposited, mitigation of residual stresses by rolling and formation recrystallized grains by heating process.

Chapter 3: Application of local mechanical tensioning and laser processing to modify the residual stress state and microstructural features of multi-pass HSLA steel welds.

Chapter 4: Application of local mechanical tensioning and laser processing to refine microstructure and modify residual stress state of a multi-pass 304L austenitic steels welds.

Chapter 5: Effect of cold rolling, laser processing and cold rolling after laser processing on microstructure and residual stress of multi-pass welds of S275 structural steel.

Chapter 6: Contains the comparison studied of the three structural alloys.

Chapter 7: Conclusion and recommendation for future work.

2 Literature Review

2.1 Multi-pass Welding

Multi-pass fusion welding by a filler wire (welding electrode) is normally carried out to join thick steel sections used in most engineering applications. Welded joints in an installation, is the area of critical importance, since they are likely to contain a higher density of defects than the parent metal and their physical properties can differ significantly from the parent metal.

These arc welding methods are widely used due to its simple assembly, operational simplicity, safety, operator skill requirement, and low price and high quality of the process compare to laser welding process. One of the processes used in multi-pass weld are briefly explained below.

2.1.1 Pulse Current and Synergic GMAW

This method of welding was developed in 1960's by J.C. Needham [35]. It utilize current pulse from the power source to control transfer of the droplet of molten filler material in the arc, in order to produce a stable and spatter-free arc. This method was not effective at the early stage due to insufficient power source technolgy. With the advancement in power source and electronics in the 1970's the method became more feasible. The technology used is known as synergic pulsed GMAW. Synergic indicate a method in such a way that the power source will authomatically select appropriate pulse parameter. Increesing or decreasing the wire feed speed, other parameters will adjust authomatically in order to maintain a suitable arc. However, if the these pulse parameters are not selected properly, defect in the weld may occur [36].

Some of the advantage of this method include but not limited to [35]:

i. The process is fully machanised and spatter free.
ii. It is possible to perform positional welding with better performace.
iii. A large wire diameter can be used: that will be less expensive and easier to feed.

iv. It is used within the normal spray arc range in order to provide better penetraion into the material.

There are different types of multi-wire welding system available with various nomenclature in the world today. The most important consideration is that, multi-wire welding can be performed using different principles [37] such as: the twin welding (one feeding unit) and the tandem welding (two feeding units and two power sources).

2.1.1.1 Tandem Pulse Gas Metal Arc Welding

GMAW is used by industry because of its increased rates of productivity as well as improvement in weld quality as compared to shielded metal arc welding (SMAW) [38].

Narrow groove tandem GMAW of high strength steels was first reported by Lassaline et al. [39]. In his experiment, he did not specified clearly whether the system will operate with one contact tip using two wires or two contact tips using single wire each. The two arcs, as shown in Figure 2-1, worked in close proximity with each other and by synchronising the pulse current waveform provided by the two power sources, the magnetic arcs blow effects were minimised [39].

Further investigation by Michie, K. [40] show that, the two welding arc, as shown in Figure 2-2 works simultaneously in the same weld pool using the tandem Pulse Gas Metal Arc Welding (PGMAW) system for narrow groove welding of pipeline [40]. His research was first demonstrated at Cranfield University and he shows the potentiality of the application of the tandem PGMAW to pipeline girth welding. The deposition rate of the processes was found to be twice as compared to single wire welding processes. In addition, an excellent mechanical property was reported by the use of the tandem PGMAW process [39]. The feasibility of the processes was also demonstrated and tested by Hudson, M. G. [41] using x100 pipeline steel.

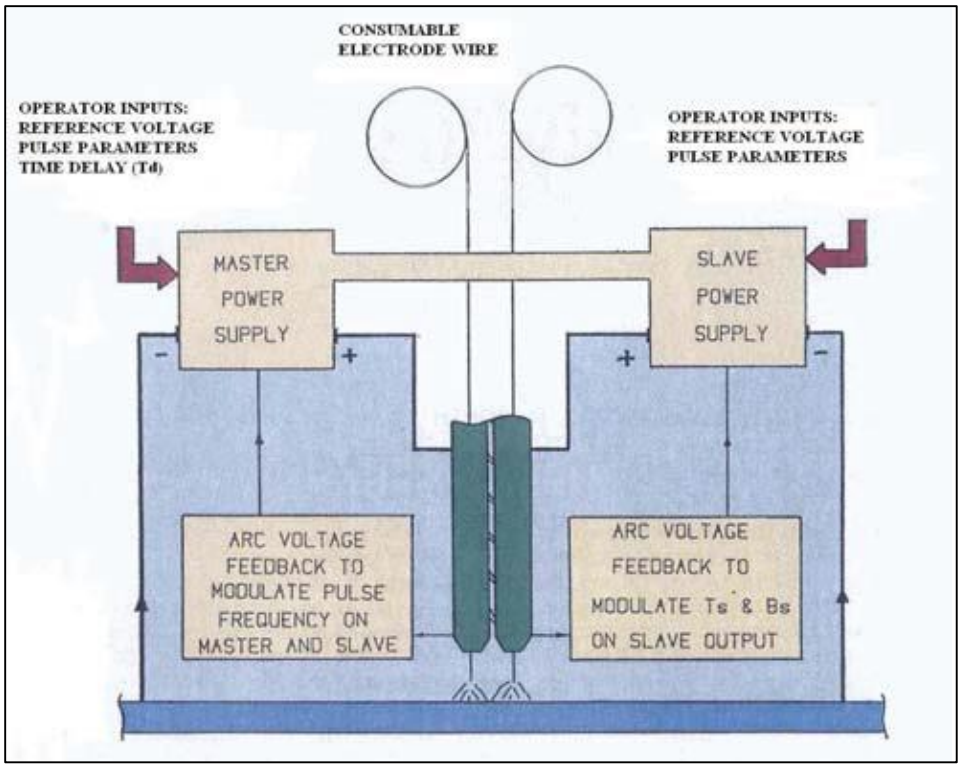

Figure 2-1: Showing the twin-wire system with synchronised power sources [39]

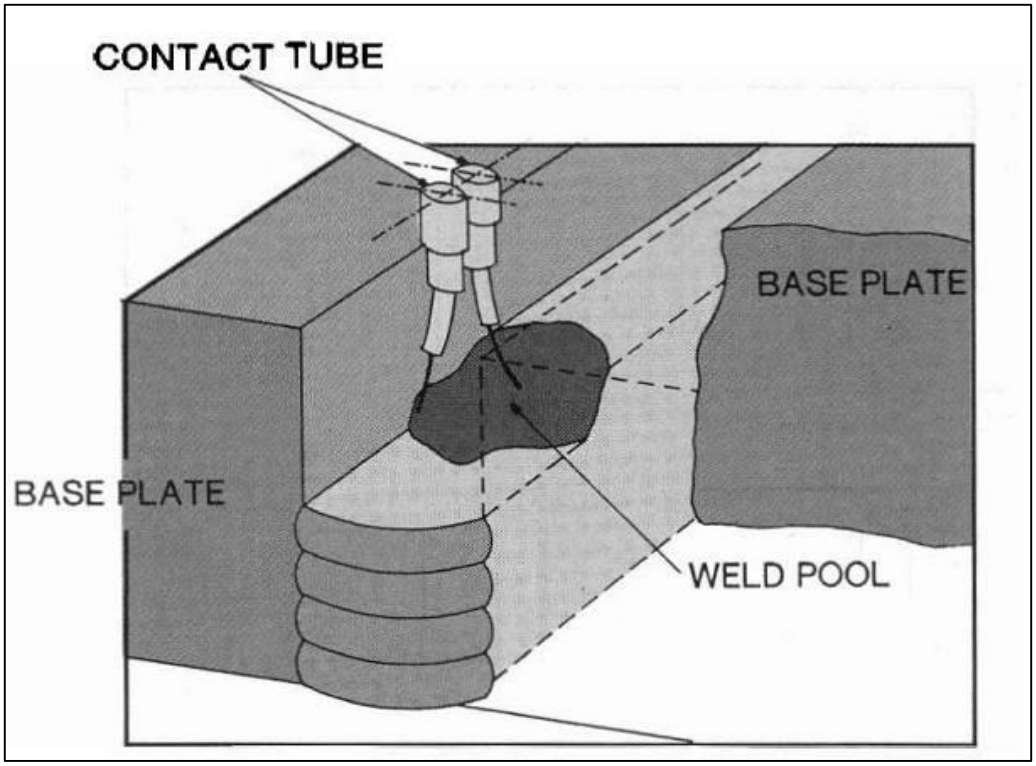

Figure 2-2: Showing the arrangements of the filler wires to ensure good sidewall fusion [39]

2.2 Narrow Gap Welding (NGW)

2.2.1 Introduction

In the recent years the demands for much thicker plate in manufacturing of welded structures has been on increased [42], [43]. This demand led to intensified efforts in search of a welding process for heavy wall fabrication. This efforts is in terms of quality and overall cost. In view of this, narrow gap welding has been consider as a promising technique. This techniques is expected to meet today's requirements. The term narrow gap welding first appears in an article published half century ago [44]. Since then, the term NGW has become a standard term in the world of welding literature. This term described a definite concept in welding development. However, there is still some misunderstanding on the concept of NGW. Some authors describe the NGW concept by use of terms such as groove, narrow groove, deep groove while others use the same terms to refer to welding process such as narrow gap electro-slag welding and narrow gap electron beam welding [43] [45]. In an attempt to clear this misconception of NGW, Malin, V. [43] summaries the feature of NGW as follows;

i. NGW is not a welding process, it is a special bead deposition technique.
ii. NGW is associated only with an arc welding process. For example, gas metal arc welding (GMAW)
iii. NGW features a fixed bead deposition layout which is characterised by constant number of beads per layer (usually between 1 – 3 layers) which are laid one on top the other.
iv. NGW requires a square groove only. However, a V or double V groove is also consistent with NGW concept, as long as a groove angle (usually very small) is provided for distortion compensation rather than for better access to the joint, and the fixed bead deposition layout is preserved.
v. NGW is a property oriented technique and therefore requires low or medium heat input.

Based on this features, narrow gap welding is define as "a property oriented bead deposition technique associate with an arc welding process characterised by a

constant number of beads per layer that are deposited one on top of the other in a deep, narrow square groove".

This technique describes welding within an essentially parallel sided joint (0-5^{o} bevel angles are commonly used) [46] in thick material. Open and closed butt root preparations have been used, both with and without backing bar systems [41], [47]. NGW has been found to be an efficient method in multi-pass welding [48].

Some of the advantages attributed to NGW when compared with other welding processes for thick joints are; (1) welding time reduction, (2) consumable costs are lower, (3) reduction in heat input which will improve the mechanical properties and reduce distortion and (4) reduction in the need for preheating and post-weld heat treatment [42],[45],[49].

The problems associated with NGW are high sensitivity to the formation of defects such as lack of sidewall fusion, undercutting and centre line cracking as a result of minor variation in welding conditions [45],[50]. Another problem associated with NGW is pore formation due to improper gas shielding and magnetic arc blow.

2.2.2 Gas Metal Arc Welding- Narrow Gap (GMAW-NG)

The welding process that was first used for NGW application is GMAW. GMAW is still the most commonly used with NGW techniques due to its ease of arc visual observation, relatively narrow groove, productivity, high welding quality and cost effectiveness [43]. Distortion and residual stress produced by GMAW-NG has been reported to be lower than that produced in comparable material thickness using other joining process [44],[47]. However, GMAW-NG is prone to defect formation in the side walls, intensive spattering and shielding gas deficiency. When compared to conventional GMAW, the real problem of GMAW-NG, which has been the major obstacle for it acceptance; is the difficulty in feeding the electrode and supplying a proper shielding gas coverage into a narrow and deep groove and obtaining well balanced arc heating between side walls and the bottom of the joint [50]. Several attempts have been made to overcome these

limitations. These include wire deposition strategy and torch design which has been proposed, developed and some of them used in industrial application since the introduction of narrow gap welding. A comprehensive review of most GMAW-NG can be found in [43].

2.2.3 Welding Conditions for Using GMAW Narrow Gap

It has been reported that GMAW-NG is much more sensitive to changes in welding parameters as compared to conventional GMAW [43]. This could be due to the operating condition of the NGW which operates in the close margins of a very narrow gap, and with restricted arc atmosphere convection as well as little loss of radiation heat during welding.

One of the major welding parameters is the voltage. This voltage or perhaps arc length provides adequate depth of penetration [47], [51], [52] and process stability [53]. Lowering the arc voltage result in the side walls receiving inadequate heat, and lack of fusion is likely to occur. Short circuiting conditions, an unstable arc and spattering can also be observed when the arc voltage is low. Increasing the arc voltage tends to widen the fusion zone. However, if the arc length become too long (as a result of high voltage) relative to the gap width, the arc tends to scramble up the groove sidewalls, resulting in damaging the contact tube and making welding almost impossible. Figure 2-3 summaries the effect of arc voltage in the performance of GMAW-NG.

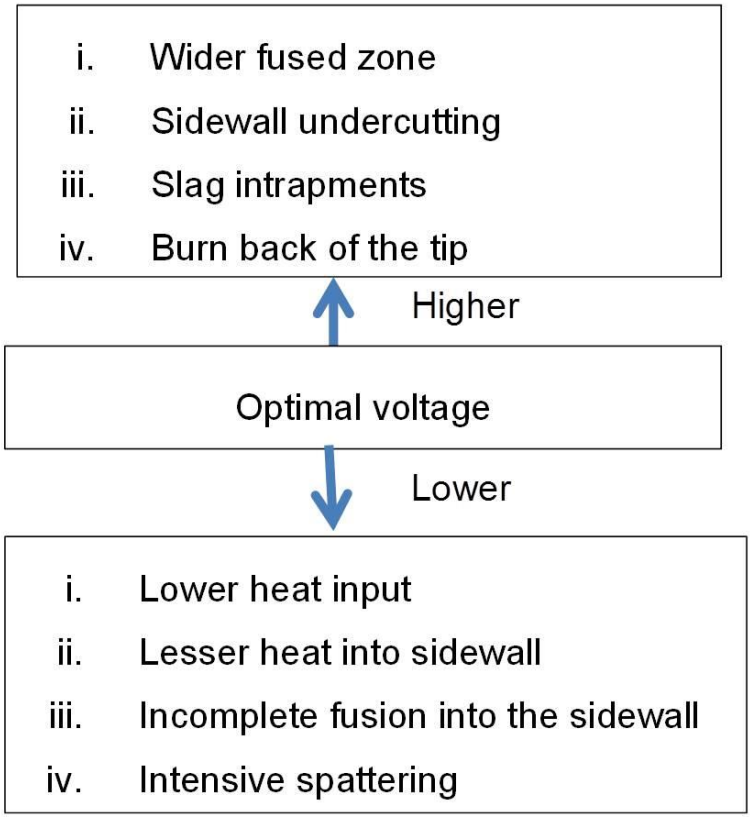

Figure 2-3: Effect of voltage on process stability and bead formation [43].

Current is also an important factor as it influences deposition rate, arc stability and bead geometry. Since current is a function of wire feed speed (wfs), as such, lowering the current decrease the deposition rate. In contrast, an increase in current results in deepening the arc penetration into the bottom of the joint much faster than into the sidewalls. This results in an unfavourable bead configuration.

The travel speed of welding influences the heat input and consequently the weld pool flow. Therefore increasing the travel speed of welds lowers the heat input in the weld. However, excessive speeds can result in incomplete fusion into the sidewall due to insufficient heating of the wall [43]. On the other hand, lowering the weld travel speed creates a large weld pool which flows under the arc causing also incomplete fusion into the side walls [51], [54]. Therefore, weld travel speed should be set in accordance with welding parameters and keep the speed low enough to allow the operator to effectively control electrode position in the groove.

Another important factor is the choice of the shielding gases in GMAW-NG as it affects many aspects of the welding procedure. The shielding gas is usually selected on the basis of arc stability, shape of the bead and properties of the welded joint. Four (4) principal gases have been considered the most important in providing the gas shielding for welding in deep grooves [43]. These gases are; argon (Ar), carbon dioxide (CO_2), Helium (He) and oxygen (O_2). However, Ar + 10 - 25%CO_2 is the most commonly used shielding gas mixture for welding mild and low alloy steel with NGW. Mixtures of gases containing higher level of carbon dioxide [51], [52], Ar - 5%CO_2 [55], Ar - 5%CO_2 - 2%O_2 [56] and mixtures containing Argon, Helium and carbon dioxide [57] have also been considered in GMAW-NG. Pure argon in conventional dc reverse polarity GMAW received very rare application in industrial steel fabrication due to its spattering metal transfer, arc radiation and high weld metal sensitivity to porosity formation. It is known that addition of carbon dioxide to argon affect both arc stability and bead shape. This explains why Ar + CO_2 mixture is the most popular gas shield for GMAW-NG.

In general, the welding conditions which are combination of welding materials, welding parameters and operating conditions are generally selected for a specific NGW technique on the basis of the following: welding position, allowable heat input, desired weld properties, distortion and other prerequisites.

2.2.4 Characteristics of Weld Bead in NGW

Arc and weld pool stability are guiding principles in maintaining high quality narrow groove welded joints. They are essential factors especially when welding around a fixed pipeline, where the effect of gravity changes the weld pool dynamics. Hence consistent and stable weld metal transfer is a prerequisite for sound joint completion [41]. Stricter control over bead shape is crucial, and in this regards, an understanding of fusion characteristics and welding parameters is extremely important.

In NGW, the best form of bead shape is regarded as being slightly concave in nature. This concave nature of the bead shape ensures ease of fusion at the toes of each preceding weld bead.

The factor(s) which influences this bead shapes are include;

i. Welding current/heat input/deposition rate
ii. Arc voltage: the greater the arc length, the greater the voltage required to maintain that arc [58]
iii. Electrode Polarity
iv. Contact tip to workpiece distance (CTWD)

2.3 Effects of Heat Input During Welding

Heat input is an essential parameter of arc welding processes. It's an important parameter because like preheating and interpass temperature, heat input influences the cooling rate. And as a consequence, it affects the mechanical properties and final microstructure of the weld metal and associated heat affected zone (HAZ). Heat input also determines residual stress distribution in a welded structure [59]. A lot of effort has been devoted in this area of welding metallurgy [10].

A number of fundamental researches in the subject of generation of welding residual stress have been carried out but the complexity of the problem is caused by the thermal elastic plastic strain-stress cycles induced by the locally non-uniform heat input [60], [61], [62]. The factors affecting welding residual stress and distortion can be classified as the material, fabrication and structure related factors.

In summary, with respect to multi-pass welding, the temperature distribution that occurs, affects the material microstructure, mechanical properties and the residual stresses that will be present in the material after cooling to room temperature [63].

2.3.1 Inter-Pass Temperature

The temperature of the material in the welded zone before the subsequent passes during a multi- pass weld is refer to as inter-pass temperature [64]. This temperature has strong influence on mechanical and microstructural properties of weldments. The strength of weld metal tends to reduce with high values of inter-pass temperature. However, where toughness of a material is required,

higher inter-pass temperatures improve toughness transition temperatures as well as provide finer grain structure [65]. The inter-pass temperature is reported to depend on the composition of the material as well as the cooling rate of the material [66].

A minimum specified inter-pass temperature is required in practice which is often equal to the minimum specified preheat temperature. The preheat temperature is the temperature to which the material is first heated, in order to avoid hydrogen cracking. According to Jones, J. E. and Luo, Y [67], preheating range depends on many factors. This factors include the chemical composition (particularly carbon content and level of alloying), the physical properties and the thickness of the weld material, electrode type, heat input and the level of standards required. With regards to the residual stresses and distortion that may develop during welding process, controlling preheat and inter-pass temperature will reduce the effect of residual stress and thus the metallurgical phases formed [68].

In summary, recent researches by [69],[70],[71], show that inter-pass temperature is important, as variations in yield strength of the weld metal were not due to compositional variations alone but also process parameters such as the weld metal inter-pass temperature which is an active determinant of the cooling rate.

2.4 Metallurgy of Ferritic Steel

Welded joint consist of three (3) regions. These are the weld metal (WM), heat affected zone (HAZ) and the parent metal (PM). A numbers of researchers have described microstructural constituents within steels and weld metals. This description lead to proposing various classification systems [72], [73], [74]. Due to heat input associated with the welding processes, several microstructural features are generated. These microstructural features often lead to confusion in describing the actual microstructure present. Due to this confusion in describing the actual microstructure, the international institute of welding (IIW) considered it as of utmost importance to unify the process of identifying various microstructural constituents [75]. These microstructural constituents are used in this research.

2.4.1 Weld Metal

Multi-pass welding of ferritic materials involves the localised injection of high heat at the fusion zone. This heat is dissipated by conduction into the parent metal. The microstructure of the weld at each point is closely associated with the thermal cycle. Where a joint is welded in more than one pass (multi-pass), the microstructure of the first pass can be altered by the heat from subsequent passes. Where the temperature rises above Ac_3, then complete transformation to austenite occurs which usually produces grain refinement [76]. This refined microstructure is normally associated with very good toughness.

Predicting the microstructure reformation during the thermal cycles of welding is always difficult since both the mechanical properties and microstructure varies within different thermal cycles [77]. However, the final structure that is produced after cooling of weld metal is determined by phase transformation [78], [79], [80]. Figure 2-4 shows different phases of weld metal transformations during solidification to room temperature.

It was reported by Babu, S.S, [81] that, as the weld cools from 2000^{o}C to 1700^{o}C, the dissolved oxygen and deoxidizing elements in liquid steel react. This reaction tends to form complex oxide inclusions (Figure 2-4 (a)). As it further cools from the temperature range of 1700^{o}C to 1600^{o}C, solidification to delta-ferrite (bcc phase) begins. This solidification then envelops the oxide inclusions as shown in Figure 2-4 (b). At this temperature, this delta-ferrite transforms to fcc phase (austenite). As the cooling continues, (at the 1600^{o}C to 800^{o}C), austenite grain growth may occur (Figure 2-4 (c)). The austenite decomposes to bcc phase (different ferrite) morphologies as it cools from the temperature range 800^{o}C to 300^{o}C, as shown in Figure 2-4 (d – g).

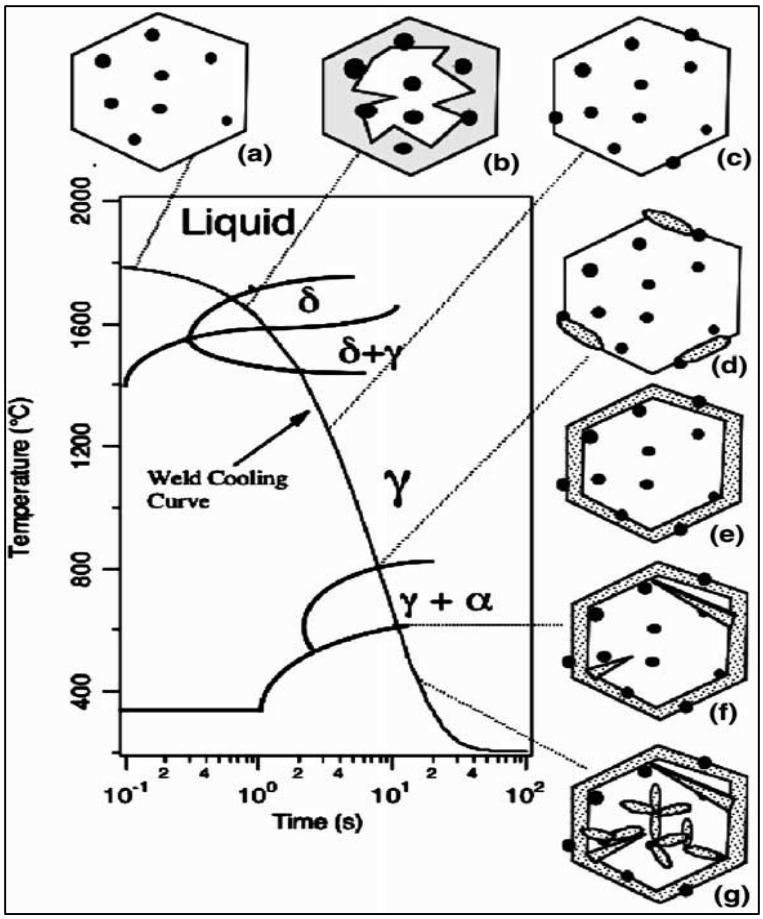

Figure 2-4: Weld metal showing the different phases of transformations during solidification at room temperature [81]

Of course, cooling rate influences the phase transformations that a weld experiences. However, the cooling rate depends on the welding process used to make the weld [82]. A number of researcher have investigated effect of cooling rates [83], [84], [85], [86], [87], [88], and it was reported that different methods of cooling rates were used to achieve the result.

The choices of filler wires when welding ferritic steel is important so as to achieve an appropriate balance between the strength and toughness of the weld. Good selection of filler wires will mitigate toughness related problems, for example, hydrogen cracking [89]. In multi-pass welds the composition of the first bead will differ from the second bead due to change in dilution level [13]. The influence of dilution on microstructure is reported to depend on mismatch between the composition of the filler wires and the parent metal. It was reported by Hunt, A.C

et al [90] that weld toughness was affected as a result of compositional changes due to dillution.

Furthermore, shielding gases play important role in protecting the weld pool from atmospheric contamination during welding process [91],[92],[93],[94]. Hence suitable process of gas selection is necessary [95]. This is because in carbon and low-alloy steels, increasing the amount CO_2 in the shielding gas results in high tensile strength and as a consequence reduces the ductility of the weld metal [96],[97]. Figure 2-5 shows a microstructure of a typical weld metal in low-carbon steels.

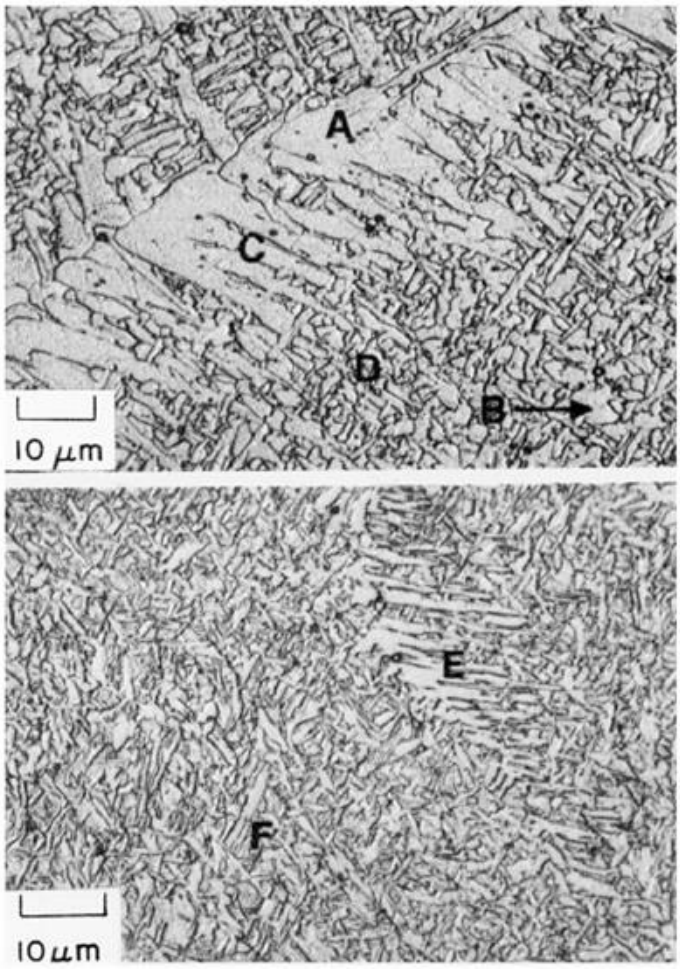

Figure 2-5: Showing micrographs of typical microstructure of weld metal in low-carbon steels [10]

In the Figure 2-5 shown above, ‘A’, ‘B’, ‘C’ and ‘D’ ‘E’ , ‘F’ is representing the grain boundary ferrite, polygonal ferrite, widmanstatten ferrite, ‘acicular ferrite, upper bainite and lower bainite respectively.

2.4.1.1 Acicular Ferrite (AF)

Acicular ferrite is widely recognized to be a desirable microstructure [6] due to its fine grain interlocking plates which are formed within the prior austenite grains [98], [99]. Acicular ferrite has microstructure that is superior in toughness and strength as compared to most of other transformation products. This microstructure appears to have the morphology of thin and lenticular plates [100] as shown in Figure 2-6. It is also generally known to have fine “grain size, high dislocation density and also high angle of grain boundaries” which serves as crack arresters [41]. The actual aspect ratio of these acicular plates has never been measured but in random sections, the plates are typically around the range of 10µm long and 1µm wide. Hence, the real aspect ratio is most likely to be smaller than 0.1 [6].

The transformation behaviours of acicular ferrite indicate that the volume fraction of AF increases with an increase in the amount of hot deformation [101]. Further investigation shows that AF form at nucleation sites within austenite grains such as dislocations [102], [103].

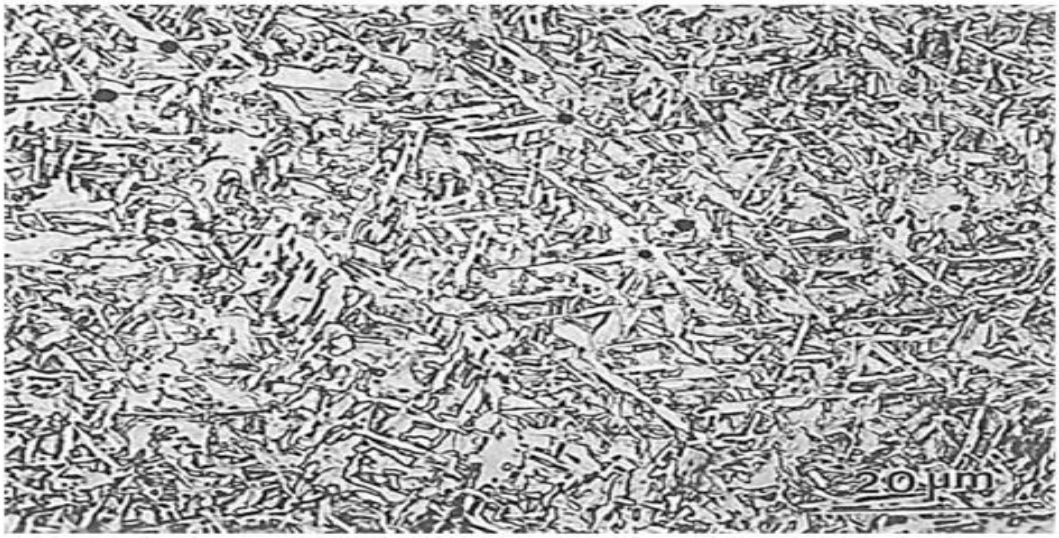

Figure 2-6: Predominately acicular microstructure [10]

2.4.2 Heat Affected Zone (HAZ)

Heat affected zone microstructures are governed by the steel chemistry and the thermal cycle experienced. Increased in the alloy content, the peak temperature, and the cooling rate through the transformation temperature range will all promote the formation of different phase constituents in the microstructure. The thermal cycle at any point in the heat affected zone is dependent on the heat input and the distance from the fusion boundary. As this distance increases, the peak temperature and cooling rate through the transformation range are reduced. Hence, the microstructures are less affected, and the hardness comes closer to the parent metal [8].

However, Zalazar, M. [104], has investigated the HAZ of multi-pass welds. He has evaluated the microstructure that arises from pipeline steel weld by using multi-pass weld with low heat input. It was found out that, with the low heat input employed during the experiment, local brittle zones (LBZ) were still noticeable [104]. LBZ decrease the fracture toughness value. This local brittle zone is as a result of complex mechanism involving compositions of the steel and the thermal cycles during the welding process. In multi-pass welding therefore, there is a significant modification of the microstructure [105].

In the HAZ of multi-pass weld, as shown in the Figure 2-7, point A (see corresponding diagram on the right) has been reheated just below the Ac_1 and is known as subcritical reheated coarse grain (SRCG) zone. The microstructure in the zone is said to be stress relieved. At point B, the reheating temperature was between the inter-critical temperature region which is between Ac_1 and Ac_3. This part is called the intercritically reheated coarse grain (IRCG) zone where partial re-austenitization occurs with high carbon contents. At this region there is a high tendency of forming brittle microstructures (M-A island). It was reported by Zalazar, M. [104], that depending on the welding process, this region normally exists at about 3 mm from the fusion line of the first pass.

When the temperature crosses the Ac_3 line as shown in the corresponding diagram (at point C), it is called the supercritically reheated fine grain (SCFG) zone. At this point, complete re-austenitization occurs, but the peak temperature

is not high enough to promote grain growth. Therefore, the microstructure becomes normalised or refined. At point D (see corresponding diagram) the reheating has moved above Ac_3 line; the high temperature promotes grain growth. This region of the weld is referred to coarse grain (CG) zone, and produces a coarse grained microstructure.

Clyde M.A [106] also developed a two-dimensional heat flow analysis equation to identify the metallurgical microstructures in the HAZ of a multi-pass weld.

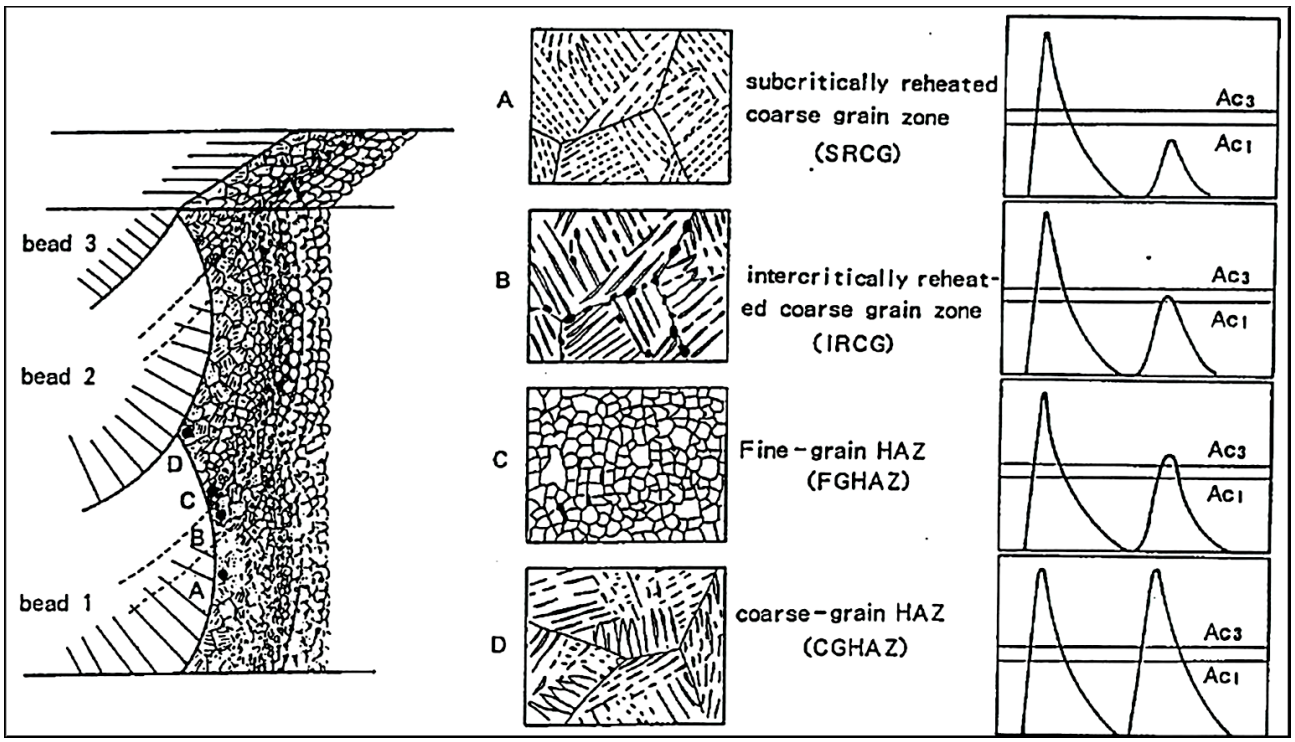

Figure 2-7: Sketch showing relationship between microstructure and thermal cycle in the HAZ. [107], [104]

2.4.3 Microstructure of Multi-pass and Single Pass

Multi-pass welds hold some excellent properties such as microstructural refinement, better toughness and lower residual stresses compared to single pass welds [108]. This is due to the fact that:

i. The thermal cycle from subsequent passes refines the grains from the previous pass.

ii. The total heat input per weld pass is reduced, therefore grain growth is effectively reduced.

iii. Previous passes provide some preheating effect that tends to extend the critical cooling time of Δt8/5 (Δt8/5 is the time taken to cool from 800℃ to 500℃).

iv. The subsequent passes have an annealing effect on the previous one, thereby relieving residual stresses from the previous passes.

Figure 2-8 shows the comparison of the microstructure of a single pass and mutli-pass welds.

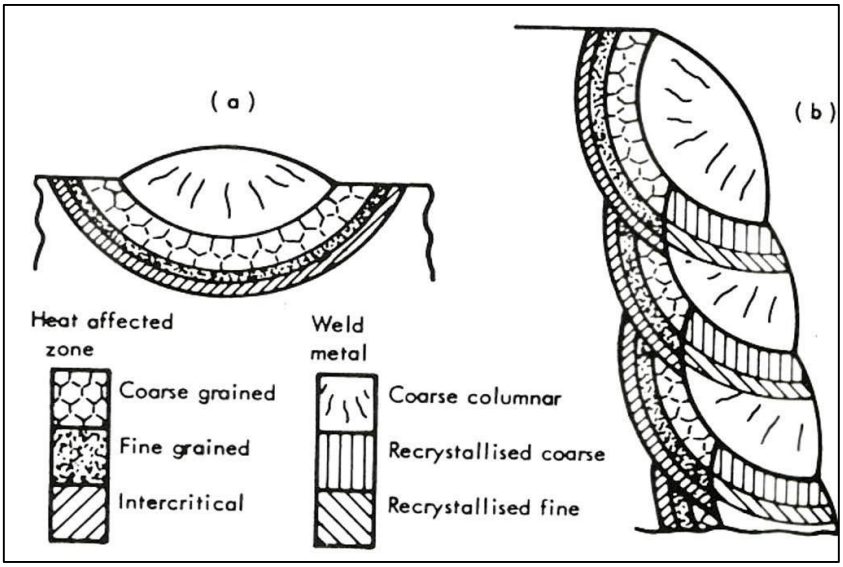

Figure 2-8: comparison of the microstructures of (a) single run and (b) multi-run welds [108]

2.5 Stainless Steels

2.5.1 Introduction

Stainless steels which are also known as corrosion-resisting steels belongs to the iron-base alloys family which has excellent resistance to corrosion. These structural alloys are used for vessels, kitchen, building, and transportation due to their low temperature toughness as well as good corrosion resistance. Austenitic steel types are the most widely used stainless steels, which contain nominally 18% chromium and 8% nickel. These materials exhibit an attractive combination

of good strength, ductility, toughness, superior resistance to high temperature corrosion properties and creep, excellent corrosion resistance and good weldability [109], [110]. Due to these attributes, this structural alloys are used in a number of industries such as thermal power generation, biomedical and petrochemical, automotive, and chemical engineering [111].

2.5.2 Weld Metal

This structural alloys (austenitic stainless) are considered weldable [112], if necessary precautions are taken into consideration. However, due to the high heat during welding, when cooling to room temperature, several metallurgical phenomena occur. These metallurgical phenomena affect the physical properties of the structural alloy weld which will result in degradation of the welded joint.

A number of researches has been conducted on the final microstructure of the weld metal of this structural alloys and the way this weld metal solidifies over the years. Based on the research, it was reported that, in austenitic stainless steel, four (4) solidification modes are possible [112], [113] [114], [115]. These modes are characterised based on the primary solidified phase. This are:

i. Fully Austenitic phase (A).
ii. Austenitic–Ferritic phase (AF)
iii. Ferritic–Austenitic phase (FA).
iv. Fully Ferritic phase (F).

It was reported that A, AF and FA phases, are mostly associated with the austenitic grades, while the fully ferritic (F) is common in duplex stainless steel grades [116]. It was also reported by Elmer et al [116] that, in the case of the austenitic and austenitic–ferritic modes, delta-ferrite was the first phase to solidify, which will then transform into austenite. While in the case of austenitic–ferritic and ferritic–austenitic modes, it was reported by Lippold, J. C. and Kotecki, D. J. [112] that, austenite, delta-ferrite and liquid (L) coexist.

However, determination of the weld metal microstructure in austenitic stainless steel and the quantity of high-temperature delta-ferrite present in the weld metal results in many constitution diagrams. The current and most widely used

constitution diagram is the WRC- 1992 diagram [117]. This WRC-1992 diagram based it specification on chromium and nickel equivalents to specified solidification mode. It also uses the ferrite number (FN) to find out the quantity of ferrite that may be present in the weld metal [117], [112]. However, the more precise way of predicting of the weld metal microstructure is by the use of neural network analysis when compared to constitution diagrams [118] .

In austenitic stainless steels, if solidification occurs in the austenitic phase mode, it was reported that, at least a little quantity of delta-ferrite in the weld metal is necessary to avoid hot cracking [119], [120]. It was also reported that, in this type of steels, cracks and fissures are potential points for corrosion [121].

However, δ-ferrite is usually between 3 to 9% in the weld metal. In order to maintain this percentage so as to minimise the effect of hot cracking [9], a change in the final composition of the weld has been suggested by many researchers. For example, Liao M. T et al [122] conducted a research using GMA and FCA welding process using different shielding gas mixtures (argon+carbon dioxide) and the results show that an increase in percentage composition of carbon dioxide in the shielding gas mixtures, decreases the amount of δ-ferrite content in the weld metal.

Other possible way of controlling the amount of δ-ferrite that may be present in the weld metal is by controlling the cooling rate, as proposed by Lin Y. C [123] and Silva C. C [124]. In this case, slow cooling rates would prolong ferrite to austenite transformation temperature range and as a consequence, a significant quantity of δ-ferrite will form into austenite. Cooling rates (particularly slow cooling rates) may result in precipitation phenomena, which may result in poor protection of the corrosion resistance of the structural alloys. However, controlling the temperature to stay for a long period of time is possible during multi-pass welding [125].

Some of the common precipitates in this structural alloys are the σ-phase [125], [126], the intermetallic χ-phase [127] and Laves phase Fe_2Mo [128],[126]. These phases result in chromium depletion at the grain boundaries leading to

intergranular corrosion. This chromium depletion is called sensitisation [112]. The HAZ of the welded structures are mostly associated with is phenomenon.

This structural alloy (stainless steel) has lower thermal conductivity and higher thermal expansion coefficients when compared to other steels such as carbon steels. Proper additions some of elements (for example Nitrogen, Carbon dioxide or Hydrogen) in the shielding gas will increase the heat input. A high heat input, creates good weld penetration [129]. However, additions of hydrogen soften the weld metal, but when moderately added increase the tensile strength [130].

Due to high amount heat input during welding, residual stresses and distortion are formed in welded joints. It was reported that stress and deformation are inversely correlated [119]. “High stresses occur where deformation is restrained. On the other hand, low stresses occur where deformation is unrestrained”.

As discussed in subsequent chapter, the presence of such tensile residual stresses can be detrimental to the service integrity of a welded joint [131]. In addition to a complex distribution of residual stress states, multi-pass welds also forms dendritic grain structures, which are repeatedly heated, resulting in segregation of alloying elements. Dendritic grain structures are weaker, and segregation of alloying elements would result in formation of corrosion microcells as well as reduction in overall corrosion prevention due to depletion of alloying elements.

2.6 Deformation, Grain Microstructure & Recrystallization

2.6.1 Deformation

In simple terms, when a structural load is applied to a metal or other structural material, the effect results in change of shape in the material. The change in shape as a result of applied load is known as deformation. This deformation behaviour of metals is critical to the forming of engineering components. The two types of deformations are elastic and plastic deformation. The former occur at low stress and the material shape is recoverable after the stress is removed while the latter occurs at high stress and the material is not recoverable when the stress

is removed (permanent deformation). What is of interest in this research is the plastic deformation.

During plastic deformation of polycrystalline materials, some new boundary structures are formed. These new boundaries composed of many dislocations [132], [133]. These boundaries subdivide the original grains into multiple elements which have different orientations from one another. As the strain increases, the evolution of these boundaries may lead to a clear subdivision of the initial grains [134]. In this case, an increasing misorientation between adjacent cells is often reported.

Dislocation movement determines the ability of material to deform because strain and micro-residual stresses are developed as a result of stress field around dislocation. However, in steel, they occur due to some aids of the solute carbon atoms present at appropriate low temperature [135]. However, the dislocation density at small angle boundaries increases with plastic tensile strain [136]. It was also reported that stress decreases as dislocation density grow in small angle boundaries after cyclic elastoplastic deformation [136], [137], [138].

In summary, all the properties of a metal that are dependent on the lattice structure are affected by plastic deformation. The microstructure and texture which determines the mechanical behaviour reflected during plastic deformation. Hence, tensile strength, yield strength and hardness increases while ductility decreases during plastic deformation [139]. Fatigue contributes to failure in structural components; and dislocations play an important functions in the fatigue crack initiation [140].

2.6.2 Grain Microstructure

Most mechanical properties of alloy depend on the grain structure. One of the mechanical properties that is influenced by the grain structure is the strength of the material [139]. Microstructure is characterised by the presence of grain boundaries. These grain boundaries are defects in the crystal structure. This defect tends to decrease the electrical and thermal conductivity of the material. At room temperature, the grain boundary affects the movement of dislocations

[141]. Small grains result in a large grain boundary area per unit volume in the microstructure. On the other hand, grain refinement (smaller grains) improves the strength of the material and vice versa.

These defect (grain boundaries) create an obstacle to dislocation movement and dislocation build-up at the grain boundaries, resulting in the formation of macroscopic deformation hardening of the material. The macroscopic properties of structural alloys depends on the grain size and the grain boundaries arrangement [142].

2.6.3 Recrystallization

Recrystallization is essential thermo- mechanical processing of metallic materials which is the device for the development of grain microstructures [141], [143]. This process is different from recovery and grain growth [144]. In recovery high angle grain boundaries do not migrate while in grain growth the driving force is only due to the reduction in boundary area.

There are two type of recrystallization. The static recrystallization which is slow and the dynamic recrystallization which is faster and is driven by plastic slip deformation of the material. In other words, static recrystallization occur on heating the deformed material to elevated temperature while dynamic recrystallization occur during plastic deformation.

In either case (static or dynamic), recrystallization occurs by growth of new grains of low dislocation density, which consume the surrounding cold-worked microstructure, effectively lowering the level of stored energy in the material. The nature of the recrystallization process is dependent on the extent of recovery, the rate of which is determined by the stacking-fault energy (SFE) of the material [145].

2.6.3.1 Measurement of Recrystallization

The traditional technique of measuring recrystallization in deformed and partially annealed metals is by using optical metallography on sectioned samples and the operator’s judgment is based on the appearance of each region [145].

Recrystallized grains are equiaxed with uniform colour while unrecrystallized grains shows deformed grains with irregular contrast. This method has spatial resolution of approximately 0.5 µm and with advancement in technological development, further methods such as Transmission electron microscopy (TEM), Scanning electron microscopy (SEM), Electron backscatter diffraction (EBSD) were developed and used.

The use of TEM allows the study of individual dislocations at a spatial resolution of approximately 5 nm [145]. Contrast mechanism of SEM is similar to that of TEM, and although individual dislocation cannot be detected [146], small changes in orientation across low angle boundaries allow the imaged to be detected. However, the widely recognised technique used for quantitative metallography now is the EBSD and details are discussed by Humphreys F. J. [147]. Using this technique (EBSD), both the size of the grains, the orientation of the grains and the subgrains may be determined.

2.6.3.2 Recrystallization Temperature

A recrystallization temperature is a temperature at which a highly cold worked structural alloy will recrystallized within a given time. In other words, recrystallization temperature is the temperature at which 99% strain free grains are produced. It has been reported that “recrystallization temperature of metal or alloy is between one-third and one-half of the absolute melting temperature (1540^{o}C for steel), which depends on several factors, including the amount of prior cold work and the purity of the alloy [141]”. The greater the amount of prior deformation, the lower the temperature for the start of recrystallization since there will be greater distortion and more internal energy driving the recrystallization [139].

2.7 Residual Stresses

2.7.1 Introduction

In a multi-pass weld, the development of residual stress depends to a large extent on the response of the weld metal, heat affected zone and parent material to

complex thermo-mechanical cycles during welding. Mechanically constrained thermal expansion and contraction leads to generation of residual stresses in the weld, with significant tensile residual stresses in and around the welded region. These residual stresses have a large tensile component in the longitudinal direction; whereas further away from the weld metal, the stresses are slightly compressive also in longitudinal direction balancing the tensile stress state [10], [11].

Residual stresses in welding are thermal stresses which are primarily cooling stresses with possibly superimposed transformation stresses [9]. These transformation stresses are formed as a result of transformation strains which occur during austenite to ferrite transformation. The development of welding residual stresses is influenced by many factors, which include thermal, mechanical and material. The effect of residual stresses in a welded structure includes distortion and amplification of the stress state which could affect the fatigue strength of the weld [12]. The knowledge of residual stress in the weld would prolong the life time of welded joints [16].

However, predicting this residual stress in welds involves the studies of interactions between various physical phenomena. These physical phenomena, include thermal expansion, phase change, material plasticity and microstructural change. However, all these phenomena: that is, plastic yielding of the weld metal across a temperature distribution which is induced by the welding process, upon cooling causes residual stresses [148].

2.7.2 Formation of Residual Stresses During Welding

Weld-induced stresses are the typical example of detrimental residual stress in structural materials due to their effect and widespread occurrence. The formation of residual stresses during welding is as a result of large amount of non-uniform heat input inherent in most forms of welding process which cause thermal expansion and contraction in the weld. The thermal stress in weld causes a non-uniform distribution of irreversible material deformation. These deformations

sometimes remain in the material after it has cooled, leading to an internal and completely self-equilibrating stress field.

Schematic illustration of residual stress formation is shown in Figure 2-9. As welding requires a large amount of heat to achieve a material bonding; high temperature causes thermal dilation of material, followed by lowering of the yield strength and eventually melting the material in the case of fusion welding [149]. On the other hand, material farther away from the weld pool remains at a relatively low temperature throughout as shown in section B–B in Figure 2-9. As the heated material begins to cooled, it solidified and hence tendency to contract, thus producing tensile stress as shown in section C-C of Figure 2-9. These result in a characteristic distribution of residual stress, with very large tensile stresses in the joint region which are balanced by compressive stresses elsewhere [10], [131], [150]. As the material is further cooled and contracted more, it produces higher tensile stresses near the weld centreline and farther away from the weld centreline is produces compressive stresses to balance the tensile stress (section D – D).

In summary, the actual magnitude and orientation of the residual stresses formation will depend on the direction of the greatest thermal gradients encountered as the material cools and on the mechanical constraint applied to the cooling weld metal.

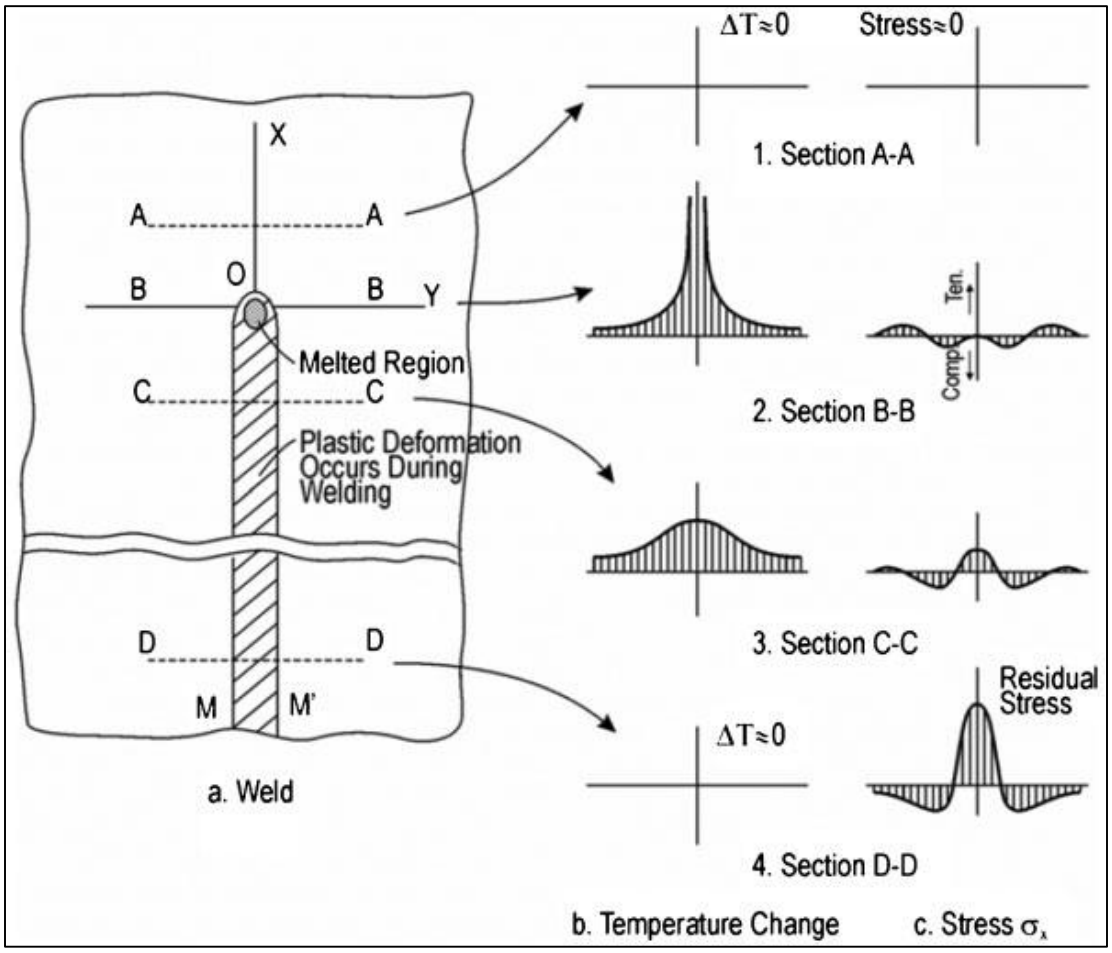

Figure 2-9: Showing residual stress formation in a weld [10], [151]

2.7.3 Effects of Welding Residual Stresses

Most of the mechanisms which result in failure of materials are because of the presence of tensile residual stress. Some of these effects include: Fracture and fatigue, Stress corrosion cracking and Distortion, which are briefly explain below.

2.7.3.1 Fracture and Fatigue

The presence of a tensile residual stress field combined with external loading modifies the stress intensity at crack tips which serve as initiation point for crack propagation [152], [153], [154], [155]. In weld fatigue lifetime, it is assumed that the effect of the mean stress applied during loading cycle are less compare to large tensile stresses that may be present in the weld region [149].

Residual stresses affect elastic fracture as well as high cycle fatigue, but they have much less influence over ductile failure due to the fact that they are rapidly accommodated by plastic deformation [156], [157].

Cracks in case of fatigue mostly start at the surface of the material, requiring tensile stresses for propagation. Therefore, the presence of tensile residual stress in the surface of the material tends to facilitate fatigue cracking, while a compressive residual stress tends to prevent the crack opening and propagating [158].

However, a number of fatigue life improvement methods (for example shot peening) depend on modifying compressive residual stresses in risk prone zones. Of course, since residual stresses must be self-equilibrating, corresponding tensile stresses must also exist somewhere else. According to Coule, H. E [149], compressive stresses are only induced in a thin surface layer as shown in the example of shot peening, while it corresponding tensile stresses form further into the material. In comparing with welds, welding tends to result in large tensile residual stresses throughout the thickness of the weld with the compressive stresses form further away from the joint [159]. Due to difference shown, methods which induce compressive surface stresses as well as the methods which reduce stresses through the entire weld thickness are useful methods for improving fatigue life of welds.

2.7.3.2 Stress Corrosion Cracking (SCC)

These forms of cracking occur when chemical and mechanical forces are present to cause crack propagation throughout the affected area in the material. Stress corrosion cracking is a form of environmentally-aided material failure. Since both chemical and mechanical are the driving factors, only materials exposed to particular corrosive area and having an elements of mechanical stress are susceptible to stress corrosion cracking (SCC). Residual stresses generated during welding are in most cases enough to promote SCC in an environment where ordinarily it would have not occur; because there is insufficient mechanical driving force [13]. But according to Fricke, S. et al [160], welding induces stress concentration and increased metallurgical susceptibility to corrosion at the

welded joint and this causes problems in gas pipeline and nuclear components where welded joints are used in a corrosive environment [161], [162].

2.7.3.3 Distortion

Residual stress fields within a material are internally self-equilibrating, and for these stress distributions to exist, there must be an internal incompatibility in strain [163]. Therefore, during manufacturing process, where residual stress are induced or relaxed as the case may be, there must be a corresponding inhomogeneous deformation so as to balance the effect. Of course, residual stresses in welding are associated with deformation which when allowed to pile-up along the length of the weld can create visible distortion of a welded material. The most problematic effect of residual stress is distortion which according to Masubuchi, K.[151], little residual strain presents in the weld, can cause different modes of distortion. In thin-walled structures, apart from shrinkage and bending mode of distortion, welds in this material mostly produce large residual stress to cause buckling which can make distortion prediction and analysis difficult [164]. Figure 2-10 shows different forms of welding-induced distortion.

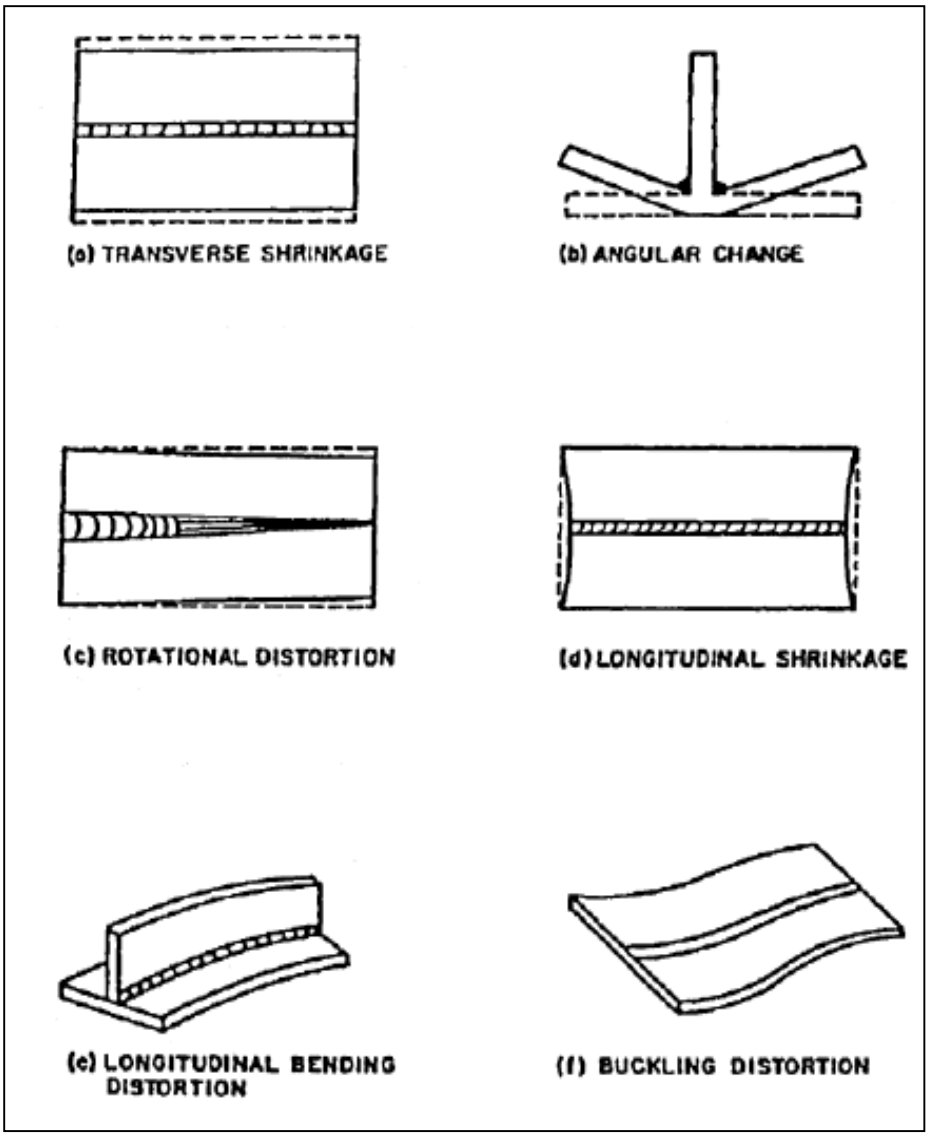

Figure 2-10: Various forms of welding- induced distortion [165]

2.7.4 Classifications of Residual Stress

Welding residual stresses arise as a result of compressive plastic flow ahead of the weld pool. The most common origins of this residual stress are those caused by;

i. non-uniform plastic flow
ii. sharp thermal gradients during welding and heat treatment operations

Welding residual stresses should be balanced because the component is in equilibrium with a stress component inside it [17]. Residual stresses can therefore

be classified according to their length scale into three types [150] [17]. A corresponding schematic of these characteristic is shown in Figure 2-11. In this figure, the top row shows a polycrystalline material at three different length scales [166]. These sketches show the microstructural constituents, i.e. the grain size as well as the size of the precipitates from a second phase. While the lower row of the figure shows the corresponding stress component in the y-direction when scanning along the x-direction.

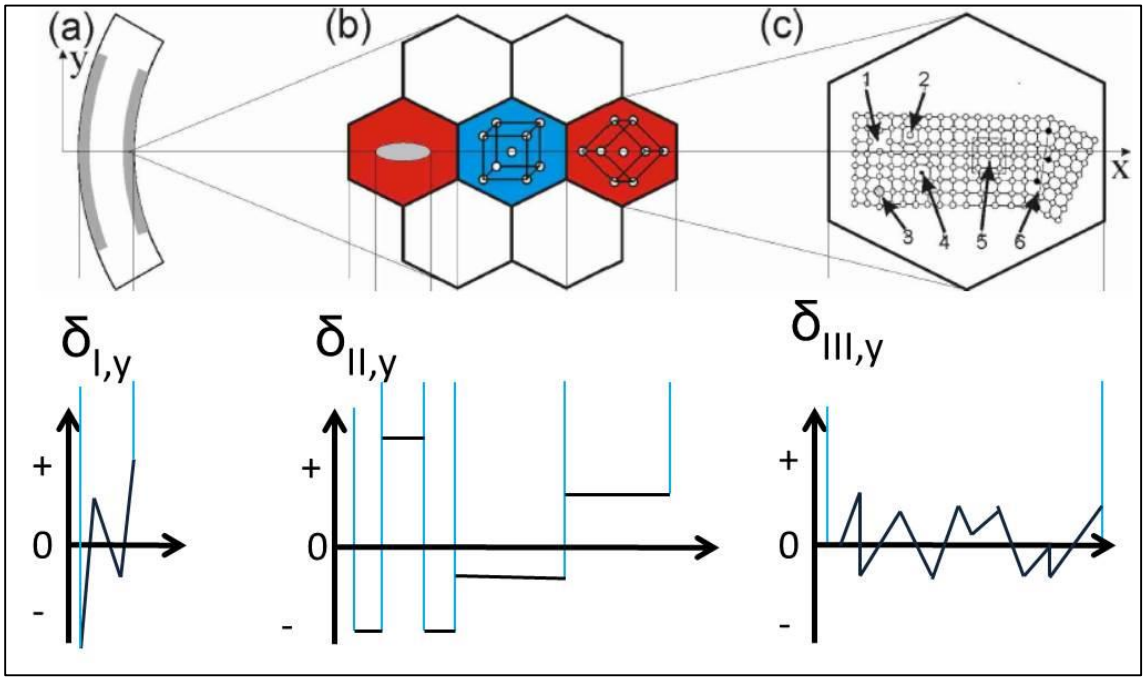

Figure 2-11: sketch showing various classifications of residual stresses [150]

As shown in this sketch, Figure 2-11 (a) is the type I stresses (σ_I) in a bent iron rod. The grey shown the plastically deformed region. Figure 2-11 (b) is the type II stresses (σ_{II}); the stresses are intergranular stresses. That is, stress form between the grains of the same material but with different orientation (for example, red and blue grain) and interphase stresses between the constituents of different materials (e.g. red and grey grain). Figure 2-11 (c) is the type III stresses (σ_{III}) which is caused as a result of strain fields around defects. For example the defect is indicated by numbers say; (1) vacancy (2) interstitial atom (3) substitution foreign atom (4) interstitial foreign atom (5) edge dislocation and (6) small angle grain boundary.

Type I stresses (σ_I) are uniform over larger regions (that is over numerous grains). These are continuum level stresses that neglect the underlying microstructure and they equilibrate over a length scale comparable to the dimension of the component. These stresses are therefore called macro- stresses. Example of these stresses is shown in Figure 2-11 (a) where the iron rod was bent. The plastically deformed region is shown in grey colour. The inhomogeneous deformation of the iron rod left residual stresses in the material, which vary along the cross-section, and these residual stresses may either be compressive or tensile.

Type II stresses (σ_{II}) are uniform on the level of the individual constituents. These are stresses between the grains of the same material but with different orientation. Figure 2-11 (b) is an example of type II stress with a microstructure taken from a plastically deform part of the iron rod. The grain in blue colour and the other grain in red colour are grains of the same material but have a different crystallographic orientation.

Type III stresses (σ_{III}) vary within the individual constituents. This occur as result of strain fields around lattice. Figure 2-11 (c) shows some of these lattice defects. These are stresses occur as a result of heterogeneous behaviour at the atomic scale.

Type II and III stresses are called microstresses since both vary on the scale of the microstructure. It is worth knowing that the real residual stress is given by the superposition of macro- and microstresses.

2.7.5 Measurement of Residual Stress

The strength, fatigue life and dimensional stability of a practical engineering component are greatly influenced by the presence of residual stresses. Knowing the size of the stresses is therefore essential, so as to take them into consideration during the design process. However, “locked-in” character of residual stresses developed especially during welding makes them challenging to measure. However, because of the wide application of residual stress measurement methods in both research and industry, a number of residual stress

measurement methods can be found in literature [16],[150],[167]. Some of these measurement techniques are destructive (“relaxation”) while others are non-destructive methods [17].

However, there are three fundamental strategies of measurement which are:-

i. Measuring the change in strain as residual stresses are relaxed by removal or cutting of material (destructive).
ii. Measuring the interatomic spacing and comparing this to the spacing in an unstressed reference specimen (non-destructive).
iii. Measuring the change in another physical phenomenon with which stress interacts.

The practical application of the first strategy includes: contour techniques which provides area maps of residual stress measurement [168], [169], and the hole drilling technique in which stresses are calculated backward from strain measurements made near a small hole as it is drilled [170]. All these techniques are relaxation method which are destructive in nature and is a subject of recent review by Schajer, G. S [167]. As the interatomic spacing in a crystalline material changes in response to applied stress, the second strategy stated above is possible to apply. Hence diffraction method can be used to measure the crystal lattice spacing, and of course, strain can be measured non-destructively in (polycrystalline) metals and ceramics. In this second strategy, stress can therefore be calculated after obtaining the strain. The third strategy uses, for example, changes in the sonic and magnetic properties of some materials to measure stress according to et al Gauthier. J. [235].

However, most researchers used neuron diffraction or high energy synchrotron X-rays to measure residual stresses produced by welding. This is due to the fact that the methods have been developed with high level of accuracy which can be used at a range of spatial resolutions. This method is conducive to the study of engineering structures and is briefly explained below.

2.7.5.1 Diffraction Techniques

Diffraction method is one of the best ways of determined residual stress fields non-destructively. The diffraction techniques for measuring strain operate by inferring the crystal lattice spacing d of the sample material from the scattering angle Θ of radiation directed at it. These two quantities are related by Bragg's Law; (n ʎ= 2d sin Θ), where "ʎ" represents the wavelength of the incident radiation. The lattice spacing is then compared with a reference value d_0 for a nominally unstressed sample of the same material. The difference in these two values is used to calculate the strain [150]. With knowledge of the strain in all directions and mechanical properties of the material, the stresses can be found. For polycrystalline materials, the unstrained lattice parameter d_0 can vary throughout the material due to differences in crystal orientation and intergranular microstresses. This means that the gauge volume (the volume of material over which diffraction occurs) must be sufficiently large compared with the microstructure of the material that the values are averaged.

As stated in the above section, there are different types of diffraction techniques, but each technique has its own advantage and disadvantage. However, neutron diffraction was proposed to use in this research. The main advantage of neutron diffraction over others is the high penetration depth in all common polycrystalline engineering materials (Figure 2-12). The high penetration depth characteristic is useful for alloys of high average atomic number [18]. Also, typical diffraction angles in neutron diffraction are much higher than those for laboratory X-ray and synchrotron X-rays, which makes it easier to measure strains in all directions, including normal to the sample's surface [171].

The majority of neutron strain-scanning instruments use a nuclear reactor as the neutron source, which produces a continuous flux of neutrons over a range of wavelengths. A monochromator is used to block out all but a small part of the spectrum. The monochromated neutron beam is directed at the sample, and the resulting diffraction pattern is scanned using movable detectors [172].

Current examples of constant flux instruments include SALSA [19]. SALSA is a good residual strain-mapping equipment that are available at the Institut Laue

Langevin France. This equipment is available for public use. It designed to accommodate all engineering component that can be mapped in terms of speed and the size.

Detailed discussions of the neutron technique are given by [171], [173] while synchrotron diffraction was explained by [174].

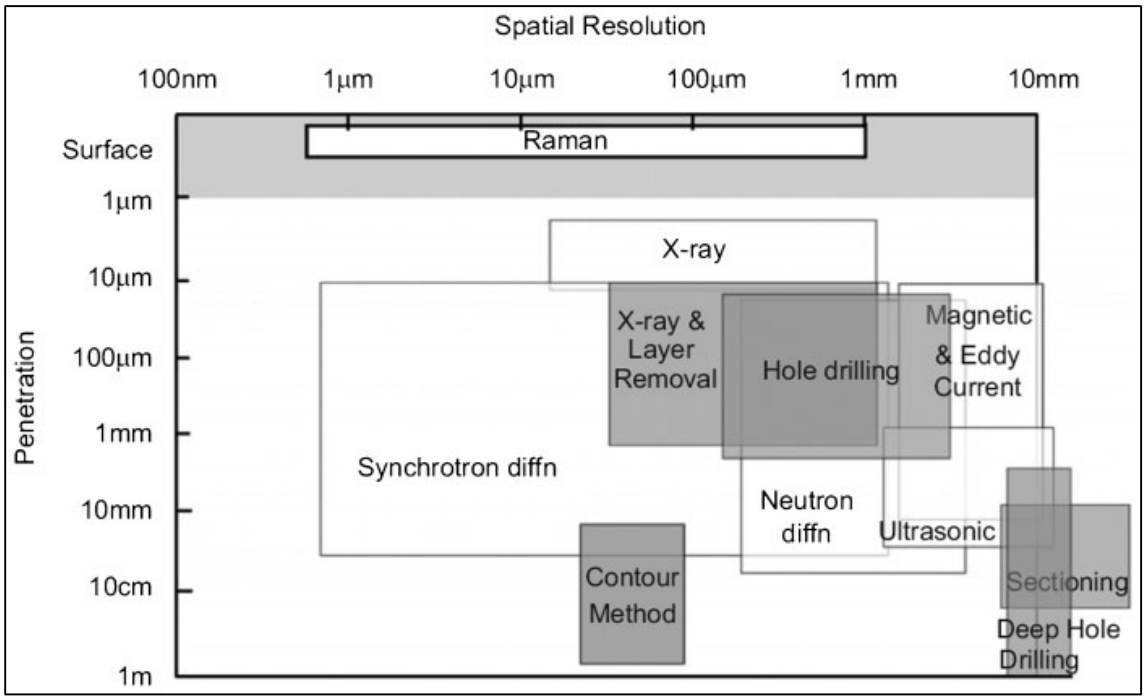

Figure 2-12: Schematic showing capabilities of the different measurement methods [168]

2.7.6 Methods of Modifying and Redistributing Residual Stress

A number of techniques are available for modification or reduction of weld residual stress distribution. The peening process have been optimised for use on welded materials. There are welding specific methods of reducing residual stresses in existence (global mechanical tensioning) which are designed to work against residual stresses produced during welding. Global mechanical tensioning (GMT) has received increased attention over the years as cheaper and more effective ways of getting the best result are always sought in engineering practice.

However, to modify the presence of residual stresses in the weld metal, a permanent plastic deformation must occur so as to modify the residual stress state in the welded joints. This deformation can be achieved by using;

i. An externally applied mechanical force.
ii. Inducing a solid state phase transformation.
iii. By application of thermal field.

It is therefore possible to group the reduction of residual stress distribution into these three groups.

In addition to the above mechanism, welding residual stress reductions have been further divided into: - Post-weld heat treatment, Control of heat input during welding, Peening, Vibratory stress relief, Localised cooling, rolling which are briefly explains below.

2.7.6.1 Post-weld Heat Treatment

This form of mitigation involves heating the material uniformly above ambient temperature to enable the residual stresses generated in the weld to relax automatically. This method is called post-weld heat treatment (PWHT), which is the most commonly accepted method of residual stress relief. This method has proven to be effective in a wide range of applications [175], [176], [177].

Experiments conducted by Smith, D. J et al [178] using ferritic steel pipe of 84 mm thickness are shown in Figure 2-13. The hoop stresses were tensile with exception of small part near the surface that is compressive, while the majority of the axial stresses across the pipe are tensile but compressive near each surface before post-weld heat treatment. After PWHT there was reduction in residual stress as shown in Figure 2-13.

High temperature reduces the yield strength which causes the material to yield locally under its own internal stresses. However, cooling (in gradual and uniform condition) is normally used to prevent further stress formation after the stress has been relaxed. This method has been proved to be effective at reducing residual stress but is not applicable in all cases. For instance, this method cannot be applied to dissimilar material welds because of the difference in their thermal

expansion coefficients. Application of PWHT is ineffective [179] in reducing residual stresses in dissimilar material and PWHT can also cause brittle failure [180].

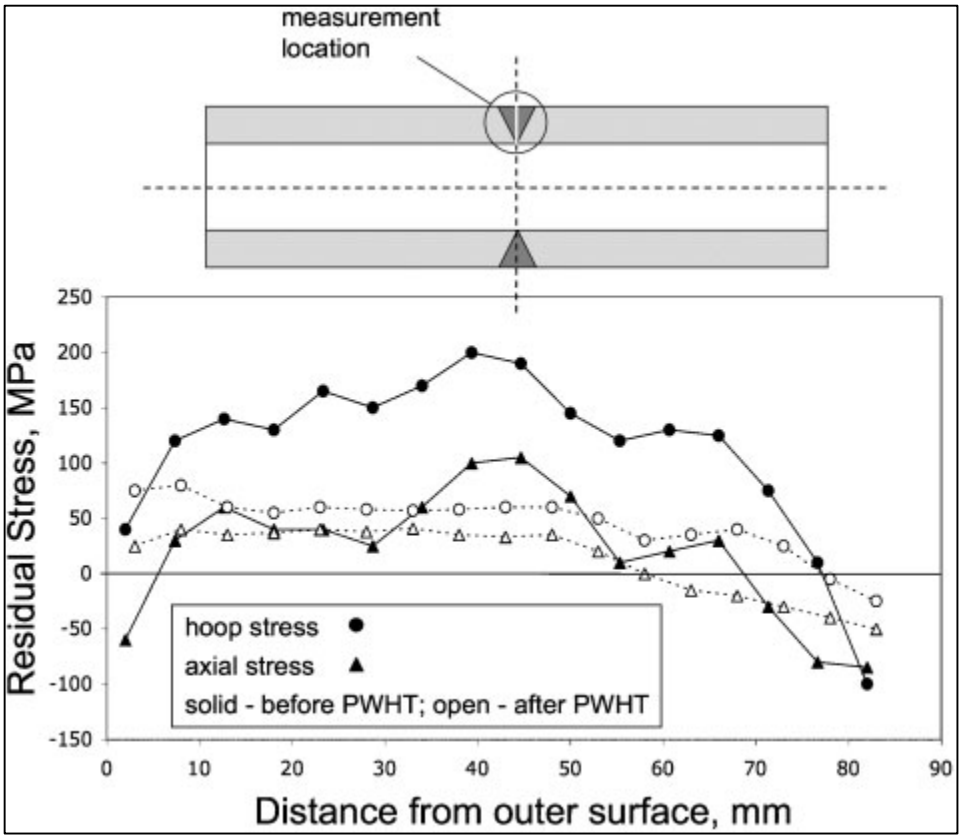

Figure 2-13: Showing axial and hoop residual stress measurements [13].

2.7.6.2 Control of Heat Input During Welding

The heat input per unit length of weld influence the distribution of temperature in the material [181] and this can affect the weld microstructure as well as the formation of residual stresses in the weld. Unfortunately, material bonding requires enough energy to fuse into each other. Hence, this limits the amount by which heat input can be reduced. Another factor that limits the control of heat input is the welding process. In some welding process (laser for example), reducing the heat input will eventually cause transition of the process from keyhole to conduction mode. However, control of welding heat input can reduce the width over which plastic strain occurs [182], [183] but cannot prevent the formation of residual stress in weld.

Another way of controlling heat input is preheating of the weld region, which is aimed at reducing the temperature gradient around the weld bead. This process also causes residual stresses [184] in some cases and hot cracking. Preheating is a good process for materials (say, aluminium) that have a high thermal conductivity and fast cooling rates [68], [185]. Hence preheat cannot be considered a universally effective method of residual stress control.

2.7.6.3 Peening

This processes described impact or the propagation of shock waves to cause deformation. It is a form of stress modification techniques which can be used to induce a stress state near to the surface of a work-piece. However, they are often stated in the context of weld fatigue life [186], where a compressive surface stress state close to the weld toe can reduce the propagation of fatigue cracks. Research conducted by Hacini, L. et al [187], show that with hammer peening, it was possible to induce a significant state of compressive stress (radial to the impact location) in a steel sample, without producing any apparent external or internal cracking. In addition, Lah, N. A. et al [188] observed that, 'the effect of the controlled shot peening (CSP) and skimming processes improved the fatigue life of the fusion weld by 50% on MMA-welded, 63% on MIG-welded, and 60% on TIG-welded samples'. In general, the effects of peening have been known to produce beneficial properties.

2.7.6.4 Vibratory Stress Relief

This technique utilizes motorised or electromagnetic equipment to vibrate the welded material strongly. The fundamental mechanism by which this techniques acts to reduce stresses is still a subject of discussion [189], [190]. Although, it was suggested by Walker, C. A. et al [191], that, this technique helps dislocation movement at the intragranular level. However, recent researches show that VSR is a localized cyclic plasticity phenomenon [192], and that the stress reduction strongly depends on the vibration's amplitude [193]. Despite recent advances in residual stress measurement techniques there is still insufficient published data on the topic of VSR.

2.7.6.5 Localised Cooling

Localised cooling is aimed at reducing the final pattern of residual stress distribution generated in the weld metal, by manipulating the temperature distribution in the welded component. Recent research uses a trailing heat sink with respect to the welding torch to create a characteristic valley-shaped temperature distribution [194], [195], [196], (see Figure 2-14). Figure 2-15 shows an example of cooling device that can be used to achieve the localised cooling. Recent research to model the process shows that heat sink placed as close as possible behind the heat source has influence in reducing tensile stresses generated during weld [195], [197] [198].

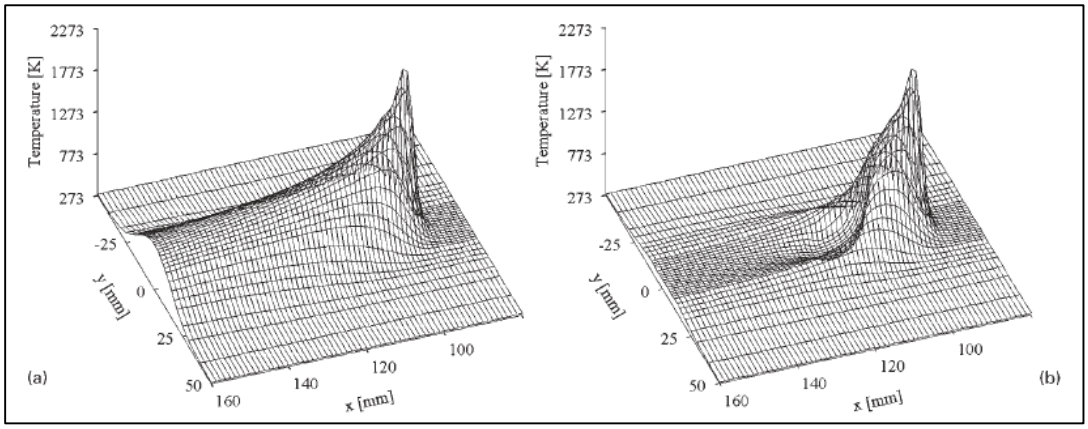

Figure 2-14: Temperature simulation profiles (a) showing the conventional arc welding; (b) showing the arc welding with trailing heat sink [195].

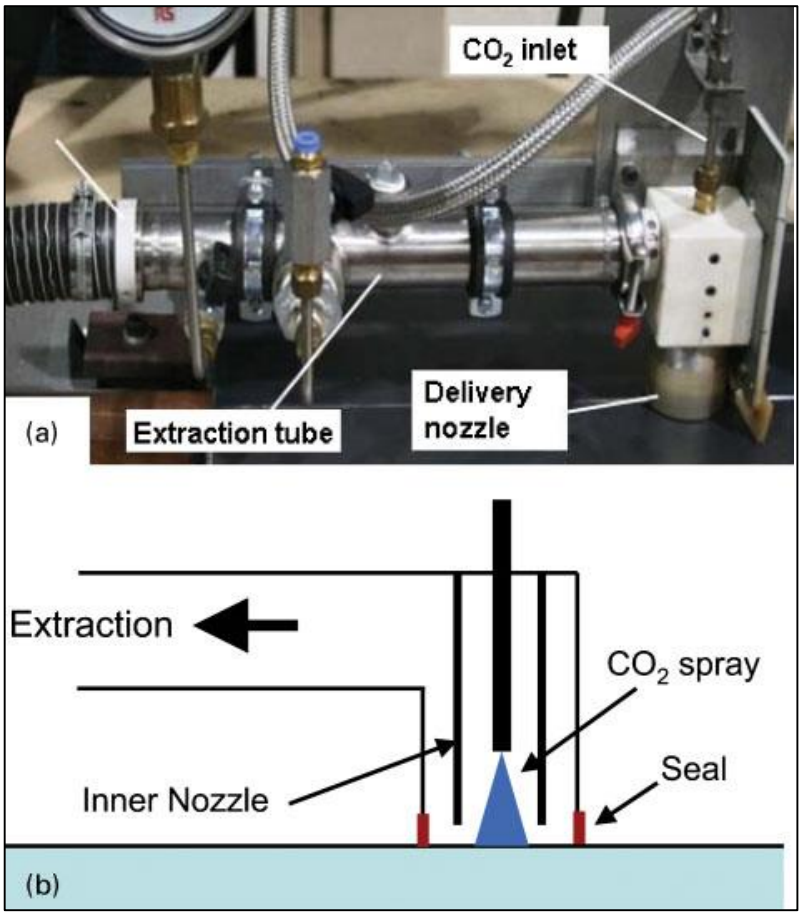

Figure 2-15: Showing design of nozzle which allow extraction of gas generated [198].

2.7.6.6 Rolling

Application of localised high pressure rolling to the welded joints causes yielding of metal in the weld region, thereby, relieving the residual stresses that may exist in the region [29], [199]. This technique depends on causing plastic deformation of the weld metal. The rolling processes, compresses the material in the direction normal to the weld's surface, thereby causing it to expand in the plane of the weld, relaxing any tensile residual stresses in the plane. This process was achieved using a single narrow roller applied directly to the weld line [199],[59], [34]. However, a pair of roller to roll in between the weld line has also been described by Altenkirch, J. et al [29]. The disadvantage of this process is that; both sides of the weld must be accessible so that the underside of the weld may be supported during rolling. Research on in situ rolling (rolling during welding)

and post weld (rolling after weld) has also been carried out by Coules, H. E. et al,[11], [200] but the results show that, post-weld rolling gives a far greater reduction in the residual stress field as compare to in situ rolling as shown in Figure 2-16.

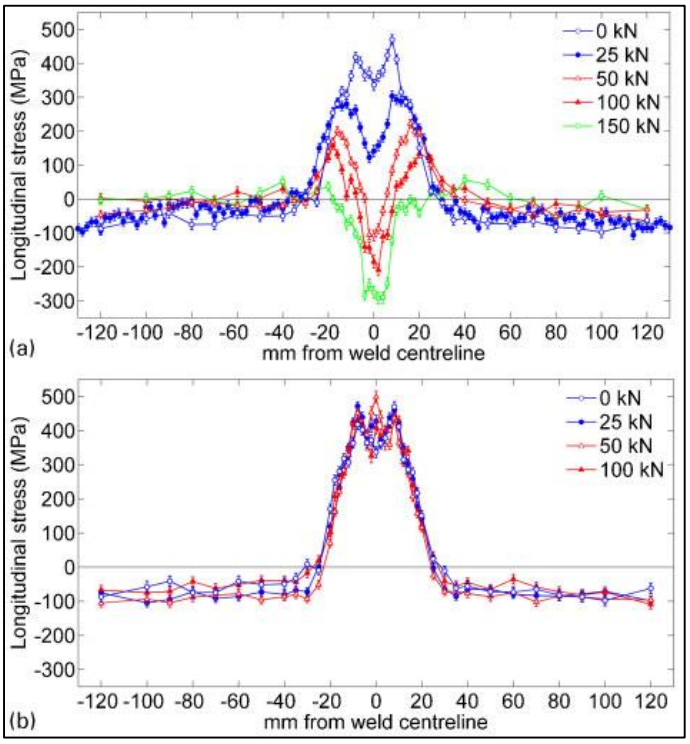

Figure 2-16: Showing cross-sectional distributions of longitudinal residual stress (a) post-weld rolling; (b) in situ rolling [11]

However, the influence of temperature of the material during rolling is of utmost importance to its final properties due to the differences in microstructure resulting from hot and cold work. Research carried out by Masubuchi, K. [151] indicates that an increased plasticity of the metal at elevated temperature allows for much greater strains. Kondakov, G. F.[34], has found experimentally that, application of hot rolling during welding in the temperature range 367-487^{o}C and strains of 10-23% resulted in superior mechanical properties of welded joints.

2.7.6.7 Global Mechanical Tensioning

A number of tensioning techniques have been tried and proved satisfactory as stress engineering method of controlling residual stress. The mechanical tensioning technique is believed to have relatively few parameters and can easily

be controlled in practice. For example, global mechanical tensioning requires only the determination of the load that should be applied in the direction of the weld. This method has a great influence in minimising the effect of local plastic strain, thereby reducing the longitudinal stresses [22], [32]. In addition, stress levelling techniques which need reasonably high tensioning loads are achieved by using post weld global mechanical tensioning techniques. This load on top of the weld would cause plastic deformation which will result in reduction of residual stress [33].

In situ global mechanical tensioning leads to reduction in residual stresses as summarised in [22]. Levels of the longitudinal tensile residual stresses are reduced as a result of plastic straining [22], [32].

The disadvantages of global mechanical tensioning methods are that they cannot be applied to large structures, as the large structure would require very strong tensioning device to apply. It is interesting to note that mechanical tensioning is only applicable on linear and simple geometries.

The use of localised mechanical processes to create residual stress effects has long been in practice, and such methods include: hammer, shot and laser peening, cold rolling, cold forging, burnishing [151]. Details of some of the work using localised mechanical processes are summarised in [186],[187],[188].

2.8 Summary/Conclusion

Welding of thick materials (pipeline steel) would introduce defect and varying distributions of residual stress field with changes in microstructural conditions. Research by Neeraj, T. et al. [201], shows tensile residual stresses formed more towards the cap (final pass) of the multi-pass weld and heat-affected-zone, which will be detrimental for crack propagation and structural integrity of the component. Therefore, it is essential to understand and characterise the residual stress distribution and device techniques to mitigate them. This would significantly improve the structural integrity and simplify its assessment procedures.

Of course, residual stress generated because of welding is a problem in engineering which affects multiple material and structural failure mechanisms. However, there has been a different approach to these problems based on different physical mechanisms, since stress formation during welding is affected by thermal, mechanical and material factors. The recent development of residual stress reduction skills is driven by the high cost and inherent limitations of conventional processes. Some techniques such as the rolling method and global mechanical tensioning have been proven capable of reducing residual stress in a weld, but each of the techniques come with its own practical shortcomings. It is believed that with advancement in technology on daily basis, the shortcomings may likely be overcome.

2.8.1 Motivation

This literature review has critically looked into changes in microstructure and the formation of residual stress in multi-pass welds. Their effect has been identified and different ways of solving the issues have been proposed and applied. But there are no reported works in the literature concerning the application of post weld cold rolling followed by laser processing of weld metal in a multi-pass weld.

The aim and objective of this research is to understand the suitability of this novel processing (application of local mechanical tensioning followed by laser processing) to create a stress free weldment with recrystallized grain structure to improve structural integrity of multi-pass welds.

3 Application of Local Mechanical Tensioning and Laser Processing to Modify the Residual Stress State and Microstructural Features of Multi-Pass HSLA Steel Welds

3.1 Introduction

In this research work, the experiments were carried out in two (2) phases. The first phase of the experiment involved three steps; welding was carried out by Tandem GMAW DC process, the post weld cold rolling was performed using an in-house rolling device and finally, the post weld cold rolling was followed by laser processing using 8 kW (peak power) continuous wave (CW) fibre laser. The laser processing in the first phase was in transient heating mode using a laser power of 3 kW with a travel speed of 0.3 m min^{-1} and laser spot dimension (beam diameter) of 20 mm. Figure 3-1 shows the schematic work flow in the first phase of the experiment. Microstructural observations, hardness scanning, tensile test and residual stress measurement were carried out after each step as shown Figure 3-1.

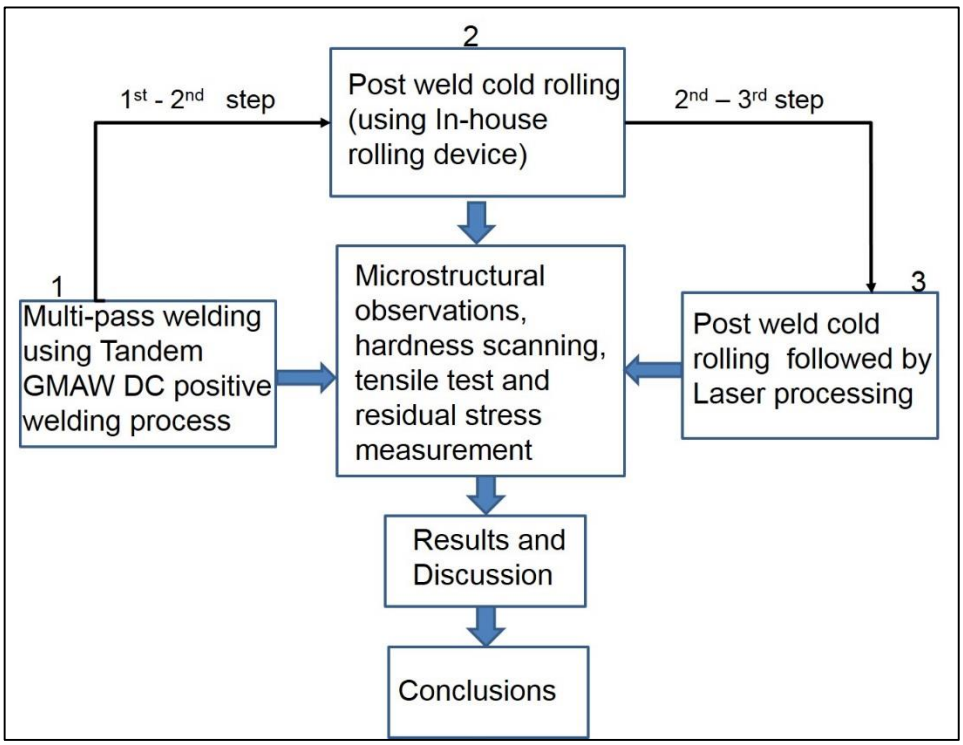

Figure 3-1: Schematic showing the work flow of the first phase

3.2 Materials

The grade of the pipeline steel plate is API 5L X100 pipeline steel plate (20 mm thick). This is a thermo-mechanically controlled processed (TMCP) structural alloy and has specified minimum yield strengths of 690 MPa [202]. Table 3-1 shows the chemical compositions of the API 5L X100 pipeline steel plate which was analysed in Exova.. The carbon equivalent for structural steel indicates the weldability of the steel; in particular, the carbon equivalent is an indicator of the requirement for preheats to achieve ideal weld properties. Standard (DNV-OS-F101) recommends that the carbon equivalent (CE) for a material should be calculated using the Pcm formula when the carbon content ≤ 0.12%, [203].

$$P_{cm} = C + \frac{Si}{30} + \frac{Mn}{20} + \frac{Cu}{20} + \frac{Ni}{60} + \frac{Cr}{20} + \frac{Mo}{15} + \frac{V}{10} + 5B \quad (3\text{-}1)$$

The standard also, recommends that for carbon content > 0.12%, the CE formula should be used.

$$CE = C + \frac{Mn + Si}{6} + \frac{Cr + Mo + V}{5} + \frac{Ni + Cu}{15} \quad (3\text{-}2)$$

Carbon equivalent numbers less than 0.40 should not require preheat, because preheat and high interpass temperatures can have a negative effect on the mechanical properties.

Table 3-1: Shows the chemical composition of the API 5L X100 pipeline steel plate

Elements	C	Si	Mn	P	Mo	Ni	Al	B	Cu	Nb	Ti	V	Cr	S	P_{cm}
Wt. %	0.06	0.25	1.79	0.016	0.16	0.13	0.03	<0.0005	0.27	0.03	0.01	0.04	0.03	<0.003	0.19

3.2.1 Filler Wire

The filler wire used was Union MoNi with a nominal diameter of 1.0 mm. The chemical composition of the filler wire is shown in Table 3-2.

Table 3-2: Shows chemical composition of the filler wire

Elements	C	Si	Mn	P	Mo	Ni	Cu	Cr	S	Others
Wt. %	0.12	0.4 -0.8	1.3 - 1.9	0.015	0.25 - 0.65	0.8 -1.3	0.3	0.15	0.018	0.25

3.2.2 Shielding Gas

The shielding gas used was 92% Ar and 8% CO_2 at flow rate of 30 lit min^{-1}. This gas was chosen because it had provided good results (mechanical properties, transfer characteristics and bead profile) in work carried earlier at Cranfield [204], [205].

3.3 Experimental Equipment

The experimental equipment used in the research are divided into four (4) sections (that is, welding, rolling, laser processing and residual stress measurement) and are presented as given below.

3.3.1 Welding

Gas-metal arc welding (GMAW) which is also called Metal-inert Gas (MIG) welding process was used in this research and some of the equipment used in welding include but not limited to: Welding Jigs, Fronius trans-pulse synergic 4000, RMS welding head oscillator.

3.3.1.1 Welding Rig

Figure 3-2, shows the linear welding rig used for tandem MIG welding process. This welding rig has a movable bed where samples are mounted. This movable bed can move in both left and right direction with a given speed. Once the sample is mounted, the welding torch is maintained in constant position, while the bed moves the sample in horizontal direction along the torch.

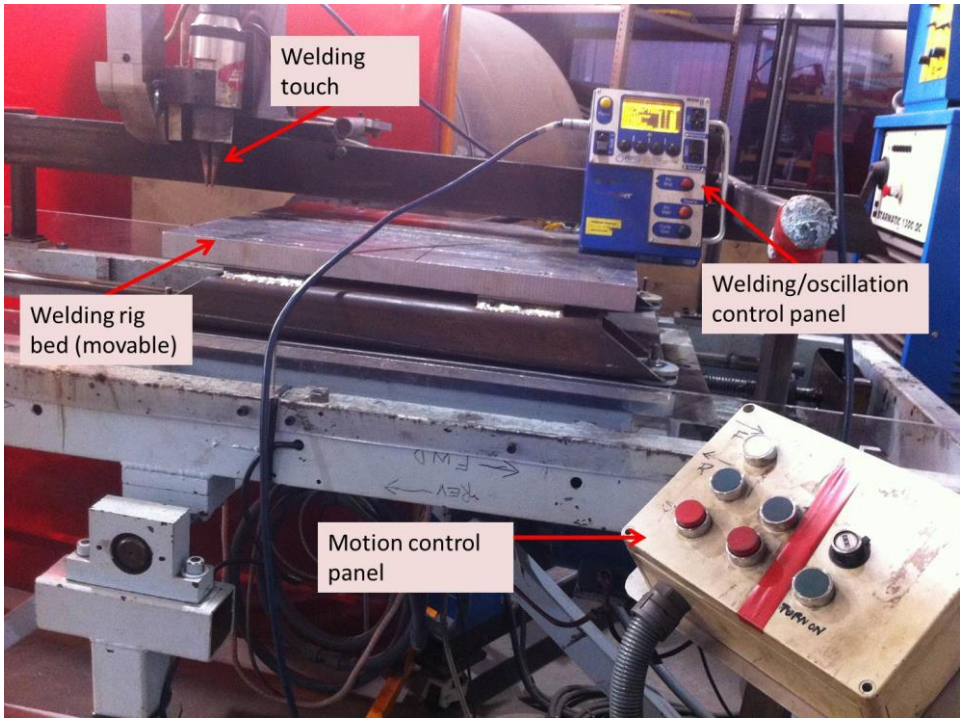

Figure 3-2: Welding rig with an RMS welding head oscillator

The travel speed was achieved by using the calibration chart made by Theocharis, L. [38]. Figure 3-3 shows the chart.

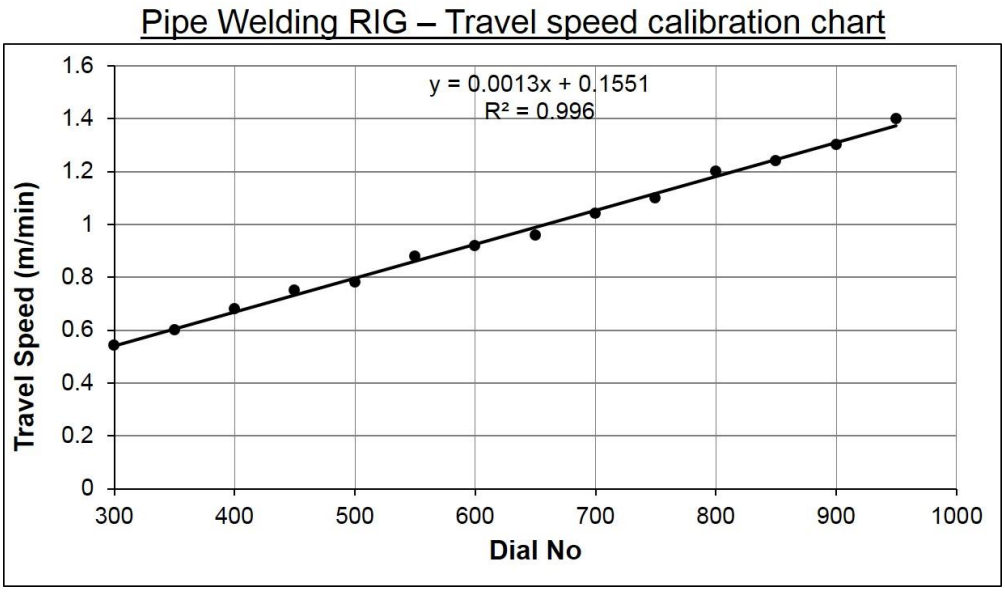

Figure 3-3: Travel speed calibration chart used [38]

This Travel speed is in millimetre per minutes (mm min^{-1}) and is plotted against the dial numbers of the control panel.

3.3.1.2 Tandem MIG Power Source

Figure 3-4 shows the sets of Fronius TPS 4000 power sources (TransPuls Synergic) fully synchronised in a tandem mode which was used for the narrow groove welding. This machine has a capacity of delivering 300 A at 100% duty cycle. At the top side of the machine are the welding setting where parameters such as wire feed speed, voltage, current, wire diameter, welding mode such as pulsed transfer mode, can be adjusted to achieve a particular purpose. This equipment is fully digitalised and equipped with microprocessors. Hence, during welding, the actual voltage and current reading are shown on the machine.

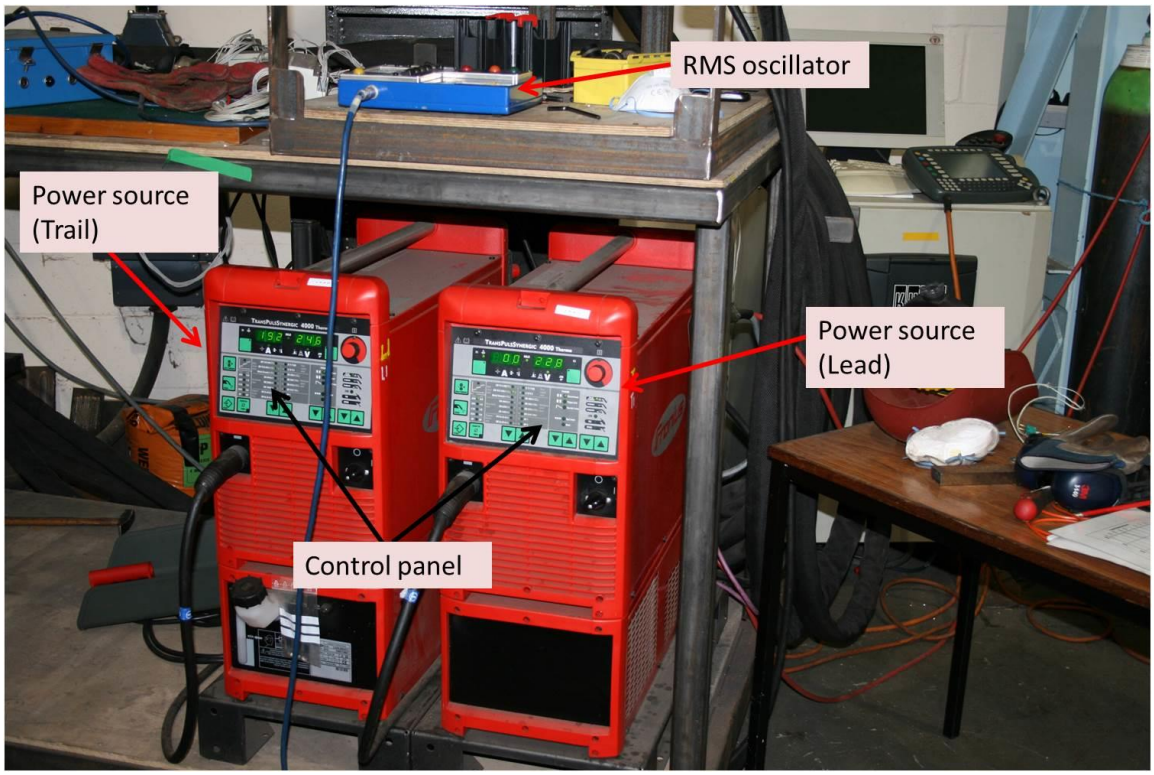

Figure 3-4: Fronius TPS 4000 thermo power welding machines

3.3.1.3 Weld Instrumentation

Instruments used for monitoring welding parameters such voltage, current and wife feed speed, and the thermal cycles generated using a thermocouple are presented here.

3.3.1.3.1 Measurement of Welding Parameters

Figure 3-5 shows the DL 750 Scopecorder used for the acquisition of transient welding current, arc voltage and wire feed speed. This device consists of twelve (12) channels which can be used at the same time to measure the welding voltage, current, wire feed speed and temperature using both R-type and K-type thermocouples. It is also capable of capturing data at a very high sampling rate. Up to 50,000 samples per second can be captured by this instrument.

This instrument is connected to the welding sample using probes. The current probe was connected to the instrument on one end while the other end was clamped to the earth wire to measure the current. In the same way, the voltage probe was connected to the instrument on one end while the other end was clamped around the welding plate to measure the voltage between the power source and the plate.

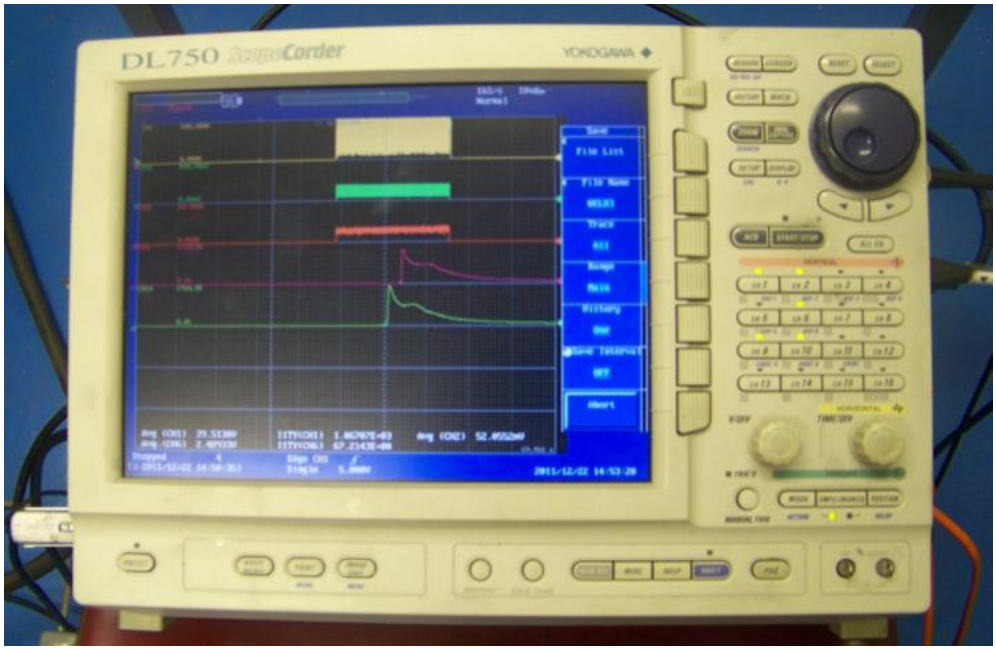

Figure 3-5: DL750 Scopecorder

R-type (Pt-13% Rh) thermocouple was used in this research to measure the temperature of the weld metal. The R-type can capture temperature up to 1600°C [41]. The R-type was dipped into the molten weld pool while the other end was connected to the Scopecorder, which logs the temperature and time during

welding. These method was used to show the transformation point in each pass of the weld.

3.3.1.4 Capacitance Discharge Welder

Figure 3-6 shows the capacitance discharge welder SR-48 which was used to join the thermocouple tips. It also used to attach the thermocouples to the samples. This equipment is designed for the fast production of thermocouple junctions and other fine wire welds. This equipment has an output of 48 joules over two power ranges allowing for two wires of up to 1.1mm diameter each to be welded.

Figure 3-6: Capacitance discharge welder

3.3.1.5 Characterisation

Instruments used for the microstructural characterisations as well as mechanical characterisations are described below.

3.3.1.5.1 Metallographic Examination

All the welded samples were prepared for metallography on the Buehler metaserv 2000 and motopol automatic grinding machines. Four (4) grinding stages; 120, 240, 1200 and 2500 grit papers were used. 6 µ diamond paste and 0.05 micron colloidal silica were used for final polishing of the samples. The following etchants were used after polishing API 5L X100 pipeline steel plate.

i. 2% Nital (2% nitric acid in ethyl alcohol) for micrographs
ii. 10%Nital (10% nitric acid in ethyl alcohol) for Macrographs

3.3.1.6 Micro Hardness Measurements

Figure 3-7 shows the Zwick Roell micro hardness testing machine that was used in measuring the hardness of all the samples under investigation. This machine has an automatic hardness tester that uses a diamond indenter. It has two lenses, the 10 and 40 times magnifications. The machine is equipped with a table that moves in the x, y and z directions.

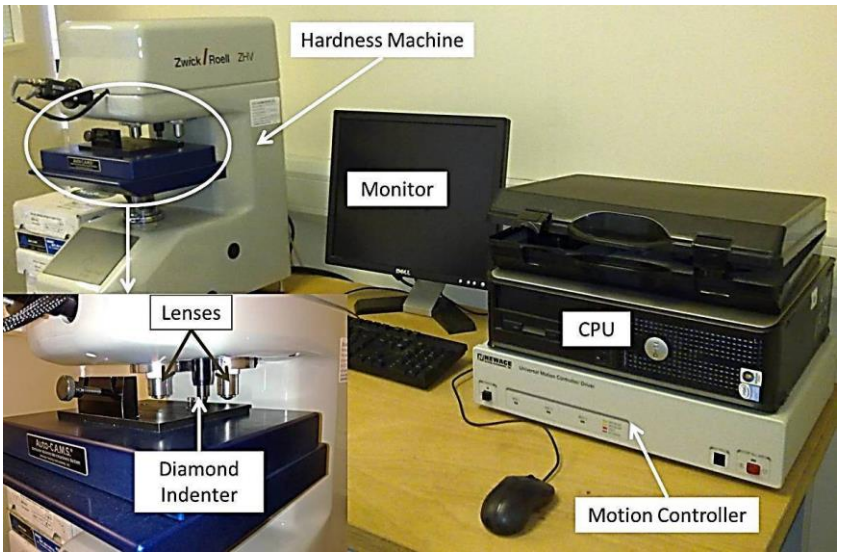

Figure 3-7: Zwick Roell micro hardness testing machine

In this experiment, the welded samples were cut, ground and polished according to standard metallographic procedures for microstructural observations and micro hardness tests. For micro hardness testing, 500 g load and 5 seconds dwell time was applied. Across and along the weld hardness scan was done with an interval of 1.0 mm within consecutive points.

3.3.1.7 Tensile Test Measurement

The all-weld metal tensile samples were machined from the welds samples in accordance to ASTM E8 / E8M – 08 standards. The equipment used was Instron 5582 50 kN tensile test machine with Serial No. 5582-K5838 in Exova. The tensile tests were designed to ensure that the samples to be tested are taken as close as possible near the cap pass in longitudinal direction (welding direction of the plate) as shown in Figure 3-8 (a). This was done to find out the effect of rolling load applied and the laser processing after rolling on the samples, since both the

load and laser processing were applied at the cap pass only. Figure 3-9 shows how the samples were machined (close to the cap pass) before it was tested.

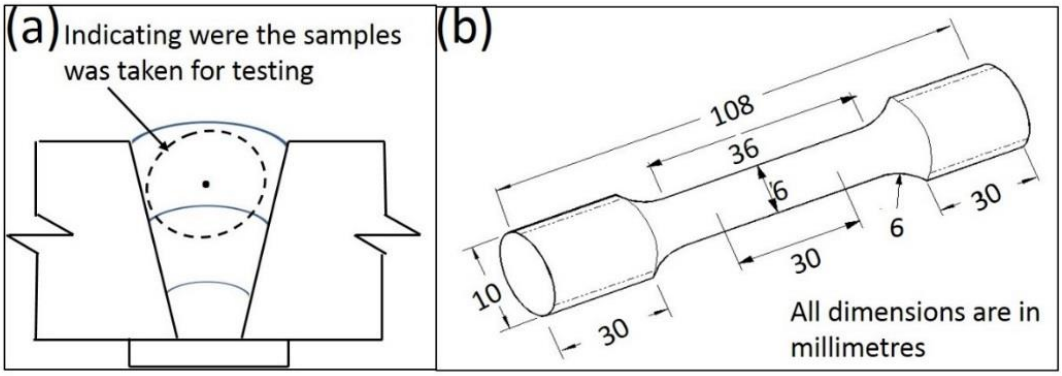

Figure 3-8: Tensile test (a) All weld metal in longitudinal direction (b) dimension of tested sample

Figure 3-9: Machined and tensile tested sample

3.3.2 Rolling (In-House Rolling Device)

The major components of the rolling system were the roller, roller fork assembly, crossbeam, oscillating mass, control panel, feed motor, main hydraulic system and vacuum clamping system. Figure 3-10 shows the rolling machine set-up. Details explanations on how this machine operates are given in section 3.4.2 of this thesis.

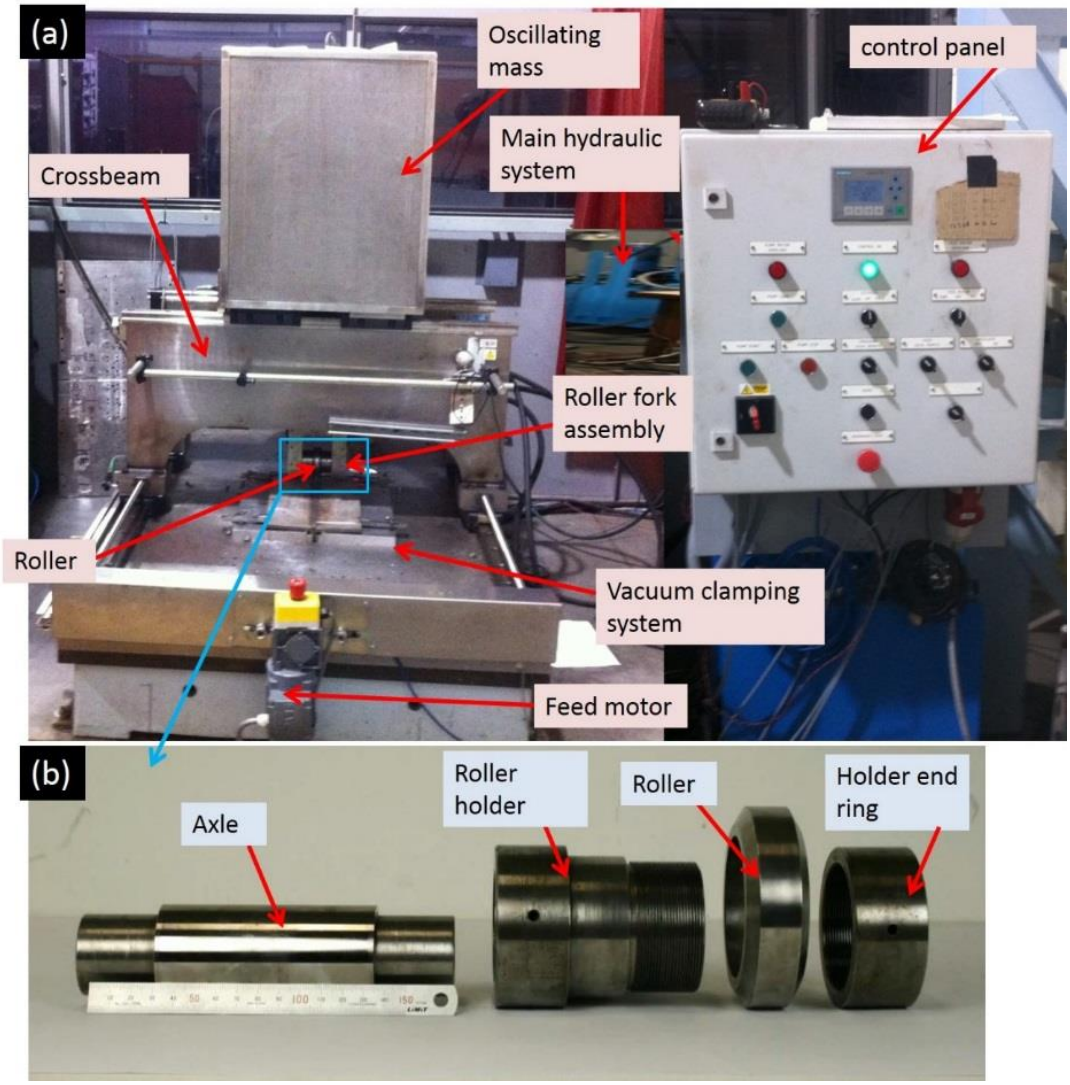

Figure 3-10: (a) Rolling device set-up (b) Roller assembly

3.3.2.1 Characterisation

Instruments used for the microstructural characterisations as well as mechanical characterisations are the same as those used in section 3.3.1.5.

3.3.3 Laser Processing

Laser processing was done by using IPG YLR-8000 Fibre Laser. During laser processing, thermal cycles were monitored by instrumentation using thermocouples. After processing, the samples were tested for metallurgical characterisation and mechanical testing.

3.3.3.1 YLR-8000 Fibre Laser

Figure 3-11 shows the photograph of IPG YLR-8000 laser system which is a diode-pumped continuous wave (CW) ytterbium fibre laser of near infrared spectral range. The IPG YLR-8000 has a high power fibre laser with a maximum output of 8 kW and has emission wavelength of 1.070µm [206]. Combinations of high power, ideal beam with quality fibre delivery give this system a unique identity.

According to IPG Photonics [206], the laser is produced from an active optical fibre and semiconductor diode. This represent a fusion of the two most innovative and advanced laser technology [207].

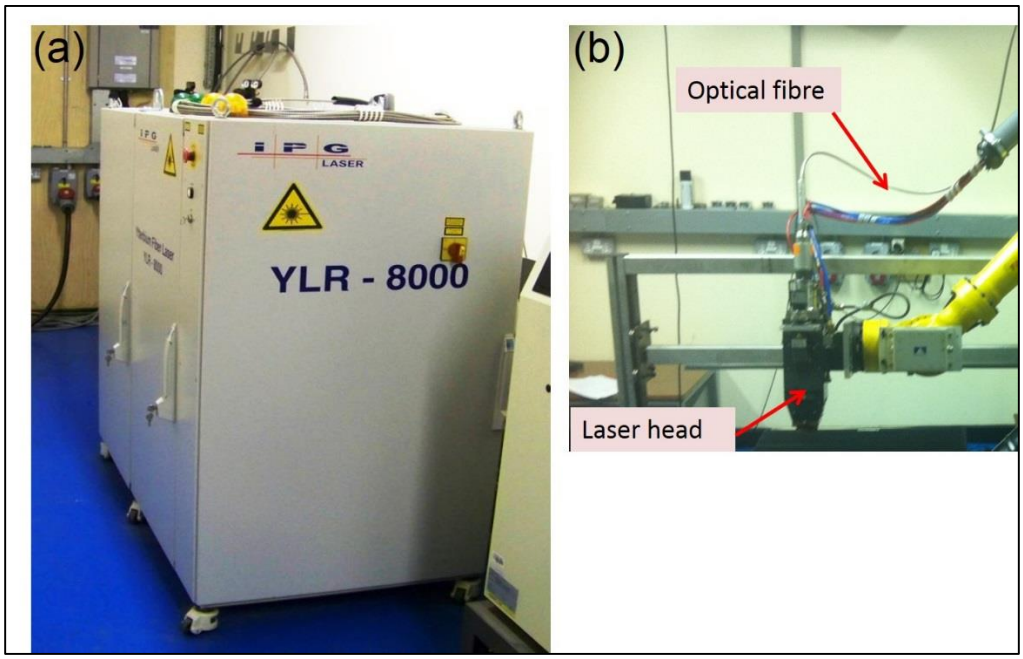

Figure 3-11: Showing (a) photograph of IPG YLR-8000 laser system (b) Laser head with the optical fibre

3.3.3.2 Weld thermal Cycles Determination

Thermocouples were used to measure the temperature-time relationship of the weld metal with the aid of a Scopecorder 750 instrument. Three holes were drilled through the plate thickness (from backing bar) to the weld metal into which K-type thermocouples was placed. The thermocouples were placed at 0.5 mm, 2.0 mm and 3.5 mm below the weld surface respectively (API 5L X100 pipeline steel

plate) as indicated in Figure 3-12. Laser travel speed of 0.3 m.min^{-1} was used in combination with laser powers of 1.5, 3.0, 4.0 and 6.0 kW. Figure 3-13 shows the photograph how the thermocouples were attached to the sample.

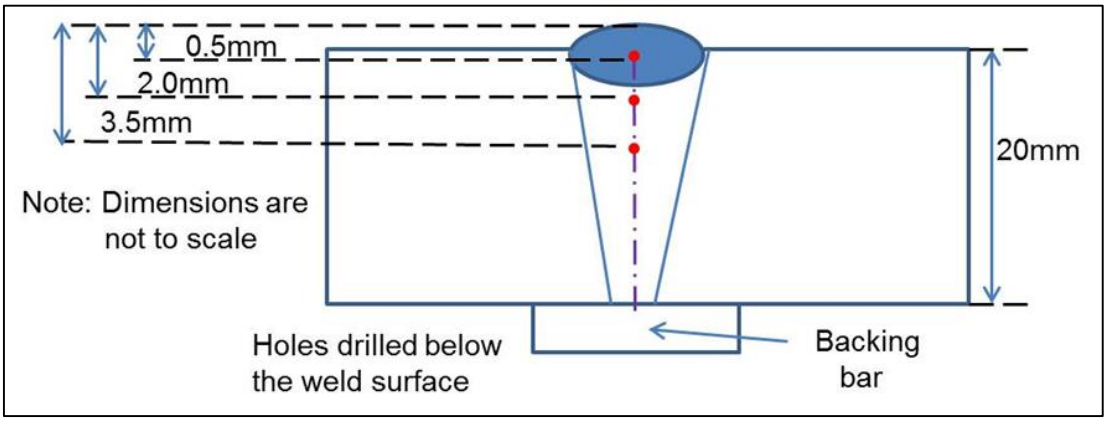

Figure 3-12: Sketch showing thermocouple positions in weld metal cross-section

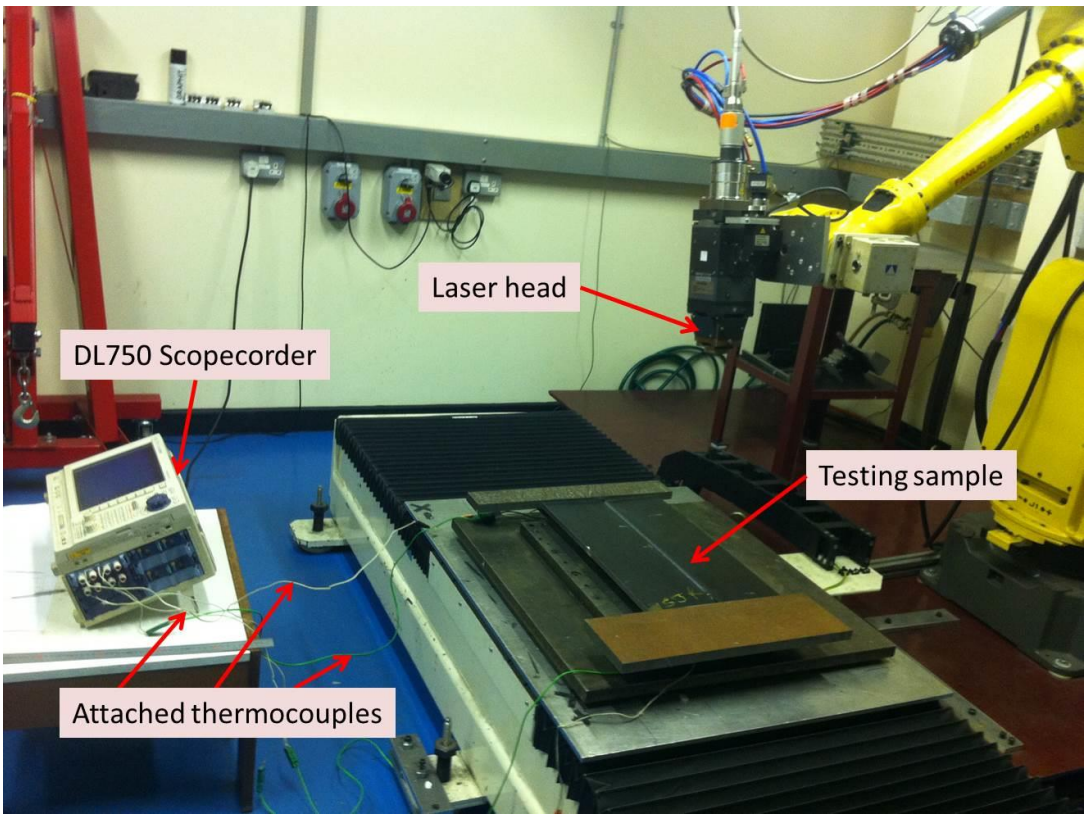

Figure 3-13: Photograph showing the laser head, scopecorder and thermocouple positions in weld metal

3.3.3.3 Characterisation

Instruments used for the microstructural characterisations as well as mechanical characterisations are the same as those used in section 3.3.1.5.

3.3.4 Residual Stress Measurement

Owing to the neutron beam's unique deep penetration and three dimensional mapping capabilities [172], neutron diffraction is widely used for stress measurements in a wide range of engineering structures. In this research, neutron diffraction was used, as it provides one of the few means of mapping residual stresses deep within the bulk of materials and components [17]. A neutron strain-scanning instrument was used. The majority of neutron strain-scanning instruments use a nuclear reactor as the neutron source, which produces a continuous flux of neutrons over a range of wavelengths. A monochromator was used to block out all but a small part of the spectrum. The monochromated neutron beam was directed at the sample, and the resulting diffraction pattern is scanned using movable detectors [172]. Although the detectors are movable, they are not in motion when the measurement are performed. Neutrons are collected across a range of 2Ɵ and then, the data is fitted to find out the actual 2Ɵ. Current examples of constant flux instruments include Strain Analyser for Large and Small scale engineering Applications (SALSA) [19]. SALSA is a dedicated residual strain-mapping instrument available at the Institut Laue Langevin for public and it is specifically designed to speed up, and extend the size and complexity of engineering components that can be mapped. SALSA is therefore designed to be very flexible equipment suitable for many materials science and engineering applications (see Figure 3-14) [19]. Figure 3-14 shows the photograph of SALSA set-up.

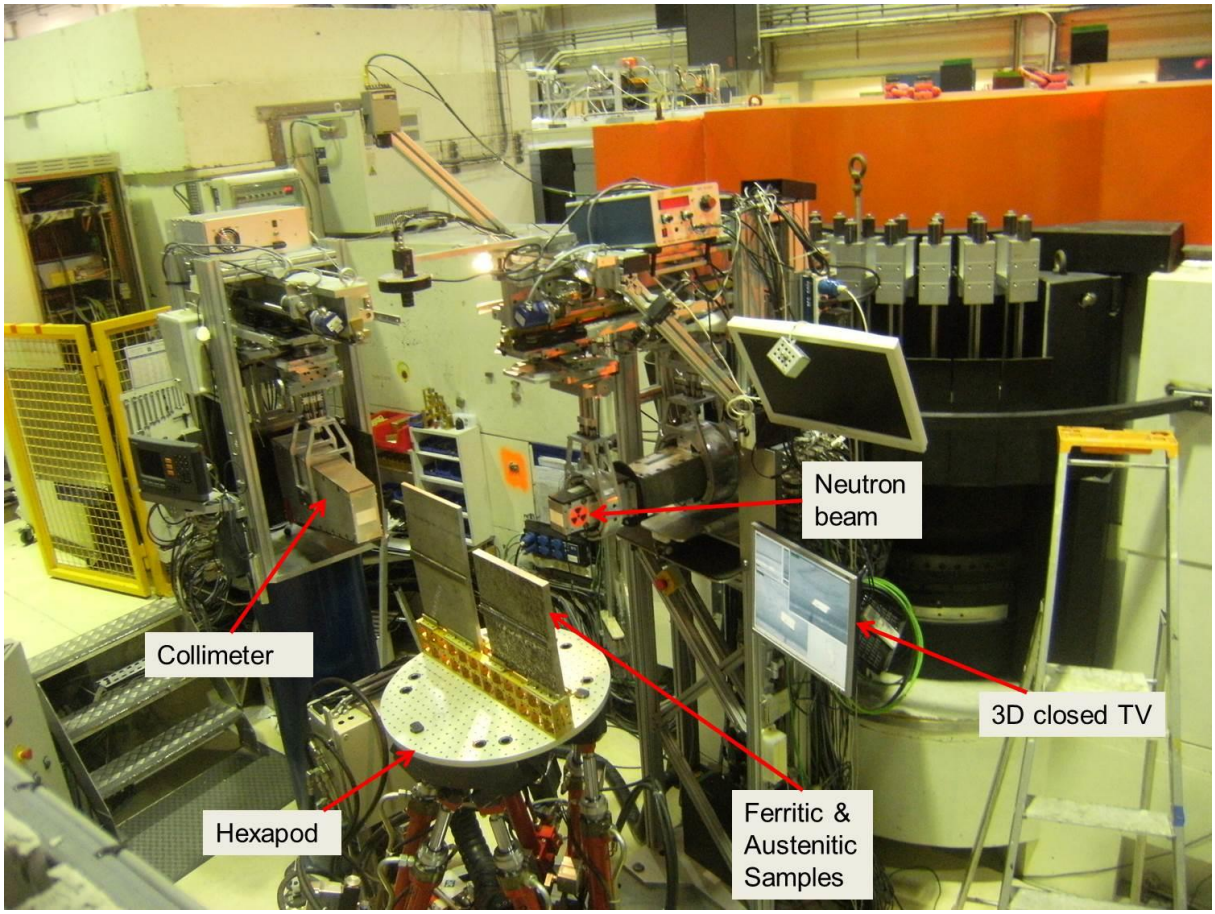

Figure 3-14: Photograph of SALSA with ferritic and austenitic plate place on hexapod table.

3.4 Experimental Method

The experimental methods are divided into four (4) headings (that is, welding, rolling method and laser processing and residual stress experimental method) and they are described in the following section.

3.4.1 Welding

The dimension of the test piece is (300 x 150 x 20) mm which was machined out from the API 5L X100 pipeline steel plate. However, before the actual welding, trial welds were carried out. Details are presented below.

3.4.1.1 Trial: Bead on Plate of API 5L X100 Pipeline Steel Plate

A bead-on-plate weld was made using different welding parameters. Significant amount of information such as welding travel speed, the wire feed speed were

generated during the trial. This trials were essential to find out the possible ways of using different parameters to achieve the desired result. In this trial, different parameters such as travel speed and wire feed speed were used interchangeable so as to have good weld profile. Figure 3-15 shows the trial made on bead on plate.

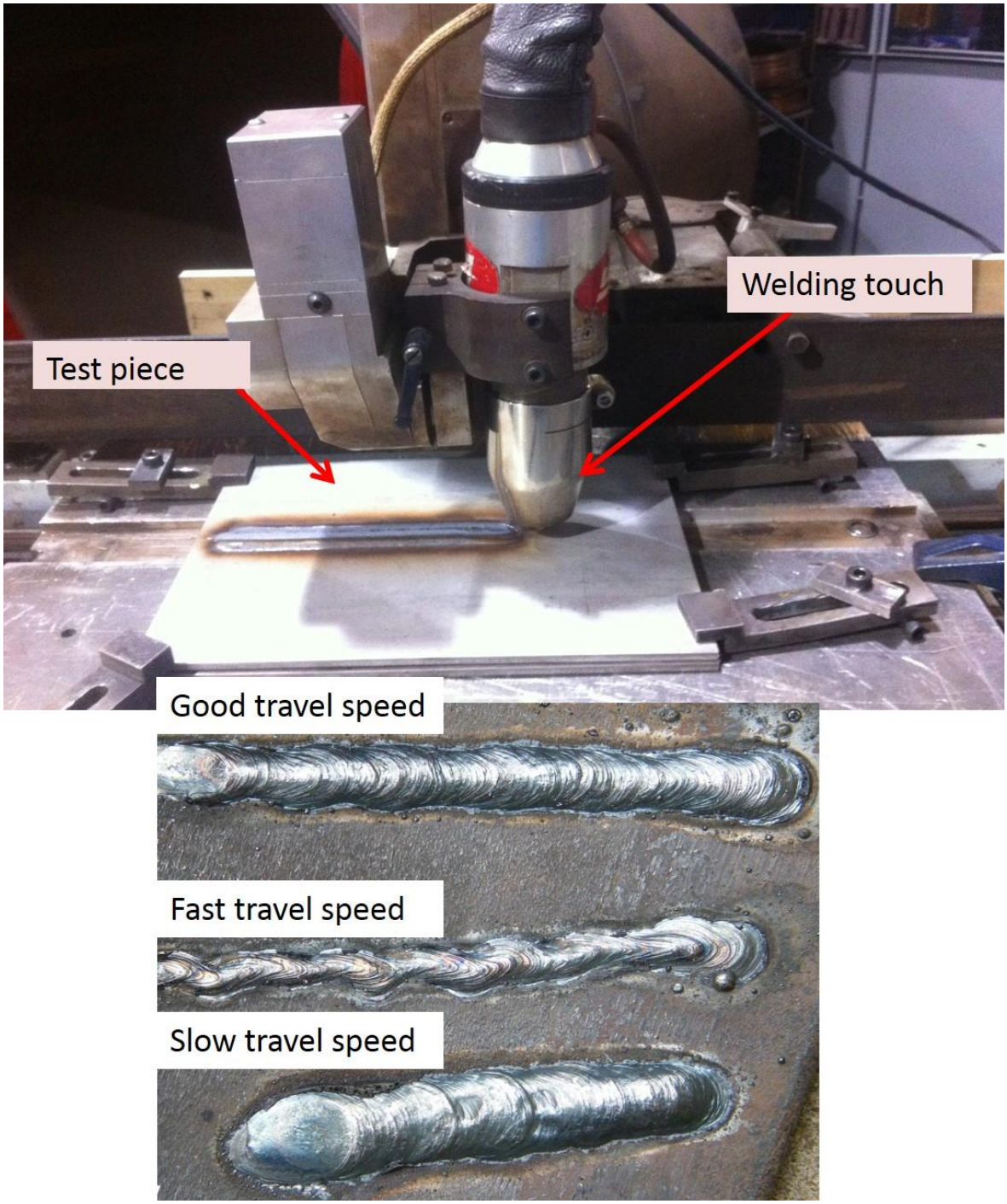

Figure 3-15: Trial bead on plate

3.4.1.2 Trial on Narrow Groove

Trial welds were made on narrow groove. In this trial welding experiment, attentions were concentrated on finding the appropriate balance between the travel speed of the weld and the wire feed speed, as well as the oscillation width and the arc length used in the research. With wide oscillation width, the wire touches the plate side walls. As a consequence, this results in instability and undercut of the welds. On the other hand, inadequate oscillation width results in a lack of sidewall fusion. Figure 3-16 shows the trials made on narrow groove using the two welding touch.

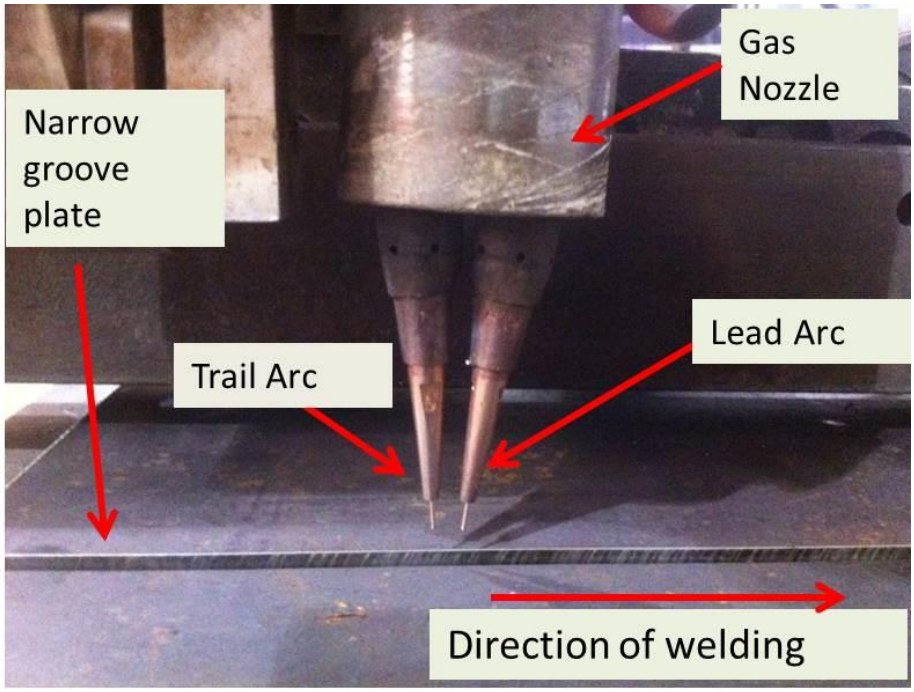

Figure 3-16: Trial made on narrow groove

3.4.1.3 Tandem MIG Welding of API 5L X100 Pipeline Steel Plate

The dimension of the test piece is (300 x 150 x 20) mm which was machined out from the API 5L X100 pipeline steel plate as stated earlier. A narrow groove edge preparation of 5° angle with backing bar (cut from the same material) was made as shown in Figure 3-17. The two plates to be welded were tacked together at both ends before commencing welding with a uniform gap of 5 mm between the plates. The tacking weld arrangement was given to the plates to minimize the effect of shrinkage and distortion. The welding sample was set and aligned in 1G

(down-hand) welding position and a total of six passes were made to fill the groove.

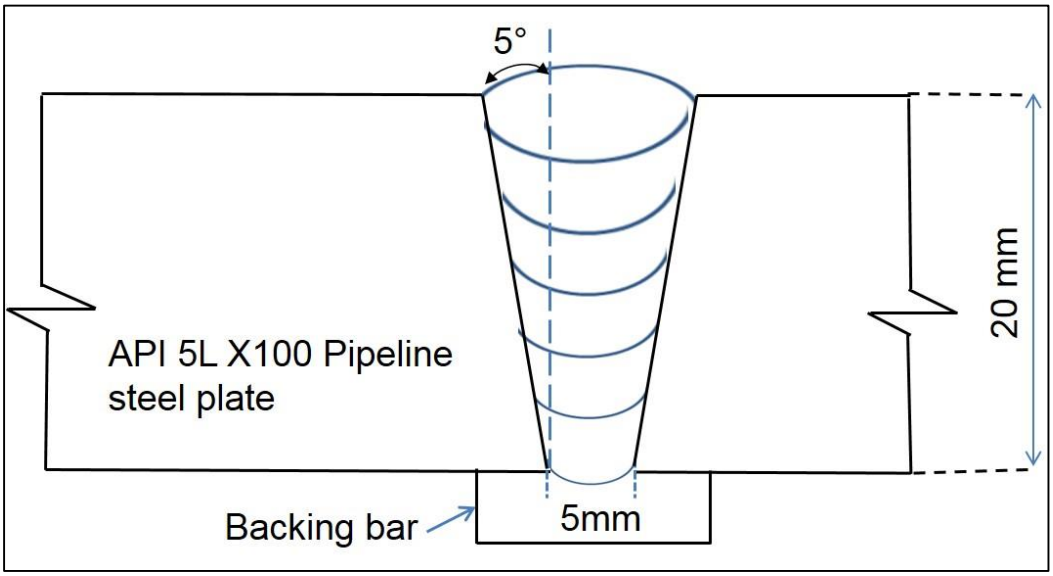

Figure 3-17: API 5L X100 pipeline steel plate set-up with backing bar

This welding process used has been developed and optimised [38]. As shown in Figure 3-18, it has two independent power sources and two independent feeding units. Each unit feeds a separate contact tip. During welding the lead arc determined the depth of penetration while the trail arc provide the final weld bead shape and reinforcement [37], [208]. Significant research on this welding process has been reported and can be found in [41], [48].

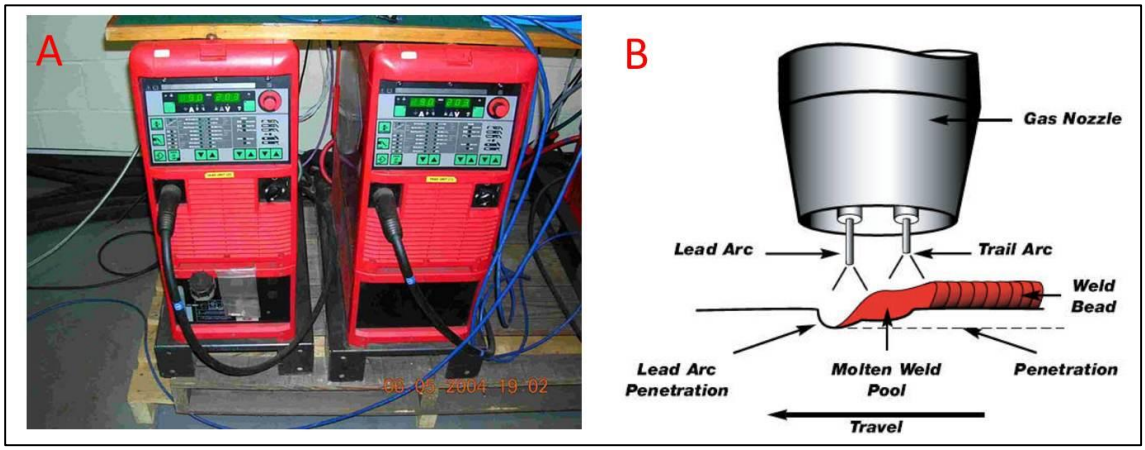

Figure 3-18: (A) Fronius TPS 4000 thermo power supplies (B) Typical tandem GMAW torch [209]

Wire feed speed (WFS) and wire diameter with the metal deposition rate are related to each other as shown in equation (3-3). The heat input was calculated using equation (3-4).

$$\text{Deposition } (mm^3/sec) = \text{Wire feed speed } (mm/sec) \times \text{Area of wire } (mm^2) \quad (3\text{-}3)$$

$$\text{Heat input} = (\text{Power} \times \text{efficiency}) / (\text{Travel speed}) \quad (3\text{-}4)$$

The efficiency used in this research is 80% of the total heat input according to Kou, S [10].

Table 3-3 shows welds made using different welding parameters at constant CTWD (14 mm).

Table 3-3: Welding parameters on narrow groove welds of API 5L X100 pipeline steel plate

		Lead			Trail			Lead	Trail
Pass	Travel speed (m/min)	Wfs (m/min)	Av. Current (A)	Av. Volts (v)	Wfs (m/min)	Av. Current (A)	Av. Volts (v)	Heat input (kJ/mm)	Heat input (kJ/mm)
1	0.9	11	188	21	11	189	21	0.21	0.21
2	0.9	12	199	21	12	199	21	0.22	0.22
3	0.9	13	219	22	13	213	21	0.26	0.24
4	0.9	14	235	22	14	226	21	0.28	0.25
5	0.9	15	249	23	15	234	22	0.31	0.27
6	0.7	13	226	21	13	215	21	0.32	0.30

3.4.1.4 Experimental Error in Tandem MIG Welding of API 5L X100 Pipeline Steel Plate

In every research, experimental errors are very important in order to have some degree of confidence in the work carried out. Like any other research, experimental errors could be divided into set-up errors and system errors.

Set –up errors could arise from;

i. Welding travel speed. The travel speed of welding influences the heat input and consequently the weld pool flow. Hence appropriate balance between the welding travel speed and the wire feed speed are ensured to minimised the error.
ii. Arc length used. The arc length has an effect on voltage, hence suitable oscillation width and the appropriate arc length were determined during the trial before the actual weld.

During the hardness measurements, errors may occur due to the size of the sample as well as device holding the sample. Appropriate measured were taken to minimised error that may arise as a result sample size and device holding the sample. Diamond indenter which is in-built in the hardness machine is in most cases interrupted when the sample holding clamps are close to it. To minimise the errors that may arise, steps were taken to reduce the error.

The welding power source and measurement instruments were calibrated before welding to avoid system errors.

3.4.2 Local Mechanical Tensioning (Cold Rolling)

3.4.2.1 Experimental Trials

In this section, application of different rolling loads were tested. Rolling loads of 50 kN, 100 kN, 120 kN and 150 kN were applied on each of the samples under investigation. This is to ensure that maximum and effective rolling load was used since the greater the amount of prior deformation, the lower the temperature for the start of recrystallization. After the trials, 150 kN was used for both API 5L X100 pipeline steel plate.

3.4.2.2 Post Weld Cold Rolling of API 5L X100 Pipeline Steel Plate

The rolling device is capable of rolling with a constant force. The principle of operation of this rolling device is that it uses hydraulic cylinder. This hydraulic cylinder applies a vertical force through a single roller supported in a fork assembly. This vertical force applied by the cylinder is determined by the cylinder pressure. The roller is made from hardened BS 4659 BH13 tool steel. It has an effective width of 30 mm and its diameter is 100 mm.

During the rolling operation, the welded plate was firmly fixed on the base plate of the rolling rig as shown in Figure 3-19 (a). The roller fork assembly is then lowered by the hydraulic cylinder to make contact with the sample and it is then translated by moving the entire crossbeam. The crossbeam has only one direction of movement which is the rolling direction as shown in Figure 3-19 (b). The control console controlled all functions of the rolling machine. See complete set up in Figure 3-10.

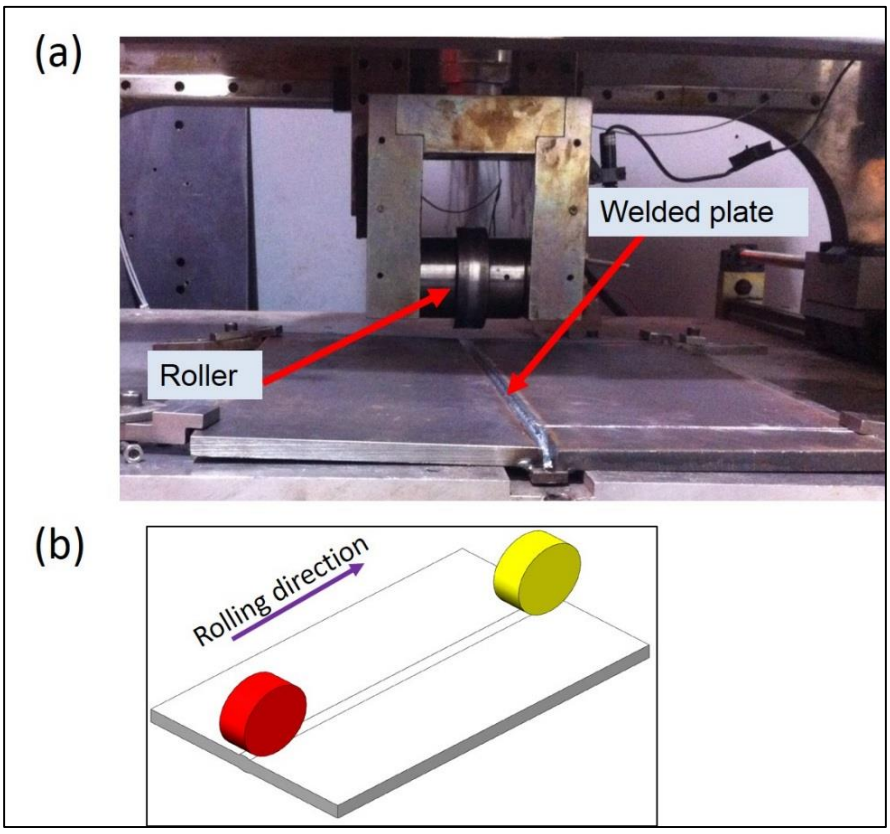

Figure 3-19: (a) Photograph of the set-up (b) Sketch of rolling direction where red roller indicate starting position and yellow roller indicate the end position

In this experiment, post weld cold rolling was carried out on the capping pass of the multi-pass weld using a rolling load of 150 kN with constant travel speed of 0.7 $m.min^{-1}$. A flat roller was used and under all rolling conditions, the rolling force was applied on the capping pass of the weld metal. The roller did not touch the plate surface on either side of the weld. As sketch in Figure 3-19 (b), the roller is released down so as to make contact with centre line of the weld metal at least 30 mm from the start of the weld and raised 30 mm before the end of the weld metal. This is done to prevent the roller from sliding off which could damage the rolling rig.

It is worth mentioning that, the rolling load in kN required in this experiment was pre-programmed into the rolling rig control station, by setting the pressure in Bar in accordance with the calibration graph shown in Figure 3-20 before rolling started. The relationship between the applied load and the cylinder pressure was generated by Harry, C. [149] and is presented in Figure 3-20.

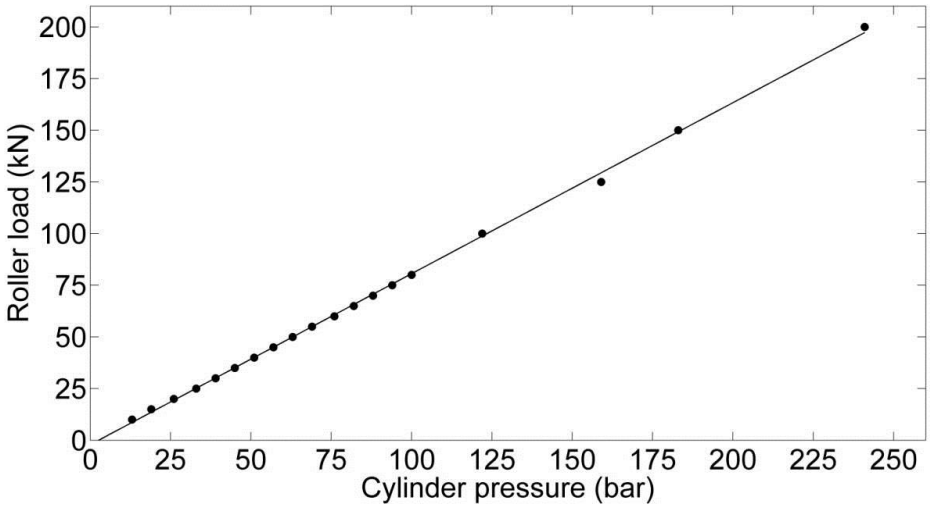

Figure 3-20: Relationship between roller load and cylinder pressure [149]

3.4.2.3 Experimental Error in Local Mechanical Tensioning (Cold Rolling)

Geometric alignment error (roller path, length of travel) were avoided by careful marking of the sample. These marks were made at the start and end part of the welded plate to determine the initial and the final position of the roller. Proper alignment of the centreline of the roller with the weld centreline were made to ensure that roller do not slip off to HAZ during rolling.

To minimised system error, proper calibrations (rolling load and travel speed) were made before the rolling start.

3.4.3 Laser Processing

In this section heat treatment was carried out using laser at specified laser power and travel speed. The laser processing in the first phase was in transient heating mode using a laser power of 3 kW with a travel speed of 0.3 m min^{-1} and laser spot dimension (beam diameter) of 20 mm. The choice of this laser parameter is explained in results and discussion (section 3.5).

3.4.3.1 Laser Processing of API 5L X100 Pipeline Steel Plate

An IPG YLR-8000 fibre laser machine was used for laser processing as shown Figure 3-21 . The principle was that the laser beam was transmitted to the laser head through an optical fibre of 300 µm diameter. Laser beam was collimated using a lens of 125 mm focal length. After collimating, a focussing lens of 250 mm focal length was used to focus the beam. This would produce a spot size of 0.61 mm at the focal point (Figure 3-22). However, the laser in this specific experiment was used to increase the temperature at a controlled rate, and so a defocussed beam of 20 mm spot size was used on the sample surface as shown in Figure 3-22. The vertical distance for defocussing was determined using a beam diagnostic system. The laser head was positioned at 10^{o} angle to avoid any back reflection which could damage the lens.

In order to determine the thermal cycle, three holes were drilled through the plate thickness (from backing bar) to the weld metal into which K-type thermocouples was placed. The thermocouples were placed at 0.5 mm, 2.0 mm and 3.5 mm below the weld surface respectively. Laser travel speeds of 0.2, 0.3, 0.4 m.min^{-1} are used in combination with laser powers of 1.5, 3.0, 4.0 and 6.0 kW. The thermal cycles at different depth of the weld are shown in the results and discussion section.

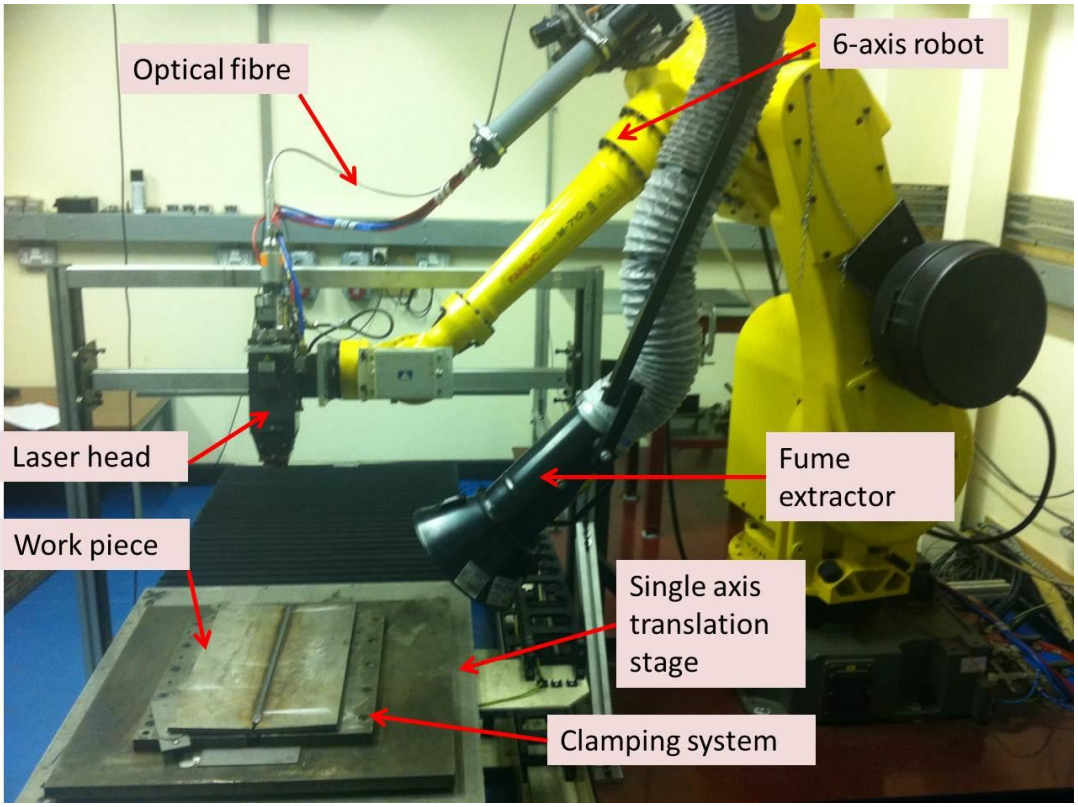

Figure 3-21: Trial set-up of laser

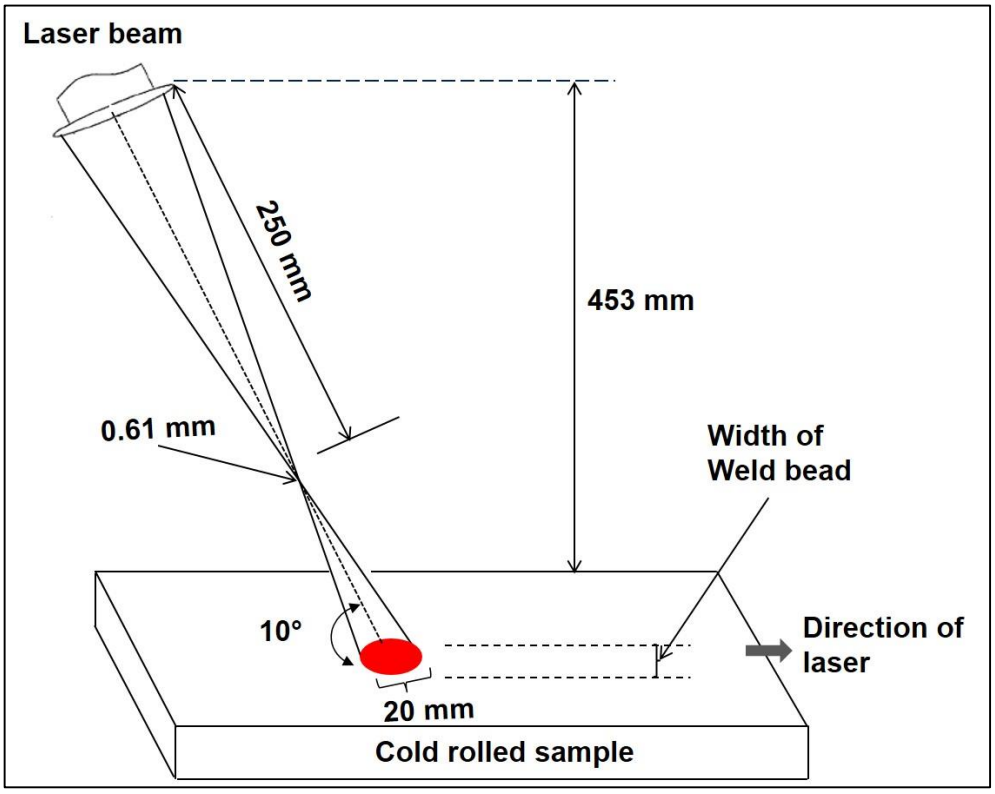

Figure 3-22: Schematic set-up of laser

3.4.3.2 Experimental Error in Laser Processing

Proper steps were taken to minimise set-up errors. However, the most likely source of error is the position of thermocouple in the welds. This is due to the fact that the holes made to insert the thermocouple were drilled manually. Hence there is the likelihood of deviations from the set position. To minimize this error, an average of three different samples was taken.

Another possibility is the error occurring in measuring the weld cooling times. The weld cooling time measured from the data obtained with these thermocouples might be affected by the holes drilled to attach the thermocouples inside the weld metal. Since these holes will create separation within the bulk material, which could affect heat transfer through conduction. However, the chances of such errors are minimised by positioning in different locations and keeping the diameters of the holes to 3 mm. The diameter of the thermocouple wire is 0.3 mm and insulator (ceramic) diameter is 2.4 mm.

3.4.4 Residual Stress Measurement of API 5L X100 Pipeline Steel Plate

Strain Analyser for Large and Small scale engineering Applications (SALSA) neutron diffractometer at the Institut Laue Langevin in France was used to measure the residual elastic strain [19]. The residual stress state was analysed from the measured elastic strain [210]. Measurements were made on the mid cross-sectional plane of a 280 mm sample (plane UVWX) shown in Figure 3-23. This was based on the assumption that the stress state in the middle will be from a steady state welding process. Longitudinal, transverse and normal strain were measured assuming these directions, by symmetry, to be the principal stress directions.

The coordinate axes shown as L, T and N in Figure 3-23, represents the longitudinal direction which is parallel to the length of the weld, transverse direction which is perpendicular to the length of the weld and parallel to the plate, and normal direction is perpendicular to the length of the weld and perpendicular to the plate respectively.

The inter-planar spacing (d) of the {211} family of crystallographic planes was chosen for measurements of all the principal strain directions. The strain response of {211} family of crystallographic planes in the BCC lattice structure closely follows the macroscopic strain response over the measured gauge volume [19]. The measurements were made using a neutron incident beam of wavelengths, 1.62 Å, which gives a diffraction angle (2Θ) of 87.62°.

However, it is important to note the two limits to the scattering angle: θ = 0 degrees and θ = 90 degrees. When θ equal to 0 degrees, the rays are not changed in direction and path lengths are the same regardless of the positions of objects. When θ is exactly 90 degrees, the waves are reflected straight back at the source.

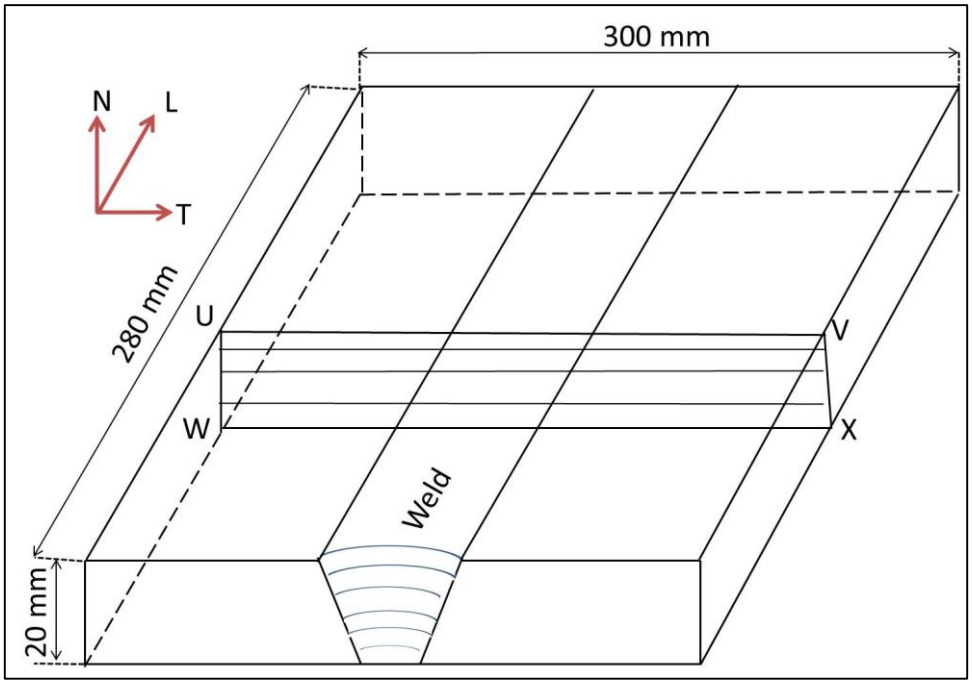

Figure 3-23: Schematic diagram of the multi-pass welded plate

Through-thickness scans were used for accurate positioning of the gauge volume within the plate. The gauge volume dimension was controlled by using slits in front of the in-coming beam and collimating the diffracted beam to maintain the through thickness resolution. An incoming beam of 2 × 2 mm^2 was used for the longitudinal strain measurement while a 2 mm collimator was used for the diffracted beam to achieve the desired spatial resolution. For transverse and

normal strain measurement an incoming beam of 2 × 20 mm was used, with the assumption that the stress state and magnitude will remain constant in the welding direction. The increase in gauge volume along the welding direction, in these two directions, allows faster measurement with more grain sampling. More grain sampling reduce the neutron counting time. In other words, a larger gauge volume which result in more grain sampling means that there are more neutrons diffracting per second in the volume.

The stress-free inter-planar spacing was measured using a comb sample of dimension 6 mm x 6 mm x 5 mm machined out from the parent plate by electrical discharge machining (EDM). The dimension of the individual comb would ensure relaxation of any macro residual stress field and will allow positional correction of the measured strain for compositional variation across the weld. The stress-free lattice spacing (d_0) were measured in all the three principal strain directions.

The lattice spacing d is related to scattering angle θ by Bragg's law as shown in equation (3-5).

$$\lambda = 2\mathrm{d}_{\mathrm{hkl}}\sin\left(\frac{\theta}{2}\right) \tag{3-5}$$

Where λ is the wavelength of the neutron source.

A Gaussian fitting routine was used to fit the intensity profile and precisely determine the peak position. The stress-free lattice spacing (d_0) measurement combined with the lattice spacing measurements were used to calculate strain (ε) using equation (3-6).

$$\varepsilon_{\mathrm{hkl}} = \left(\frac{\mathrm{d}_{\mathrm{hkl}} - \mathrm{d}_{0\mathrm{hkl}}}{\mathrm{d}_{0\mathrm{hkl}}}\right) \tag{3-6}$$

Where ε is strain, hkl is the measured crystal plane, d is the lattice spacing and d_0 is strain- free spacing (measured in the same plane).

Once the strain is determined, the principal stress could be analysed using the Hooke's law for three dimensional state of stress as shown in equation (3-7, using the appropriate elastic constants for the specific crystallographic plane.

$$\sigma_{ii} = \frac{E}{(1+\upsilon)}\left[\varepsilon_{ii} + \frac{\upsilon}{(1-2\upsilon)}(\varepsilon_{11} + \varepsilon_{22} + \varepsilon_{33})\right] \quad (3\text{-}7)$$

Where E and υ are the Young's modulus and Poisson ratio respectively, and i, = 1, 2, 3 indicate the directional component of stress and strain in an orthogonal coordinate system. Linearly elastic and isotropic material properties were assumed, and the plane-specific elastic constants used to calculate stress from measured strains (E = 225.5 GPa and υ = 0.28), were Kröner model predictions [172].

Note that the measurements of the residual strain were taken at 2, 10 and 18 mm below the plate surface on which the capping pass was laid as shown Figure 3-24. In the measurement of the longitudinal direction, strains were measured with 3 mm step in the region between −36 mm and 12 mm position. This gives a total of 17 points with zero point inclusive in each line (say 2 mm). The time taken per point of measurement was 8 minutes. Hence for measurement at 2, 10, and 18 mm below the weld surface; approximately 6.8 hours of neutron counting time was required for each plate sample (excluding d_0 measurements).

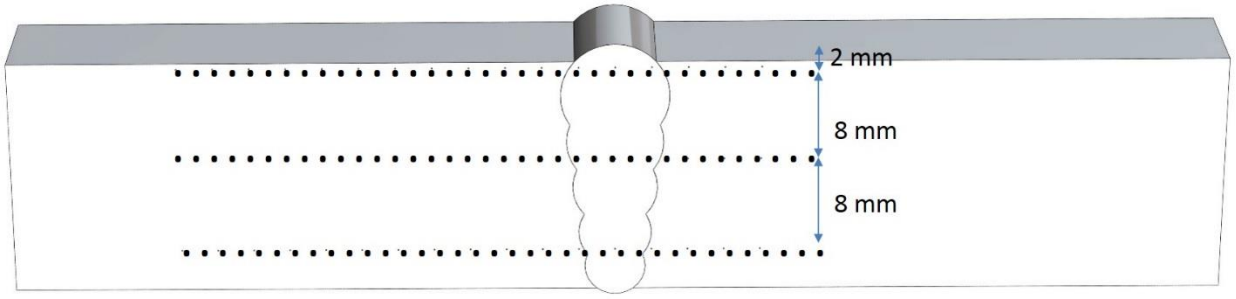

Figure 3-24: Sketch showing a cross section of the point of measurements (Transverse distance, each point is 3 mm apart)

3.4.4.1 Determination Lattice Parameter

The most important parameter to be considered during the measurement of residual strain in welds is the positional variation of the stress-free lattice parameter (a_0), to which the change in measured lattice parameter in the weldment is referred. Difference in a_0 can be as a result of:

i. Variations in the solute content of the lattice owing to the thermal cycling of the parent material in the HAZ.
ii. Difference in composition due to the combine effect of parent metal and filler wire in the weld metal.

Hence, good understanding of any lattice parameter variation with position in the weldment would provide appropriate residual strain measurement which in turn gives accurate residual stress measurement.

3.4.4.2 Full Width at Half Maximum (FWHM)

FWHM diffraction profiles are used to characterize different material properties. Analysis of diffraction peak profiles indicates that FWHM is sensitive to the changes in microstructure as well as stress–strain accumulation in the material. A number of researchers have identified various material properties through the FWHM of X-ray diffraction peaks. For example, it has been reported that, an increase in stacking faults and structural disorder widens the diffraction peaks [211] . Tung H-M et al [212] also report that increases in hardness and density of point defects affect the crystallinity and grain boundary mobility, which in turn causes a linear increase in the FWHM of diffraction peak. The presence of tensile stress in the material causes increase in the FWHM while relaxation of tensile stress cause reduction of FWHM [213]. “A decrease in FWHM with cyclic softening in a cold rolled high strength low alloy steel was observed while alloy, in hot rolled condition, exhibited a stable stress response accompanied with an increase in FWHM after fatigue cycling [214]”.

All the data were obtained by using Large Array Manipulation Program (LAMP) software. Since changes in full width at half maximum of diffraction profile indicates plastic deformation, measurement of full width at half maximum

diffraction profiles enables one to see the effect of the load at the surface and through the thickness of the material.

3.4.4.3 Experimental Error in the Residual Stress Measurement

A potential source of error arises from d_0 values. The use of inappropriate d_0 values due to weld shape variation can caused a change in the location of the maximum measured residual strain.

Errors could also arise in the use of incorrect elastic constants (Young's modulus and Poisson ratio), counting time, misalignment of diffractometer and specimen position. Hence, precise positioning and alignment of the sample to be examined in the diffractometer is necessary. It worth mentioning that spatial resolution of a neutron measurement depends on the gauge volume. Potential problem arise from inaccurate positioning of the gauge volume.

This error is applicable to all the structural alloys presented in chapter 4 and 5 of this thesis.

3.5 Results and Discussion

This chapter present the results and discussion from the experiments conducted in the first phase of this research with their interpretations. Direct and indirect comparisons with earlier research work was also made.

3.5.1 Welding

Several trials were made as described in section 3.4.1 of this thesis. However, since welds were made in narrow groove, emphasis were placed on how to find appropriate balance between the welding travel speed and the wire feed speed, oscillation width as well as the arc length to be used. Observation of these trials on the narrow groove showed that given a wide oscillation width, the wire touches the plate side walls in the groove. This then resulted in instability and undercut of the welds. Using smaller oscillation width results in lack of sidewall fusion.

3.5.1.1 Tandem MIG Welding

Narrow groove tandem MIG welding has been optimised at Cranfield University in the past decade. Research works carried out previously by [38], [41], [205], [48] have already designed appropriate welding procedure specifications using this welding process. In this particular research, appropriate welding parameters were selected based on the trials to achieve the designed results. The welding parameter used in this material is shown in Figure 3-25. The weld thermal cycle is shown in Appendix A.1.

Cranfield UNIVERSITY

Welding process	Tandem GMAW DC +ve
Welding position	1G
Material Grade	X100 Pipeline steel plate
Thickness	20 mm
Electrode Wire	ϕ = 1 mm
Brand	Union MoNi
Preparation	Saw cut
Backing System	X100 Backing Strip
Cleaning Method	Wire Brush or Grinding
Shielding Gas	92%Ar - 8%CO_2
Flow rate	30 L/min

Designer: Jibrin Sule

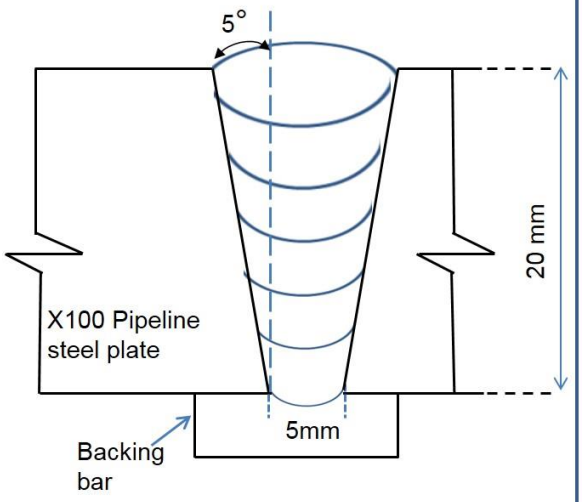

Pass	Travel Speed (m/min)	Lead			Trail			Oscillation		CTWD (mm)
		WFS (m/min)	Amps (I)	Volts (V)	WFS (m/min)	Amps (I)	Volts (V)	Freq. (HZ)	Osc. width	
Root pass	0.9	11	193.3	20.3	11	176.2	21.5	350	90	14
Fill 1	0.9	12	191.9	21.5	12	177.7	21.7	350	135	14
Fill 2	0.9	13	209.3	22.2	13	192.3	21.7	350	190	14
Fill 3	0.9	14	226.6	21.9	14	195.6	21.3	350	225	14
Fill 4	0.9	15	231.7	23.9	15	184.4	22.9	350	270	14
Cap pass	0.7	13	215.0	21.5	13	168.7	21.4	350	400	14

Figure 3-25: Welding parameters

3.5.1.2 Hardness on As-Welded Sample

Figure 3-26 shows the scan hardness of the six (6) deposited welds across the weld metal of as-welded sample, showing clearly that the root pass is harder than the cap pass. The higher hardness in the root pass may be due to dilution of the

weld metal by the parent metal. Figure 3-26 also shows that the maximum hardness occurred in the heat affected zone. The hardness in the weld metal is lower than that obtained HAZ, while the parent metal has the minimum hardness values. The high hardness profile at the HAZ observed in this research, is due to the HAZ hardening, which is the same with what has been reported by Eroglu [215] in his research work. This high hardness at the heat affected zone has also been reported by Katsina [204] on welding of API X100 pipeline steel. High hardness value at the HAZ could also be attributed to the presence of martensite in the microstructure. The presence of martensite was caused by relative low heat input in the zone leading to high cooling rate.

Hardness in weld matal is higher than the parent metal as shown in Figure 3-26. This increase in hardness at the fusion zone could be attributed to variation in the morphology of ferrite and martensite at the zones as well as compositional enrichment by the filler wire [216], [217].

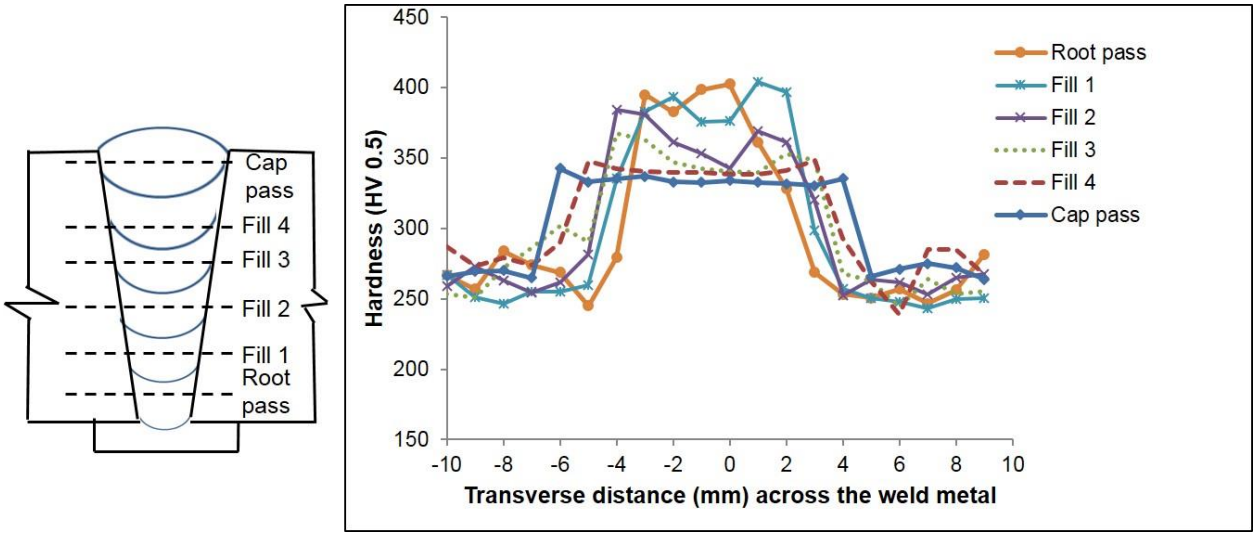

Figure 3-26: Hardness profile across the weld metal of all the six passes in as-welded sample.

3.5.2 Post Weld Cold Rolling

The in house rolling device was used in this research. Trials were also carried out before the actual experiment. Figure 3-27 shows the hardness profile from the different rolling loads used in experimental trials. The hardness values increase

with increasing load. In the result presented here, the rolling load of 150 kN was used for both the API 5L X100 pipeline steel plate and S275JR structural steel plate presented in chapter 5 of this thesis. It is important to mention here that the in-house rolling device used in this research was only capable of using a rolling load of 200 kN. The maximum load was avoided to prevent unexpected friction between the roller and the weld metal. The choice of the load was also based on the assumption that the higher the deformation (high load) the lower the temperature to activate recrystallization.

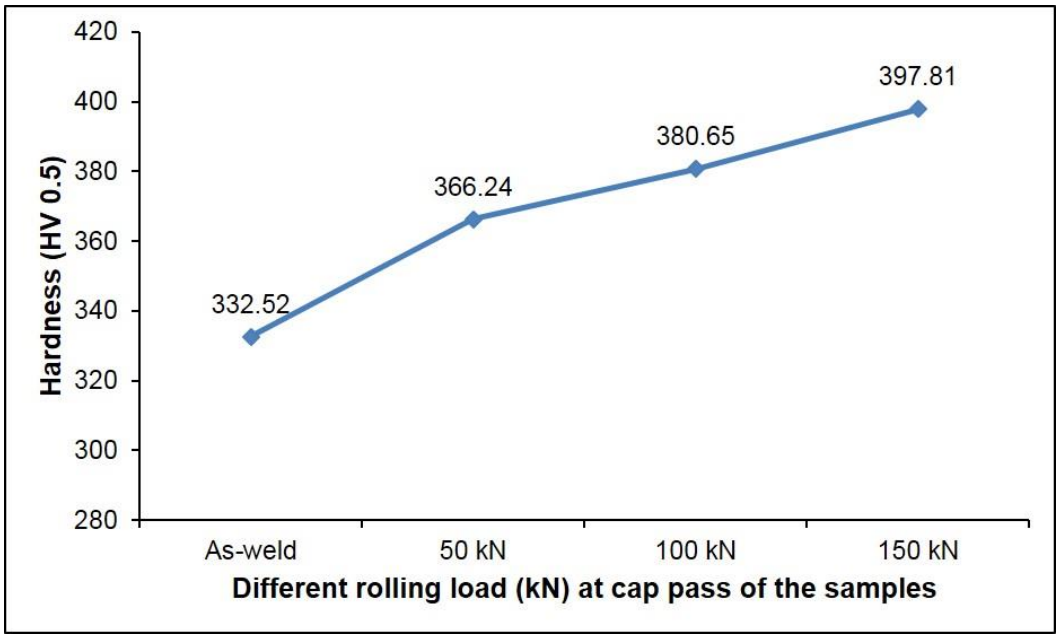

Figure 3-27: Hardness profile at different load

3.5.2.1 Effect of Post Weld Cold Rolling on Hardness Profile

Figure 3-28 shows the Vickers micro hardness measurement across the weld metal of the three processing condition. The processing conditions are the as-welded condition, post weld cold rolling and laser processing condition

Note that, the laser processing presented is for purpose of comparison. (The laser parameter are 3 kW laser power with the travel speed of 0.3 $m.min^{-1}$ and the beam diameter of 20 mm which will be in section 3.5.3).

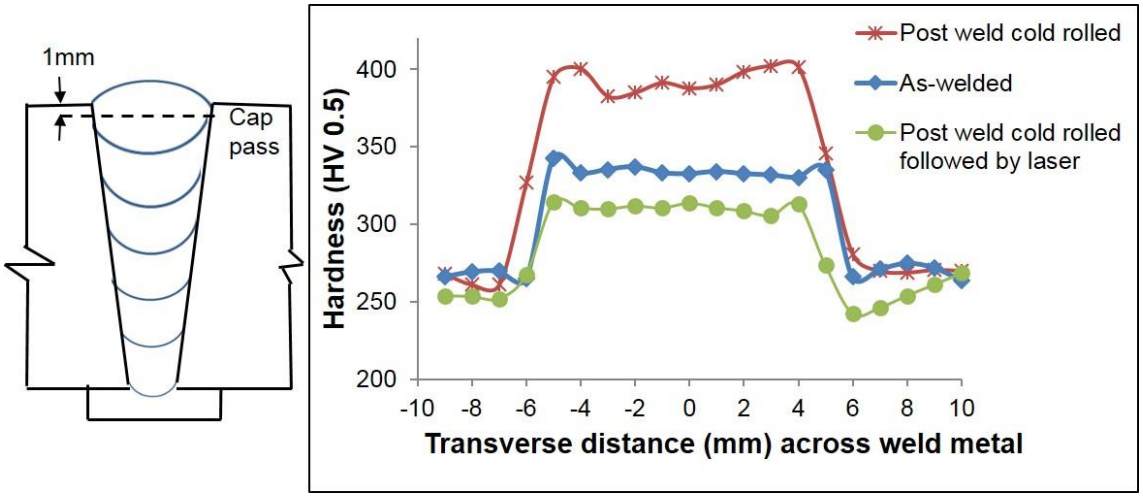

Figure 3-28: The hardness profile across the weld metal at the cap pass

Figure 3-29 shows the Vickers micro hardness measurement along the weld metal of the three processing conditions.

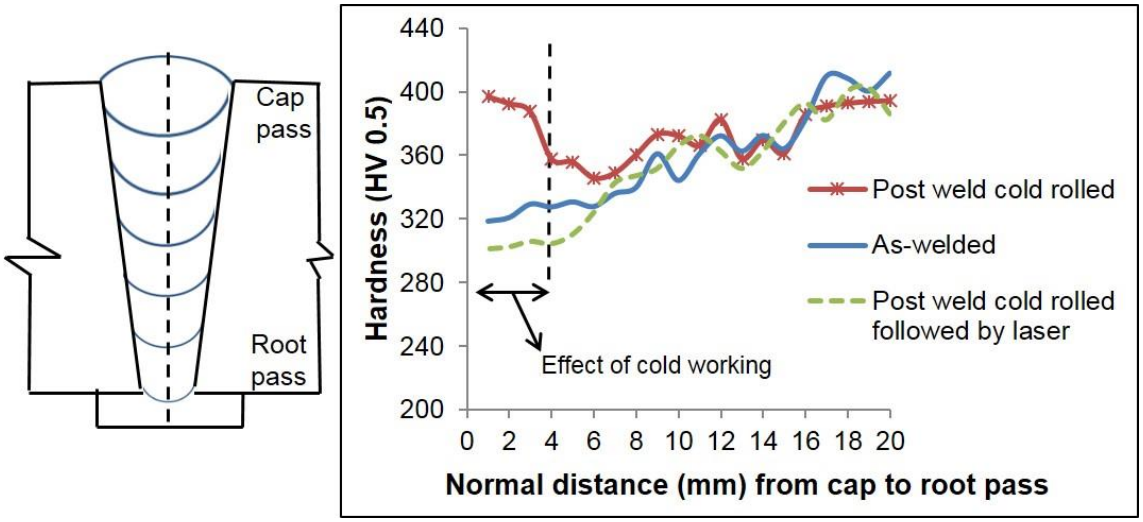

Figure 3-29: The hardness profile along the weld metal from cap to root pass

Hardness values are lowest in the parent metal, but sharply increase in the heat affected zone, and at the weld metal, the hardness remains fairly uniform (Figure 3-28). Post weld cold rolling increases the hardness value from 332 HV to 388 HV at the weld metal. This effect of post-weld cold rolling is predictable, since work-hardening is an inevitable consequence of the plastic deformation induced during rolling.

Figure 3-29 shows a hardness that scan was performed from the reinforcement bead (cap pass) to the root pass. The effect of cold working was observed up to about 12 mm below the weld cap. Up to about 4 mm the effect is more pronounced and from 4-12 mm the effect is less pronounced. The as-welded plate shows an increase in hardness value from the cap to the root pass of the weld metal, which suggests that the root pass is harder than the cap pass (also see Figure 3-26). This increase from cap to root pass suggests thermal straining by successive passes. Again the grains at the cap pass are columnar grains not refined grains and these decreases the hardness value at the cap pass.

Another possible reason could be strain induced by the root passes. This because the root passes were laid when the samples were cold. Therefore, the surrounding material would have quenched the bottom material. In other words, high hardness in the root pass can be explained with the fact that the root pass experience fast cooling resulted in small grain size thus increase in hardness value.

The scattering of the hardness along the weld metal could be due to the absence of a controlled inter-pass temperature, since there is no particular temperature that was maintained in each pass. Some of the deposited layers were made when the temperature from the previous layer was high, while others were made when the temperature was low. Differences in this temperature could affect the hardness profile.

Another reason could be associated with the placement of the indentations within the weld metal. Indentations placed within reheated weld metal will result in the hardness value being higher as compared to the non-reheated weld metal. In other words, the minor scattering in hardness could be due to micro-structural variation from re-heating by subsequent passes. It was also reported that re-melting of columnar grains by subsequent reheated zone, could change the micro structure of the previous bead layer, thus reducing the hardness values [218].

3.5.3 Post Weld Cold Rolling Followed by Laser Processing

In this section, heat treatment trials were conducted in the API 5L X100 pipeline steel plate after the post weld cold rolling. The different trials were made (using different laser power combined with different travel speed) to give a reasonable amount of thermal energy to applied on the sample to activate recrystallization. This trials were also carried out to see how heat was conducted through the thickness (from cap to root pass) of the weld metal.

Figure 3-30 shows the sketch of the influence of temperature on the grains size.

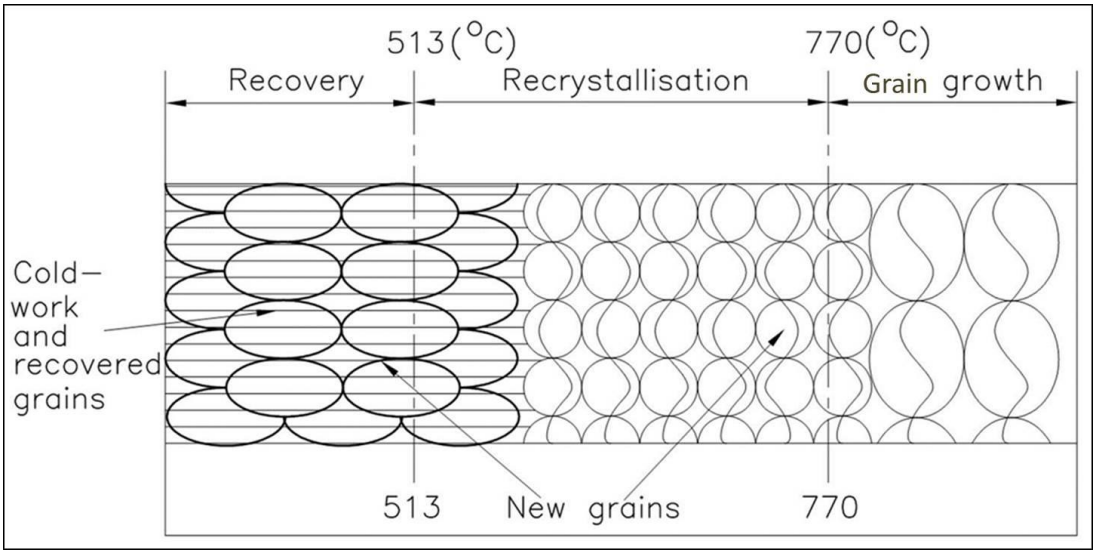

Figure 3-30: The sketch showing the influence of temperature [141]

Figure 3-31 shows the laser thermal cycle for a travel speed of 0.3 $m.min^{-1}$ at a constant beam diameter of 20 mm, combined with four different laser powers. Other trials using the travel speed of 0.2 $m.min^{-1}$ and travel speed of 0.4 $m.min^{-1}$ are shown in appendix A.2

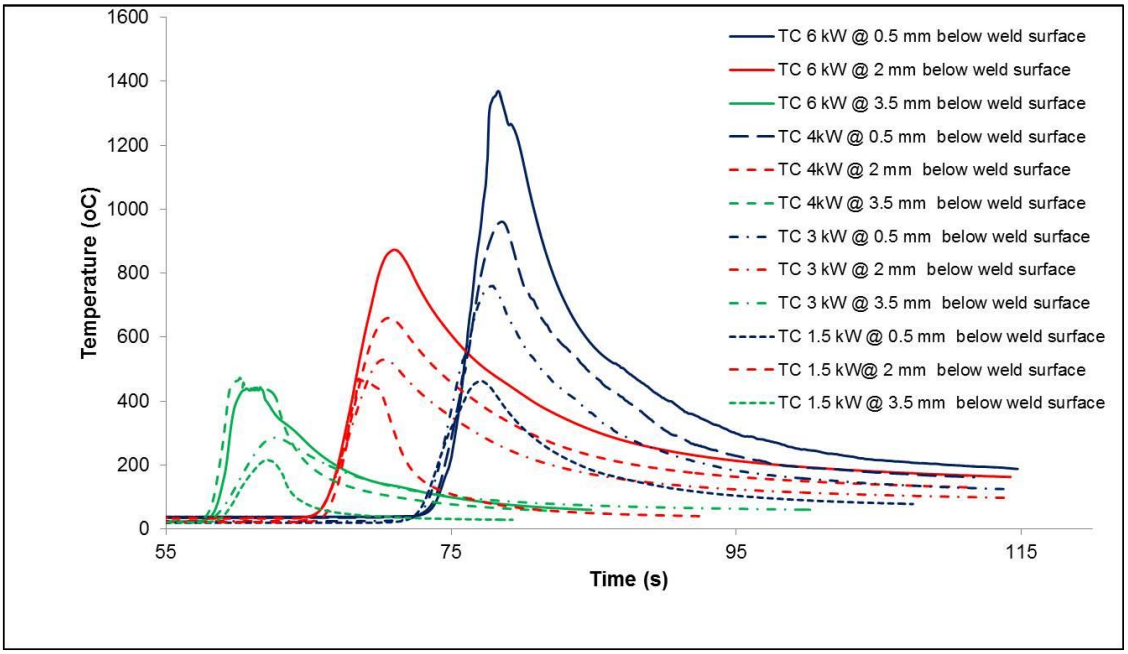

Figure 3-31: Thermal cycles of laser powers of 1.5 kW, 3.0 kW, 4.0 kW and 6.0 kW with travel speed of 0.3 m.min^{-1} at constant beam diameter of 20 mm

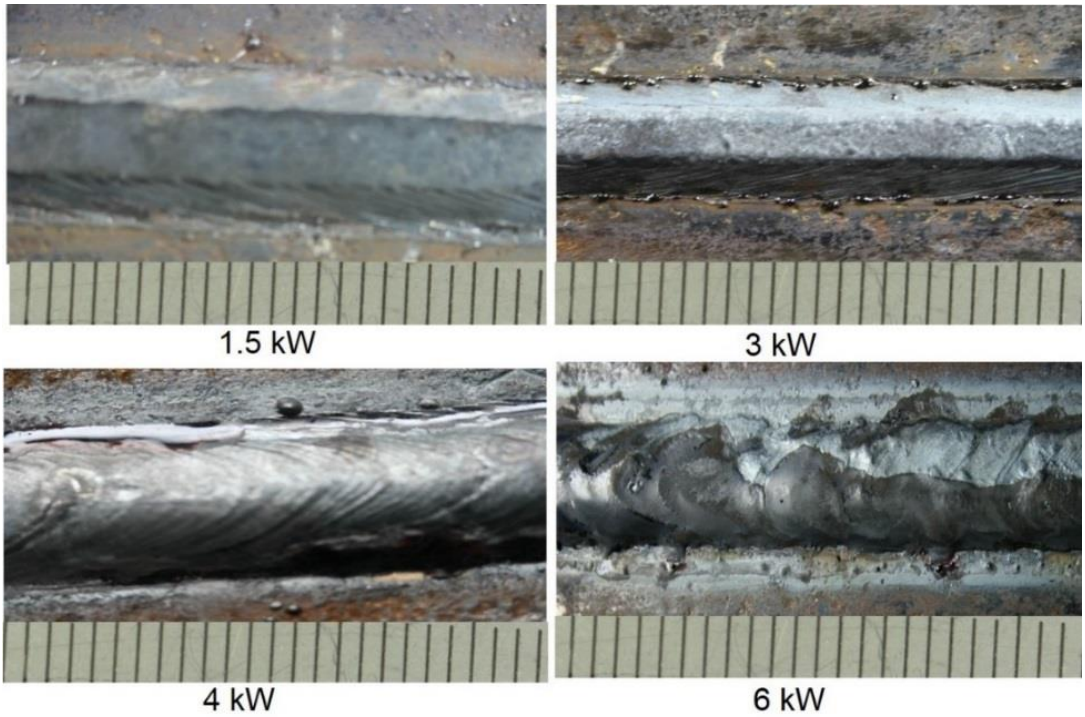

Figure 3-32: Physical weld appearance (top view) of laser powers of 1.5 kW, 3.0 kW, 4.0 kW and 6.0 kW with travel speed of 0.3 m.min^{-1}

Figure 3-32 shows the physical weld appearance of laser powers of 1.5 kW, 3.0 kW, 4.0 kW and 6.0 kW with travel speed of 0.3 $m.min^{-1}$ at a constant beam diameter of 20 mm. The physical weld appearance using the travel speed of 0.2 $m.min^{-1}$ and travel speed of 0.4 $m.min^{-1}$ at different laser power are shown in appendix A.2. The effect of the laser power of 6 kW with travel speed of 0.3 $m.min^{-1}$ at a constant beam diameter of 20 mm through the thickness is shown appendix A3.

As shown Figure 3-31, the laser power of 3 kW at a travel speed of 0.3 m min^{-1} was used. This is because, the peak temperature at 0.5 mm below the weld surface was approximately 759^{o}C (1032 K).The selection of the temperature used on this material was based on the fact that: “the recrystallization temperature of metal or alloy is between one-third and one-half of the absolute melting temperature (1540^{o}C for steel), which depends on several factors, including the amount of prior cold work and the purity of the alloy [141]”.

3.5.3.1 Effect of Laser Processing on Hardness Profile

Post weld cold rolling followed by laser processing resulted in softening of the weld metal up to about 12 mm below weld surface (Figure 3-29) but like hardening, the softening is also more pronounced up to 4 mm (388HV to 313HV). The combination of laser power and travelling speed used indicates that the thermal energy applied was not sufficient to supply enough energy for complete recrystallization as shown on the micrograph. This necessitates the second phase of the experiment presented in section 3.6.

3.5.4 Tensile Strength

Figure 3-33 shows the all weld metal tensile tests taken close to the capping pass. All samples were taken in the longitudinal direction of the welds.

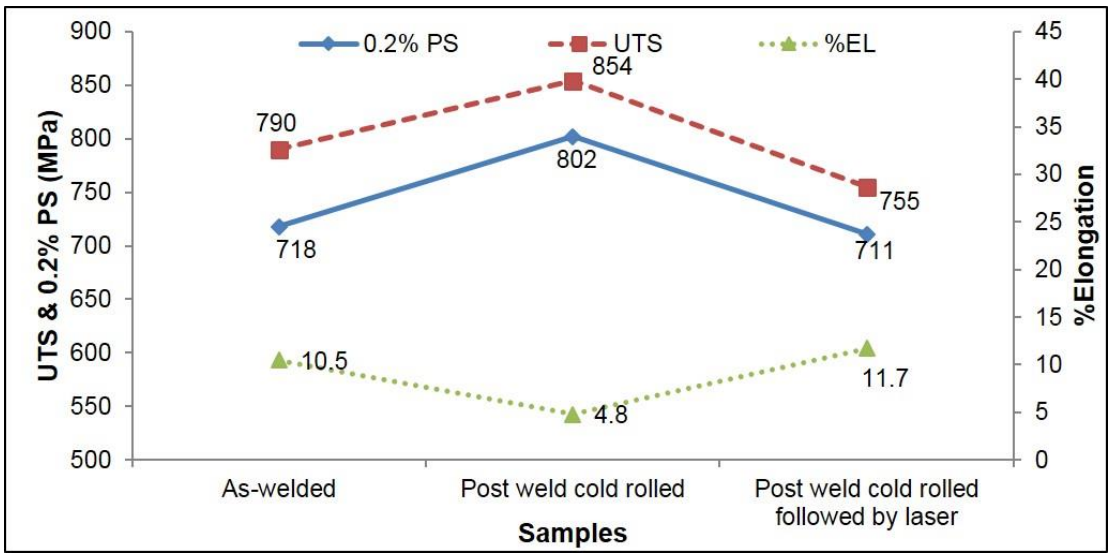

Figure 3-33: Tensile test close to the capping pass

Figure 3-34 shows the result of the all weld metal tensile tests of samples taken close to the root pass. All samples were also taken in the longitudinal direction of the welds.

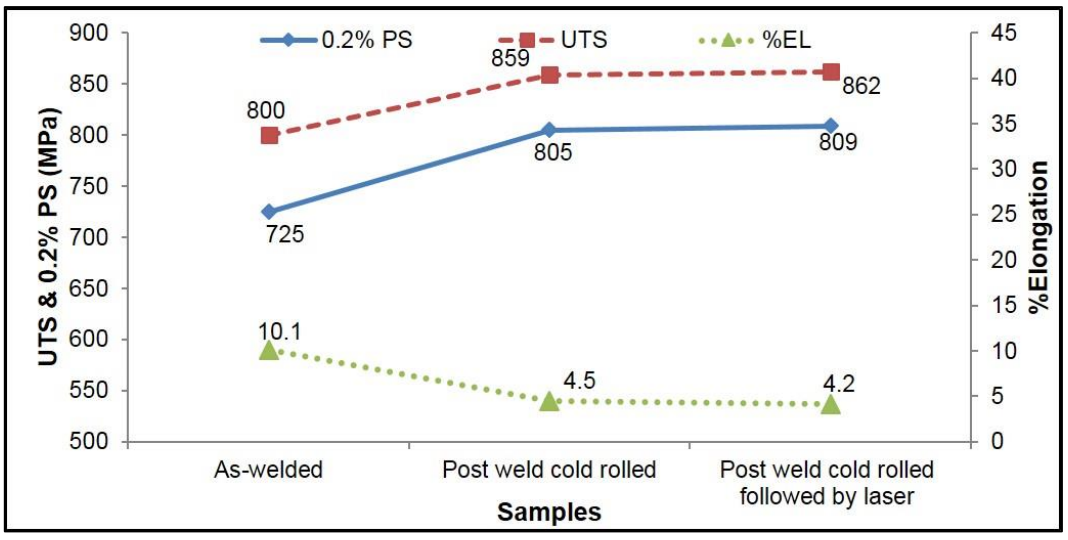

Figure 3-34: Tensile test close to the root pass

3.5.4.1 Effect of Post Weld Cold Rolling on Tensile Strength

Post weld cold rolling increases the proof strength (PS) by 10.5% and ultimate tensile strength (UTS) by 7.5% at the cap pass as shown in Figure 3-33, with corresponding reduction percentage elongation (10.5% - 4.8%). This is due to effect of cold working. This permanent deformation as a result of cold rolling, causes the dislocations (defects in the lattice structure) to pile up, which increases the strength of the material, while the ductility (percentage elongation), decreases with the effect of cold working. However, fracture becomes much more likely if the material is less able to plastically deform. Similarly, the tensile test taken close to the root pass (Figure 3-34), shows a similar trend as the cap pass when the post weld cold rolling was applied.

However, it was observed that, the tensile strength obtained close to root pass (Figure 3-34), is higher than those obtained close to the cap pass indicating that tensile strength increases with the number of passes. Another possible reason is that, the plastic strains generated by thermal cycling, increase the yield strength at the root pass. Since root pass had experienced a higher number of thermal cycles than cap pass, it is logical to expect that the contribution to the yield and tensile strength from this factor could be higher at the root pass.

In this work also, it was also clear that an anisotropy of deformation occurred in the all-weld metal tensile tests (post weld cold rolled), as it can be observed by cross-sections of the fractured shown in Figure 3-35. This anisotropic deformation could be attributed to preferred crystallographic orientations of grains in the weld metal. The coordinate axes shown as TD and ND in Figure 3-35, represents the transverse direction and normal direction respectively.

Figure 3-35: Macrostructure of the cross section of fractured tensile sample (post weld cold rolled sample)

3.5.4.2 Effect of Post Weld Cold Rolling Followed by Laser Processing on Tensile Strength

Post weld cold rolling followed by laser processing decreases the PS by 7.5% and UTS by 11.5% and with corresponding increase the percentage elongation (4.8% -11.7%) close to the cap pass as shown in Figure 3-33. These decrease in PS and UTS can be associated with the formation of soft ferrite matrix in the microstructure of the annealed sample by cooling. However, at the root pass, post weld cold rolled followed by laser processing (Figure 3-34) shows an increase in PS by 0.5% and UTS by 0.3% with corresponding decreases the percentage elongation (4.5% - 4.2%) indicating that the heat applied by the transient laser processing was not sufficient to conduct through the thickness.

3.5.4.3 Yield/Tensile Ratio

The ratio of PS to UTS of a line pipe material is a measure of the margin of safety against failure by plastic collapse. This ratio also indicates the ability of a pipeline material to experience plastic deformation before failure. In a situation where yield strength is the same with the ultimate tensile strength, any plastic deformation of the pipeline material could result in rupture. However, with a difference between proof strength and ultimate tensile strength, the ability for the steel to exhibit cold

working provides some protection for the pipe against fracture, especially during laying of the pipeline material.

It has been reported by Pisarski, H. G. [219] that small percentage of overmatching could be of benefit by allowing axial stress to exceed the Specified Minimum Yield Strength of the parent material.

The API 5L requires a maximum PS/UTS factor of 0.93 for X80 pipe steel grade. High values of the yield to tensile ratio are expected as the material yield strength increases. In this research, the PS/UTS (Figure 3-33 and Figure 3-34) are summarised in the Table 3-4 below. All this values are within the SMYS according to report presented by British steel [220].

Table 3-4: Summary of the variation of 0.2% proof stress to ultimate tensile stress ratio

Position of samples	As-welded (PS/UTS)	Post weld cold rolled (PS/UTS)	Post weld cold rolled followed by laser (PS/UTS)
Close to cap pass	0.91	0.939	0.942
Close to root pass	0.91	0.937	0.938

3.5.5 Metallographic Examination

The macrostructure and microstructure of the weld samples under investigation are presented here. In this section, the as-welded, post weld cold rolled and post weld cold rolled followed by laser Processing are presented.

3.5.5.1 Macrographs

Figure 3-36 shows macrographs of the three samples, that is, as-welded, post weld cold rolled and post weld cold rolled followed by laser processing. All the macrographs show good weld profiles with excellent penetration and good side wall fusion. The heat affected zones are also clearly shown. Internal defects such as porosity and solid inclusions were not detected in most of the welds except for Figure 3-36 (b).

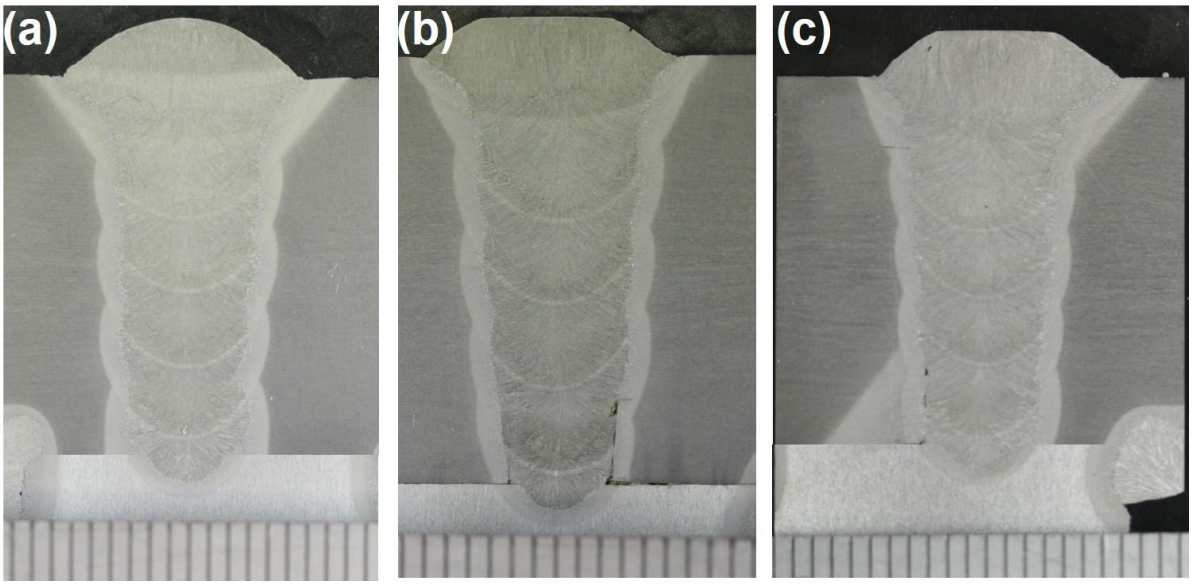

Figure 3-36: Macrographs of weld deposited layers of API 5L X100 pipeline steel (a) as-welded (b) post weld cold rolled (c) post weld cold rolled followed by laser processing

However, Figure 3-36 (b) shows some lack of side wall fusion and porosity at the second and third pass of the welds. These could be as result of the shielding gas used. The CTWD or arc length used could also cause lack of side wall fusion in the welds.

Inadequate shielding gas flow could be a possible cause of the porosity in the welds. Misalignment of the gas shroud is another potential cause of porosity in the welds. Although Theocharis [38] suggested the use of 30 Litre/minute gas flow rate in his work to overcome the problem of porosity, which was used in this work, porosity was still evident in some of the welds made in this research. The

presence of porosity in this research could therefore be attributed to the fact that, when carbon monoxide (CO) and oxygen (O_2) dissociated and dissolved in the weld pool, some percentage of these gases then react with iron (Fe) and deoxidants in the weld pool. Thus the remaining gas (CO) can become trapped in the weld during the solidification which form the porosity. It was reported by Chung B.G. et al [221] that diffusion rate of the gas and solidification rate are function of porosity. If solidification rate is faster than the diffusion rate of the weld pool, the carbon monoxide will be trapped in as porosity in the weld which could be the case in this research.

Another possible cause of porosity could be the reaction of the weld metal with the anti-spatter spray since anti-spatter was used to spray in the shroud and around the weld plate before welding. Anti-Spatter Spray is non-flammable agent for the prevention of weld-spatter adhering to metal surfaces during the welding process. Maintenance of the correct CTWD was vital in ensuring a stable metal transfer of the correct arc length, in this research approximately 3 mm CTWD was ensured for correct arc length.

3.5.5.2 Optical Microstructure

Optical micrographs in Figure 3-37 compare the effects of post weld cold rolling on the weld microstructure. As-welded weld metal (cap pass) consists of heterogeneous mixture of acicular ferrite (AF), grain boundary ferrite (GBF), Sideplate ferrite (SPF) and polygonal ferrite (PF), fine bainitic ferritie which is typical for a low carbon steel weld. In welding of ferritic steel, competitive growth occurs between ferrite growing from the austenite grain boundaries and intragranularly nucleated acicular ferrite during austenite to ferrite transformation [222], [223]. Some factors that influence these transformations include the cooling rate, prior autenite grain size and density of intragranular inclusion [81], [224].

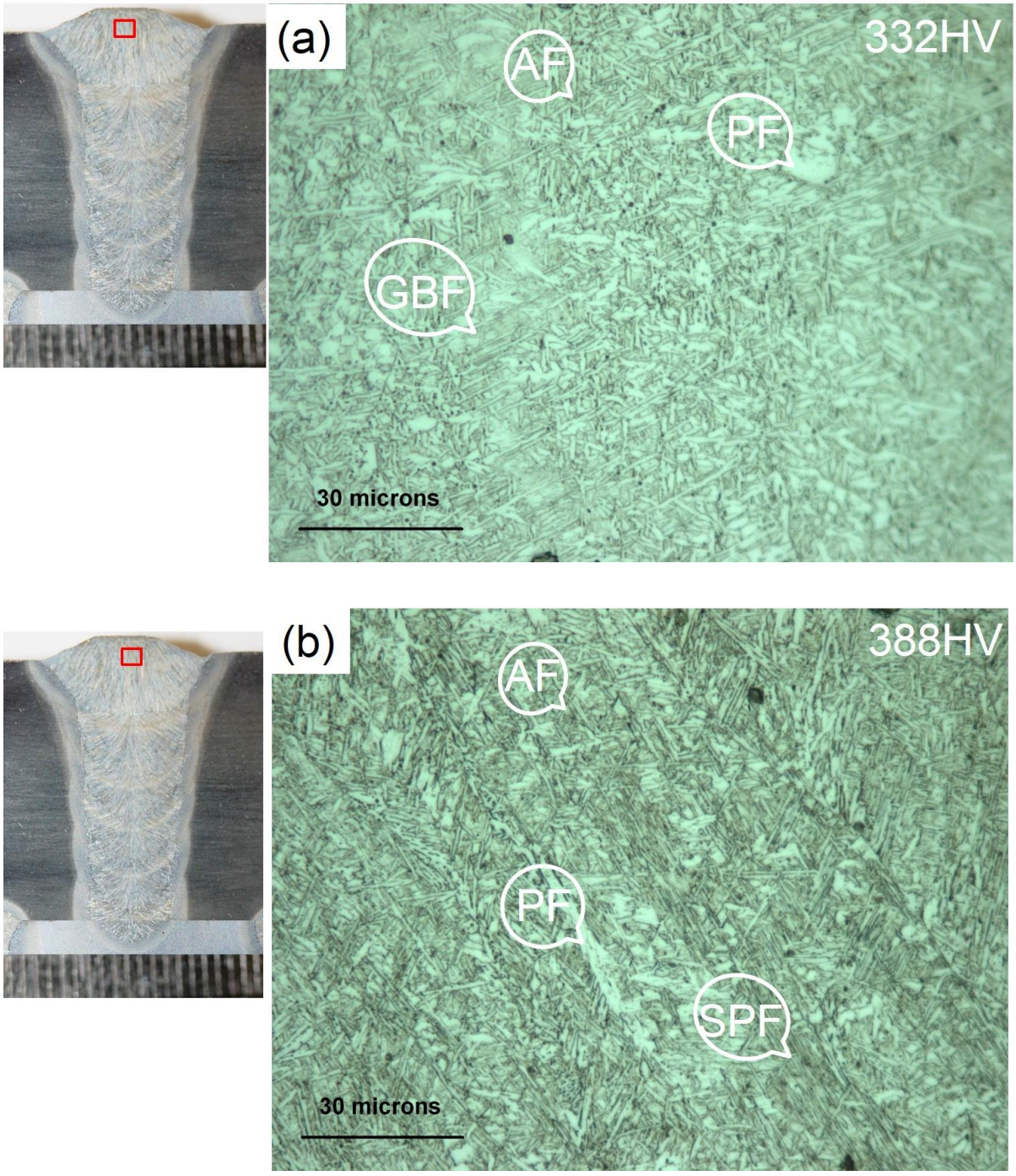

Figure 3-37: Optical micrographs at cap pass (a) as-welded (b) post weld cold rolled

Post weld cold rolling followed by laser processing shows some changes in microstructure (change in phase) which resulted in lowering the hardness value (see Figure 3-38). However, the thermal energy applied was not sufficient to supply enough energy to sustain a complete recrystallization kinetic.

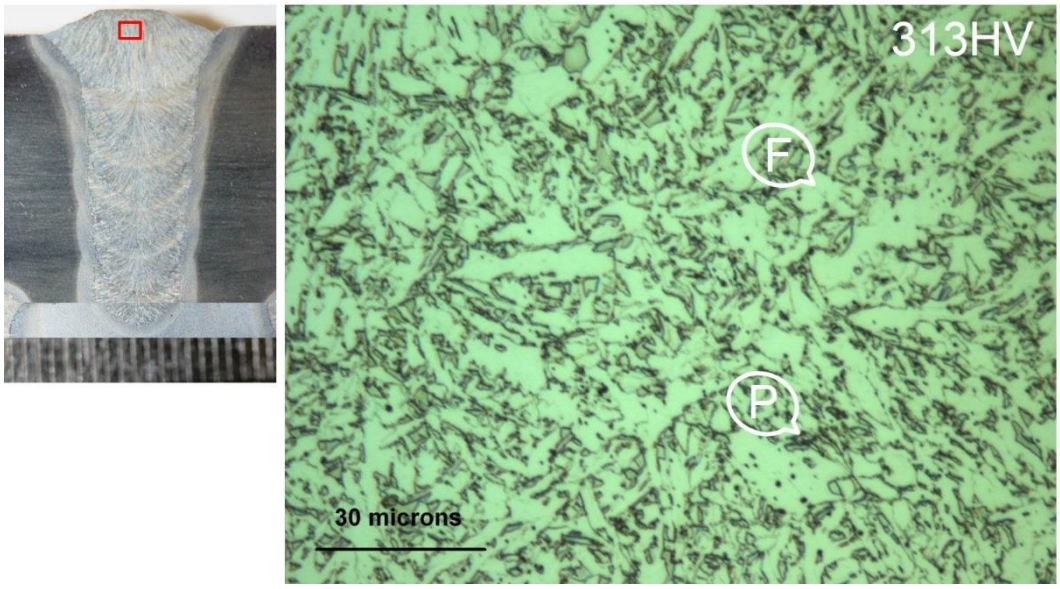

Figure 3-38: Optical micrographs at cap pass of post weld rolled followed by laser processing

Figure 3-39 is the optical micrographs of as-welded showing the microstructures at the third pass, which include the HAZ, the fusion line and some part of the weld metal. This figure shows how the parent material responds to the welding thermal cycles, as well as phase formations that formed as a result of thermal cycles. From left to right of Figure 3-39 is weld metal, fusion line and HAZ of the third pass.

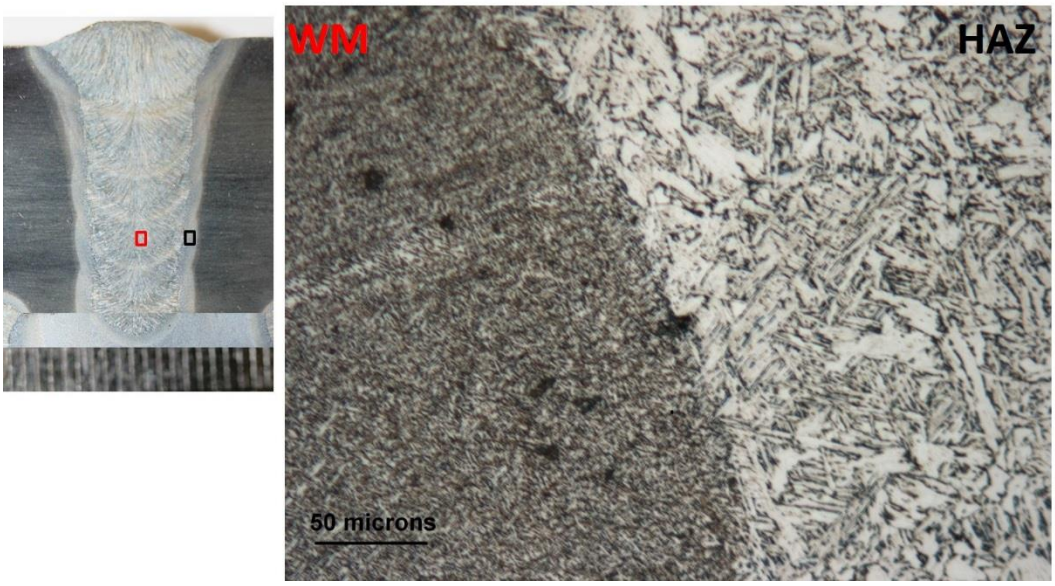

Figure 3-39: Optical micrographs showing the change in phase transformation

3.5.5.2.1 Effect of Post Weld Cold Rolling on Microstructure

Post weld cold rolling (weld metal at the cap pass) also consists of heterogeneous mixture of acicular ferrite, grain boundary ferrite, Sideplate ferrite and polygonal ferrite, fine bainitic ferritie which is typical for a low carbon steel weld. However, as shown in Figure 3-37 (b), post cold weld rolling has not shown any change in phase transformation since there is no change in temperature to create or alter phase composition. However, the formation of acicular ferritic in the welds are of great importance. This acicular ferrite is widely recognized to be a desirable microstructure [6] due to its fine grain interlocking nature [98], [99]. The formation of upper bainte is detrimental to weld toughness since its microstructure provide easy crack propagation path [10].

3.5.5.2.2 Effect of Post Weld Cold Rolling Followed by Laser processing on Microstructure

As shown in Figure 3-38, there are significant changes in terms of carbon diffusion and aspect ratio of different phases. However, as stated before, this thermal energy applied was not sufficient to supply enough energy to sustain a complete recrystallization kinetic.

3.5.5.2.3 Micrographs by Electron Backscatter Diffraction (EBSD)

For further analysis of grain structure, the crystallographic characteristics of the weld metal were examined with electron back-scatter diffraction (EBSD) techniques. The EBSD crystal orientation maps are shown in Figure 3-40 and Figure 3-41. These micrographs were obtained from data collected over an area of 255 µm x 190 µm with step size 0.21 µm. It is important to emphasize that the grid step size limits the size of the structure elements that can be analysed using EBSD. However, based on the step size used, the average grain size of the as-welded sample was 12.18 µm at cap pass. When the rolling load (post weld cold rolling) was applied on the same position, the average grain size was found to be 16.51 µm, similarly; average grain size of 10.15 µm was found when post cold rolling followed by laser processing was applied on the sample (see Figure 3-42). Among many other factors, grain boundary area poses as one of the major obstacles for movement of dislocations. Reduced grain size (10.15 µm), in laser

processed samples would, therefore, have the potential of improving the strength and toughness of the weld metal.

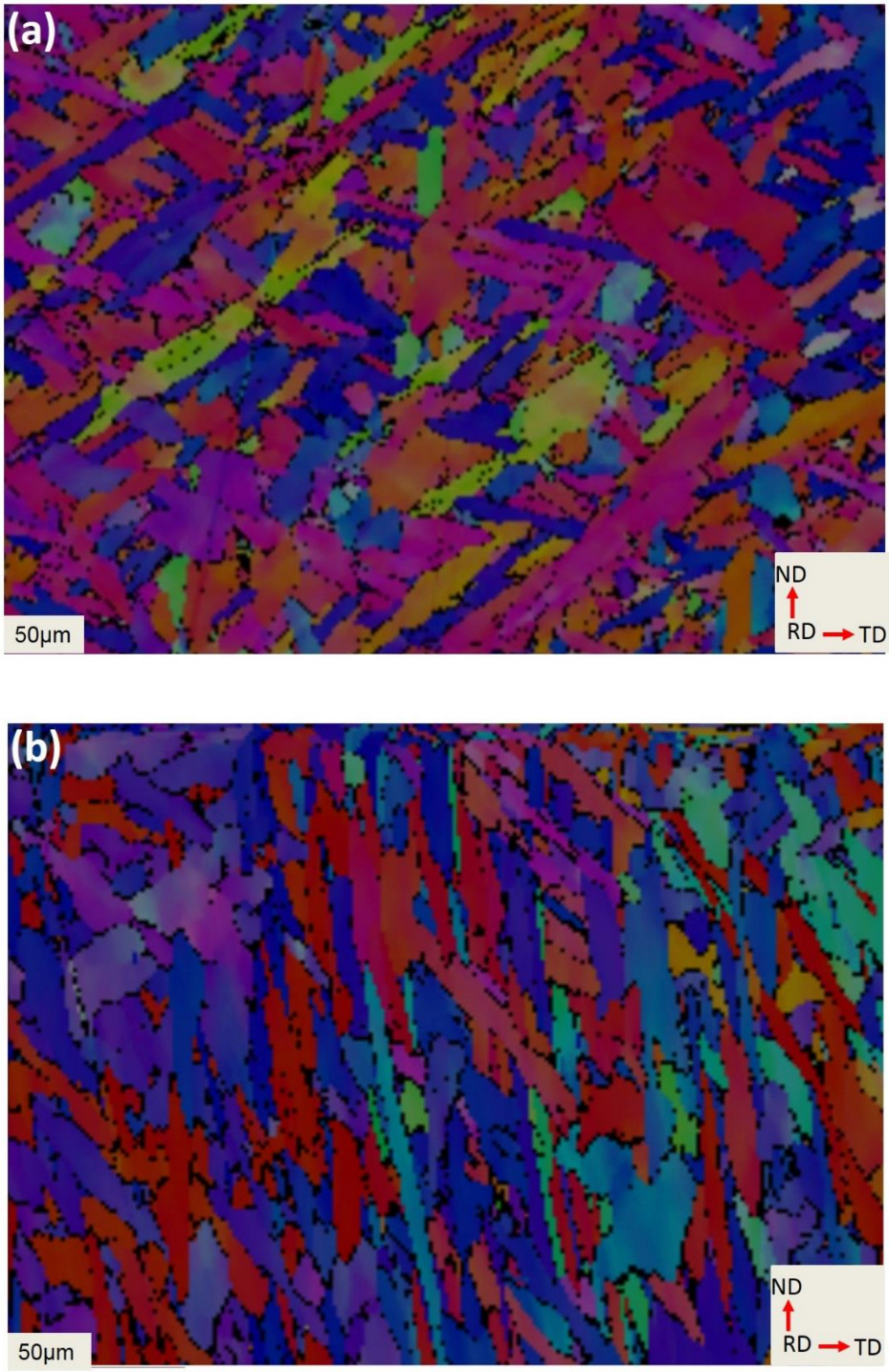

Figure 3-40: EBSD micrograph of X100 pipeline steel at the cap pass of (a) as-welded (b) post weld cold rolled samples.

The post weld cold rolled followed by laser processing obtained from EBSD shows the grains with different orientations (Figure 3-41).

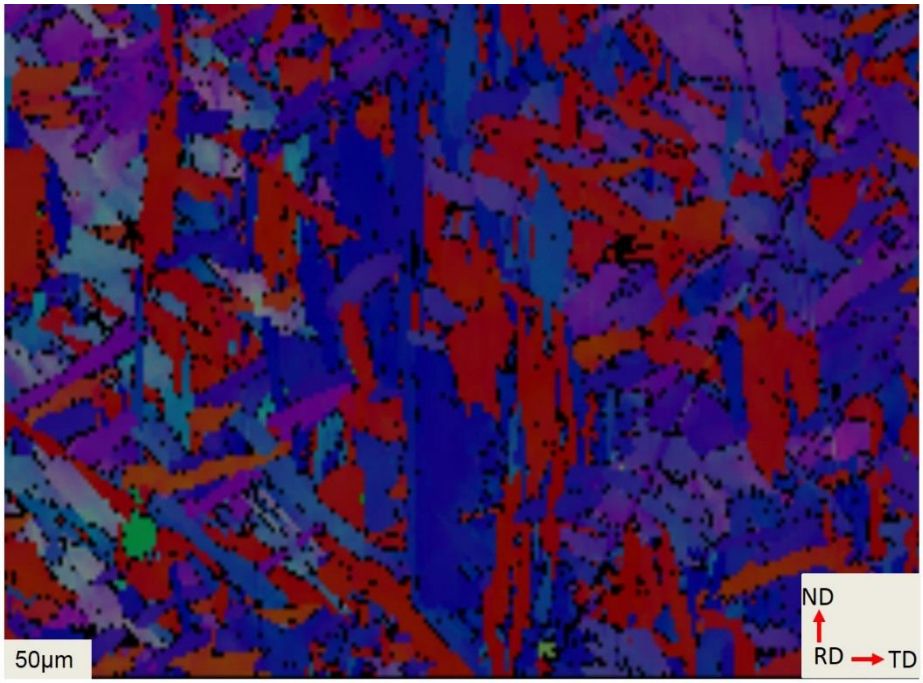

Figure 3-41: EBSD micrograph (cap pass) of post weld cold rolling followed by laser processing

Mechanical properties of polycrystalline metals and alloys are very sensitive to their grain size. Table 3-5 shows the statistical distribution of the as-welded sample. The table shows that the average grain size increase from root pass to cap pass. The smaller grains at the root pass can be attributed to fast cooling rate at the root pass.

Table 3-5: showing the statistical distribution of the grain size

	Root pass	Fill 1	Fill 2	Fill 3	Fill 4	Cap Pass
Ex (µm)	6.28	8.58	9.65	10.37	11.86	12.18
σ^2x (µm)	184.38	170.15	248.55	285.55	231.59	352.86
σ (µm)	13.58	13.06	15.77	16.90	15.22	18.77
σ^2x/Ex (µm)	2.16	1.52	1.63	1.63	1.28	1.54
X_{min} (µm)	1	1	0.73	0.58	0.73	0.73
X_{max} (µm)	337	149	105	92	58.77	89.79
N (µm)	1799	982	118	112	95	100
Raster (μm^2)	222 x167	222 x 166	316 x234	407x304	316x225	317x225
Step size (µm)	0.21	0.21	0.73	0.58	0.73	0.73

Where: Ex = average grain size

σ^2x = variance

σ = standard deviation

X = each value in the data set

N = number of value in the data set

Figure 3-42 shows the average grain size of all the samples with post weld cold rolled sample having a longer average grain size.

Its well known that refined grain size increases the strength of a polycrystalline material, post weld cold rolling followed by laser processing has reduce the grain size as shown Figure 3-42.

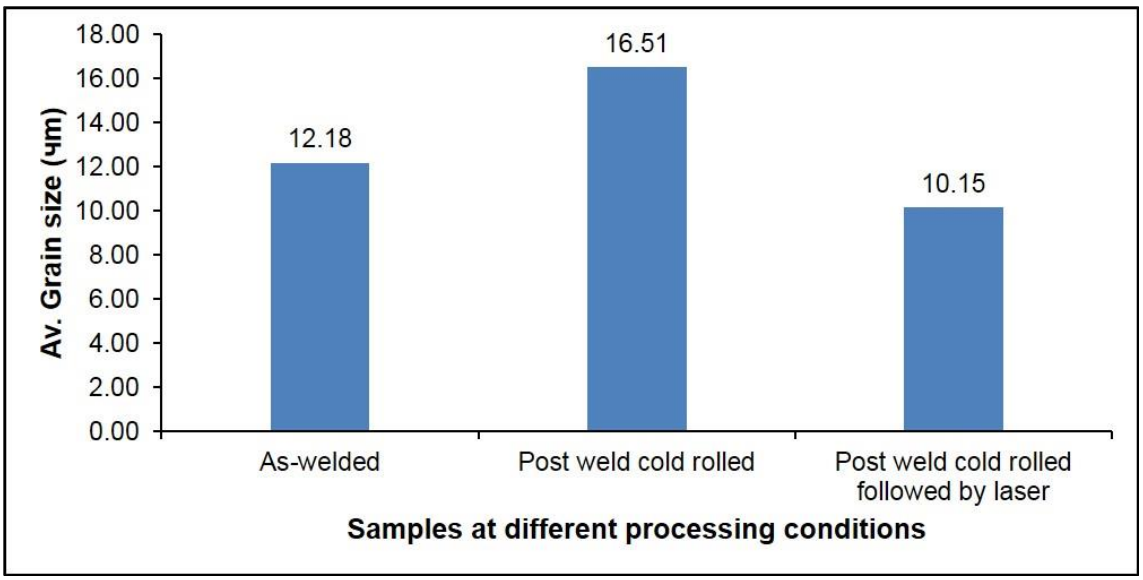

Figure 3-42: showing the average grain size at cap pass of all the three samples

3.5.5.2.4 Pole Figure

The {211} pole figures measured by the X-ray diffraction (XRD) obtained from the as-welded, post weld cold rolled and post weld cold rolled followed by laser processing are shown in Figure 3-43 and Figure 3-44 respectively. The pole figure shows that the texture intensity of the samples decreases as the sample was rolled and further decrease when post weld cold rolling followed by laser processing was applied, indicating that the texture was modified by grain reorientation induced by plastic deformation.

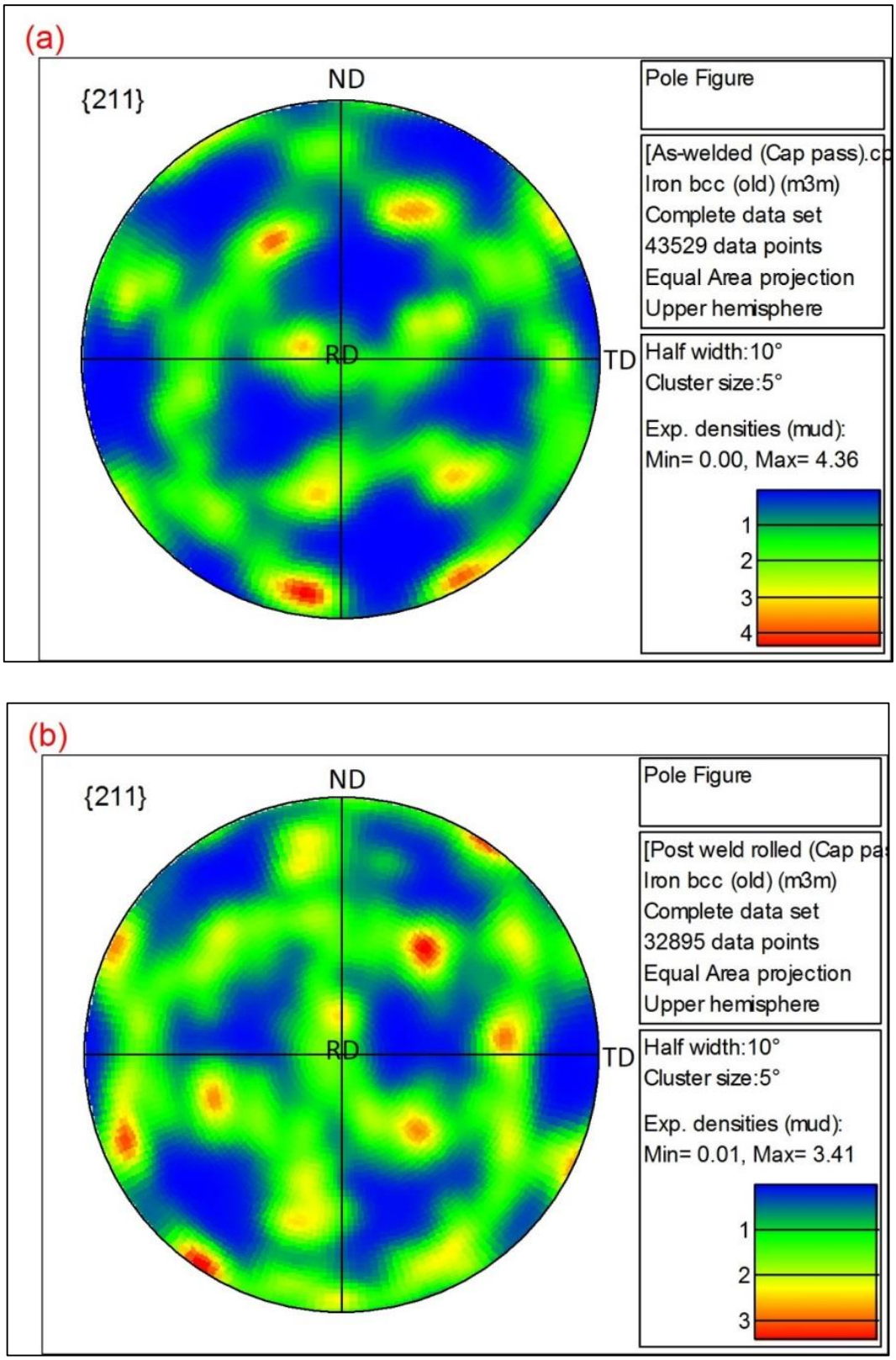

Figure 3-43: Crystallographic texture of the cap pass (a) as-welded (b) post weld cold rolling

The post weld rolling followed by laser processing further decrease the texture intensity of the samples as shown in Figure 3-44.

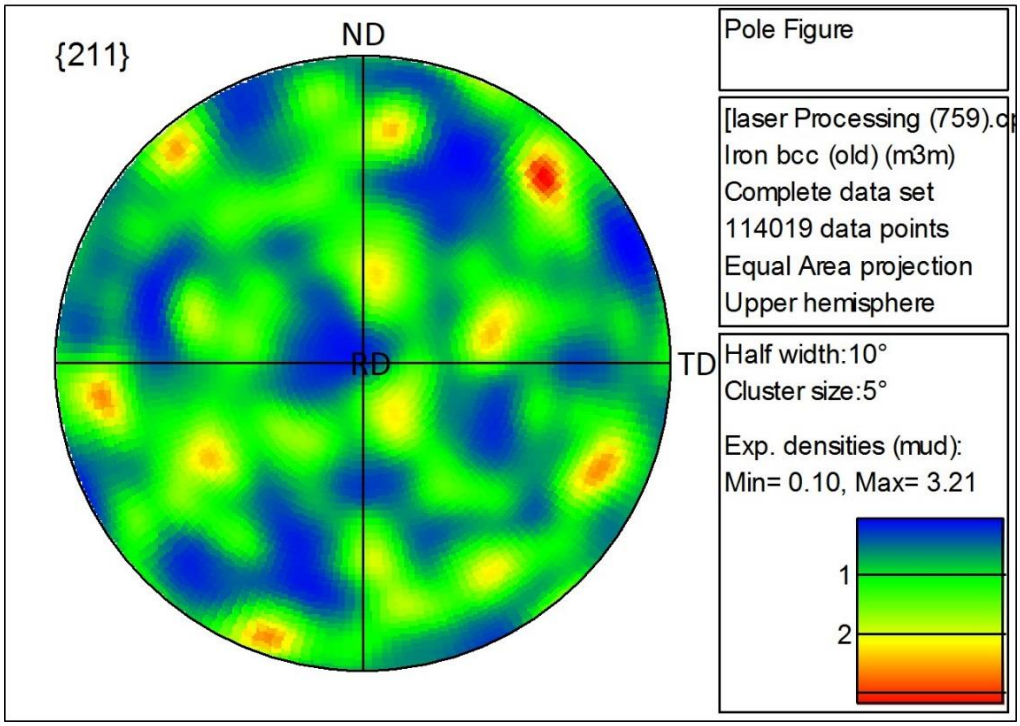

Figure 3-44: Crystallographic texture (cap pass) of post weld cold rolling followed by laser processing

3.5.6 Residual Stress Measurement

Measurement was taken at 2 mm below the top surface. This region is almost at the fifth pass. This fifth pass will be affected by tempering from the deposition of the last layer (sixth pass), and the previous layer (fourth pass) welding will have had a preheating effect on the parent metal. These processes reform the microstructures of weld metal and HAZ, and also affect the internal stresses that may be formed. A multi-pass welding process amounts to performing a heat treatment on the microstructure of the weld zone and HAZ and, in most cases, due to an uneven distribution of welding thermal history, the multiple depositions result in modification of stress magnitude and distribution.

However, the precise measurement of a stress-free reference lattice parameter is important when determining residual stress by neutron diffraction. The reference parameter variation as measured in the comb samples, for the

longitudinal directions as observed by monochromatic neutrons at the ILL in France is shown in Figure 3-45.

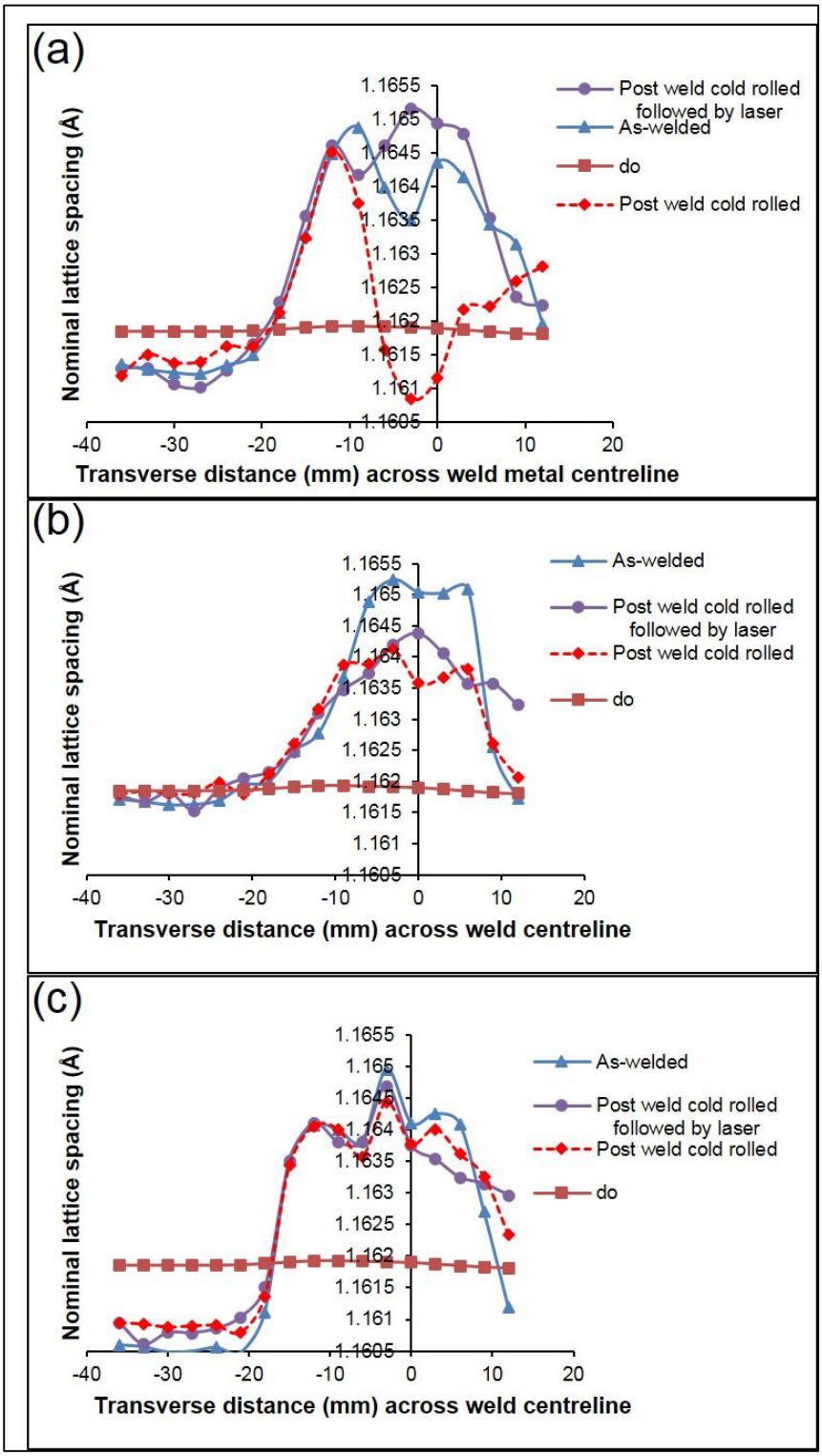

Figure 3-45: Variation in the unstressed αFe {211} lattice spacing d_0 measured. Measurement taken at (a) 2 mm (b) 10 mm (c) 18mm below weld surface

In this research, the residual stress analysed from the measurements of elastic strain showed a variation in residual stress across the weld at 2 mm below the weld surface (Figure 3-46). These are familiar distributions of longitudinal residual stress(σ_{xx}) during welding, showing tensile stresses close to the weld line and slightly compressive further away from it. The transverse and normal residual stress are shown in Figure 3-47 and Figure 3-48 respectively.

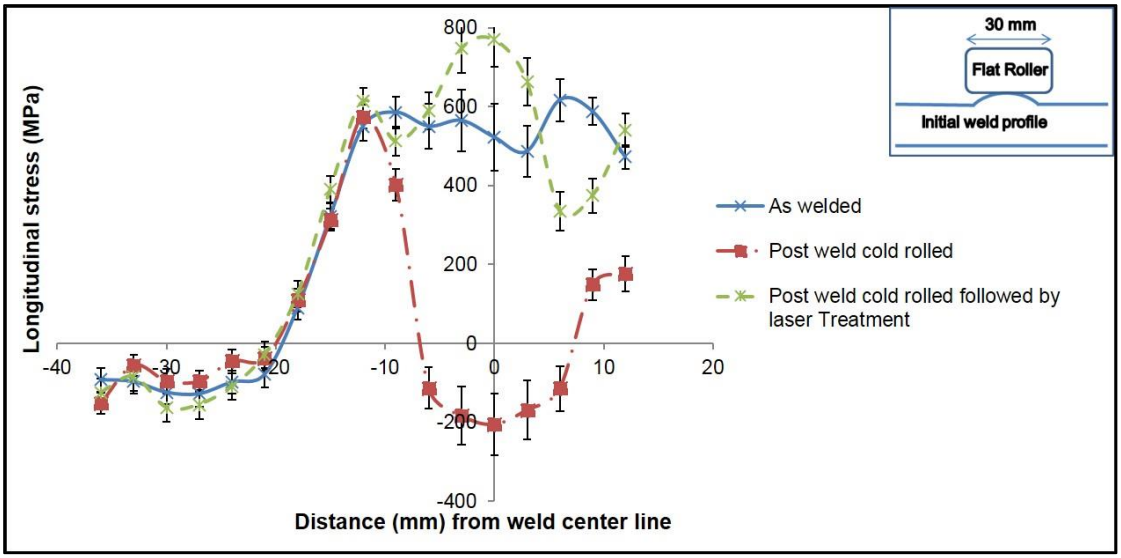

Figure 3-46: Longitudinal residual stress profile across the weld in specimens with different processing conditions (measured 2 mm below the top surface)

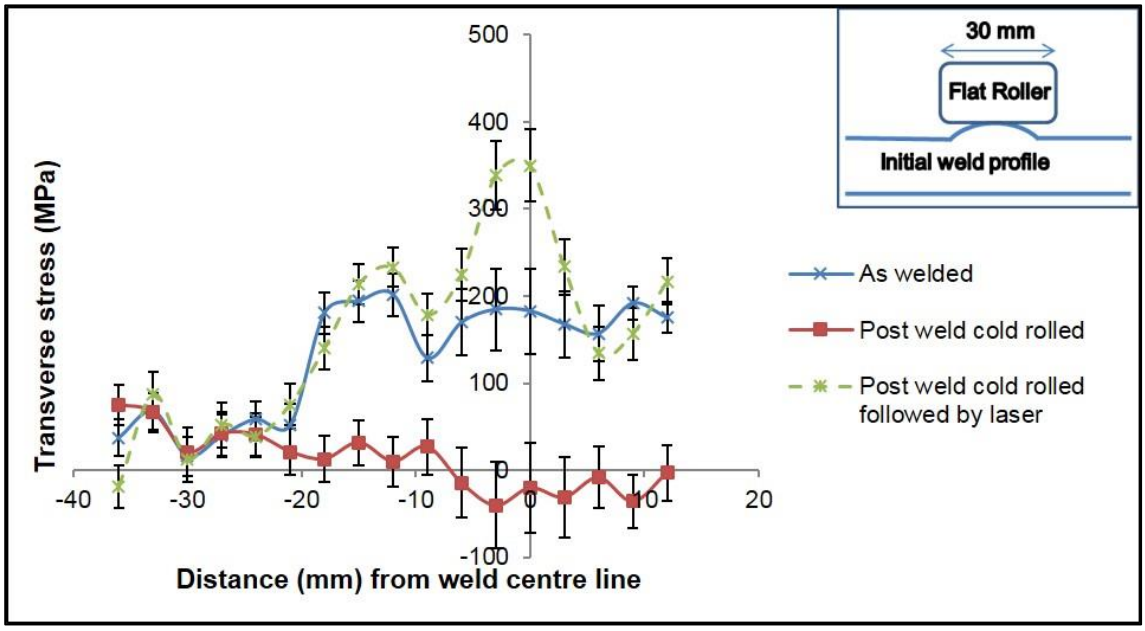

Figure 3-47: Transverse residual stress profile in the weld with different processing conditions (measured 2 mm below the top surface)

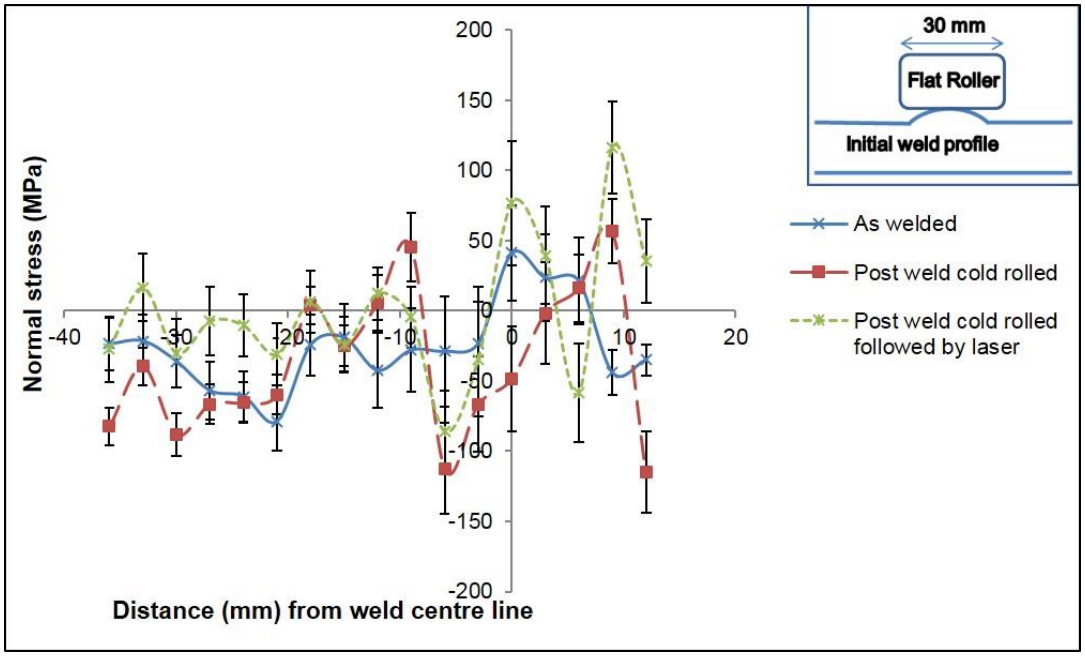

Figure 3-48: Normal residual stress profile in the weld with different processing conditions (measured 2 mm below the top surface)

3.5.6.1 Residual Stresses Across the Weld of As-welded Sample

Figure 3-46 shows the distribution of the longitudinal residual stress distribution profile. As shown, both the weld zone and HAZ show mainly tensile stress (as-welded). This stress, with a maximum value of 522 (+/-23) MPa at the weld metal centreline, was produced by not only longitudinal compressive plastic flow but also transverse compressive plastic flow. With increasing distance from the weld centreline as shown in the figures, the temperature declines sharply which lead to uneven heat input between the weld metal and base metal. These thermal contraction of the material in the high temperature zone is been restricted by the materials around it, resulting in the tensile stress. The variation in the stress profile of the weld metal can be attributed to the fact that the fusion zone is within the arc centre, and is predominately affected by the heat input, traveling speed and other welding parameters.

Formation of residual stress and microstructure to a large extent are dependent on heat input, and in most cases, near the fusion boundary which is the HAZ, the size of the grains are found to be relatively coarser at high heat input (if the heat is sufficient to take the temperature above the AC_3 line) and finer at low heat input

[225]. It was also reported that residual stresses were tensile near the welded region which has highest heat input, while at the lowest heat input region, the residual stress becomes compressive balancing the tensile stress [226]. This research has also confirmed the same phenomena.

Figure 3-47 shows the distribution of transverse residual stress. It was observed that the transverse residual stresses are mainly tensile with a maximum value of 183 (+/-20) MPa at the weld metal centreline. As shown, this magnitude is lower than that of longitudinal stress direction. This could be attributed to the fact that during the cooling stage, solidification shrinkage is restrained by base metal in the transverse direction, which also contributes to the formation of the tensile stress after welding. Another possible reason of lower transverse stress could be the propagation of heat in transverse direction. Heat transfer is faster in transverse direction than in longitudinal direction, hence, the heat quantity transferred in transverse direction is more than in longitudinal direction which may also affect the stress distribution in the transverse direction.

Figure 3-48 shows the distribution of the normal residual stress (as-welded). Comparing the normal stress value to the longitudinal and transverse residual stress, the stress in normal direction is smaller. Maximum value obtained at weld centreline was 41 (+/-25) MPa. The weld zone shows tensile residual stress and the HAZ and base metal shows compressive residual stress. Further away from the weld centreline the stress decreases gradually and then declines to zero. This tensile residual stress was observed around the centreline of the weld because of the solidification of weld metal and constriction around the base metal.

3.5.6.2 Residual Stresses through the Thickness of Weld (As-welded Condition)

The residual stress analysed showed a reduction in magnitude from cap to root in the as-welded state (Figure 3-49). This diminishing in magnitude through the thickness of a multi-pass weld can be attributed to the fact that multiple passes result in thermal straining of previously laid pass from successive passes. The thermal cycling would cause macroscopic plastic deformation of previously laid passes.

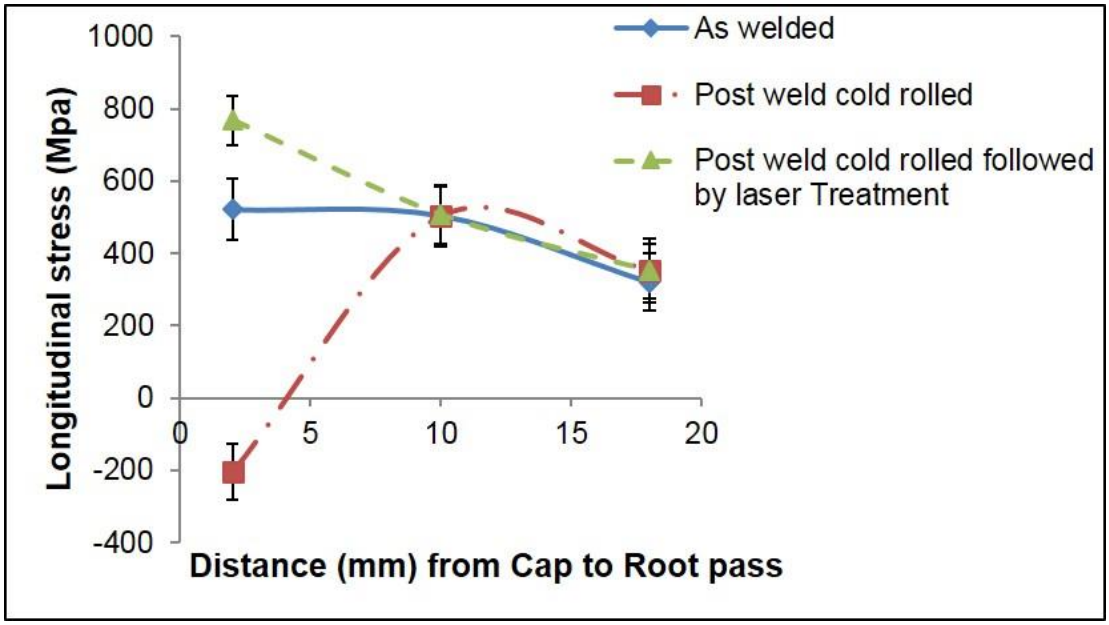

Figure 3-49: Variation of peak residual stress magnitude through the thickness (measured at 2, 10, and 18 mm below the top surface)

3.5.6.3 Effect of Post Weld Cold Rolling Through the Thickness

As shown in Figure 3-46, post weld cold rolling (measurement was taken at 2 mm below the weld surface) has changed the longitudinal residual stress state causing it to become compressive around the weld metal (from peak tensile stress of 522 MPa to compressive stress of 205 MPa). Up to about 4 mm below the weld surface, compressive residual stress was observed (Figure 3-49). Application of rolling to the welded joints causes yielding of material in the weld region, thereby, redistributing the residual stresses that may exist in the region. These rolling processes compress the material in the direction normal to the weld's surface, thereby causing it to expand in the plane of the weld, relaxing any tensile residual stresses in the plane.

A flat roller of 30 mm width was used which determines the extent to which localized plastic strain is induced and thereby compressive longitudinal stress is generated (Figure 3-46,). However, the compressive zone width is narrower than the width of roller because the contact area of the roller is smaller compared to the width of roller. Hence rolling causes plastic deformation around that region of the weld which is approximately 17 mm in width.

It was observed that, at about 10 mm below the weld surface (Figure 3-49) the rolling load has little influence on the residual stress state of the weld. The rolling changes the peak tensile stress from 505 MPa to 405 MPa suggesting little impact of the rolling in this region. Similarly, at 18 mm below the weld surface (Figure 3-49); the rolling load did not show any insignificant change in the residual stress state.

3.5.6.4 Effect of Post Weld Cold Rolling Followed by Laser Processing

Laser processing after cold rolling (measurement was taken at 2 mm below the weld surface) has been shown to increase the longitudinal residual stress from compressive stress of 205 MPa to peak tensile stress of 770 MPa (Figure 3-46) indicating a low heat input but fast cooling condition of the material, thus generating inhomogeneous plastic deformation and tensile residual stresses. Similarly, at about 10 mm and 18 mm below the weld surface (Figure 3-49), application of laser processing to the rolled samples did not show any significant change in the residual stress state. This indicates that the heat conducted through the material at that region was not sufficient to cause in changes in the residual stress state.

3.5.6.5 Full Width at Half Maximum (FWHM)

Figure 3-50 shows the effect of FWHM on (a) as-welded sample at different depth (b) Post weld cold rolling at different depth and (c) the three samples 2 mm below weld surface.

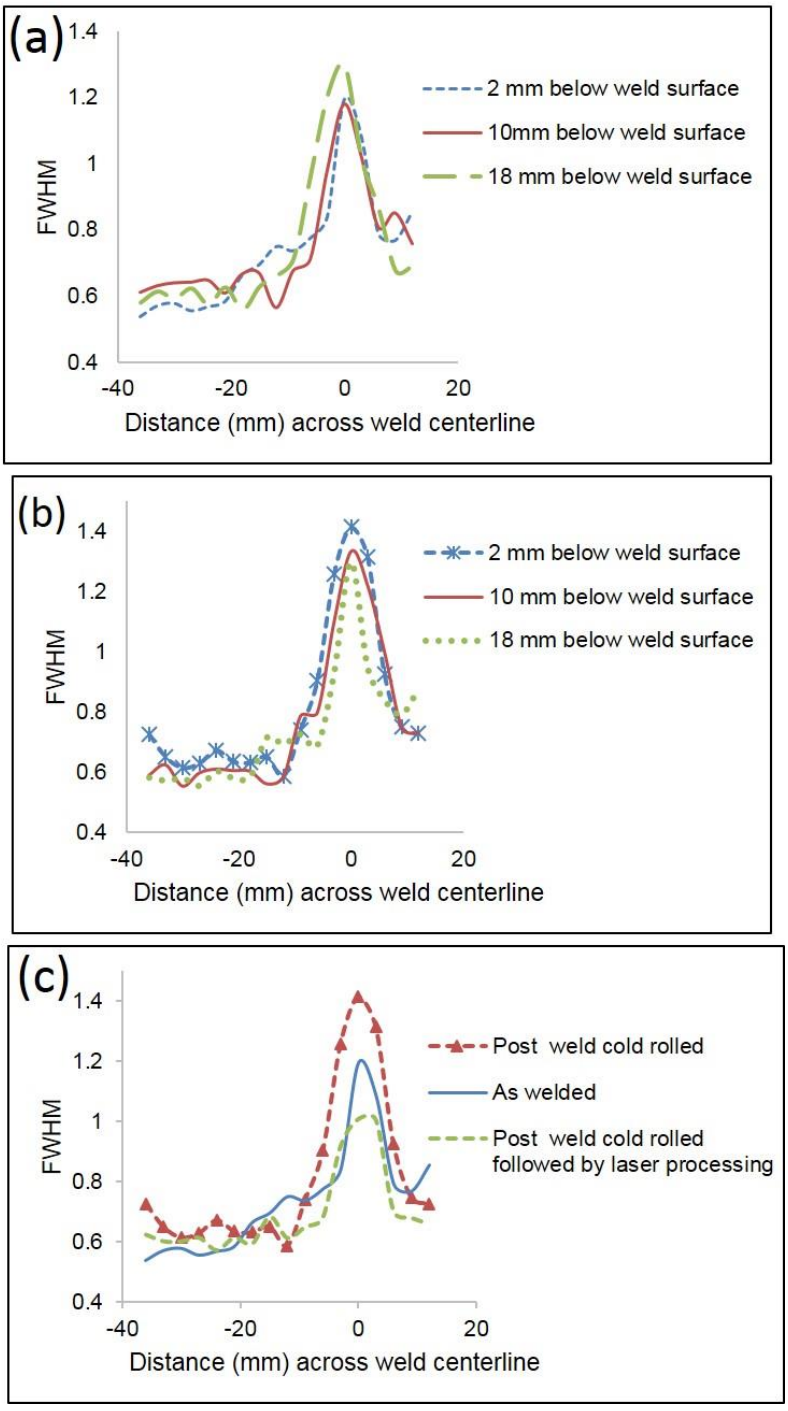

Figure 3-50: Effect of FWHM on plastic deformation at (a) as-welded at 2 mm, 10 mm and 18 mm below weld surface (b) post weld cold rolling at 2 mm, 10 mm and 18 mm below weld surface and (c) The three samples at 2 mm below weld surface

FWHM indicate the plastic strain history of a crystalline structure. As shown in Figure 3-50 (a), the FWHM at 18 mm below the weld surface was higher than the FWHM at 2 mm below the weld surface. This is due to the fact that root regions experience more thermal cycles than any other region in the multi-pass weld. Thus, the root pass undergoes more thermal straining compared to cap pass. Similarly, in the post weld cold rolled sample, FWHM at 2 mm below the weld surface was higher because of the direct contact between local mechanical tensioning (roller) and cap pass indicating more plastic deformation at that region (Figure 3-50 (b)).

As the effect of the load applied by the roller diminishes through the thickness (Figure 3-50b), the peak FWHM reduces, indicating that FWHM is influenced by the work hardening effect of the rolling process. FWHM profile reduces when rolling followed by laser processing was applied (Figure 3-50(c)). This could be due to the thermal energy from laser which induces recovery and dislocation density reduces.

3.5.7 Conclusion

The effect of rolling was realized up to about 4 mm below the weld surface. Minimal grain refinement was observed at the cap pass when post weld cold rolling followed by laser processing was applied to the sample. The post weld cold rolling modifies the stress state and a compressive residual stress was formed below the weld metal. As the modification of stress state is achieved by localized plastic deformation an increase in hardness of the weld metal was also observed. Post weld cold rolling followed by laser processing resulted in formation of refined microstructure with strain free grains due to recrystallization. However, laser processing reinstated the as-welded residual stress state profile with even higher magnitude of peak stress. Following this observation, a further processing route was proposed, which form the second phase of the experiment.

The peak tensile residual stress of the as-welded sample diminishes in magnitude through the thickness of a multi-pass weld. This is attributed to the fact that, multiple passes result in thermal straining of previously laid pass from successive

passes. The thermal cycling would cause macroscopic plastic deformation of previously laid passes.

The analysis of FWHM data shows that the root pass of multi-pass welds undergo more deformation (as-welded sample) due to the fact that root regions experience more thermal cycles than any other region. These indicate that the root pass undergo more deformation, thus, FWHM was higher at the root pass compare to cap pass. Similarly, post weld cold rolling, resulted in an increase in FWHM at 2 mm below the weld surface due to direct contact between local mechanical tensioning (roller) and the cap pass, indicating that FWHM is influenced by the work hardening effect of the rolling process.

3.6 Second Phase of Experimentation

This second phase of the experiment was based on the observation made in the first phase of the experiment, that post weld cold rolling followed by laser processing reinstated as-welded residual stress state profile with even higher magnitude of peak stress and also resulted in minimal refinement of microstructure. This indicated that the re-crystallisation is partial because the transient thermal cycle is not sufficient to supply enough energy to sustain the entire recrystallization kinetics. Based on this observation, a new laser processing was adopted.

The new laser processing involves applying thermal energy for a prolonged period which would ensure full recrystallization of the grain structure.

In order to overcome the problem of restoration of residual stress after laser processing of the post weld cold rolled samples as observed in the first phase of the experiment, further cold rolling was applied. This cold rolling after laser processing is to redistribute and eliminate the tensile residual stress state which would have formed during laser processing. Figure 3-51 shows the sketch of the work flow for the second phase. As shown in the sketch, the second phase of the experiment involved four steps; welding was carried out by Tandem GMAW DC process, the post weld cold rolling was performed using an in-house rolling device, the post weld cold rolling was followed by laser processing using 8 kW

(peak power) CW fibre laser and finally cold rolling after post weld cold rolling was followed by laser processing.

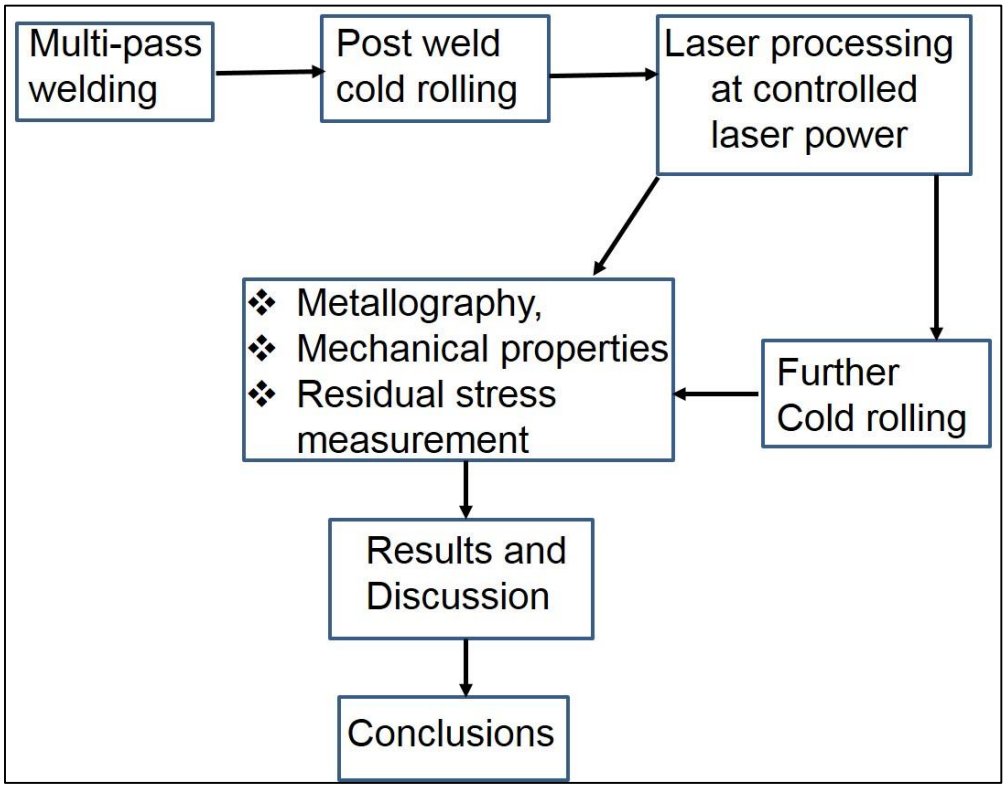

Figure 3-51: Sketch of the work flow of the second phase

In this second phase of experiment, the material and experimental equipment used in the first phase were used.

3.6.1 Experimental Method

The experimental methods are divided into five (5) stages (that is, welding, post weld cold rolling, laser processing, cold rolling after laser processing and residual stress measurement) and they are presented here.

3.6.1.1 Welding

The same principle of welding process used in section 3.4.1 was adopted in this second phase of the experiment.

3.6.1.2 Local Mechanical Tensioning (Cold Rolling)

The rolling method used in section 3.4.2 was applied in this section.

3.6.1.3 Laser Processing

The new laser processing involves applying thermal energy for a prolonged period which would ensure full recrystallization of the grain structure and formation of new set of strain free grains. In order to understand the time-temperature cycle required for full recrystallization, experiment using reheating furnace was carried out on post weld cold rolled samples.

3.6.1.3.1 Experiment Using Reheating Furnace

In these experiments, different temperatures were tried. Thermocouples were attached to each sample so as to differentiate between the furnace temperature and sample temperature. Each sample was heated and held for 60 s.

Carbolite chamber furnaces was used for these trials so as to understand the time-temperature cycle required for full recrystallization of post weld cold rolled samples. This carbolite furnaces are designed under an ISO 9001:2008 standard. In this carbolte furnance, the silicon carbide heating elements was used, which are good heating element required in laboratory furnaces. Figure 3-52 shows the Carbolite chamber furnaces used at Cranfield University.

Figure 3-52: Carbolite chamber furnaces

3.6.1.3.2 New Laser Processing

In the new laser processing, the same continuous wave (CW) laser was used as in first phase, but instead of transient heating mode, the post weld cold rolling samples were gradually heated by controlling the laser power at a large beam diameter of 110 mm. Figure 3-53 shows an experimental set up while Figure 3-54 shows the schematic diagram for design laser set-up. The laser head was positioned at 25^{o} angle to avoid any back reflection which could damage the lens.

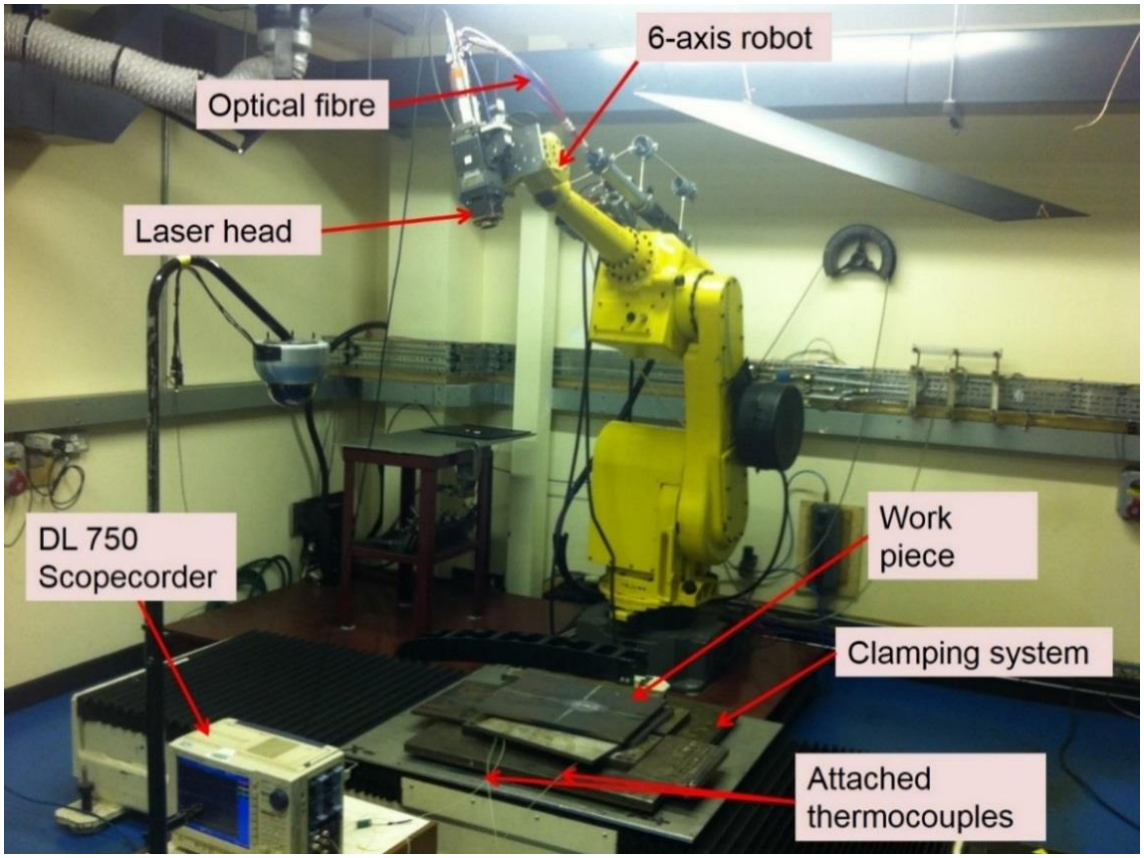

Figure 3-53: New laser experimental set-up

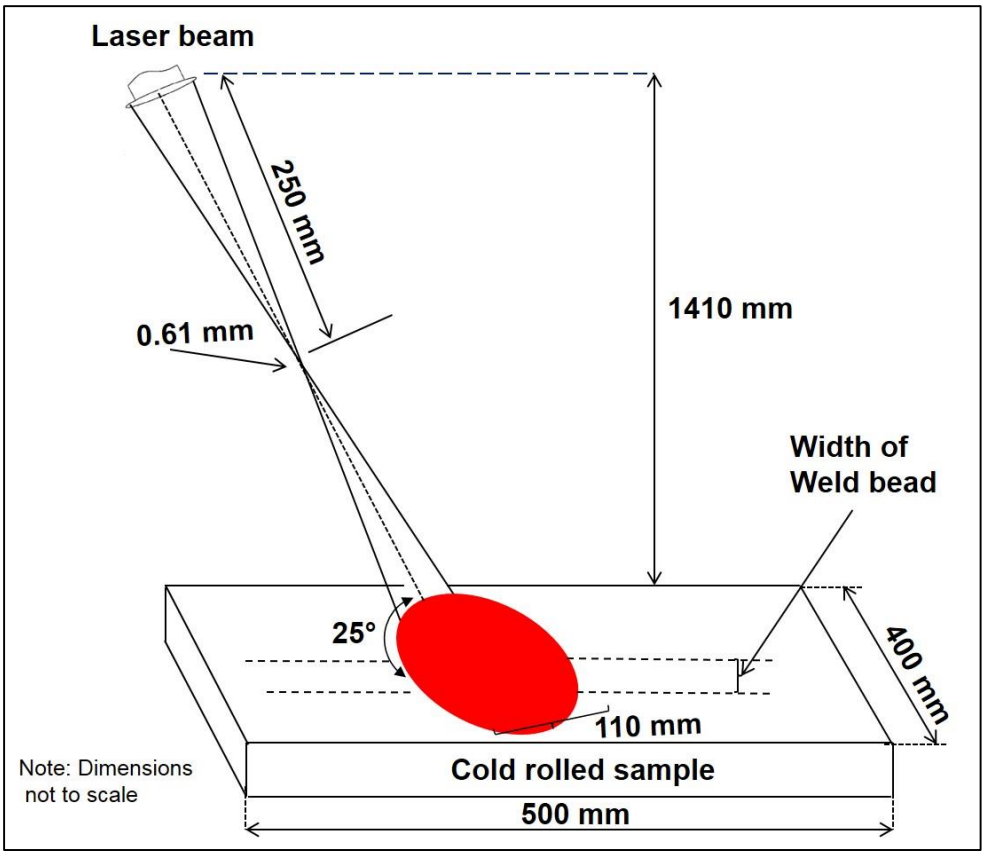

Figure 3-54: Schematic diagram for new laser set-up

3.6.1.4 Further Cold Rolling After Laser Processing

The same principle used in section 3.4.2 of this thesis was also applied here.

3.6.1.5 Method of Residual Stress Measurement

The SALSA neutron diffractometer at the Institut Laue Langevin in France was used in a similar condition as stated in section 3.4.4 to measure the residual elastic strain [19]. In this second phase, the following parameters are different from the first phase;

1. The measurements in the second phase were made using a neutron incident beam of wavelengths, 1.6 Å, which gives a diffraction angle (2Θ) of 84.2^{o}
2. The measurements of the residual strain were taken at 3.5, 11.5 and 19.5 mm below the plate surface on which the capping pass was laid

3.6.2 Results and Discussion

The furnace experiment, new laser processing, cold rolling after laser processing and their effect on this structural alloy is presented in a comparative manner where ever possible.

3.6.2.1 Experiment Using Reheating Furnace on API 5L X100 Pipeline Steel Plate

The post weld cold rolled samples were heated on the furnace and their hardness and microstructure were checked before designing the new laser processing route. The size of the samples heated on this trial was 50 mm long by 40 mm wide by 20 mm thick. In these experiments, the samples were heated to different temperatures (600^{o}C, 800^{o}C, 900^{o}C, 1000^{o}C and 1200^{o}C). A thermocouple was attached to each sample so as to differentiate between the furnace temperature and sample temperature. Each sample was heated and hold for 60 seconds. The thermal cycle at different temperatures are shown in Figure 3-55. The hardness profile and optical micrographs are also shown in Figure 3-56, Figure 3-57 and Figure 3-58 respectively.

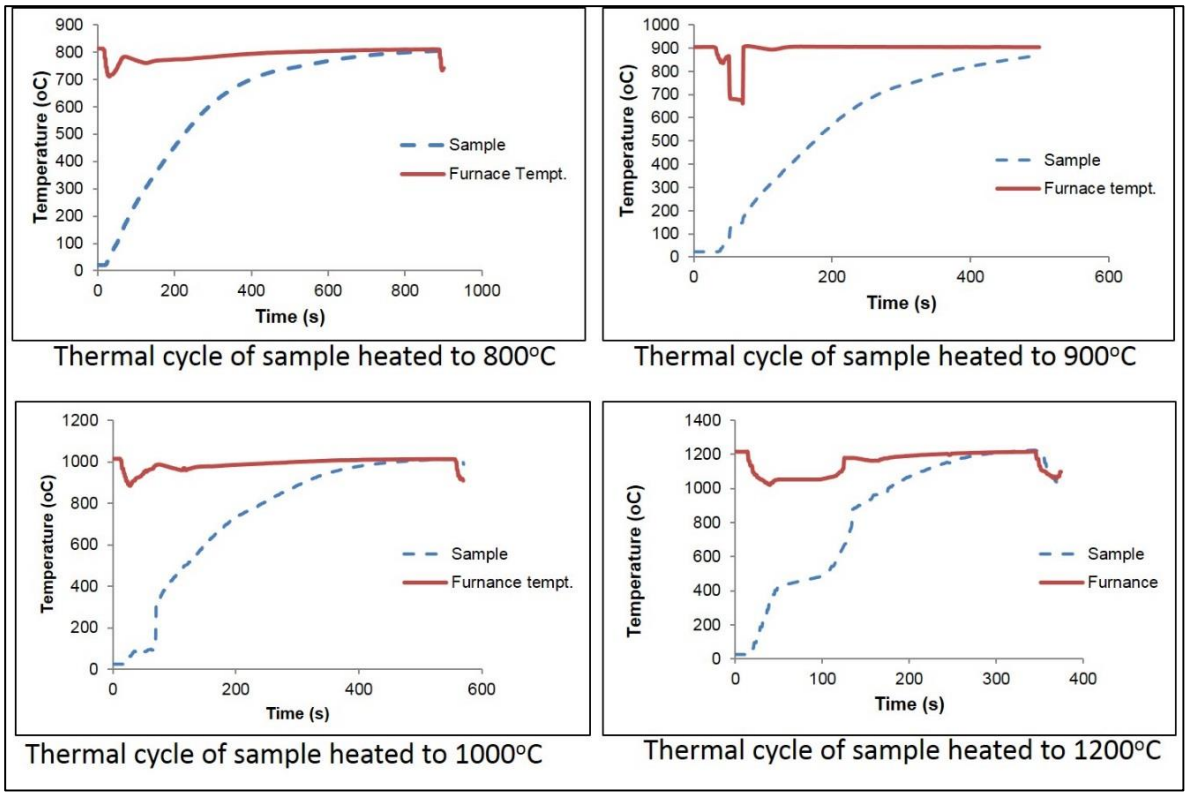

Figure 3-55: Thermal cycles of furnace treatment at different temperature

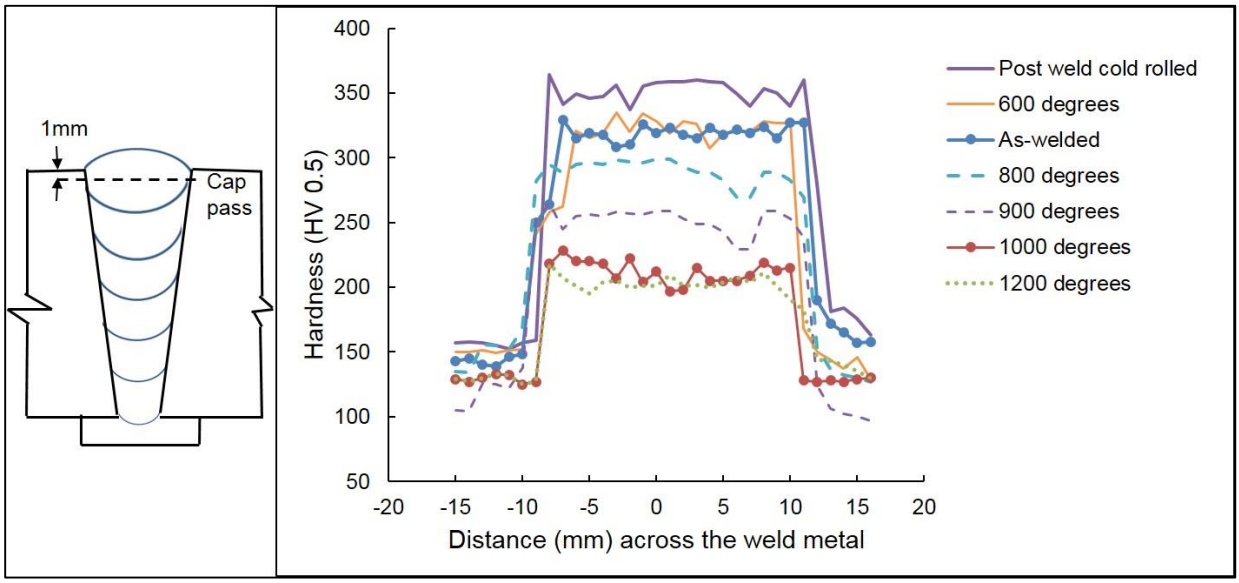

Figure 3-56: Hardness profile across weld metal (cap) at different temperature

As shown in Figure 3-56, the hardness values across the weld metal decreases with increase in temperature. This reduction in hardness values is as a result of formation of other softer phases e.g. ferrite.

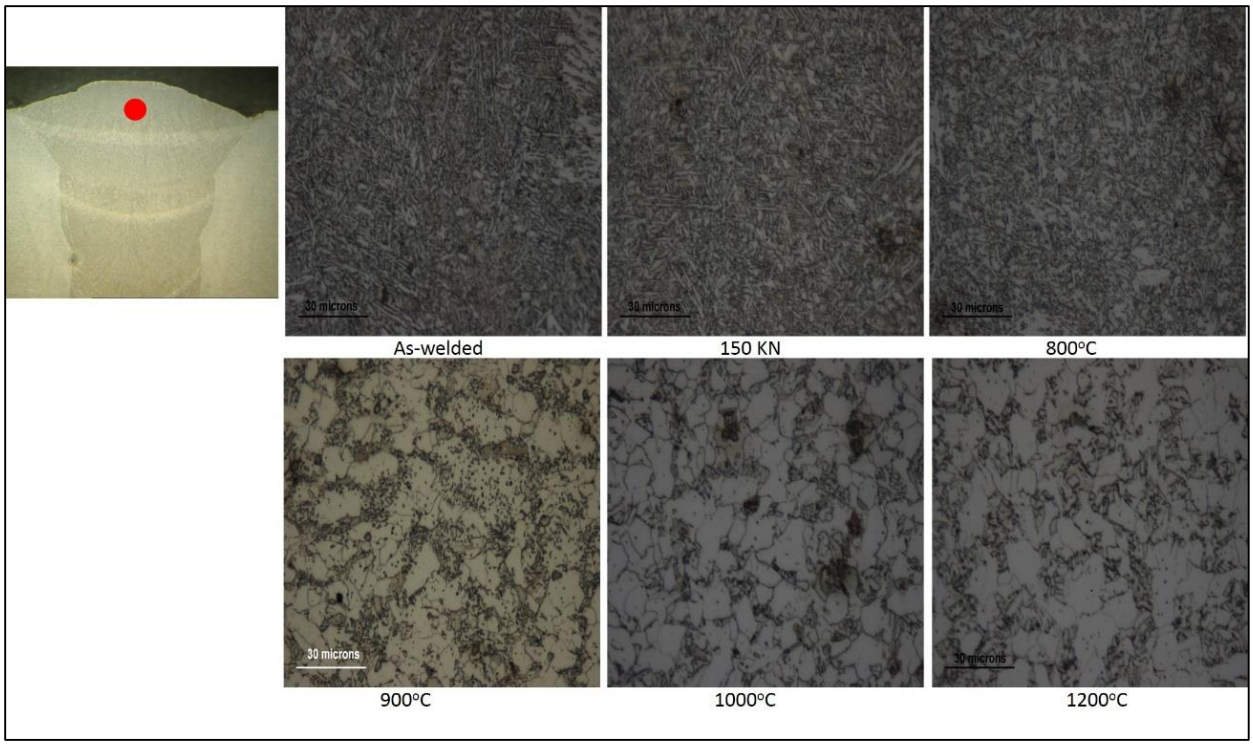

Figure 3-57: An optical micrographs of the welds metal (cap pass)

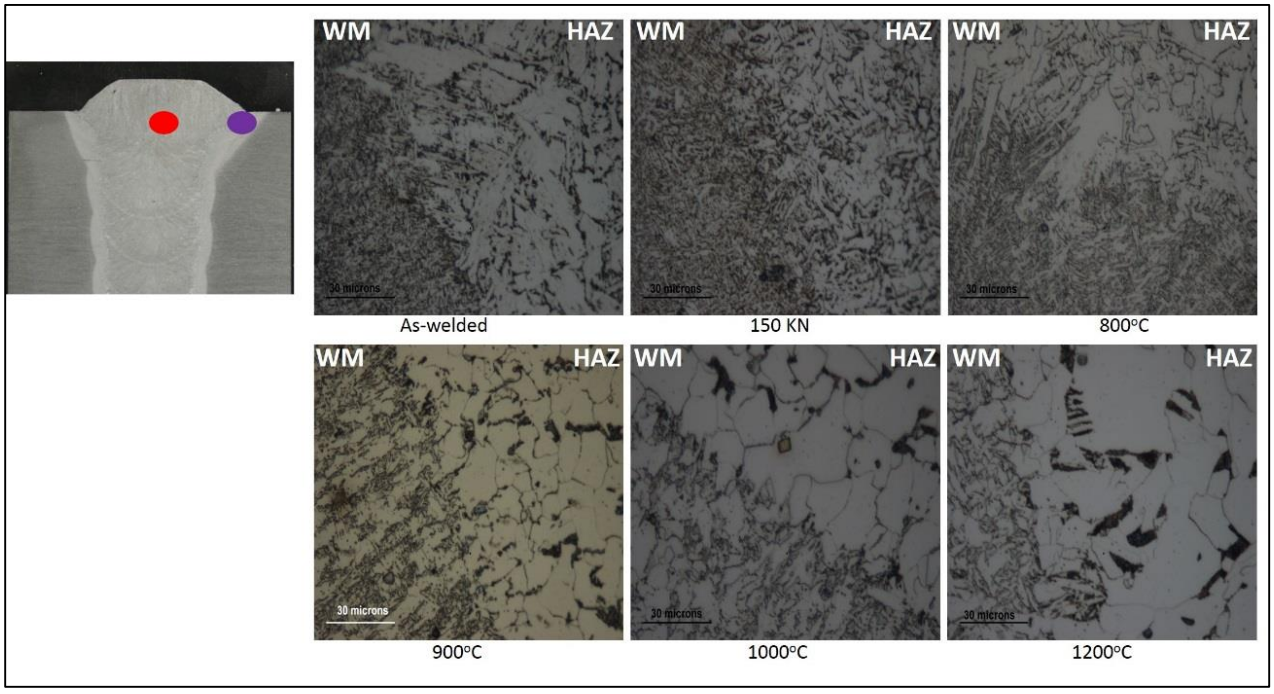

Figure 3-58: An optical micrographs of the welds metal and HAZ (cap pass)

3.6.2.2 Conclusion for the Furnace Experiment

The result in the furnace experiment shows that recrystallized grains can be formed after heating the API 5L X100 pipeline steel plate to 900ºC. Based on this observation, the laser processing in the second phase of the experiment was designed.

3.6.2.3 New Laser Processing

In this phase the same CW laser was used as in first phase, but instead of transient heating mode the post weld cold rolled samples were gradually heated by controlling the laser power at a large beam diameter of 110 mm. The API 5L X100 pipeline steel plate was heated up to 900ºC using identical laser parameters. The thermal cycle of the laser processing is shown in Figure 3-59.

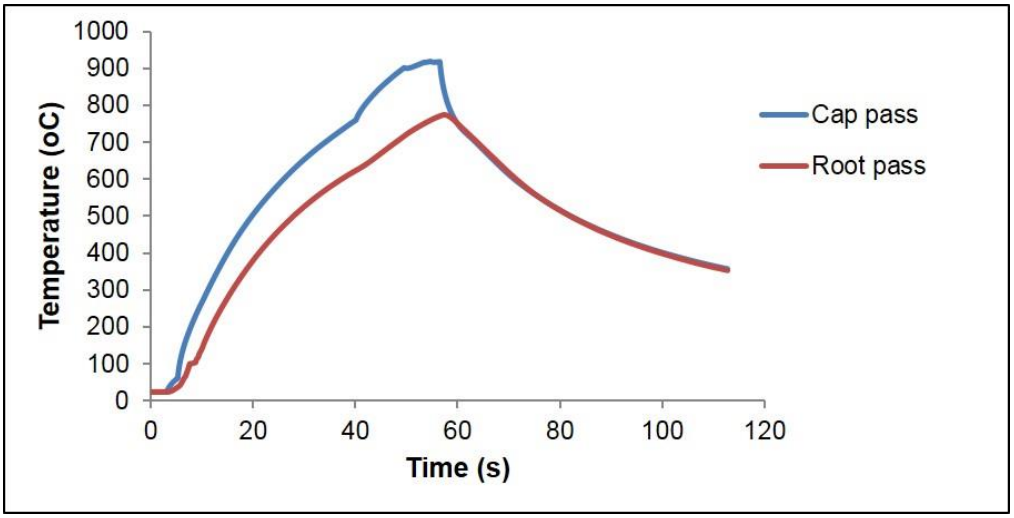

Figure 3-59: Thermal cycles of control laser power (heated to 900ºC) at constant beam diameter of 110 mm

The effect of the new laser processing on hardness, tensile strength, metallography and residual stress measurement are presented and discussed.

3.6.2.3.1 Effect of the New Laser Processing on Hardness Profile

Figure 3-60 shows the hardness measurement profile at the cap pass of the welds in the three processing conditions for purpose of comparison.

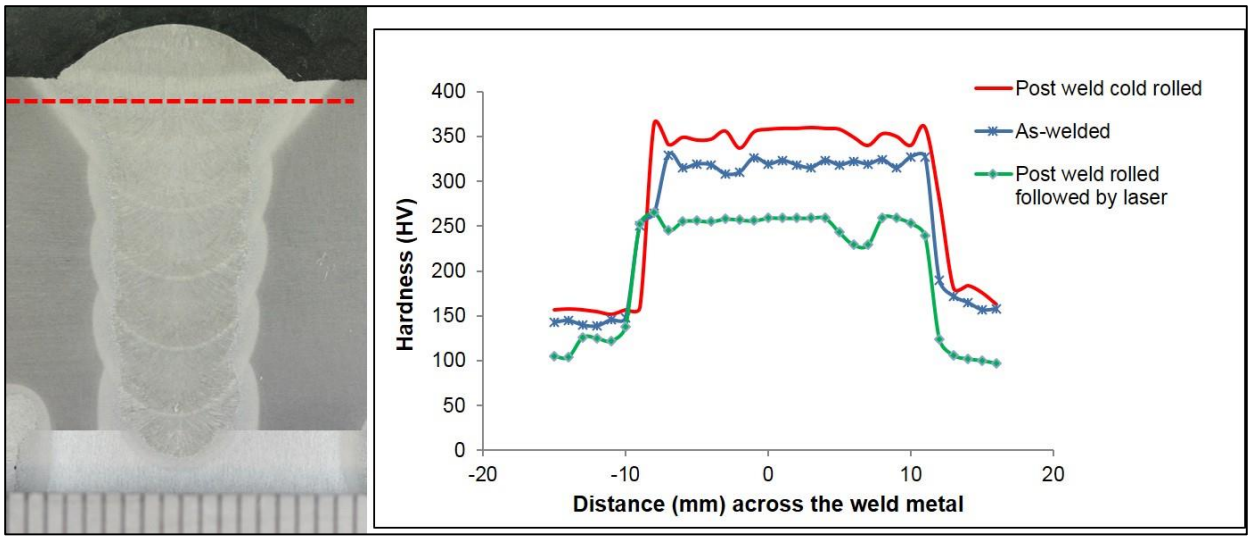

Figure 3-60: Hardness profile at the capping pass across the weld metal

Figure 3-61 shows the hardness profile from the reinforcement bead (cap pass) to the root pass.

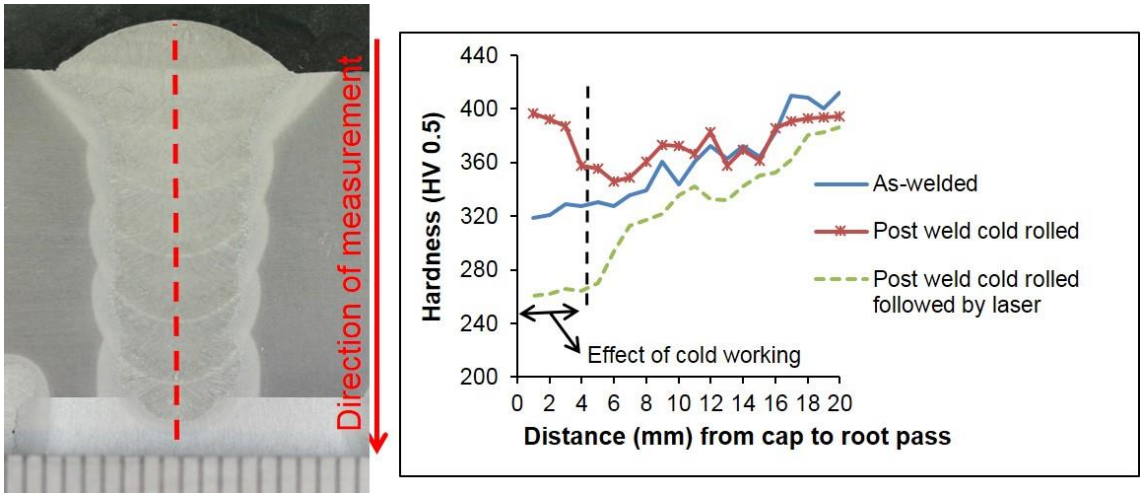

Figure 3-61: Showing hardness scan position along the weld metal and the hardness profile

This method resulted in softening of the weld metal throughout the entire thickness (Figure 3-61). Figure 3-60 shows the hardness measurement (HV0.5) across the capping pass of the welds. The hardness values drop from 388 HV to 258 HV at the cap pass. This softening resulted in significant refinement of the grain structure. This grain refinement may improve the mechanical behaviour of the weld metal and also increase resistance to fatigue and fracture failure. In

other words, laser processing following cold rolling has resulted in refining of the cold worked grains, which will relax the strains and also allow diffusion of interlocked carbon atoms making a more tempered structure.

3.6.2.3.2 Effect of the New Laser Processing on Tensile Strength

Figure 3-62 shows a graphical representation of the all-weld metal tensile test.

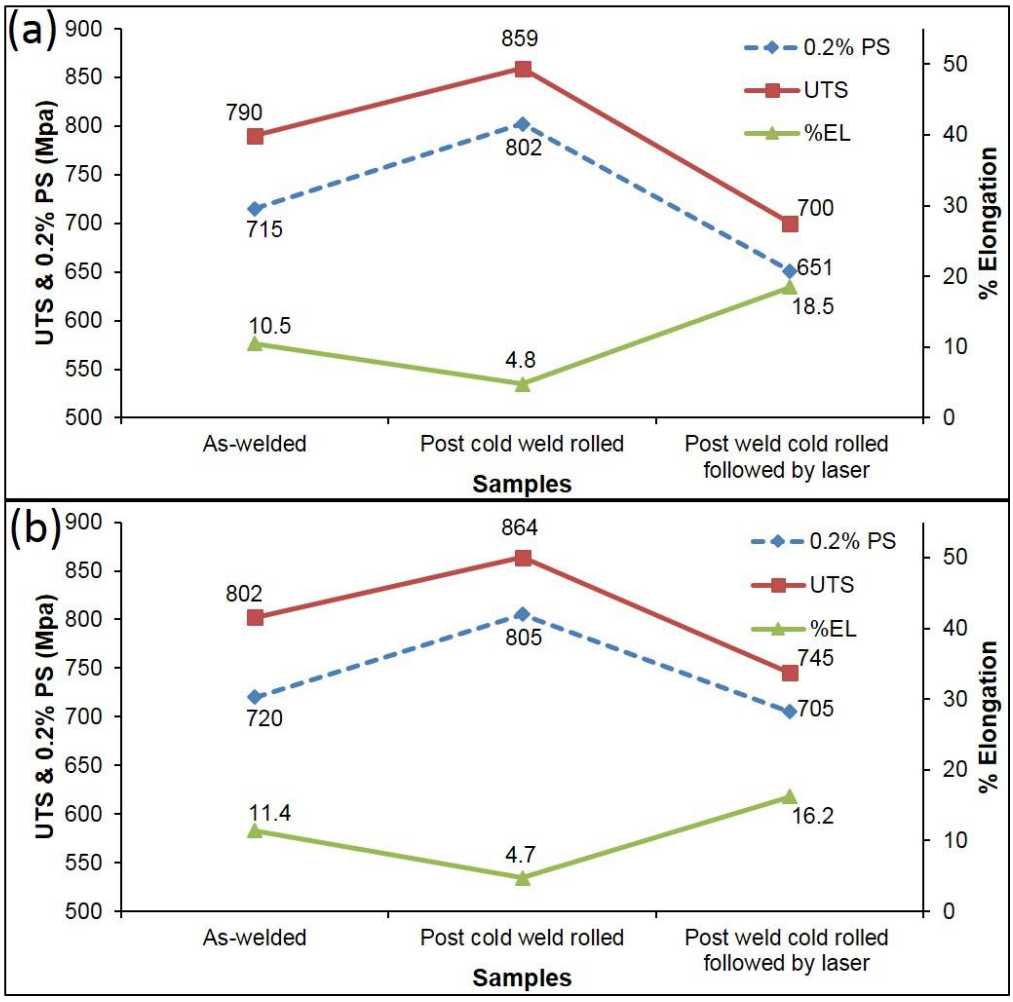

Figure 3-62: Tensile test for API 5L X100 pipeline steel plate close to (a) cap pass (b) root pass

In this second phase, post weld cold rolling followed by laser processing shows a greater decrease in the PS by 18.8% and UTS by 18.5% and with corresponding increase the percentage elongation (4.8% to 18.5%) close to the cap pass as shown in Figure 3-62 (a). These decrease in PS and UTS can be associated increase in temperature. However, at the root pass, post weld cold

rolling followed by laser processing also shows a decrease in PS and UTS with corresponding increase in percentage elongation indicating that the heat applied by the laser processing was sufficient through the thickness to change the microstructural feature at the root pass which is a clear improvement on first phase of the experiment.

Table 4-3-6: Sowing the Tensile test of the samples

samples	UTS (MPa)	0.2%PS	%EL
As-welded	780	738	10.5
Post weld rolled	844	802	4.8
Post weld rolled followed by laser treatment	700	651	18.5

As shown in Figure 3-62, PS/UTS of samples close to the cap pass are 0.91, 0.93 and 0.93 for as-welded, post weld cold rolling and post weld cold rolling followed by laser respectively. The PS/UTS measured close to the root pass are 0.90, 0.93 and 0.95 for as-welded, post weld cold rolling and post weld cold rolling followed by laser respectively. All this values are within the SMYS according to report presented by British steel [220].

3.6.2.3.3 Optical Microstructure

The as-welded and post weld cold rolled samples which consist of heterogeneous mixture of acicular ferrite (AF), grain boundary ferrite (GBF), Sideplate ferrite (SPF) sometimes called widmanstatten ferrite, and polygonal ferrite are shown in Figure 3-63 are compared. While, post weld cold rolling followed by laser processing shows a typical ferrite (F) and pearlite (P) structure (see Figure 3-64).

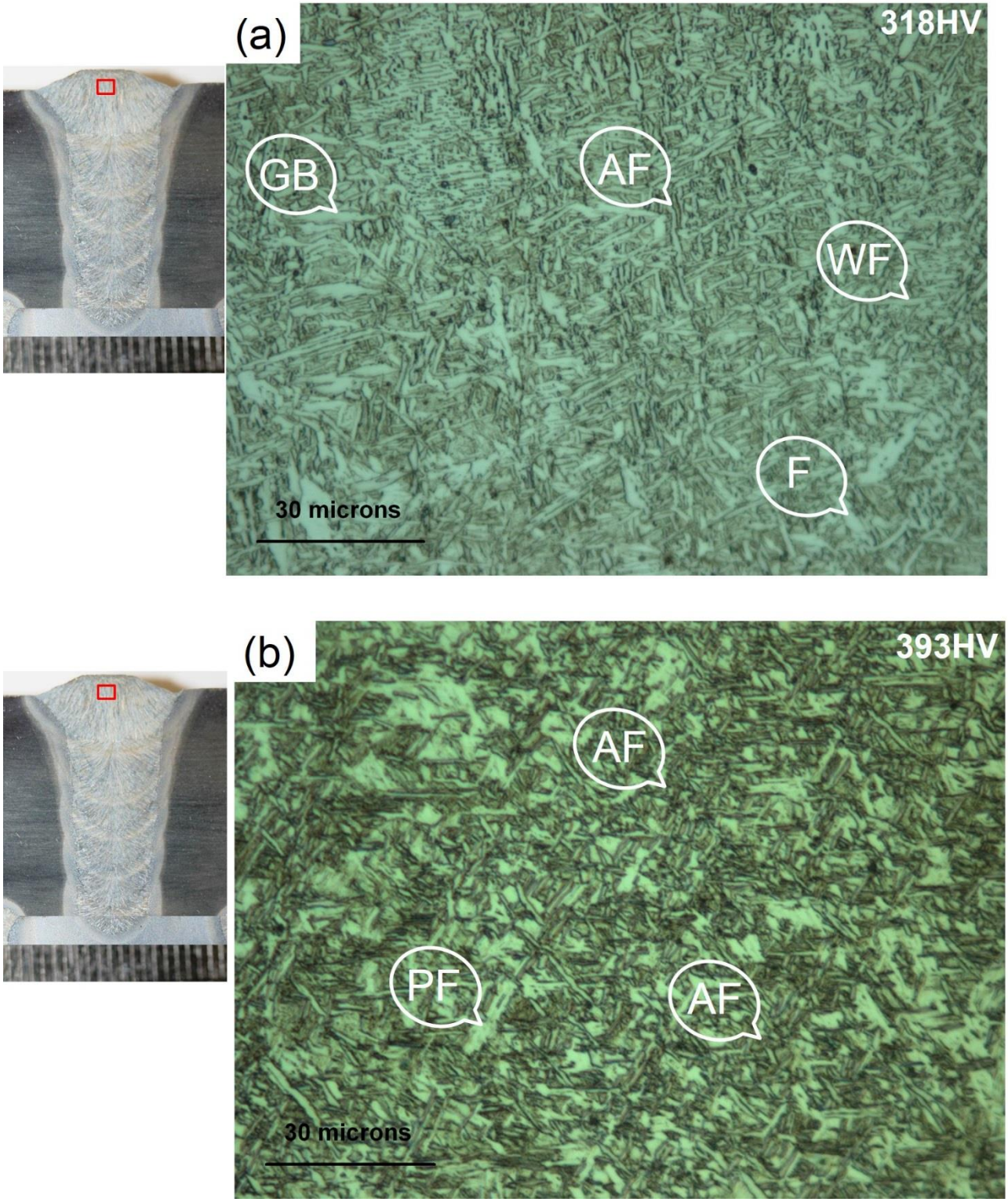

Figure 3-63: Optical micrographs at cap pass (a) as-welded (b) post weld cold rolling

Post weld cold rolling followed by laser processing shows a typical ferrite (F) and pearlite (P) structure (see Figure 3-64 (a)). For purpose of comparison, parent metal is shown in Figure 3-64 (b).

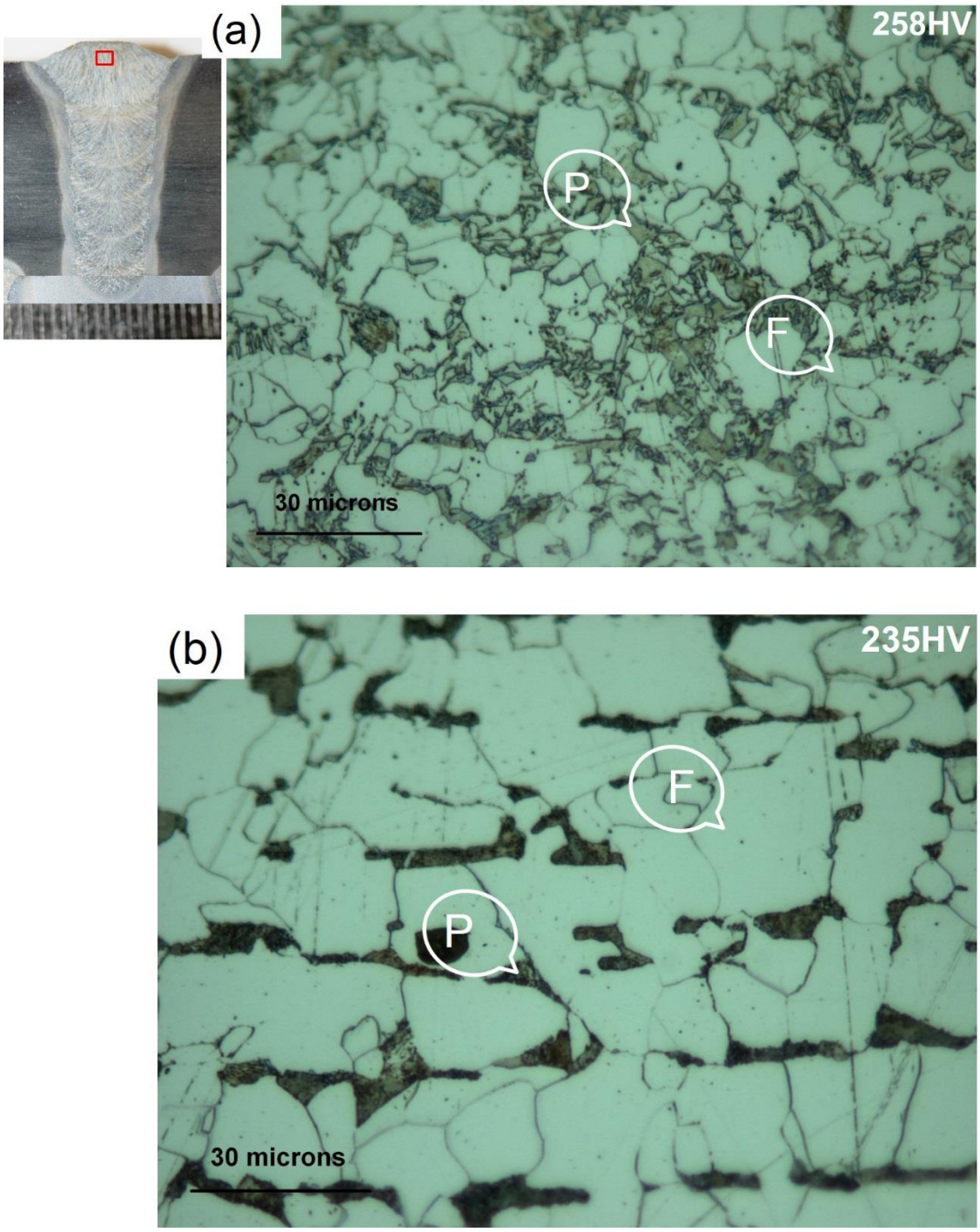

Figure 3-64: Optical micrographs at (a) cap pass of post weld rolling followed by laser processing (b) parent metal

Post weld cold rolling followed by laser processing (Figure 3-64) produce a typical ferrite (F) pearlite (P) structure. This process produced the expected coarse grained ferrite-pearlite microstructure; the coarse grains being caused by the long time at high temperatures (900ºC). As the temperature is high, phase transformation occurs and created a ferrite- pearlite structure associated with cooling of low carbon materials. Although, in most cases, pearlite regions are generally associated with the solidification boundaries, more noticeably in high heat input welds where initial segregation is probably greater.

For further analysis of grain structure, the crystallographic characteristic of the weld metal was examined with the electron back-scatter diffraction (EBSD) techniques (Figure 3-65).

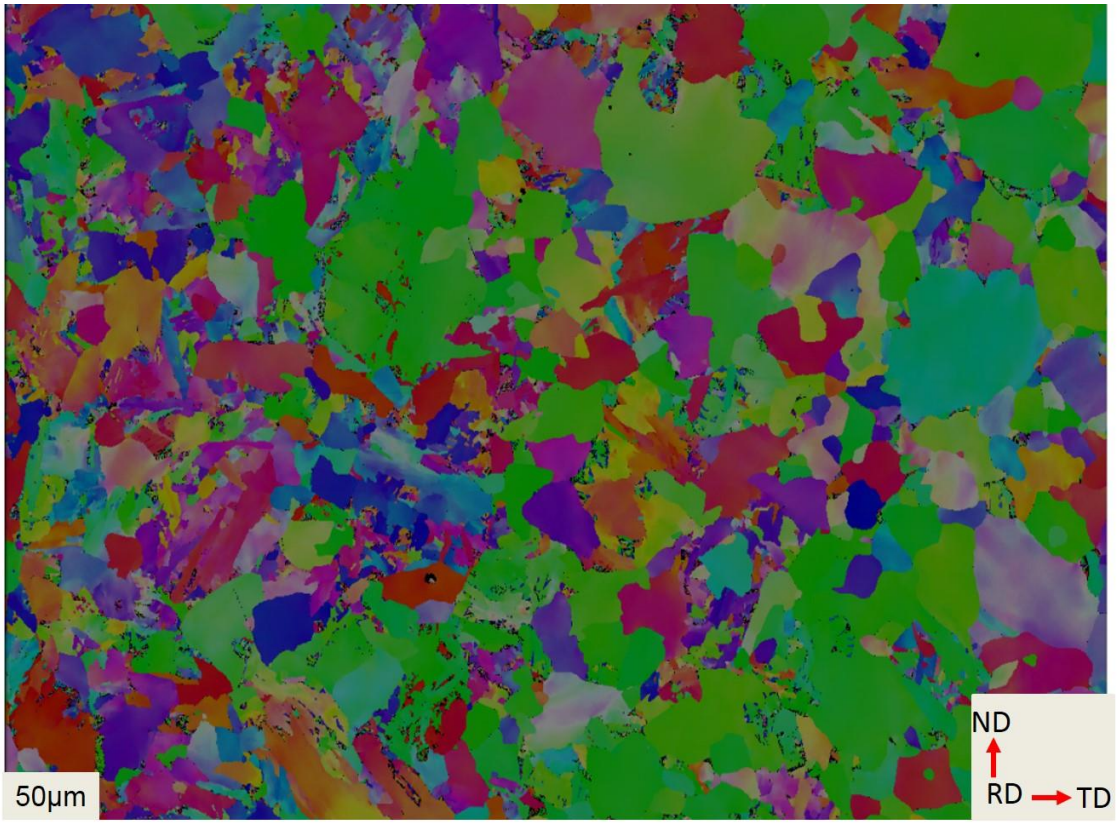

Figure 3-65: EBSD micrograph (cap pass) of post weld rolled followed by laser processing heated to 900ºC

These grain orientation maps were acquired from data produced over an area of 255 µm x 190 µm with step size 0.21 µm. The average grain size was found to

be 5.2 µm. This generation of the recrystallized microstructure with large proportion of high angle grain boundaries would increase the strength and toughness of the material which is lower in as-welded dendritic grain structures [10], [108].

3.6.2.3.4 Residual Stress

Due to the nature of heat flow in a welding process, large magnitude tensile residual stresses are formed parallel to the welding direction and close to the weld zone. In this section, the discussion is focussed on the longitudinal direction.

Figure 3-66 shows the variation in the unstressed αFe{211} lattice spacing d_0 measured, and Figure 3-67 shows the longitudinal residual stress profile analysed from the measurements of elastic strain. The transverse and normal residual stress are shown in appendix A4. The as-welded sample was not measured in this second phase but as-welded used in the first phase serves as a reference sample since the same welding parameters are used in manufacturing the weld. Post weld cold rolling presented here is to confirm it effect as stated in the first phase.

As shown in Figure 3-67, post weld cold rolling has modified the longitudinal residual stress to compressive, confirming the effect of post weld cold rolling observed in the first phase. However, post weld cold rolling followed by laser processing (measurement was taken at 3.5 mm below the weld surface) has change the compressive residual stress (155 MPa) obtained during post weld cold rolling to peak tensile stress (139 MPa). Although this effects is not surprising since the same effect were observed in the first phase of the experiment. What is noticeable here is the reduced tensile stress when compared the value obtained in the first phase. This could be attributed to the fact that, the second experiment was heated for a long period and this gives room for expansion during cooling as compared to the first phase of the experiment whose heating was on transient mode. Another possible reason is the interaction time associated with the two experiment; the first phase was heated for four seconds, whereas the second phase was heated for sixty seconds (see Figure 3-59) which is likely to be the effect.

The interaction time is calculated using equation (3-8).

$$T_i = \frac{d}{v} \tag{3-8}$$

Where d is the beam diameter and v is the travel speed.

As expected, post weld cold rolling followed by laser processing then cold rolled has changed the longitudinal residual stress state once again to become compressive around the weld metal (from peak tensile stress of 139 MPa to compressive stress of 74 MPa in Figure 3-67). The presence of this compressive stress component would likely inhibit crack propagation across the weld under longitudinal fatigue loading.

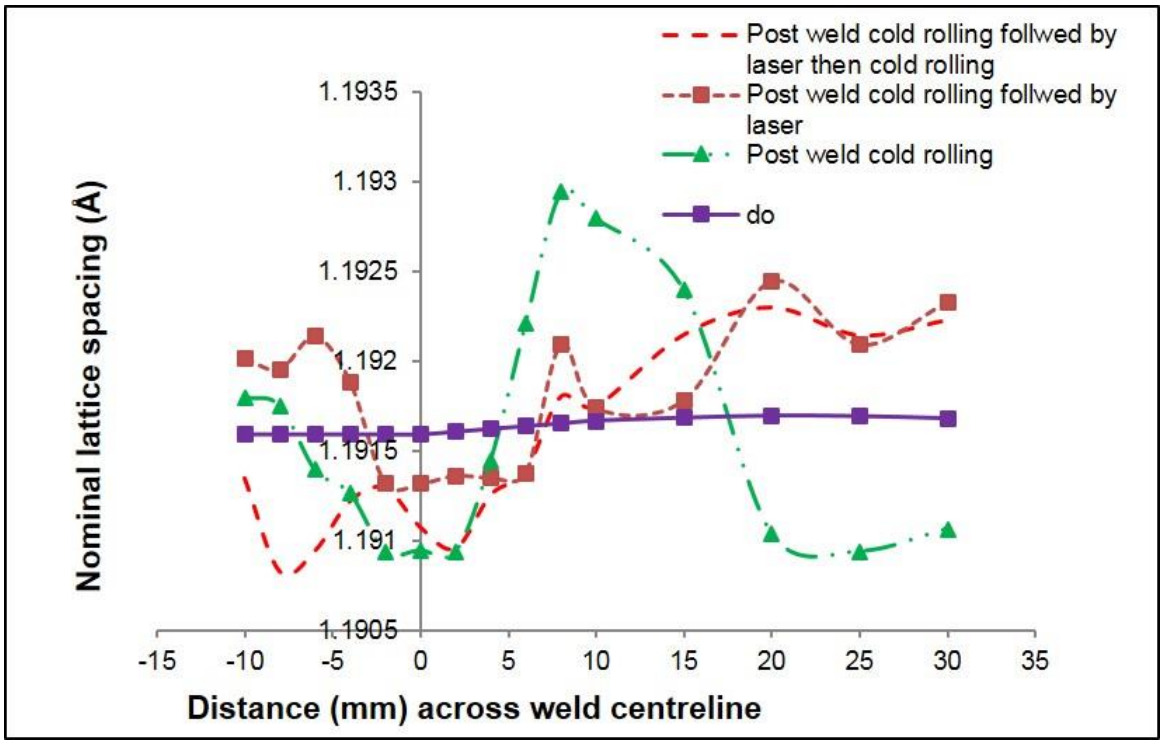

Figure 3-66 : Variation in the unstressed αFe {211} lattice spacing d0 measured (measured 3.5 mm below the top surface)

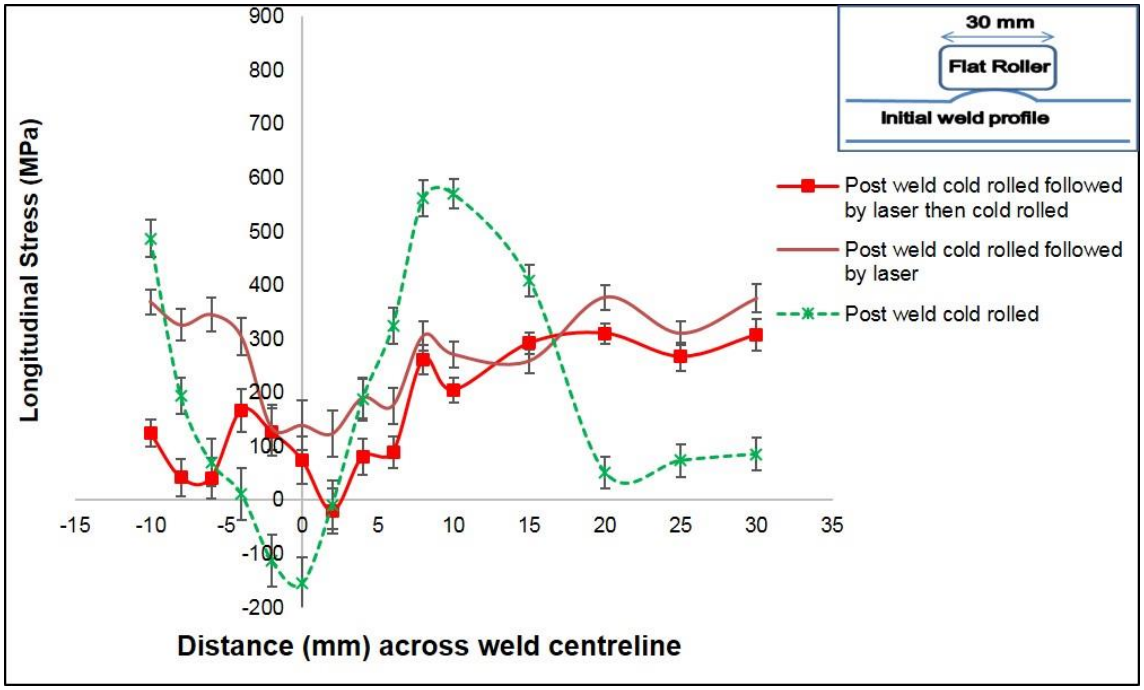

Figure 3-67 : Residual stress profile across the weld in the sample (measured 3.5 mm below the top surface)

3.6.2.3.5 Conclusion

The new laser processing in this second phase of experiment has demonstrated that full recrystallization of the grain structure and formation of new set of strain free grains can be achieved.

The cold rolling after laser processing has redistributed and eliminated the tensile residual stress state formed during laser processing of the post weld cold rolled samples observed in the first phase of this experiment.

4 Application of Local Mechanical Tensioning and Laser Processing to Refine Microstructure and Modify Residual Stress State of a Multi-pass 304L Austenitic Steels Welds

4.1 Introduction

Austenitic stainless steel types are the most widely used stainless steels which contain nominally 18% chromium and 8% nickel. This material exhibits an attractive combination of good strength, ductility, toughness, excellent corrosion resistance and good weldability [109], [110]. Due to these attributes, this type of structural alloy is used in a variety of industries such as thermal power generation, biomedical and petrochemical, automotive, and chemical engineering [111].

In this research, the experiments were also carried out in two (2) phases. The first phase of the experiment involved three steps;

i. Welding which was carried out by using Tandem GMAW DC process
ii. The post weld cold rolling in structural alloy was performed using an in-house rolling device and finally,
iii. The post weld cold rolling was followed by laser processing using 8 kW (peak power) CW fibre laser.

The laser processing in the first phase was in transient heating mode using a laser power of 1 kW with a travel speed of 0.3 m min^{-1} and laser spot dimension (beam diameter) of 20 mm. Figure 4-1 shows the schematic work flow in the first phase of the experiment. Microstructural observations, hardness scanning, tensile test and residual stress measurement were carried out after each step as shown Figure 4-1.

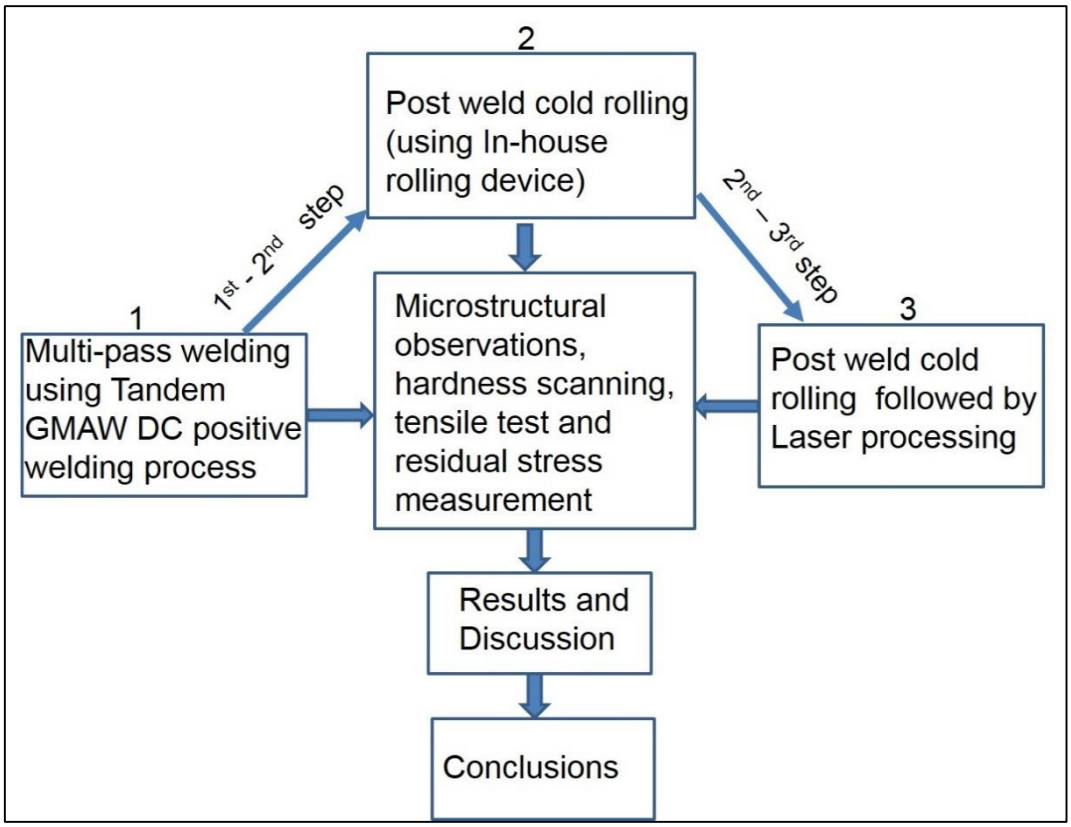

Figure 4-1: Sketch of the work flow of the first phase

4.2 Materials

AISI 304L grade of austenitic stainless steel plate (12 mm thick) was used and chemical compositions of the austenitic stainless steel plate is shown in Table 4-1.

Table 4-1: Showing chemical composition of AISI 304L austenitic stainless steel plate

Element	C	Si	Mn	Cr	P	Mo	Ni	Al	S	Cu	Nb	Ti
Wt. %	0.021	0.36	1.48	18.2	0.022	0.15	8.10	< 0.01	< 0.005	0.19	0.01	< 0.01

4.2.1 Filler Wire

The filler wire used for austenitic steel was Lincoln MIG 308L Si with a nominal diameter of 1.0 mm. The chemical composition of the filler wire is shown in Table 4-2.

Table 4-2: Showing chemical composition of austenitic steel filler wire

Element	C	Si	Mn	Cr	P	Mo	Ni
Wt. (%)	0.01	0.75	1.6	20	0.015	0.20	10

4.2.2 Shielding Gas

The shielding gas used was 98% Ar and 2% O_2 at flow rate of 30 lit min^{-1}. Weldment properties strongly depend on the shielding gas. This is because shielding gas dominates the mode of metal transfer. The GMAW process uses four basic modes (Short-circuit Transfer, Globular Transfer, Spray Transfer Mode and Pulse-Spray Transfer) to transfer metal from the electrode to the workpiece. Each mode of transfer depends on the welding process, the welding power supply, and the consumable, and each has its own distinct characteristics and applications). The choice of this gas was based on the experiment carried out by Yilmaz R. [227].

4.3 Experimental Equipment

The experimental equipment used in this structural alloy is the same as those use in API 5L X100 pipelines steel plates (see chapter 3) except for the metallographic examination.

In this case, all the welded samples were prepared for metallography on the Buehler metaserv 2000 and motopol automatic grinding machines. Four (4) grinding stages; 120, 240, 1200, 2500 grit papers were used. 6 µ diamond paste, 3 µ diamond paste and 0.05 micron colloidal silica were used for final polishing of the samples. The samples were electrolytically etched using the following condition:

i. Electrolyte used is the oxalic acid (10 g) + Distilled water (100 ml),
ii. 6 V cell voltages were used.
iii. Etching time: 60 seconds.

All the etched samples were examined using an optical microscope, energy dispersive X-ray spectroscopy (EDS) and electron back-scatter diffraction (EBSD).

4.4 Experimental Method

The experimental methods are divided into four (4) headings (that is, welding, rolling method, laser processing and residual stress experimental method) and they are presented here.

4.4.1 Welding

The dimension of the AISI 304L austenitic stainless steel plate for making the welds are 300 x 150 x 12 mm thick. However, before the actual welding, trial welds were performed. Details are presented below.

4.4.1.1 Trial: Bead on Plate of 304L Austenitic Stainless Steel Plate

Bead-on-plate was made using different welding parameters. In this trial, significant amount of information such as welding travel speed, the wire feed speed were generated as austenitic stainless steel grades are considered weldable if necessary precautions are taken into consideration. This bead on plate welds were made to purposely capture the weld bead profile before applying it on the narrow groove welds. This trial was also helpful in identifying suitable welding parameters to be used during the real multi pass welds. Figure 4-2 shows the different bead on plate trials that were made using different parameters to achieve the desired result.

Figure 4-2: Trial made on austenitic stainless steel plate

4.4.1.2 Tandem MIG Welding of Austenitic Steel Plate

Trial welds were made on narrow grooves before the actual welding. In this trial welding experiment, welding parameters such as welding travel speed, the wire feed speed as well as oscillation width, and the welding arc length were carefully examined. Figure 3-16 in chapter 3 of the thesis, shows a similar trials made on narrow groove using the two welding touch.

In austenitic stainless steel plate, the same welding preparation as that of API 5L X100 pipeline steel plate was maintained. The dimension of this sample was 300 x 150 x 12 mm. The backing bar was cut from the same material. However because of the thickness of the austenitic stainless steel plate used compare to the thickness of API 5L X100 pipelines steel plates, a total of three passes were required to fill the groove. Table 4-3 shows the welding parameters at constant CTWD (14 mm) and Figure 4-3 shows the sketch of preparation of the austenitic stainless steel plate.

Table 4-3: Welding parameters on narrow groove welds

		Lead			Trail			Heat Input		
Pass	Travel speed ($m.min^{-1}$)	Wire feed speed ($m.min^{-1}$)	Average. Current (A)	Average. Volts (v)	Wfs ($m.min^{-1}$)	Average. Current (A)	Average. Volts (v)	Lead Heat input ($kJ.mm^{-1}$)	Trail Heat input ($kJ.mm^{-1}$)	Total Heat Input ($kJ.mm^{-1}$)
Root pass	0.9	11	193.3	20.3	11	116.2	44.5	0.24	0.14	0.38
Fill 1	0.9	12	191.9	21.5	12	177.7	21.7	0.26	0.24	0.50
Cap pass	0.7	13	209.3	22.21	13	192.3	21.7	0.29	0.26	0.55

The wire feed speed (WFS) is related to wire diameter and metal deposition rate as shown in equation (4-1). The calculation of heat input is shown equation (4-2).

$$\text{Deposition } (mm^3/sec) = \text{WFS } (mm/sec) \times \text{Area of wire } (mm^2) \quad (4\text{-}1)$$

$$\text{Heat input} = (\text{Power x efficiency})/ (\text{Travel speed}) \quad (4\text{-}2)$$

The efficiency used in this research is 80% of the total heat input according to Kou, S [10].

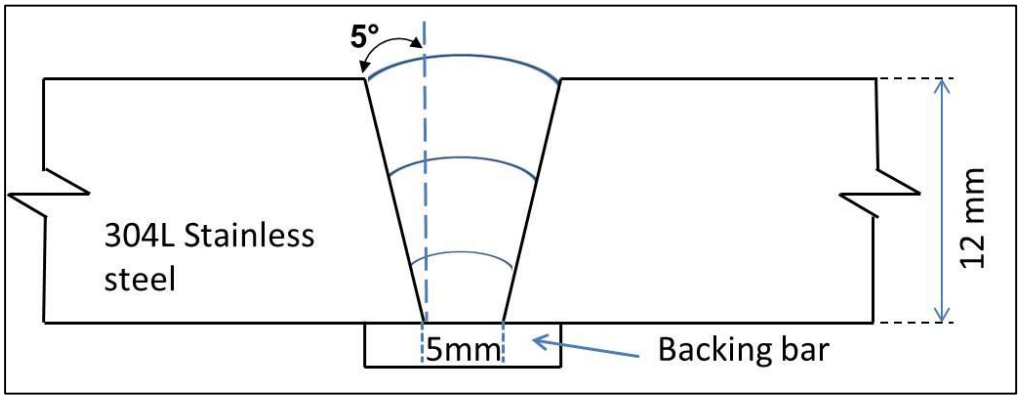

Figure 4-3: 304L stainless steel plate set-up with backing bar

4.4.1.3 Experimental Error in Tandem MIG Welding of Austenitic Steel Plate

The same source of error as shown in section 3.4.1.4 of the thesis.

4.4.2 Local Mechanical Tensioning (Cold Rolling)

4.4.2.1 Post Weld Cold Rolling of 304L Austenitic Stainless Steel Plate

After the different trials described in section 3.4.2.1, a rolling load of (100 kN) was applied and the same principle as in section 3.4.2.2 was used. The lower rolling load of 100 kN was used instead of 150 kN used in API 5L X100 pipeline steel plate due to ductile nature of the material which make it easier to deform. Hence, using high rolling load in this material can create a friction between the roller and weld metal. The deformity ability of austenitic steel is higher than the ferritic steel because of the greater number of active slip planes in austenitic steel. In other words, lattice structures with closely packed planes (austenitic steel) allow more plastic deformation than those that are not closely packed (ferritic steel) [141].

4.4.2.2 Experimental Error in Local Mechanical Tensioning (Cold Rolling)

The sources of errors stated in section 3.4.2.3 are also applicable in this structural alloy. In addition, the rolling load used can constitute source of error. For example, high rolling load create ripple and cumulate weld in front of the roller due to ductile nature the material thereby impede the rotation of the roller.

4.4.3 Laser Processing of 304L Austenitic Stainless Steel,

The same principle of laser processing used in section 3.4.3.1 was applied in this structural alloy. However, unlike the laser power of 3 kW used in section 3.4.3, the transient heating mode using a laser power of 1 kW with a travel speed of 0.3 m min^{-1} and laser spot dimension (beam diameter) of 20 mm was used. The choice of this laser parameter is explained in results and discussion section (section 4.5).

4.4.3.1 Experimental Error in Laser Processing of 304L Austenitic Stainless Steel

The sources of error stated in section 3.4.3.2 are also used in this structural alloy.

4.4.4 Method of Residual Stress Measurement of 304L Austenitic Stainless Steel,

SALSA neutron diffractometer at the Institut Laue Langevin in France was also used to measure the residual elastic strain. In this structural alloy, measurements were made at the centre of the cross-sectional plane of 200 mm sample (plane PQRS) as shown in Figure 4-4 with the assumption that, the stress state at the centre of the sample represent the original weld samples. The coordinate axes L, T and N shown in Figure 4-4, represents the longitudinal direction, transverse and normal direction respectively.

The lattice spacing (d) of austenite {311} family of crystallographic plane was chosen for measurements of all the principal strain directions, since this plane gives the macroscopic average strain over the measured gauge volume [19]. The measurements were made using a neutron incident beam of 1.62 Å wavelength, which gives a diffraction angle (2Θ) of 95.99^{o}. A through-thickness scan was used to position the gauge volume accurately. In longitudinal measurements, the gauge volume of 2 × 2 × 2 mm^3 was used to achieve the desired spatial resolution. In transverse and normal directions, the gauge volume of 2 × 20 × 2 mm^3 was used in measurements. The increase in gauge volume along the welding direction was with assumption that the stress state would remain the same over the length of the welds. Increase in gauge volume result in more grain sampling leading to reduction in counting times for transverse and normal

measurements. The measurements were taken at 2, 6 and 10 mm below the weld surface.

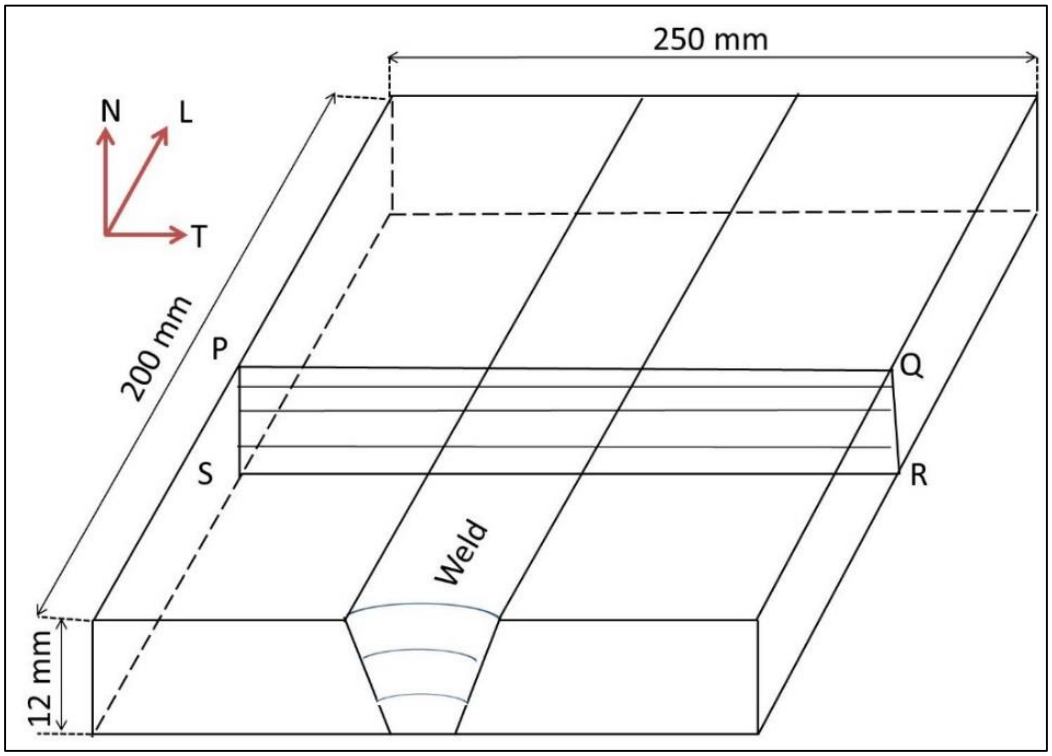

Figure 4-4: Schematic diagram of the multi-pass welded sample

The stress-free lattice spacing was also measured using comb of dimension 6 mm x 6 mm x 5 mm samples machined out by electrical discharge machining (EDM). This comb dimensions are assumed to be small enough to relax any macroscopic stress within the comb. Figure 4-5 and Figure 4-6 shows how the comb samples were machined.

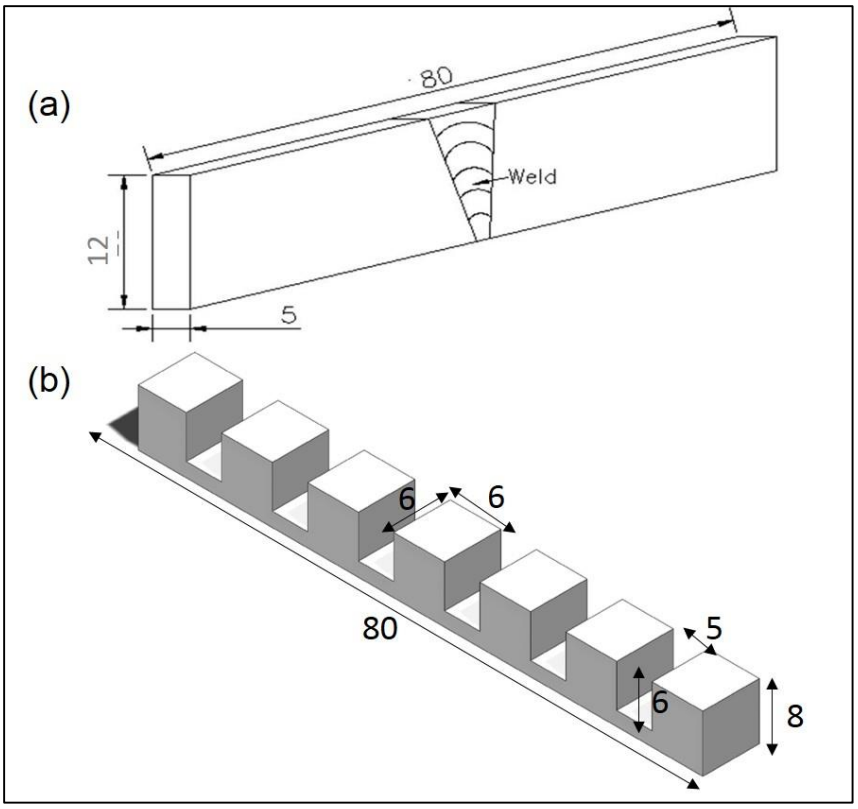

Figure 4-5: Sketch showing (a) side view (b) Comb

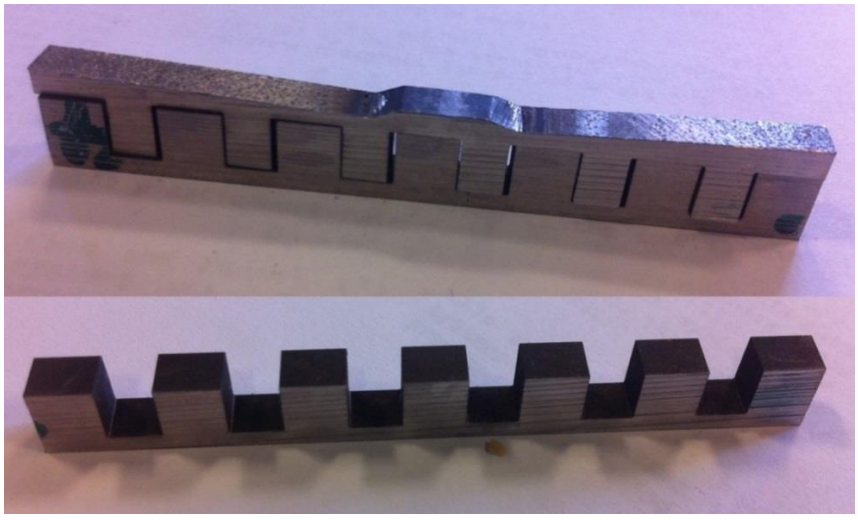

Figure 4-6: Electrical discharge machining (EDM) of (d_0)

The stress-free lattice spacing (d_0) measurements were taken in the three directions corresponding to the sample coordinate axes, and these values were interpolated to yield representative (d_0). Data from the measurements were

analysed using LAMP software. LAMP has an in-built Gaussian fitting routine which was used to fit the raw data and determine the peak position precisely.

Note that, to have good spatial resolution, appropriate gauge volume must be defined. However, as shown in Figure 4-7, the gauge volume are defined by incident and receiving collimators and the neutrons were counted in a position sensitive detector (PSD). Measurements of strain components along the principal directions (longitudinal, transverse and normal) were made by an alignment of the sample. This is necessary so that the corresponding direction was along the scattering vector as indicated in Figure 4-7 [171], [228].

It worth mentioning here that the scattering vector is the bisector of the primary (beam into sample) and secondary (beam out of sample) neutron beams and must be aligned with the strains in the direction being measured.

The same equations used in calculating the strain and the stress stated in section 3.4.4.1 were used in this section, using the elastic constants values of E= 200 GPa and υ = 0.29 [229].

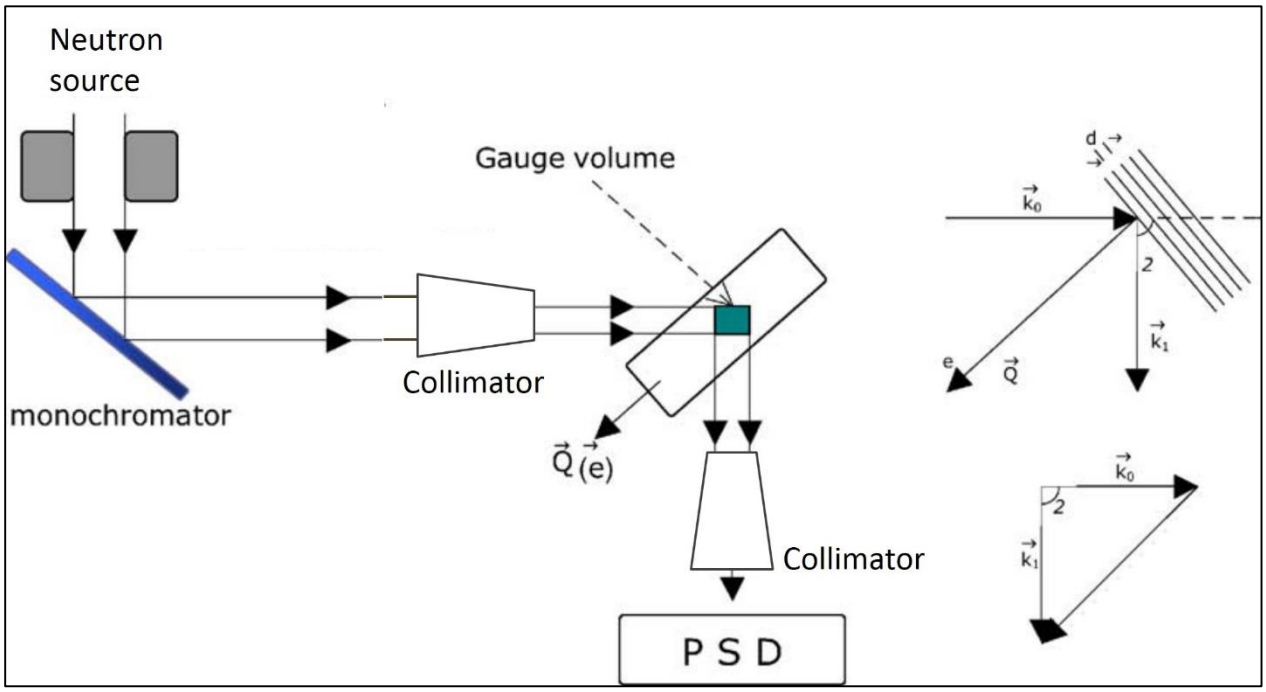

Figure 4-7: Sketch of strain measurement

Figure 4-8 shows the longitudinal measurement of the austenitic stainless steel.

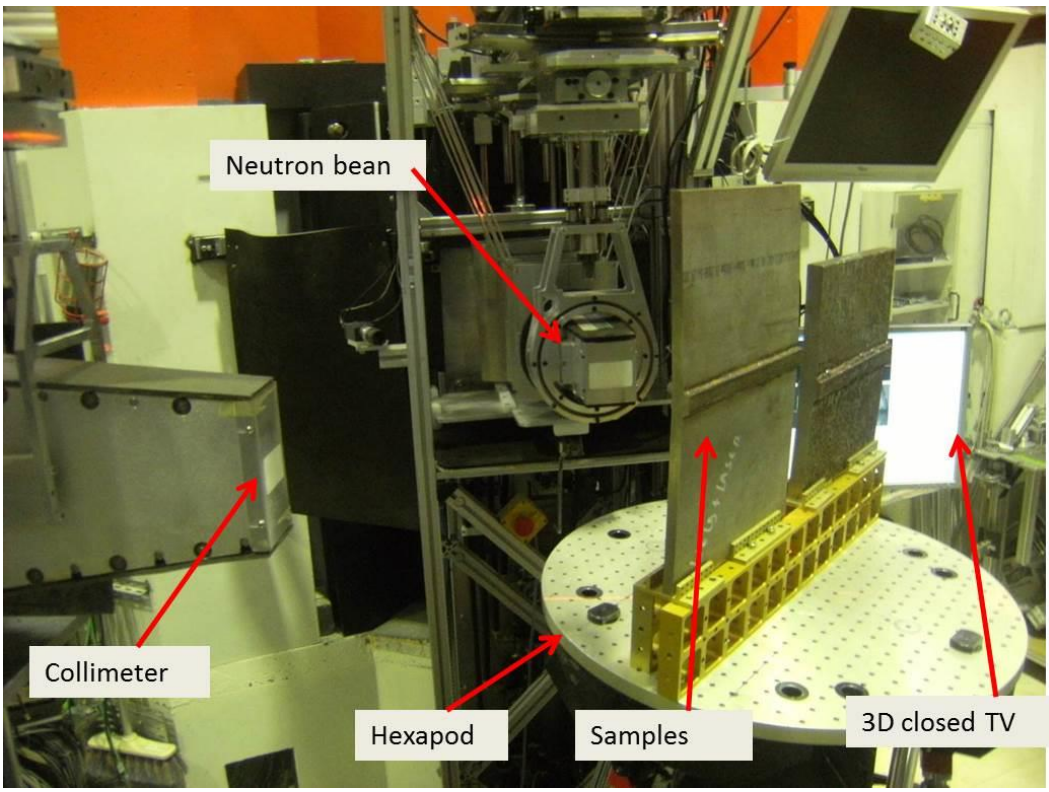

Figure 4-8: SALSA set-up (longitudinal measurement of the austenitic stainless steel)

4.4.4.1 Full Width at Half Maximum

The same principle applies as explained in section 3.4.4.1.2.

4.4.4.2 Experimental Error in Residual Stress Measurement of 304L Austenitic Stainless Steel,

The same source of errors which occur in section 3.4.4.2 applies in this section.

4.5 Results and Discussion

This section present the results and discussion from the experiments conducted in first phase of this research with their interpretations. Direct and indirect comparisons with earlier research works were also made.

4.5.1 Welding

4.5.1.1 Tandem MIG Welding

The result of the trials made on narrow groove shows that too wide or small oscillation width can result in the following weld defects;

i. Instability and undercut of the welds.
ii. Lack of sidewall fusion.

Welding travel speed influences the heat input and weld pool flow. Hence, increasing the weld travel speed lowers the heat input in the weld as vice versa. However, excessive speeds also result in incomplete fusion into the sidewall due to insufficient heating of the wall. Figure 4-9 shows the welding parameters used on this structural alloy.

Cranfield UNIVERSITY

Welding process	Tandem GMAW DC +ve
Welding position	1G
Material Grade	304L Stainless steel plate
Thickness	12 mm
Electrode Wire	ϕ = 1 mm
Brand	MIG 308L Si
Preparation	Saw cut
Backing System	304L Backing Strip
Cleaning Method	Wire Brush or Grinding
Shielding Gas	98%Ar - 2%O_2
Flow rate	30 L/min

Designer: Jibrin Sule

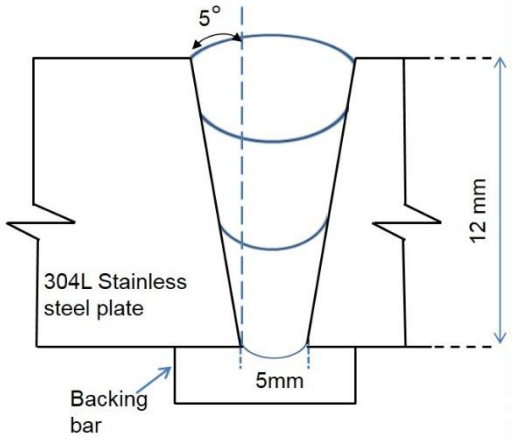

Pass	Travel Speed (m/min)	Lead			Trail			Oscillation		CTWD (mm)
		WFS (m/min)	Amps (I)	Volts (V)	WFS (m/min)	Amps (I)	Volts (V)	Freq. (HZ)	Osc. width	
Root pass	0.9	11	218.9	21.1	11	216.1	21.0	350	90	14
Fill 1	0.9	12	232.3	21.9	12	230.3	22.3	350	190	14
Cap pass	0.7	10	222.5	23.5	10	219.8	23.9	350	400	14

Figure 4-9: Welding parameters used for 304L stainless steel plate

4.5.1.2 Hardness on As-Welded Sample

Figure 4-10 shows the effect of the passes on the weld metal. In this figure, the root pass showing higher hardness compare to cap pass suggesting thermal straining by successive passes.

As show in Figure 4-10, during welding and subsequent cooling of material, residual stresses are generated in weldments due to differential heating and cooling rates [109],[151]. When this material is cooling after welding, the stresses generated may exceed the yield strength, causing plastic deformation and work hardening in the weld metal. Since the root regions experience more thermal cycles than any other region, they undergo more thermal straining. The enhanced plastic deformation in the root regions is responsible for the high hardness values observed in the root pass. The increase in hardness at the root pass (as-welded) could also be attributed to increase in chromium content in weld metal which is about 20.43 wt % at the root pass (the root pass weld metal in this research was analysed using EDS), since high chromium content combining with niobium presence in the weld metal increases solid solution strengthening.

HAZ in the as-welded sample is also harder than the base metal. This is due to the strain-hardening of the HAZ.

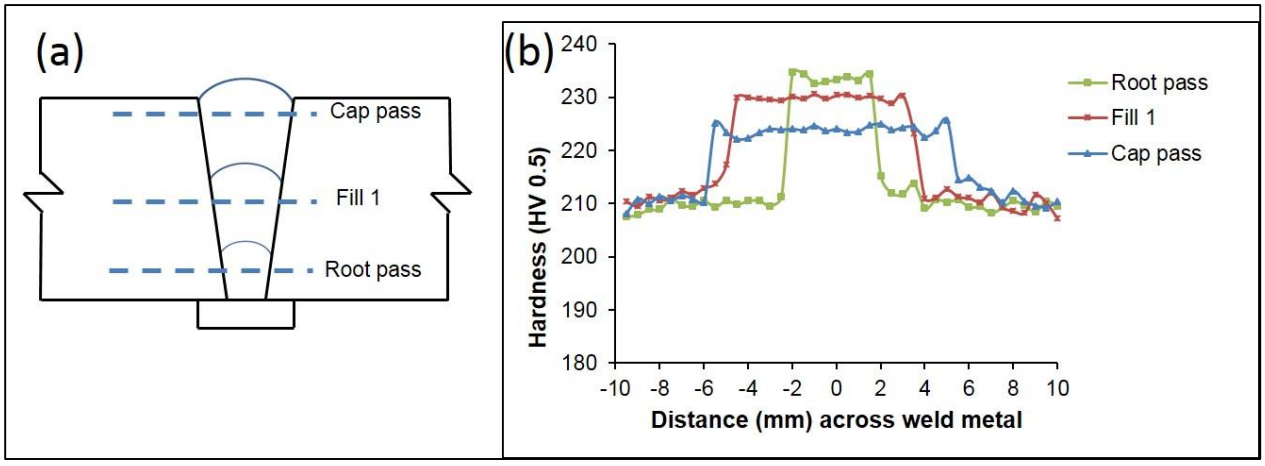

Figure 4-10: Hardness profile of 304L austenitic steel (as- welded) across the weld metal

4.5.2 Post Weld Cold Rolling

The rolling load of 100 kN was used based on the reason(s) stated in section 4.4.2.2.

4.5.2.1 Effect of Post Weld Cold Rolling on Hardness Profile

A hardness scan was performed from the cap pass to the root pass as shown in Figure 4-11, while Figure 4-12 shows the hardness scan across the weld metal. The effect of cold working was observed throughout the entire thickness of the material when a load of 100 kN was applied (Figure 4-11). Up to about 4 mm below the cap, the effect was very significant. The effect of cold working observed throughout the entire thickness of 304L stainless steel could be attributed to the closely packed crystal structure and large number of active slip systems in the FCC alloy.

Hardness in the weld metal can also be because of formation of strain-induced martensite as result of cold deformation. Although a number of researches have been carried out on the formation of martensite in stainless steels as a result of cold working [230], [231],[232], it was not clear in literature about the amount of plastic deformation that could introduce martensite in stainless. However, in this research, it can be deduced that cold working is mainly responsible for the increase in hardness of the weld metal.

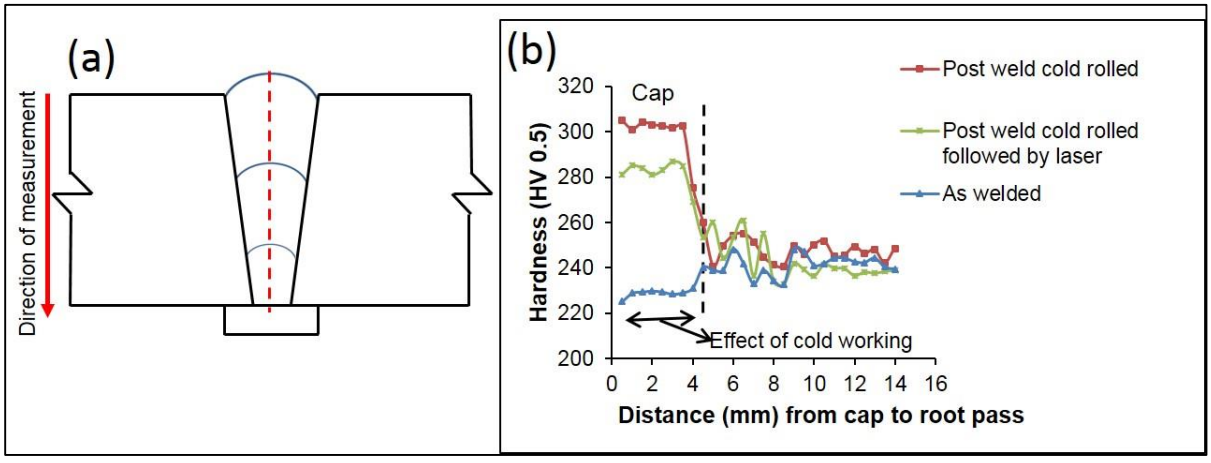

Figure 4-11: showing (a) hardness scan position along the weld metal (b) hardness profile

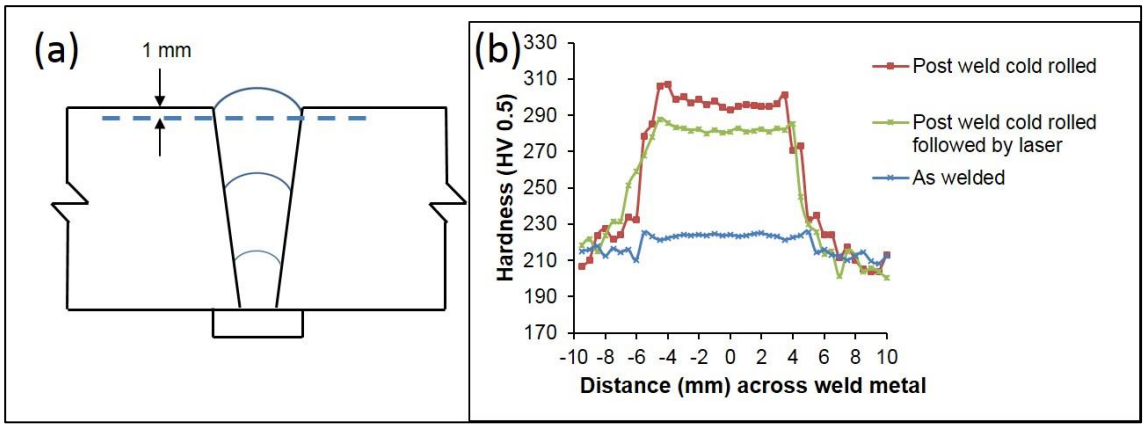

Figure 4-12: (a) hardness scan position across the weld (b) hardness profile

4.5.3 Post Weld Cold Rolling Followed by Laser Processing

Different trials were made using different laser power combined with different travel speed before the appropriate laser parameters were used. Figure 4-13 shows thermal cycles of a travel speed combined with different laser powers at constant beam diameter. Other trials are shown in appendix B.1.1.

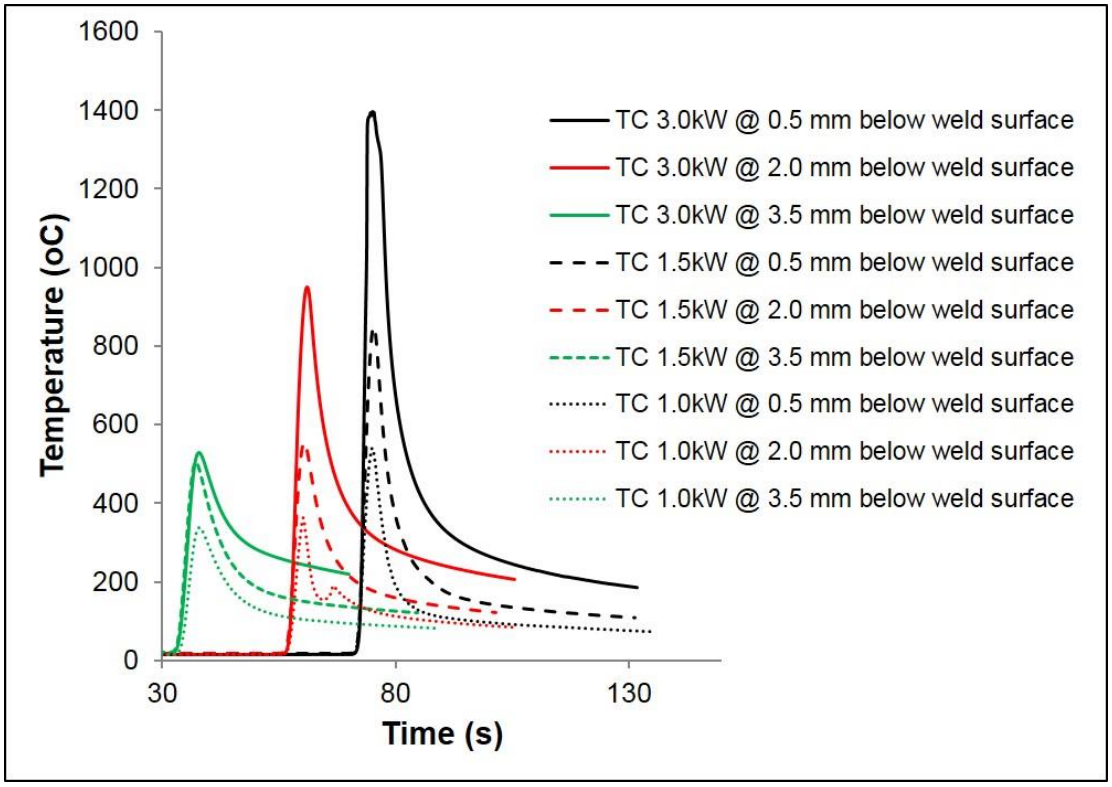

Figure 4-13: Thermal cycles of laser powers of 1.0 kW, 1.5 kW and 3.0 kW with travel speed of 0.3 m.min^{-1} at constant beam diameter of 20 mm

Laser power of 1.0 kW with the travel speed of 0.3 m.min^{-1} was used (Figure 4-13). As shown in the figure, the peak temperature of the 1.0 kW at 0.5 mm below the weld surface using a travel speed of 0.3 m.min^{-1} was approximately 537^{o}C (810 K). The selection of the temperature also based on the fact that: the recrystallization temperature of metal or alloy is reported to be between one-third and one-half of it absolute melting temperature (1540^{o}C for steel) [141].

4.5.3.1 Effect of Post Weld Cold Rolling Followed by laser processing on Hardness Profile

The application of the laser after post weld cold weld rolling shows a decrease in hardness values (307HV to 280HV) at the cap pass (Figure 4-11). This diminished hardness value could be attributed to changes in microstructural phases as result of the applied thermal energy. Although, the thermal energy applied was not sufficient to supply enough energy to sustain a complete recrystallization kinetic as it was evident in the change in grain sizes measured (see Figure 4-19).

4.5.4 Tensile Strength

Figure 4-14 shows the all weld metal tensile tests taken close to the capping pass.

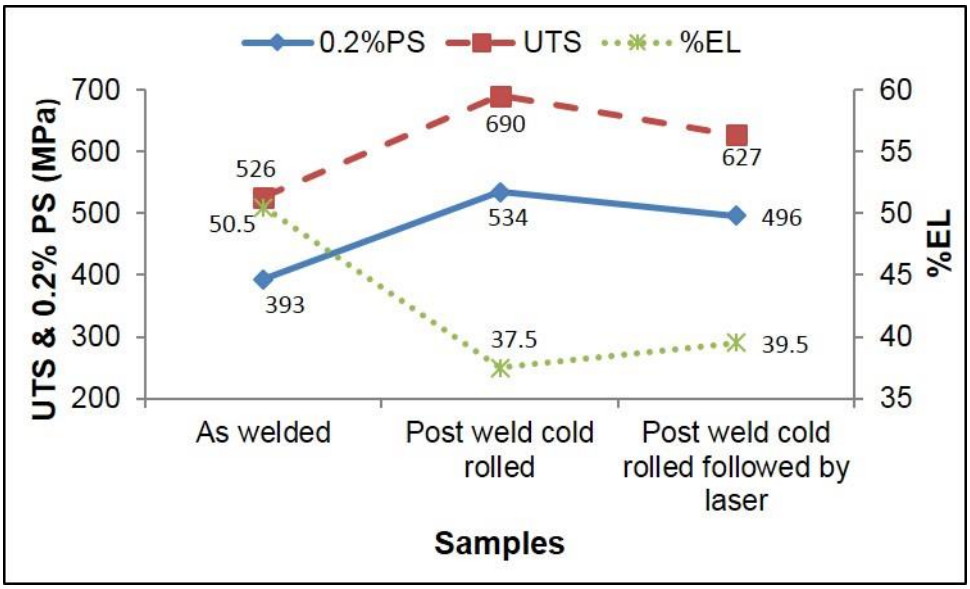

Figure 4-14: 304L Austenitic steel tensile test close to the capping pass

4.5.4.1 Effect of Post Weld Cold Rolling on Tensile Strength

Figure 4-14 shows both ultimate tensile strength (UTS), 0.2% proof strength (PS) and percentage elongation (%EL). Post weld cold rolling increase both PS and UTS, and decreases the ductility (%EL). As shown in Figure 4-14, post weld cold rolling brought about 35% increase in proof strength (393 MPa to 534 MPa) with corresponding reduction in percentage elongation (50.5% to 37.5%) in the fusion zone. Of course one of the main mechanism by which plastic deformation takes place is the movement of dislocations by slip planes. The post weld rolling increases dislocation density which restricts the slipping of dislocations. In other word, plasticity of the material reduces due to cold working. This results in lowering of ductility and increase the strength.

4.5.4.2 Effect of Post Weld Cold Rolling Followed by Laser Processing on Tensile Strength

As shown in Figure 4-14, Post weld cold rolling followed by laser processing brought about a decrease in proof strength (534 MPa to 496 MPa) and slight increase in percentage elongation (37.5% to 39.5%). This indicates that some of the stored internal strain energy was relieved as a result of enhanced atomic diffusion at higher temperature. An effective indication of recrystallization can be drop in proof strength [139] due to releasing of internal energy; the higher the amount of prior deformation, the lower the temperature to initiate recrystallization, as the activation energy gap needed to initiate recrystallization would be less.

4.5.4.3 Yield/Tensile Ratio

As stated earlier, PS/UTS is only a convenient means of expressing a material's ability for plastic deformation. Thus, other related characteristics should also be considered. For instance, the interaction between strain hardening, toughness, ductile tearing resistance, and overall global deformation needs to be considered, especially when assessing the practicality of using the PS/UTS ratio as a measure of plastic strain capacity of cracked components.

The PS/UTS ratio obtain in this research is within acceptable limits as it was reported that present design codes permit the PS/UTS ratio to vary between 0.70 and 0.93 [233].

4.5.5 Metallographic Examination

The macrostructure and microstructure of the 304L austenitic stainless welds are presented here.

4.5.5.1 Macro Structures of the Welds

Figure 4-15 shows macrographs of the three samples. All the macrographs show an excellent weld with good penetration and good side wall fusion and porosity free welds. These could be attributed to the proper use of shielding gas and maintenance of the correct CTWD which was vital in ensuring a stable metal transfer of the correct arc length.

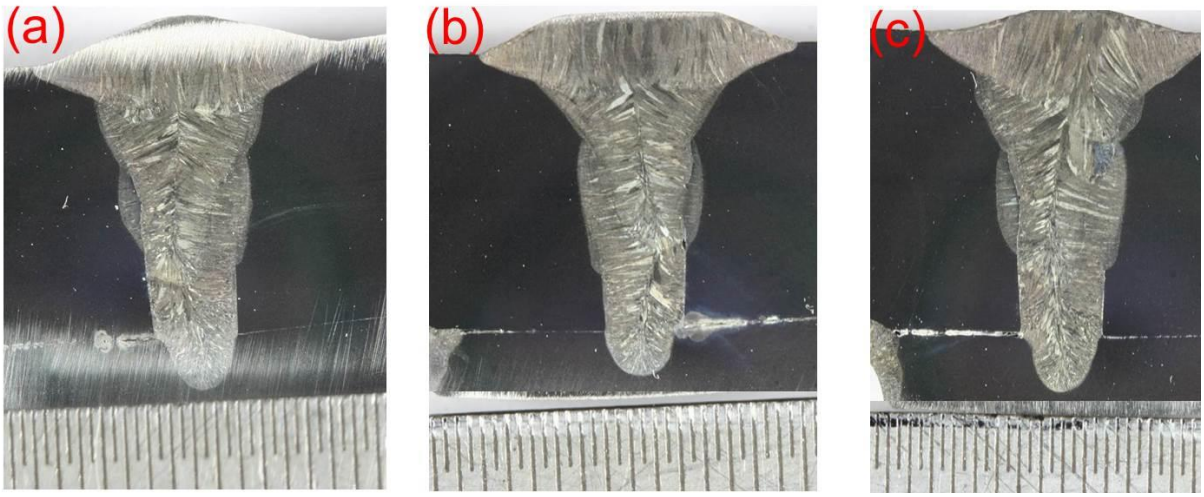

Figure 4-15: Macrographs of weld bead profiles of 304L austenitic steel (a) as-welded (b) post weld cold rolled (c) post weld cold rolled followed by laser processing

4.5.5.2 Micro Structures of the Welds

4.5.5.2.1 Optical Microstructures

Figure 4-16 shows the optical microstructures of the capping pass of the three samples consist of austenite and ferrite structures. These structures are as a

result of both the solidification behaviour and subsequent solid-state transformations which are controlled by both composition and weld cooling rates. Under normal conditions, austenitic stainless steels will exhibit a single phase that is maintained over a wide temperature range. However, austenitic microstructure containing a small amount of ferrite is less crack (solidification cracking) sensitive compared to a fully austenitic microstructure [112]. Figure 4-16 (a), shows a dendritic and columnar grains structure. This is attributed to the fact that, during solidification of the weld metal, grains tends to grow in the direction perpendicular to pool boundary. This dendritic solidification of the weld metal often leads to segregation of alloying elements within the grain structures which would result in formation of localised region with reduced corrosion protection. It was also reported that columnar growth influences mechanical properties [30] and microstructural features, such as microsegregation [31]. The post cold rolling shown in Figure 4-16 (b) has modified the grain structure. It was observed that the deformation cause by cold rolling does not initiate any measurable transformation. This is because austenite is a stable phase and the cold working did not bring any change in temperature.

Post weld cold rolling follower by laser resulted in refining the grains as shown in Figure 4-16 (c). This refine grains would increase the strength and toughness of the material which is lower in the as-welded state due to the formation of dendritic grain structure.

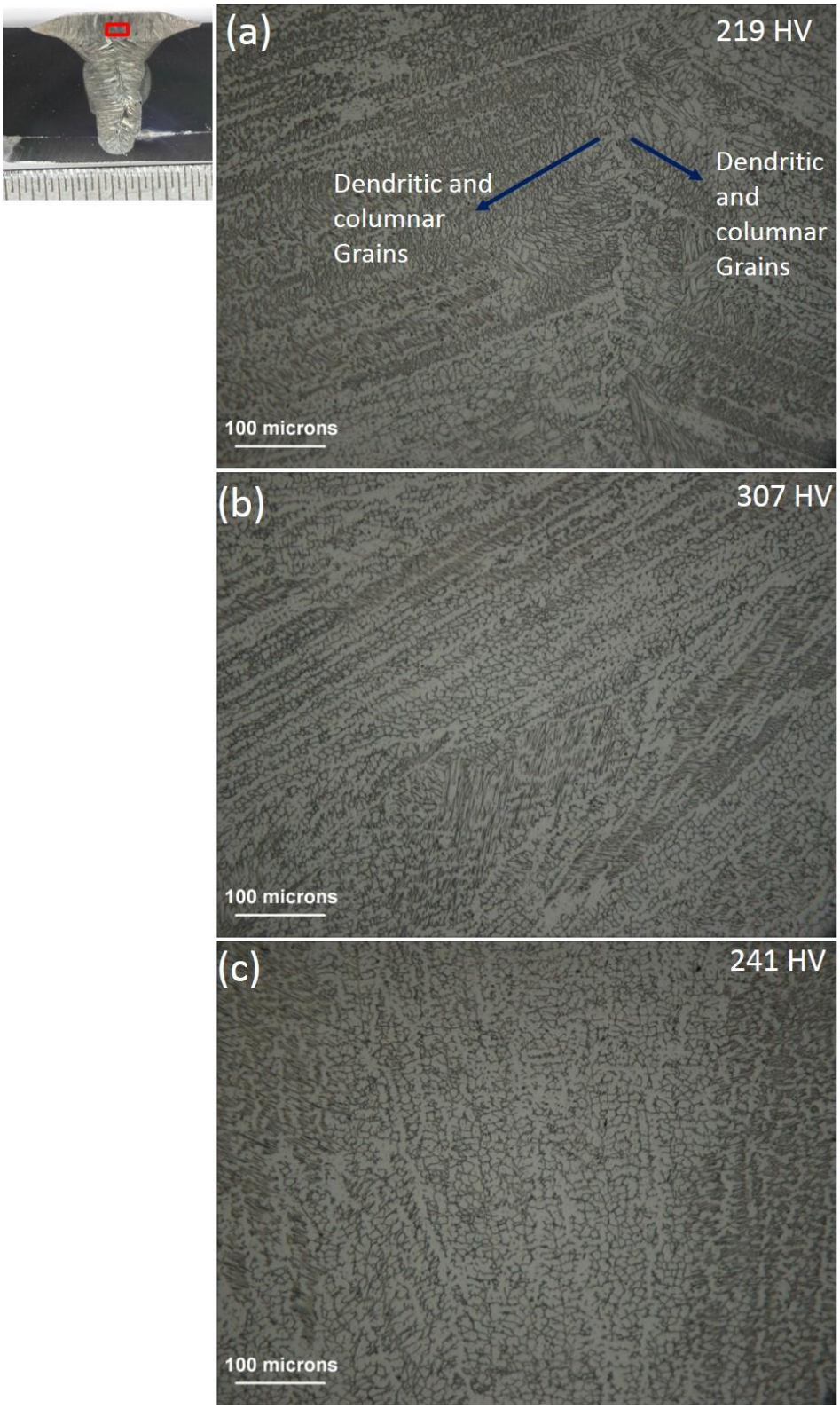

Figure 4-16: Optical micrograph of 304L stainless steel at the cap pass (a) As-welded (b) Post weld cold rolling (c) Post weld cold rolling followed by laser

4.5.5.2.2 Micrographs by Electron Backscatter Diffraction (EBSD)

For further analysis of the grain structure, the crystallographic texture of weld metals were obtained by EBSD. The pole figure plots are shown in Figure 4-17 and Figure 4-18. These textures were acquired from data obtained over an area of 316 µm x 234 µm with step size 0.73 µm. It is important to emphasize that the grid step size limits the size of the structure elements that can be analysed using EBSD. However, based on the step size used, the average grain size of the as-welded sample was 14.81 µm at cap pass. When the rolling load was applied on the same position, the average grain size was found to be 19.78 µm, similarly an average grain size of 11.00 µm was found when post weld cold rolling followed by laser processing was applied on the sample at the same position (Figure 4-19). Among many other factors, the grain boundary area poses as one of the major obstacles for movement of dislocations. Although, there are no significant changes in the grain sizes, the reduced grain size (11.00 µm) in laser processed samples would, therefore, have the potential to improve the strength and toughness of the weld metal and also limit Cr segregation which would result in formation of corrosion microcells. It was also evident that in as welded sample, the grain size increase from root pass to cap pass. The root pass, fill 1 pass and the cap pass have the grain sizes of 4.20 µm, 10.37 µm and 14.81 µm respectively (Figure 4-20). This could be attributed to the fact that thermal cycles from subsequent passes refine the grains from the previous pass. It can be added that subsequent passes have a stress relieving effect on the previous pass, thereby relieving residual stresses from the previous passes.

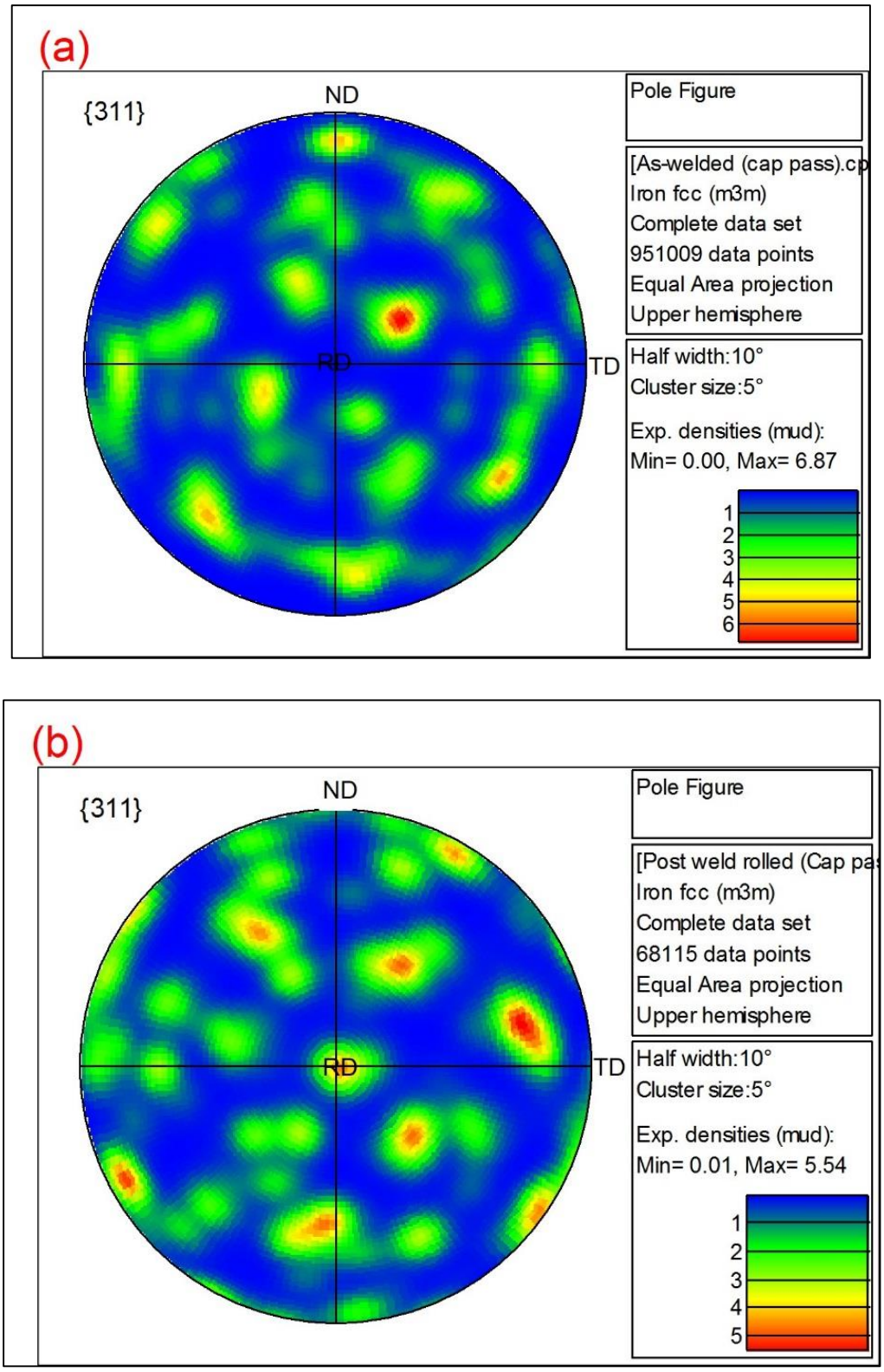

Figure 4-17: Pole figure of the cap pass (a) as-welded (b) post weld cold rolling

Figure 4-18 shows the pole figure of the post weld cold rolling followed by laser processing at cap pass.

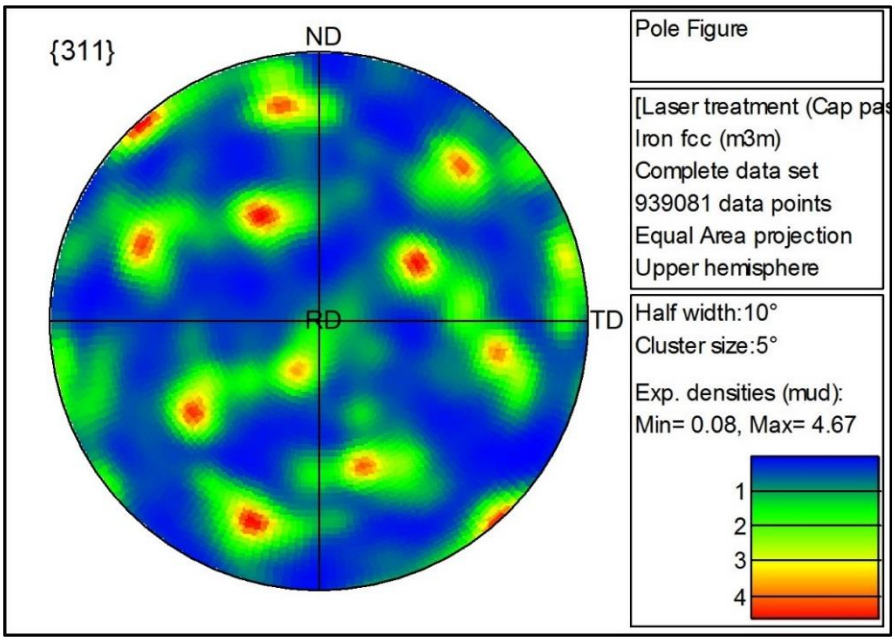

Figure 4-18: Pole figure of the post weld cold rolling followed by laser processing at cap pass

Figure 4-19 shows the average grain size at different processing condtions. the post weld cold rolled followed by laser processing has a reduced grain sizes.

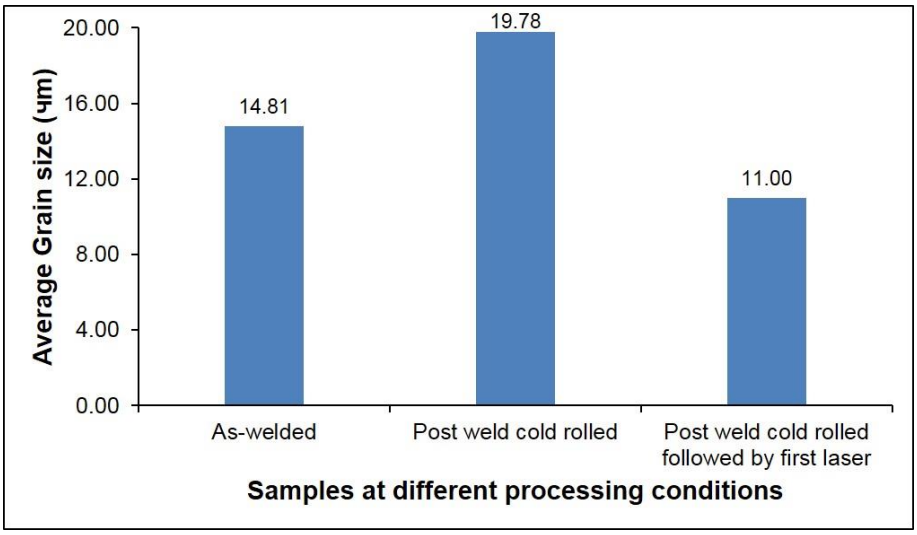

Figure 4-19: Showing the average grain size at different processing conditions

Figure 4-20 shows the average grain size of the as-welded sample. As shown, the grain sizes increases from the root pass to cap pass.

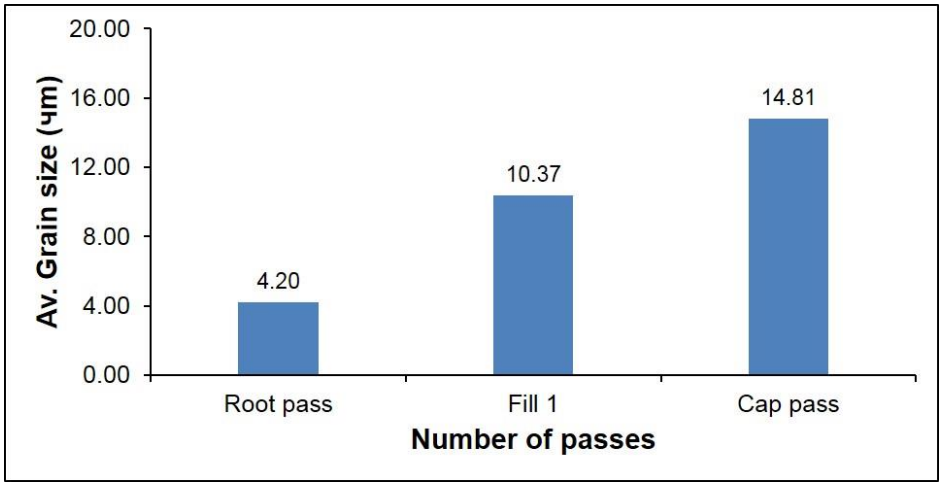

Figure 4-20: Showing the average grain size of each pass in the as-welded sample

4.5.6 Residual Stress Measurement

The reference parameter variation as measured in the comb samples, for the longitudinal directions as observed by monochromatic neutrons at the ILL in France is shown in Figure 4-21.

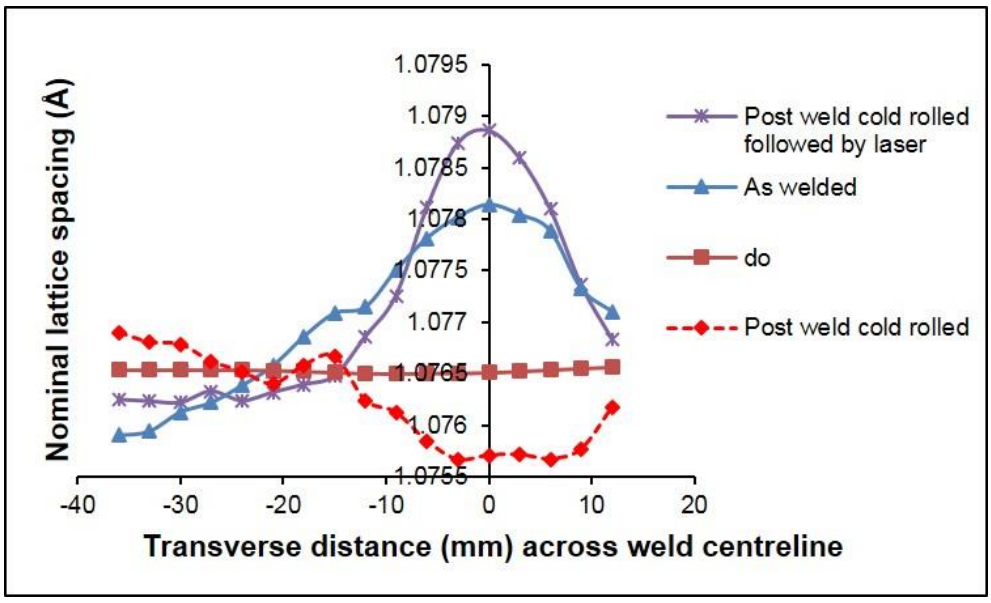

Figure 4-21: Variation in the unstressed austenitic {311} lattice spacing d0 measured (measured at 2, mm below the top surface)

The variation in residual stress distribution across the weld metal at 2 mm below the weld surface is shown in Figure 4-22. These are the longitudnal residual stress(σ_{xx}) distribution showing tensile stresses close to the weld centreline and slightly compressive further away from it to balance the tensile stress. The discussion here is focussed on the longitudinal direction due to the fact that the largest residual stresses are expected parallel to the welding direction. However, transverse and normal direction are presented for purpose of comparison in the different processing conditions.

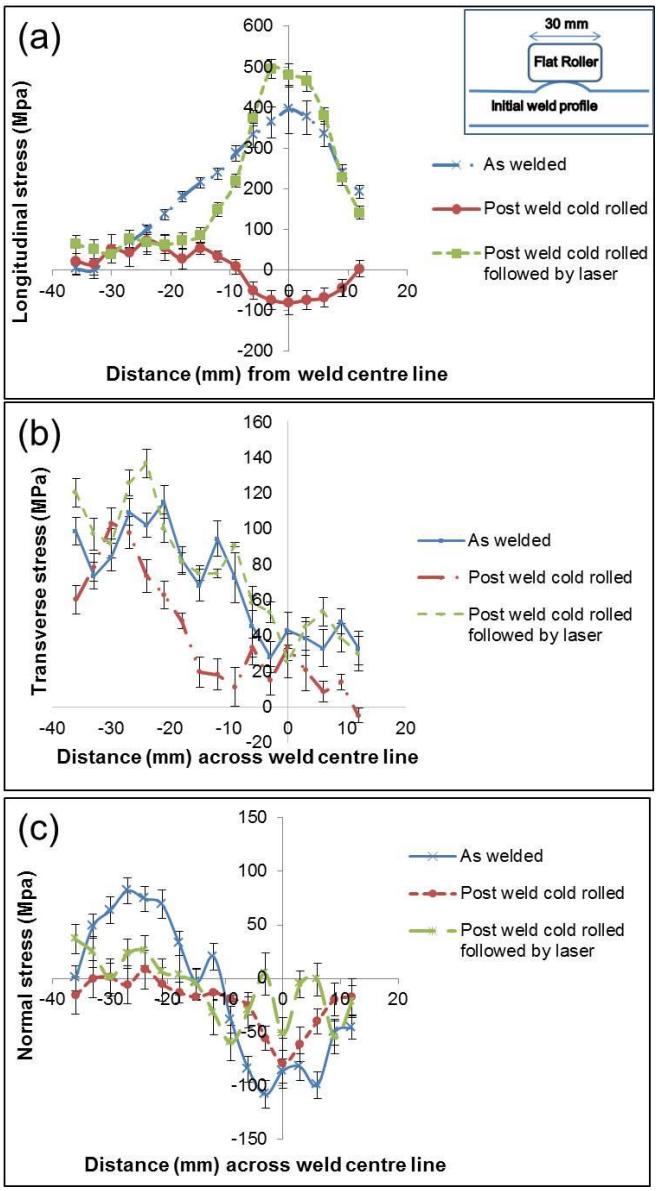

Figure 4-22: Residual stress profile across the weld metal with different processing conditions (a) Longtudinal (b) Transverse (c) Normal direction

4.5.6.1 Effect of Post Weld Cold Rolling Through the Thickness

A flat roller of 30 mm width was used, which determines the extent to which localized plastic strain is induced, and thereby generation of compressive longitudinal stress (Figure 4-22 (a)). However, the compressive zone width is narrower than the width of roller because the contact area of the roller is smaller compared to the width of roller. Hence rolling causes plastic deformation around that region of the weld which is approximately 20 mm in width.

As shown in Figure 4-22 (a), post weld cold rolling has changed the longitudinal residual stress state causing it to become compressive around the weld metal (from peak tensile stress of 395 MPa to compressive stress of 80 MPa). Application of rolling to the welded joints causes weld metal to yield thereby relieving the residual stress that exists in the region. In other word, these rolling processes compress the material in the direction normal to the weld's surface, thereby causing it to expand in the plane of the weld, relaxing any tensile residual stresses in the plane.

It was evident that at about 6 mm below the weld surface (Figure 4-23), the rolling load has a significant influence on the residual stress state of the weld (changing the peak tensile stress from 319 MPa to 50 MPa). These suggest that the closely packed atoms of the FCC crystal make it easier to deform through the thickness which enables the reduction in the residual stress to extend through the thickness. Deformability of austenitic steel is higher than the ferritic steel because of more active slip planes in the austenitic steel.

Similarly, at 10 mm below the weld surface (Figure 4-23), the rolling load changes the residual stress state (peak tensile stress from 208 MPa to 74 MPa) suggesting some impact of the rolling in this region. It can therefore be deduced from this work that post weld cold rolling was effective in modifying the residual stress.

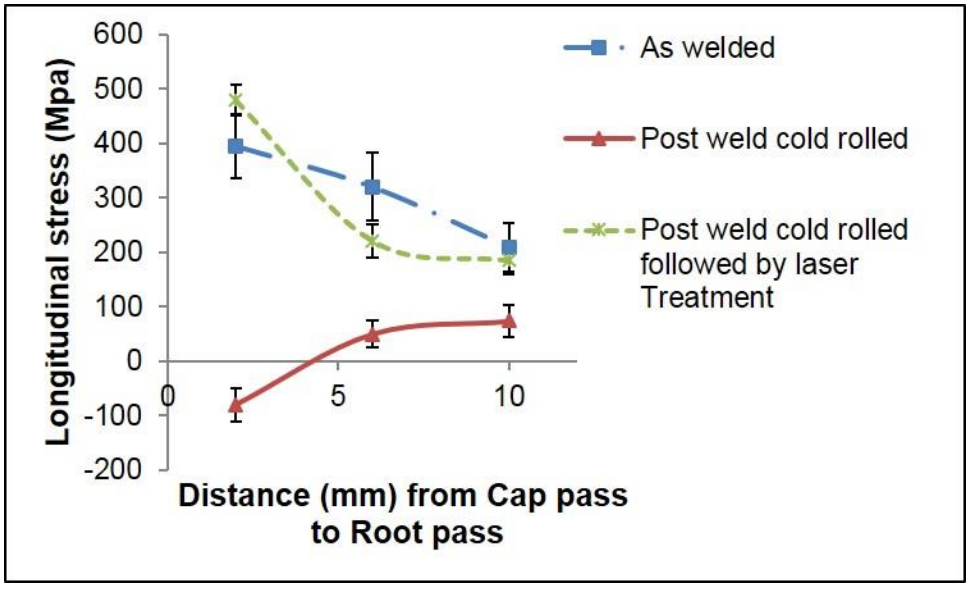

Figure 4-23: Variation of peak residual stress magnitude through the thickness (measured at 2, 6, and 10 mm below the top surface)

4.5.6.2 Effect of Post Weld Cold Rolling Followed by Laser Processing

Laser processing after cold rolling has been shown to increase the longitudinal residual stress from compressive stress of 80 MPa to 479 MPa (Figure 4-22(a)). This indicates a high thermal input and non-uniform cooling of the welded plate, thus generating inhomogeneous plastic deformation and tensile residual stresses.

With reduced heat input below the weld surface (6 mm) a change in the longitudinal residual stress state was observed, modifying the peak tensile stress from 50 MPa to 220 MPa (Figure 4-23). This could be attributed to low thermal conductivity and high coefficient of thermal expansion of the austenitic steel.

Similarly, at about 10 mm below the weld surface (Figure 4-23), application of laser processing to the cold rolled samples reinstated residual stress distribution profile to as-welded state. This indicates that the heat conducted through the material at that region was not sufficient to cause any changes in the residual stress state.

4.5.6.3 Full Width at Half Maximum (FWHM)

Figure 4-24 shows the effect of FWHM on (a) an as-welded sample at different depth (b) Post weld cold rolling at different depth and (c) the three samples at 2 mm below weld surface.

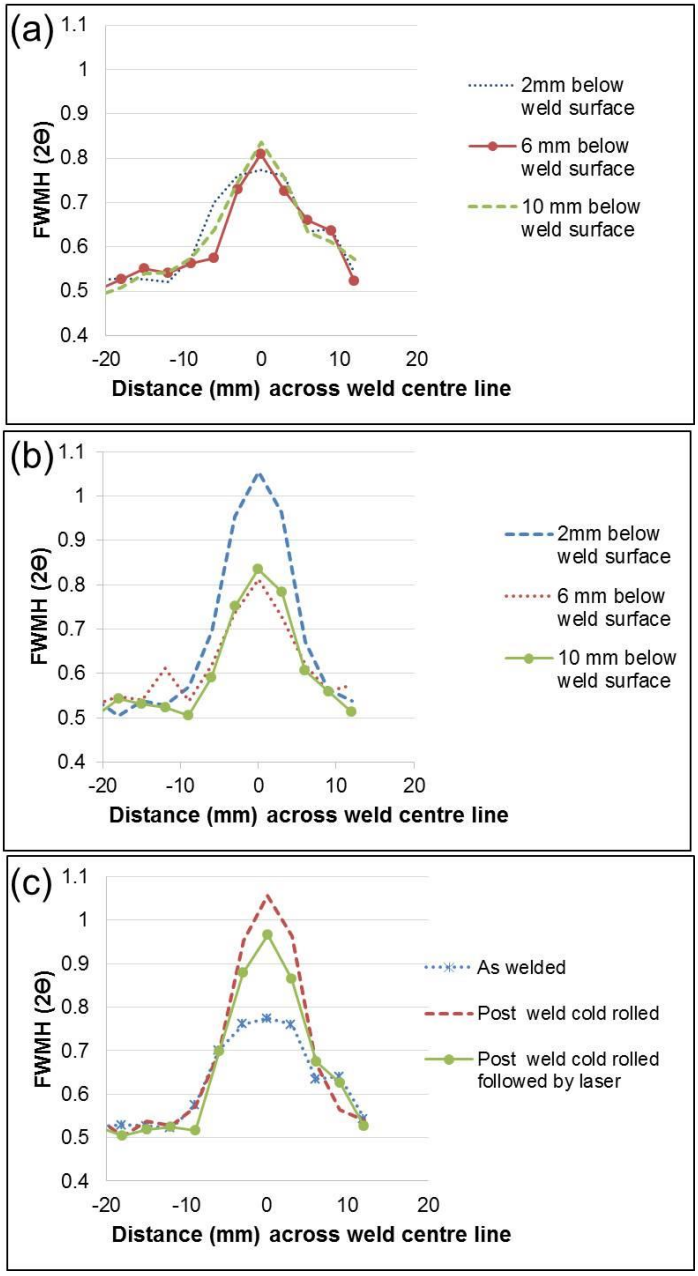

Figure 4-24: Effect of FWHM on plastic deformation at (a) As-welded at 2, 6, and 10 mm below weld surface (b) Post weld cold rolling at 2, 6 and 10 mm below weld surface (c) The three samples at 2 mm below weld surface

FWHM values of the diffraction peaks were obtained from Large Array Manipulation Program (LAMP) software. As stated earlier, FWHM indicates the plastic strain history of a crystalline structure. Hence as shown the in the as-welded sample (Figure 4-24 (a)), the FWHM at 10 mm below the weld surface was higher than the FWHM at 2 mm below the weld surface. Since the root regions experience more thermal cycles than any other region, the root pass undergo more thermal straining compare to cap pass. Figure 4-24 (b) shows a significant increase in FWHM profile at the cap pass when the cold rolling was applied to the weld metal. This shows that the FWHM increases with hardening (increasing plastic deformation). Of course, because of the direct contact between the cap pass and the roller, the cap pass of the weld experience more deformation as compared to passes below the cap pass. In addition, as the effect of the applied load by the roller diminishes through the thickness (Figure 4-24 (b)), the peak FWHM decreases, indicating that FWHM is influenced by the work hardening effect of the rolling process. FWHM profiles were reported not only to be influenced by plastic deformation but it is also sensitive to residual stress [214]. However, the FWHM profile reduces when the post weld cold rolling followed by laser processing was applied (Figure 4-24 (c)). This means there was a lot of dislocation when laser processing was applied.

4.5.7 Conclusion

Very minimal grains refinement was observed at the cap pass of multi-pass welds when post weld cold rolling followed by laser processing was applied to the sample. These refine grains (average grain size of 11.00 µm) in laser processed samples would limit Cr segregation which would result in the formation of corrosion microcells as well as a reduction in overall corrosion prevention due to depletion of alloying elements.

The post weld cold rolling modifies the tensile residual stress state, and a compressive residual stress was formed below the weld metal. As the modification of stress state is achieved by plastic deformation, 31% increase in ultimate tensile strength and 36% increases in proof strength with corresponding

reduction in percentage elongation (50.5% to 37.5%) in the fusion zone was observed.

Post weld cold rolling followed by laser processing resulted in the formation of a refined microstructure. However, from the grain structure it is clear that re-crystallisation is not complete because the transient thermal cycle is not sufficient to supply enough energy to sustain the complete kinetics. However, laser processing reinstated as-welded residual stress state profile with even higher magnitude of peak stress.

Peak tensile residual stress of the as-welded sample diminishes in magnitude through the thickness of a multi-pass welds. This is attributed to the fact that, multiple passes result in thermal straining of previously laid pass from successive passes. The thermal cycling would cause macroscopic plastic deformation of previously laid passes.

The FWHM in this experiment shows an increase with increase in plastic deformation (post weld cold rolling).

4.6 Second Phase of Experimentation

Based on the observation made in the first phase of the experiment (section 4.5.7), that post weld cold rolling followed by laser processing reinstated as-welded residual stress state profile with even higher magnitude of peak stress and also resulted in minimal refinement of microstructure, the second phase of the experiment was considered necessary to perform. In this second phase, new laser processing route was adopted.

The new laser processing involves applying thermal energy for a prolonged period which would ensure that grain structures are fully recrystallized with formation of new set of strain free grains.

Cold rolling after laser processing was also adopted so as to redistribute and eliminate the tensile residual stress state which would have formed during laser processing. Figure 4-25 is the schematic showing the work flow for this phase. As shown in the sketch, the second phase of the experiment involved four steps;

welding was carried out by Tandem GMAW DC process, the post weld cold rolling was performed using an in-house rolling device, the post weld cold rolling was followed by laser processing using 8 kW (peak power) CW fibre laser and finally cold rolling after post weld cold rolling was followed by laser processing.

Note that in this second phase, the same material and equipment used in the first phase were used.

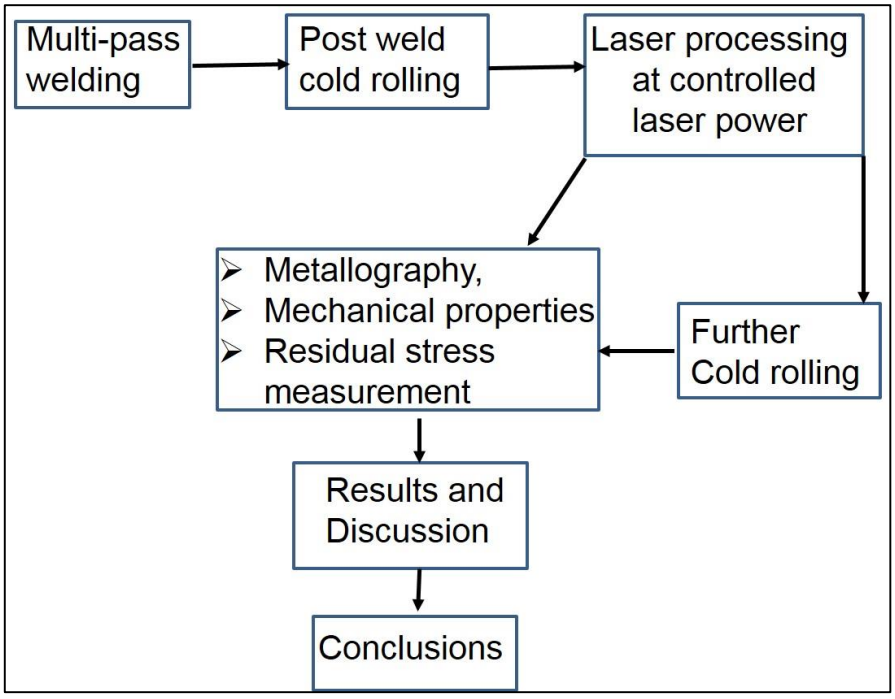

Figure 4-25: Sketch of the work flow of the second phase

4.6.1 Experimental Method

The experimental methods are divided into five (5) stages (that is, welding, post weld cold rolling, laser processing, cold rolling after laser processing, residual stress measurement) and they presented here.

4.6.1.1 Welding

The same welding process used in section 4.4.1 was used.

4.6.1.2 Local Mechanical Tensioning (Cold Rolling)

The principle of rolling used in section 4.4.2 was applied in this section.

4.6.1.3 Laser Processing

The new laser processing involves applying thermal energy for a prolonged period which would ensure that grain structures are fully recrystallized. In order to understand the time-temperature cycle required for full recrystallization, an experiment using reheating furnace was carried out on post weld cold rolling samples.

In this reheating furnace experiment, different temperatures were tried. Thermocouples were attached to each sample so as to differentiate between the furnace temperature and sample temperature. Each sample was heated and hold for 60 s.

4.6.1.3.1 New Laser Processing

In the new laser processing, the same continuous wave (CW) laser was used as in first phase, but instead of transient heating mode the post weld cold rolling samples were gradually heated by controlling the laser power at a large beam diameter of 110 mm. Figure 3-53 and Figure 3-54 in chapter 3 section 3.6.3.3.2 of this thesis shows an experimental set up and schematic diagram for new laser set-up respectively. The laser head was positioned at 25^{o} angle to avoid any back reflection which could damage the lens.

4.6.1.4 Cold Rolling After Laser Processing

Rolling has been performed under identical set up and principles as described in section 4.4.2.2, of this thesis.

4.6.1.5 Method of Residual Stress Measurement

The principle used in section 4.4.4.1 was used here except that the following parameters are different from those used in first phase;

1. The measurements were made using a neutron incident beam of wavelengths, 1.6 Å, which gives a diffraction angle (2Θ) of 93.2^{o}
2. The measurements of the residual strain were taken at 3, 7 and 11 mm below the plate surface on which the capping pass was laid

4.6.2 Results and Discussion

4.6.2.1 Experiment Using Furnace Treatment on 304L Austenitic Stainless Steel

In this experiment, the samples were also heated inside the furnace and their hardness and microstructure were check before designing the experiment using laser. The size of the samples heated on this trial was 50 mm long by 40 mm wide by 12 mm thick. In these experiments, different temperatures (800ºC, 900ºC, 1000ºC and 1200ºC) were tried. Each sample was heated and hold for about 60s. Figure 4-26, Figure 4-27 and Figure 4-28 shows the thermal cycle, hardness profile and the optical micrographs respectively.

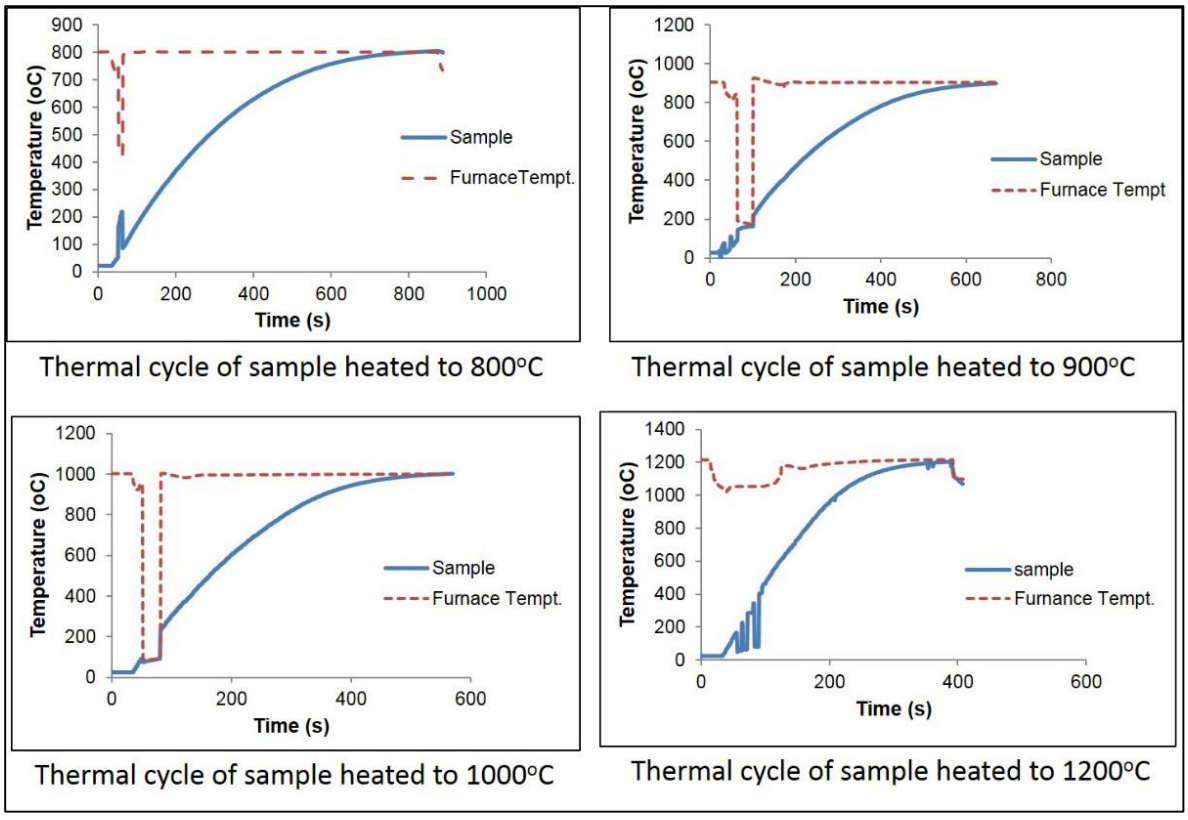

Figure 4-26: Thermal cycles of furnace at different temperature

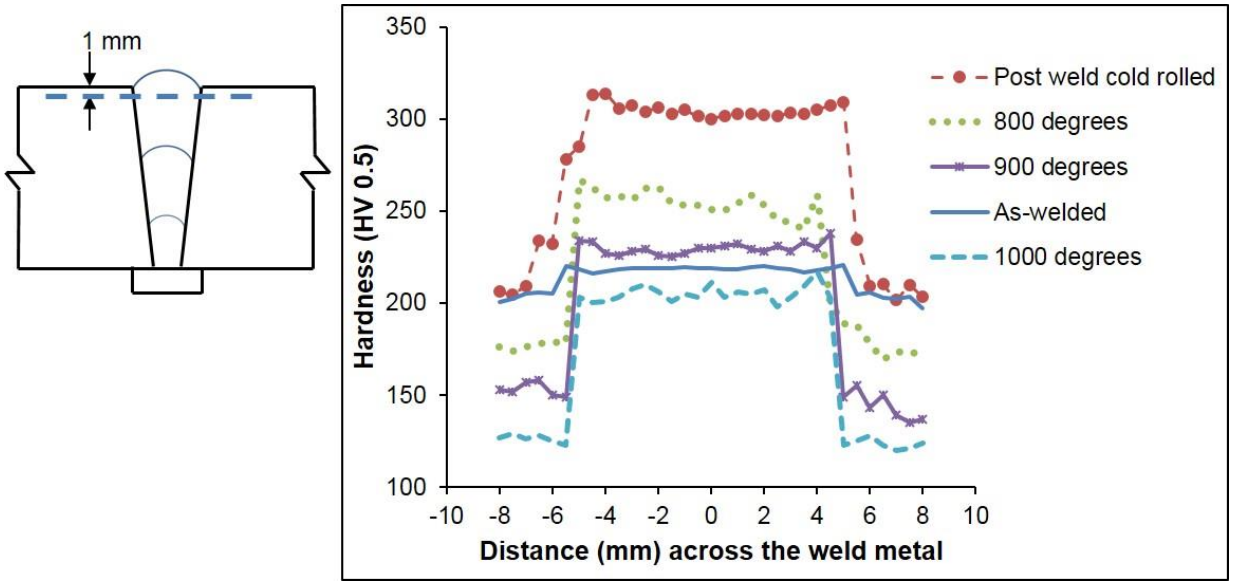

Figure 4-27: Hardness profile across weld metal (cap) at different temperature

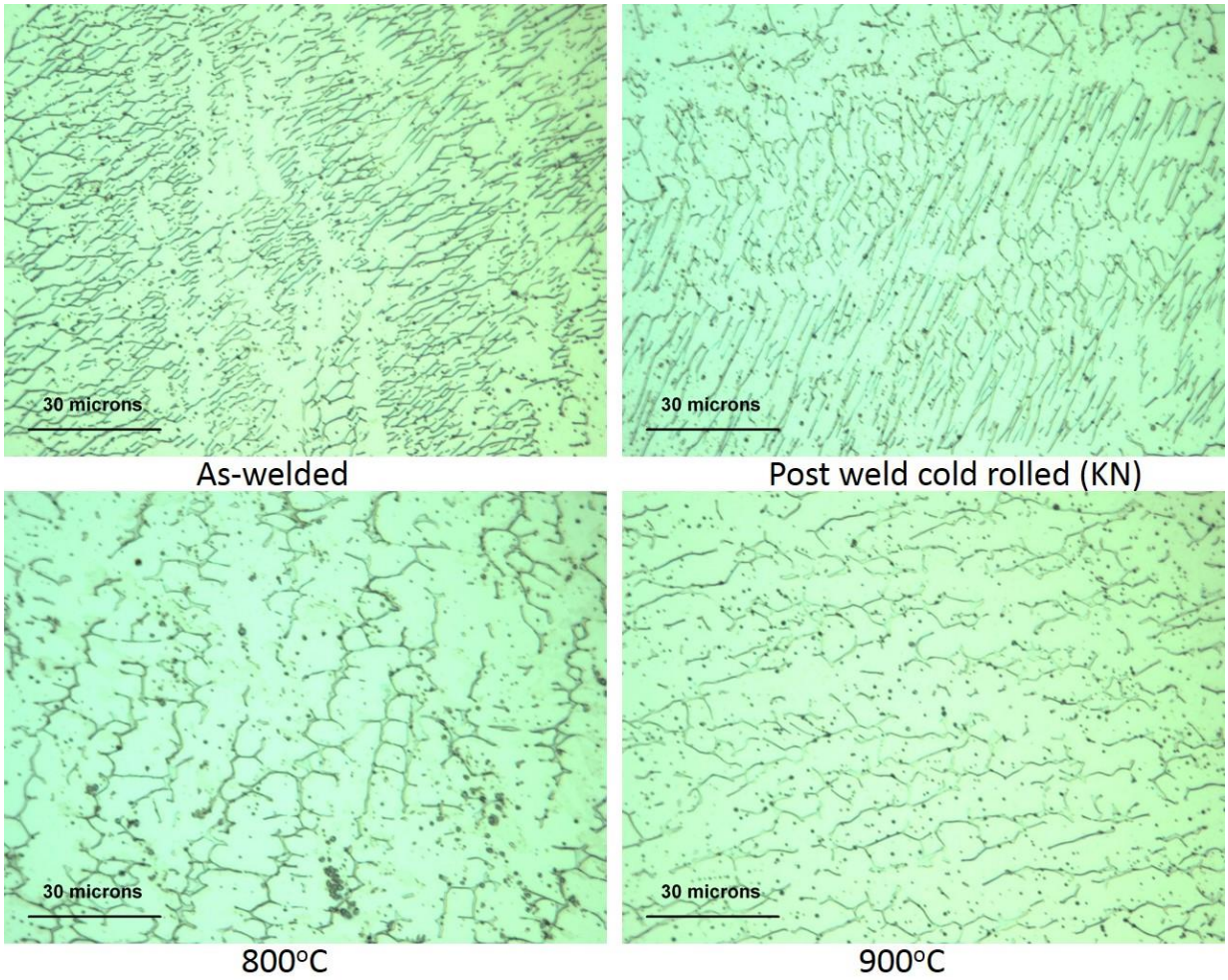

Figure 4-28: Optical micrographs of the welds metal of 304L (cap pass)

4.6.2.2 Conclusion for the Furnace Experiment

The furnace experiment result showed that a recrystallized grain was formed after heating 304L austenitic stainless steel up to 800^{o}C. Based on this observation, the laser processing in the second phase of the experiment was designed.

4.6.2.3 The New Laser Processing

In this phase the same CW laser was used as in first phase, but instead of transient heating mode the post weld cold rolling samples were gradually heated by controlling the laser power at a large beam diameter of 110 mm. The 304L austenitic steel was heated to 800^{o}C using identical laser parameters.

The thermal cycle of the laser processing are shown in Figure 4-29 for 304L austenitic steel plate.

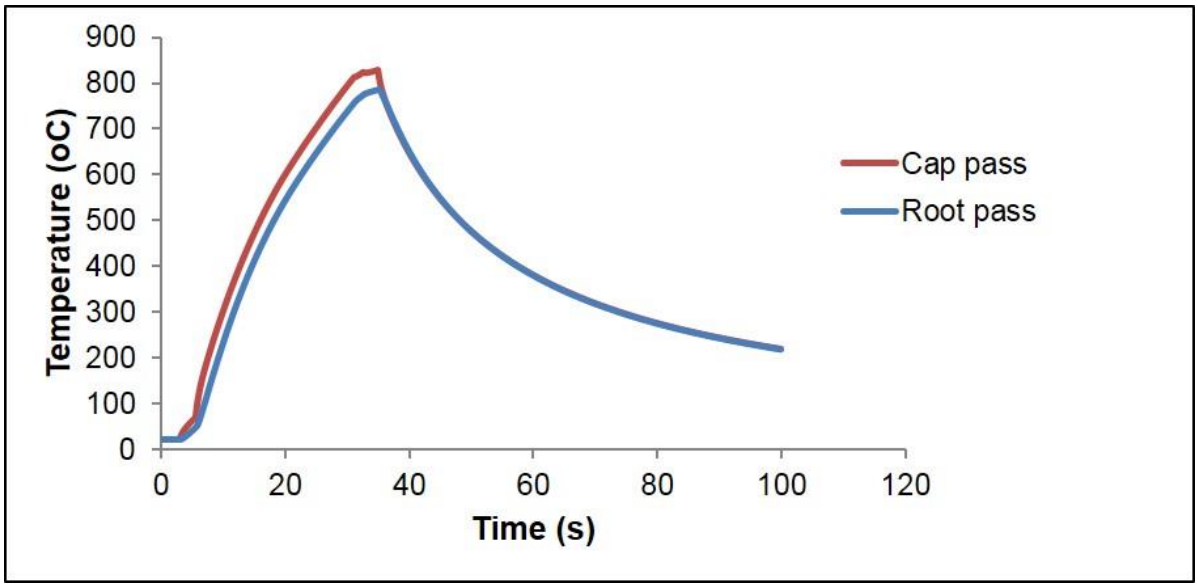

Figure 4-29: Thermal cycles of control laser power (heated to 800^{o}C) at constant beam diameter of 110 mm

The effect of the designed laser processing on hardness, tensile strength, metallography and residual stress measurement are presented and discussed.

4.6.2.3.1 Effect of Laser Processing on Hardness Profile of 304L Austenitic Stainless Steel

For the purpose of comparison, the hardness profile of as-welded, post weld cold rolled, post weld cold rolled followed by laser processing and cold rolling after laser processing are presented.

A hardness scan was performed from the reinforcement bead (cap pass) to the root pass as shown in Figure 4-30. The effect of cold working was observed throughout the entire thickness of the material when a load of 100 kN was applied. The designed laser processing applied after post cold weld rolling shows a significant decrease in hardness values (307HV to 241HV) at the cap pass and the effect continues throughout the thickness. This Indicates that the thermal energy applied was sufficient to supply enough energy to sustain a complete recrystallization kinetic as is evident in EBSD micrograph shown in Figure 4-34. The cold rolling after laser processing once again show the effect of cold working which would be beneficial in terms of residual stress modification.

Figure 4-31 shows the hardness distribution at the cap pass of the welded samples with different processing conditions. Figure 4-31 (a) shows the indentation point or hardness scan position (measurement at 1 mm below the plate surface) on the sample while Figure 4-31 (b) shows the hardness profile. The heat-affected zone (HAZ) in all the samples were harder than the base metal. This could be attributed to the strain-hardening of the HAZ.

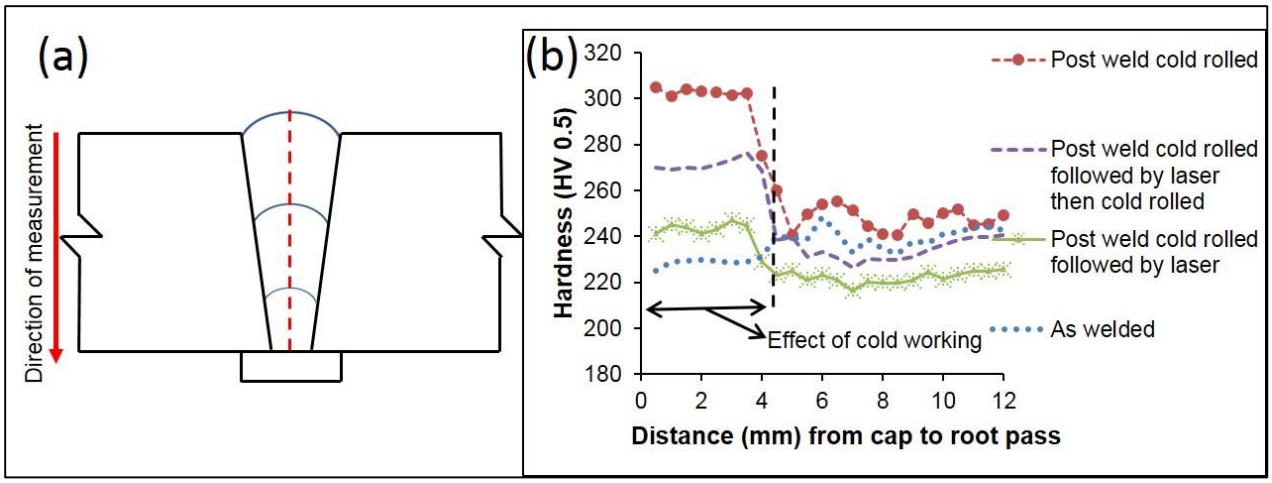

Figure 4-30: Showing (a) hardness scan position along the weld metal and (b) hardness profile

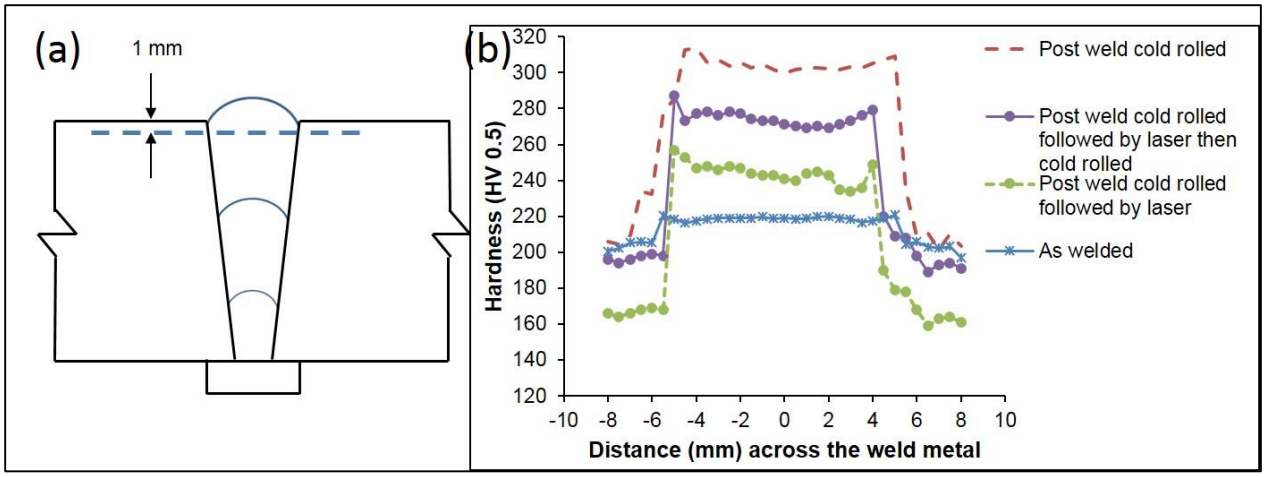

Figure 4-31: Hardness profile at the capping pass across the weld metal of the four different samples

4.6.2.3.2 Effect of Laser Processing on Tensile Strength

Tensile properties of the all-weld metal samples tested are shown graphically in Figure 4-32. This figure shows the different processing conditions. For the purpose of comparison, post weld cold rolling followed by laser processing brought about a decrease in proof strength (534 MPa to 496 MPa) and slight increase in percentage elongation (37.5% to 39.5%) in the first phase (Figure 4-14). This new laser processing shows a further decrease in proof strength (534 MPa to 370 MPa) and an increase in percentage elongation (37.5% to 42.11%) as shown in Figure 4-32.

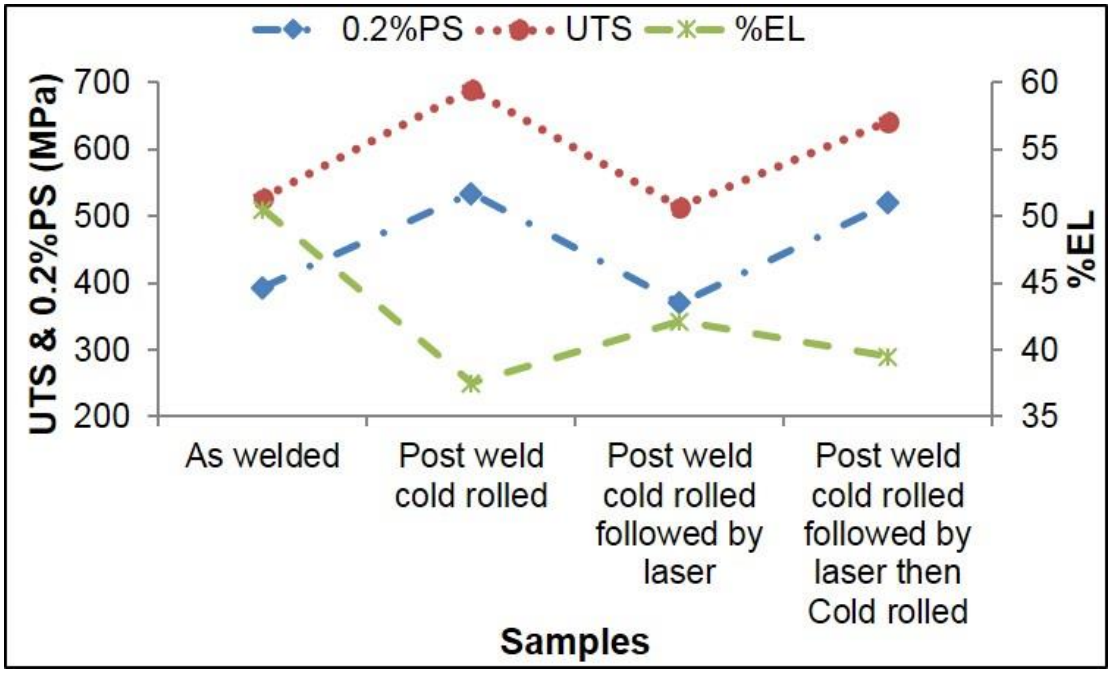

Figure 4-32: Tensile test of the 304L austenitic steel samples

This indicates that, some of the stored internal strain energy was relieved as a result of enhanced atomic diffusion at higher temperature. An effective indication of recrystallization can be a drop in proof strength [139] due to releasing of internal energy; the greater the amount of prior deformation, the lower the temperature to initiate recrystallization, as the activation energy gap needed to initiate recrystallization would be less.

However, the application of cold rolling after laser processing shows an increase in UTS (513 MPa to 641 MPa) and PS (370MPa to 520 MPa), with corresponding decrease in ductility (42.11% to 39.50%) as shown Figure 4-32, indicating the effect of cold working after laser processing. This effect of cold working would be helpful in terms of residual stress relaxation.

4.6.2.3.3 Micrographs by Electron Backscatter Diffraction (EBSD)

In this new laser processing, the grain structure was studied using EBSD techniques. For the purpose of comparison, the as-welded and post weld cold rolling samples are presented. Figure 4-33 shows the crystallographic texture of the cap pass of both as-welded and post weld cold rolling samples obtained from EBSD. These micrographs were obtained from data collected over an area of 316 µm x 235 µm with step size 0.729 µm. Each colour indicates the orientation of the grains.

The analysis of grain structure using EBSD shows a dendritic grain structure in as-welded and post welded cold rolling samples (Figure 4-33). This dendritic and columnar grains structure could be attributed to the fact that during weld metal solidification, grains tends to grow in the direction perpendicular to pool boundary. This dendritic solidification of the weld metal often leads to segregation of alloying elements within the grain structures which would result in formation of localised region with reduced corrosion protection. Columnar grain growth was reported to influence mechanical properties [30] and microstructural features, such as microsegregation [31]. However, based on the step size used, the average grain size of 5.10 µm was found when post weld cold rolling followed by new laser processing was applied on the sample at the same position (see Figure 4-37). This value was lower than that obtained in the first phase (Figure 4-19). Among many other factors, grain boundary area poses as one of the major obstacles for movement of dislocations. This reduced grain size (5.10 µm), in laser processed samples would, therefore, have the potential of improving the integrity of the weld metal. This is true since generation of the recrystallized microstructure with large proportion of high angle grain boundaries would increase the strength and toughness of the material which is lower in the as-welded dendritic grain structure state [10] [108].

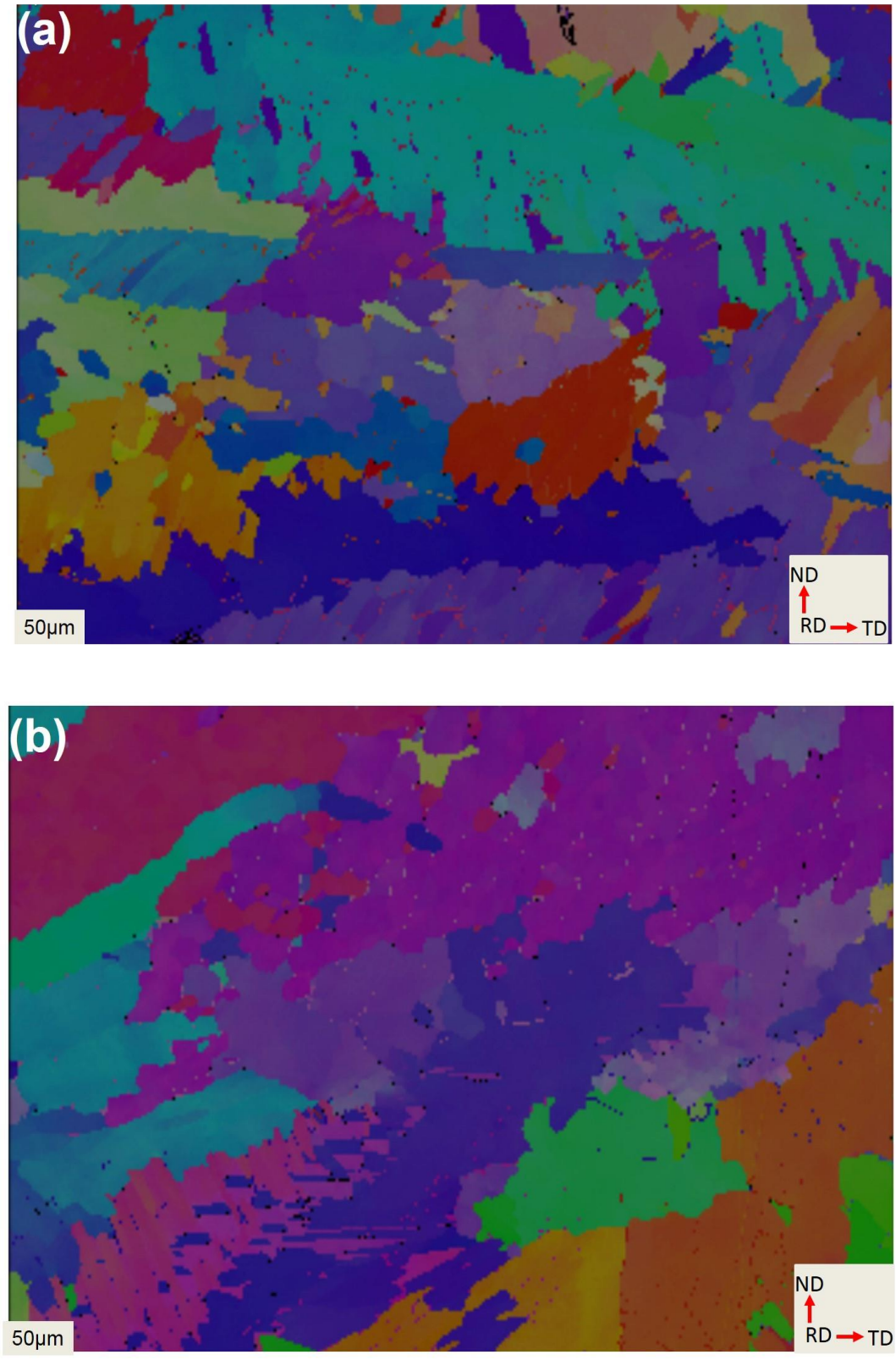

Figure 4-33: EBSD micrographs of 304L austenitic steel at the cap pass of (a) as-welded (b) post weld cold rolling

Figure 4-34 showing the presence of twin and a clear grains with different orientations after laser processing.

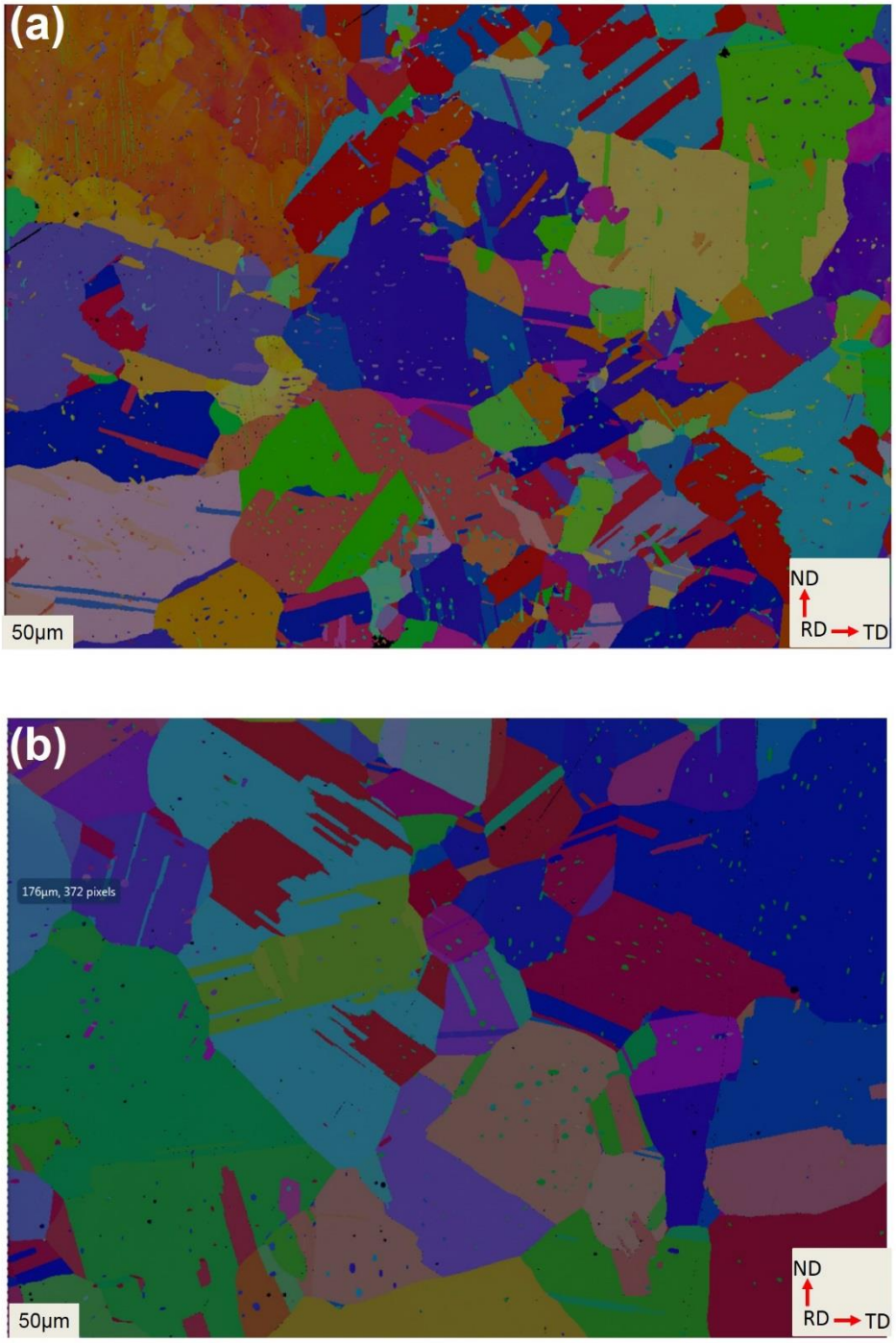

Figure 4-34: EBSD micrographs of 304L austenitic steel at the cap pass of (a) post weld cold rolling followed by laser processing (b) cold rolling after post weld cold rolling followed by laser processing

Figure 4-35 shows the {311} pole figures measured by XRD obtained from the as-welded, post weld rolled. The texture intensity of the samples decreases as the sample was rolled and further decrease when post weld rolled followed by laser processing was applied.

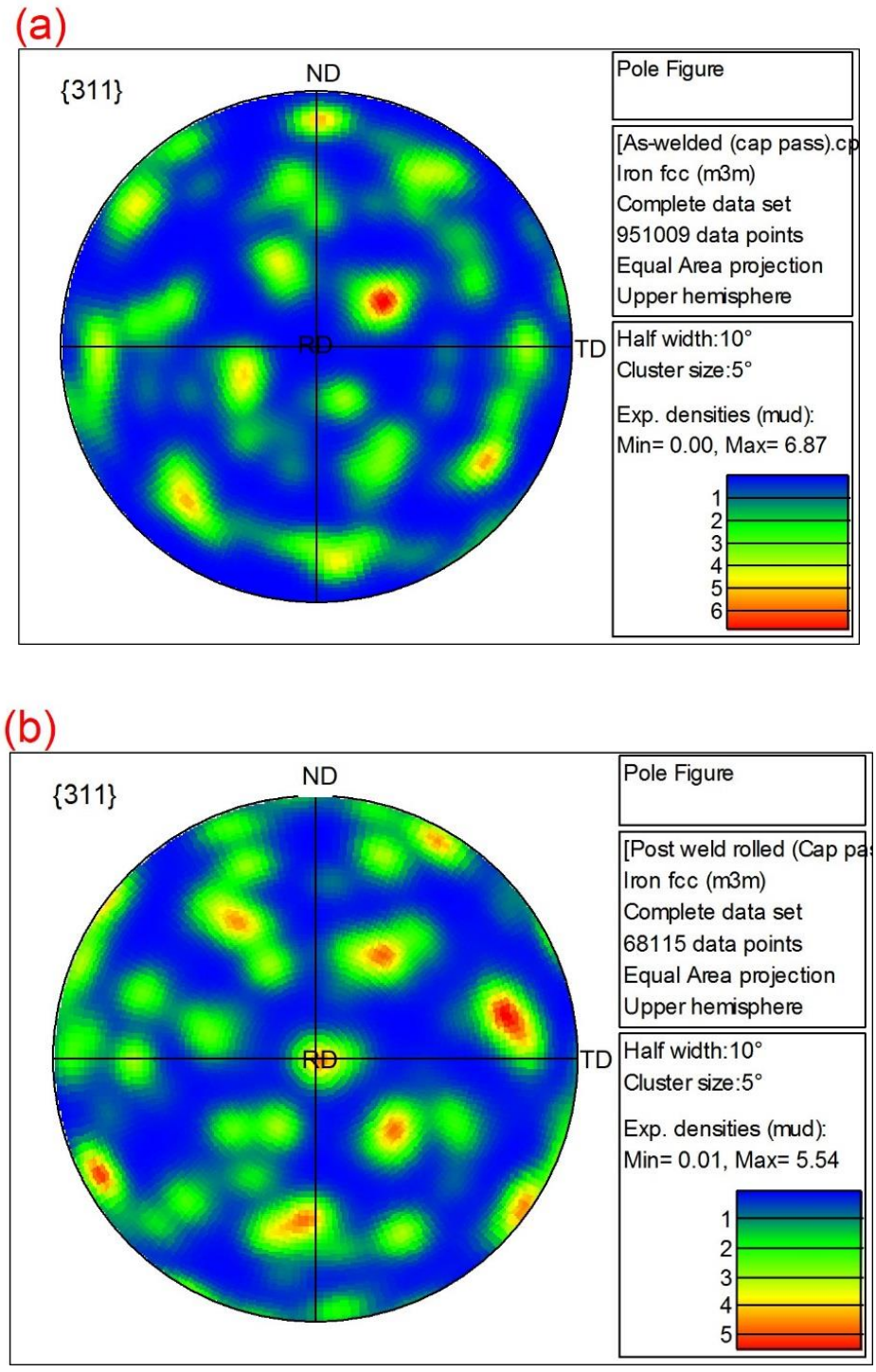

Figure 4-35: Pole figure of the cap pass (a) as-welded (b) post weld cold rolling

Figure 4-36 shows the pole figure of the post weld cold rolling followed by laser processing at cap pass.

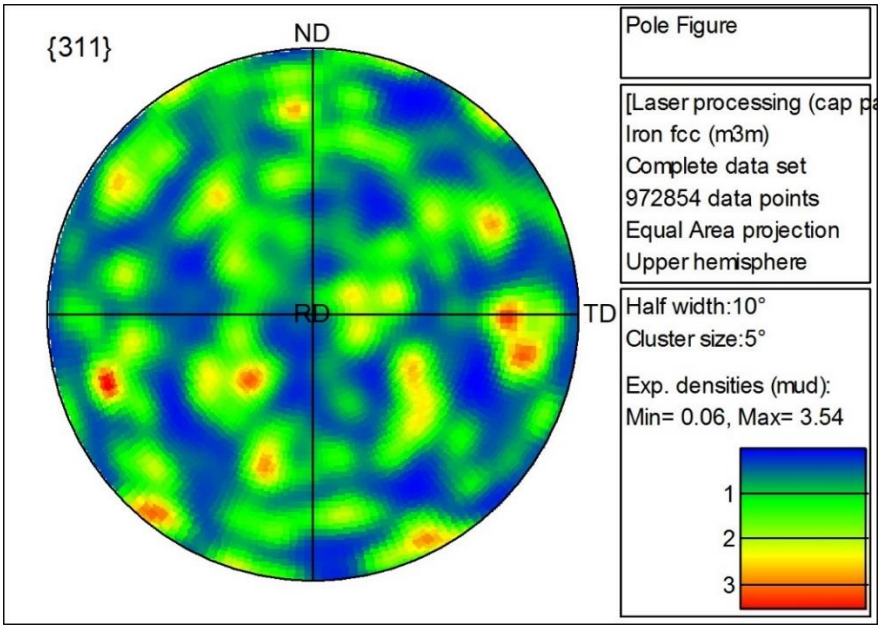

Figure 4-36: Pole figure of the post weld cold rolling followed by laser processing at cap pass

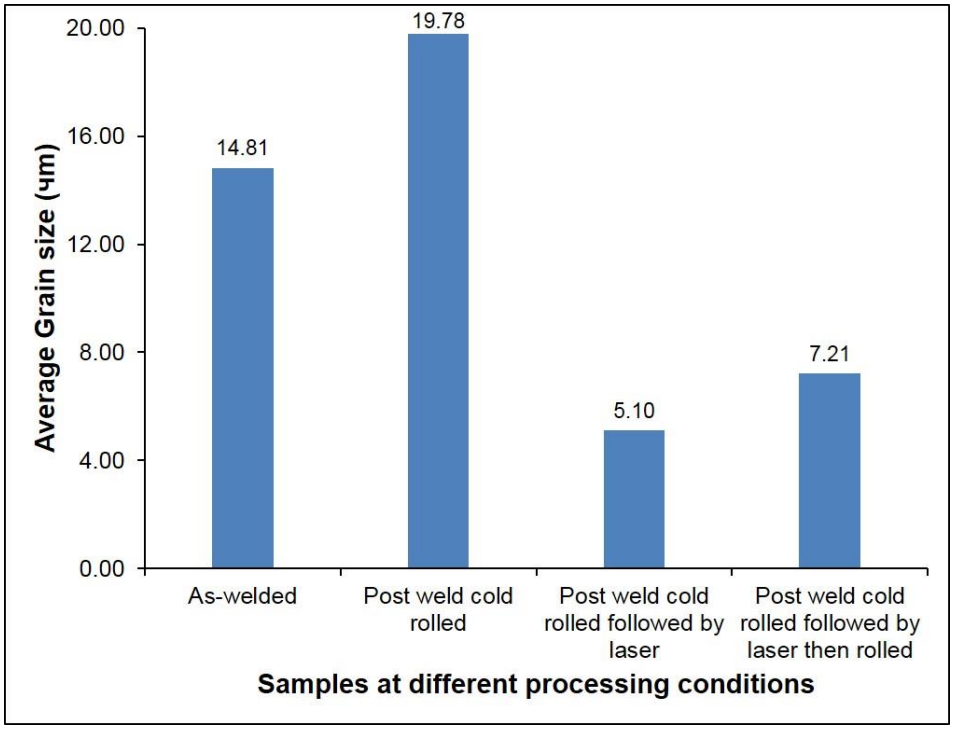

Figure 4-37: Showing the average grain size at the cap pass of the different processing conditions

Changes in texture intensity of the samples were observed when different processing condition were applied (Figure 4-35 and Figure 4-36). The change is more pronounced in this sample (austenitic stainless steel) compare to low carbon steel for structural pipeline (ferritic steel). This confirm that, the texture can be affected by grain reorientation induced by plastic deformation.

4.6.2.3.4 Residual Stress

Figure 4-38 shows the variation in the unstressed austenitic {311} lattice spacing d0 measured and Figure 4-39 shows the residual stress profile analysed from the measurements of elastic strain. The post weld cold rolling sample measured (residual stress) in first phase is used as a reference sample since the same welding parameters are used in making the weld (see Figure 4-22). In Figure 4-22 which is reproduce in (Figure 4-39 (a)), post weld cold rolling has changed the longitudinal residual stress state causing it to become compressive around the weld metal (from peak tensile stress of 395 MPa to compressive stress of 80 MPa).

As shown in Figure 4-39 (b), post weld cold rolling followed by laser (measurement was taken at 3.5 mm below the weld surface) has change the compressive residual stress (80 MPa) obtained during post weld cold rolling to peak tensile stress (536 MPa). Although this effects is not surprising since the same effect were obtained in first phase of this research.

However, further cold rolling after post weld cold rolling followed by laser processing has changed the longitudinal residual stress state once again to become compressive around the weld metal (from peak tensile stress of 536 MPa to compressive stress of 162 MPa in Figure 4-39 (b). The presence of this compressive stress component would likely inhibit crack propagation across the weld under longitudinal fatigue loading which is essential for structural integrity of an engineering or structural component.

As stated earlier, the largest residual stresses are expected parallel to the welding direction and close to the weld zone. Hence, the discussion above was focussed on the longitudinal direction. However, transverse and normal direction are

presented in appendix B.3.1. For the purpose of comparison through the thickness, the measurement at 7 mm below the surface is shown in appendix B.3.2.

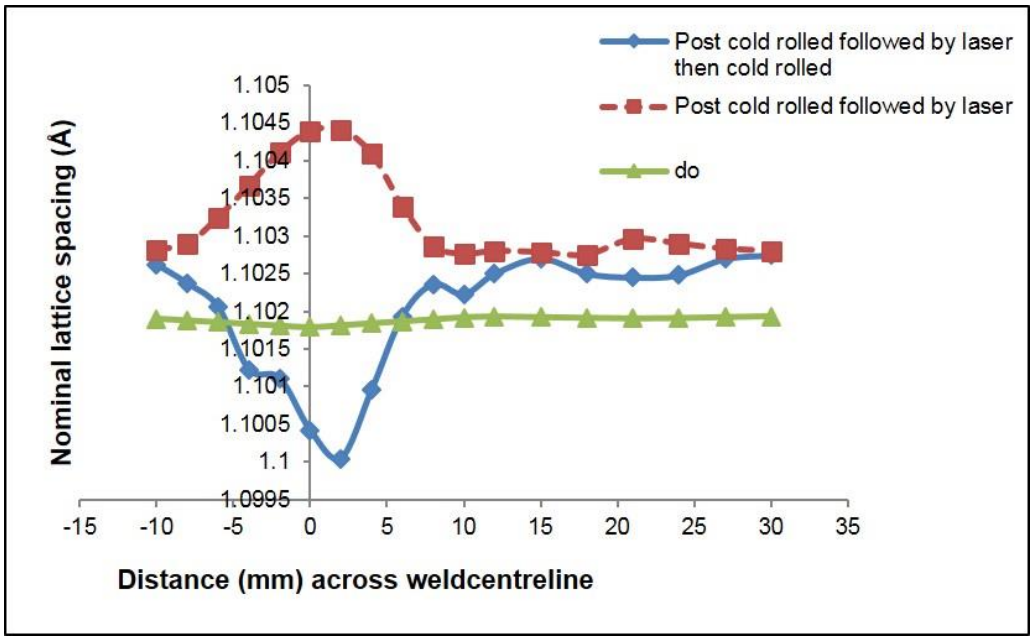

Figure 4-38 : Variation in the unstressed austenitic {311} lattice spacing d0 measured (measured 3 mm below the weld surface)

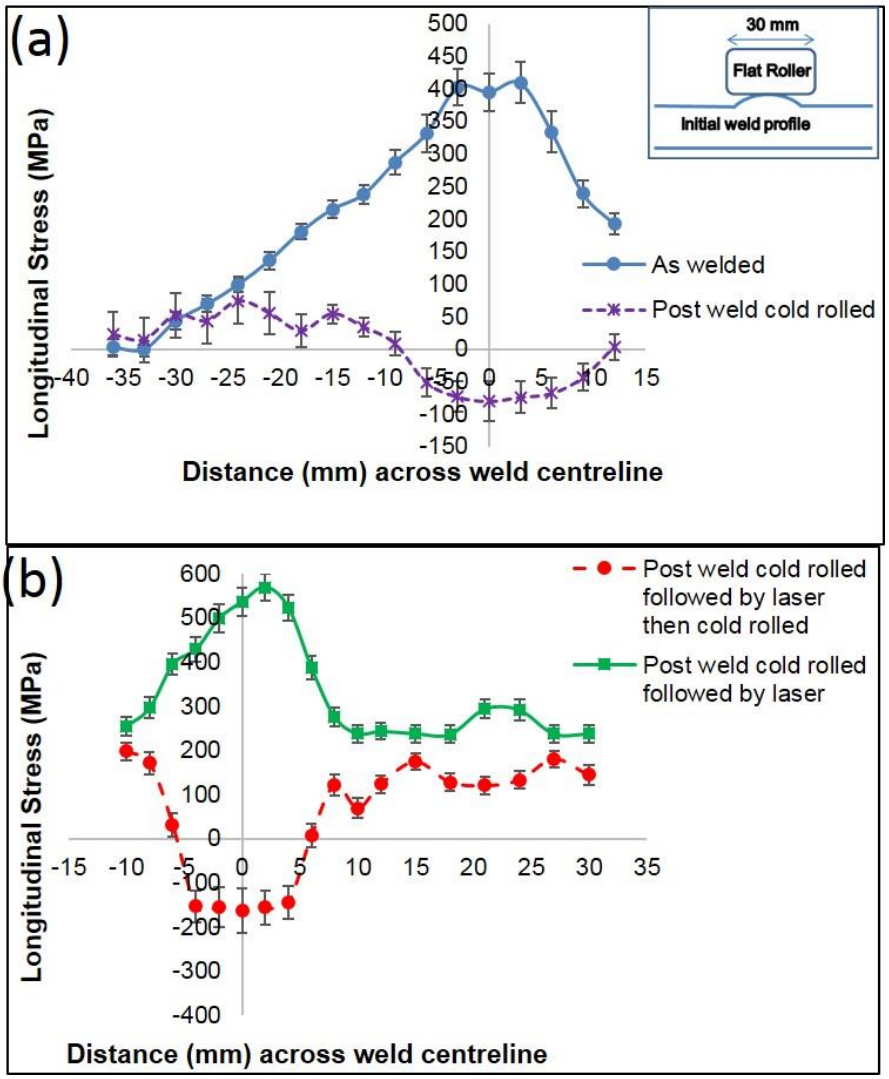

Figure 4-39 : Longitudinal Residual stress profile across the weld in sample with different processing conditions (a) as-welded and post weld cold rolling at measured 2 mm below the weld surface (b) post weld cold rolling followed by laser and further cold rolling after processing post weld cold rolled followed by laser processing measured 3 mm below the weld surface

4.6.3 Conclusion

The second phase of this experiment has demonstrated that a complete recrystallized microstructure with compressive state of stress can be formed when a further cold rolling is applied on the laser processed, recrystallized microstructure.

5 Effect of Cold Rolling, Laser Processing and Cold Rolling After Laser Processing on Microstructure and Residual Stress of Multi-pass Welds of S275 Structural Steel

5.1 Introduction

S275 is also another form of steel which is common among the low carbon steel grade. This structural alloy is suitable for many general engineering and structural applications especially in construction, maintenance and manufacturing industries.

This experiment using this material (12 mm thick S275 Structural Steel) was based on the observation made on the two structural alloys (20 mm thick API 5L steel and 12 mm thick 304L austenitic steel) in this research. In both 20 mm thick steel plate and 12 mm thick plate used, up to 4 mm below the weld surface, the post weld cold rolling was effective in modifying the residual stress. In this particular material, the residual stress was measured was analysed at 6.5 mm and 10.5 mm below the weld surface. The transient mode of laser processing applied in the two structural alloys reinstated as-welded residual stress profile with even higher magnitude of peak stress, and also resulted in minimal refinement of microstructure. In this material, a new laser processing was adopted. The new laser processing involves applying thermal energy for a prolonged period which would ensure full recrystallization of the grain structure. Further cold rolling after laser processing was also adopted to redistribute and eliminate the tensile residual stress state which would have formed during laser processing. Hence, this experiment aim at comparing the effect of the different processing conditions through the thickness of the materials.

5.2 Materials

The material used in this experiment was the S275JR structural steel plate (12 mm thick) and chemical compositions of the S275JR structural steel plate are shown in Table 5-1.

Table 5-1 shows the chemical compositions of the S275JR structural steel

Elements	C	Si	Mn	P	Mo	Ni	Al	N	Cu	Nb	Ti	V	Cr	S	CE
Wt. (%)	0.14	0.24	1.1	0.013	0.005	0.03	0.044	0.006	0.03	0.005	0.005	0.005	0.04	0.002	0.337

5.2.1 Filler Material

The filler material used was Union MoNi with a nominal diameter of 1.0 mm and the composition of the filler wire is shown in Table 5-2.

Table 5-2: Shows chemical composition of the filler material

Elements	C	Si	Mn	P	Mo	Ni	Cu	Cr	S	Others
Wt. (%)	0.12	0.4 -0.8	1.3 - 1.9	0.015	0.25 - 0.65	0.8 -1.3	0.3	0.15	0.018	0.25

5.2.2 Shielding Gas

The shielding gas used was 92% Ar and 8% CO_2 at flow rate of 30 lit min^{-1}. This gas was chosen because it had provided good results (mechanical properties, transfer characteristics and bead profile) in work carried earlier at Cranfield [204], [205].

5.3 Experimental Equipment

The experimental equipment used in this structural alloy is the same as those use in API 5L X100 pipelines steel plates (see chapter 3).

5.4 Experimental Method

In this material this phase of the experiment involved four (4) steps, which are;

i. Welding which was carried out by using Tandem GMAW DC process.
ii. The post weld cold rolling using an in-house rolling device.
iii. The post weld cold rolling was followed by laser processing using 8 kW (peak power) CW fibre laser.

iv. Cold weld rolled after laser processing of the post weld cold rolled.

5.4.1 Welding

The same welding process used in section 3.4.1 was applied in this section. Except for the difference in the plate thickness. The dimension of the S275JR structural steel plate for making the welds are 300 x 150 x 12 mm thick.

5.4.2 Local Mechanical Tensioning (Cold Rolling)

The principle of rolling method used in section 3.4.2 was also applied in this section.

5.4.3 Laser Processing

The laser processing in this chapter involves applying thermal energy for a prolonged period which would ensure full recrystallization of the grain structure. In this laser processing, the same continuous wave (CW) laser was used as explain in section 3.3.4 of this thesis, but instead of transient heating mode, the post weld cold rolling samples were gradually heated up to 900^{o}C using identical laser parameters, by controlling the laser power at a large beam diameter of 110 mm. The thermal cycle of the laser processing is shown in Figure 5-1.

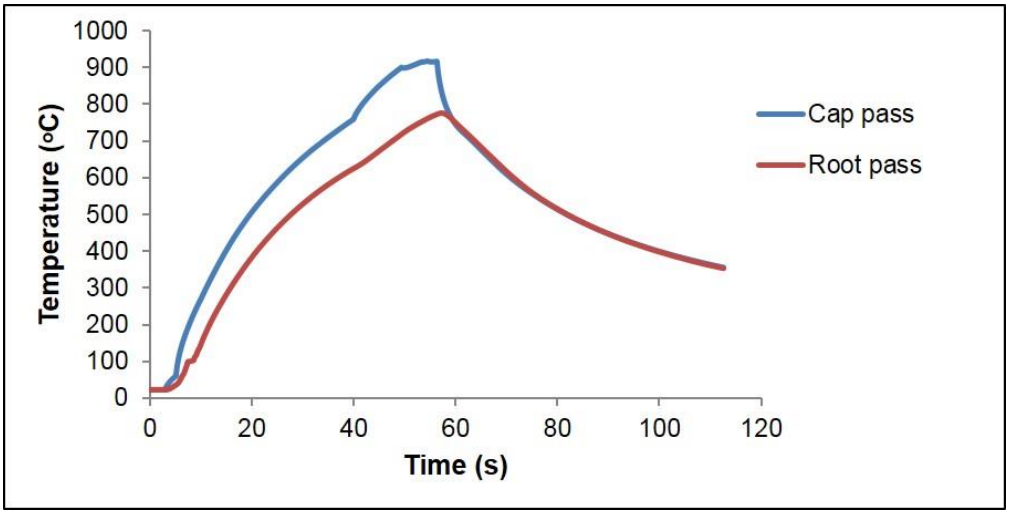

Figure 5-1: Thermal cycles of control laser power (heated to 900^{o}C) at constant beam diameter of 110 mm

5.4.4 Cold Rolling After Laser Processing

The principle of cold rolling used in section 3.4.2 of this thesis was also applied here.

5.5 Residual Stress Measurement Method

The principle used in section 3.4.4 was used here except that the following parameters are different;

1. The measurements were made using a neutron incident beam of wavelengths, 1.6 Å, which gives a diffraction angle (2Ɵ) of 84.2^{o}
2. The measurements of the residual strain were taken at 2.5, 6.5 and 10.5 mm below the plate surface on which the capping pass was laid

The same equation used in calculating strain and stress in section 3.4.4 in these thesis are used here, which are reproduced in equation (5-1) and (5-2).

$$\varepsilon_{\mathrm{hkl}} = \left(\frac{\mathrm{d_{hkl}} - \mathrm{d_{0hkl}}}{\mathrm{d_{0hkl}}}\right) \tag{5-1}$$

Where ε is strain, hkl are the coordinate planes, d is the lattice spacing and d_0 is strain- free spacing (measured in the same plane).

The principal stress can be analysed once the strain is determined using the Hooke's law for three dimensional state of stress as shown in equation (3-7, using the appropriate elastic constants for the specific crystallographic plane.

$$\sigma_{ii} = \frac{E}{(1+\upsilon)}\left[\varepsilon_{ii} + \frac{\upsilon}{(1-2\upsilon)}(\varepsilon_{11} + \varepsilon_{22} + \varepsilon_{33})\right] \tag{5-2}$$

Where E and υ are the Young's modulus and Poisson ratio respectively, and i, = 1, 2, 3 indicate the component of stress and strain (relative to chosen to the principal strain directions). Elastic constants values of E = 225.5 GPa and υ = 0.28 [11] are used to calculate stress from measured strains.

5.6 Results and Discussion

This section present the results and discussion of the experiment carried out with their interpretations.

5.6.1 Tandem MIG Welding

Tandem MIG welding was also used. The dimension of the test piece was (300 x 150 x 12) mm^3 which was machined out from the S275JR structural steel plate. A narrow groove edge preparation of 5° angle with backing bar (cut from the same material) was made as shown in Figure 5-2. The two plates to be welded were tacked together at both ends. The gap between the tacked edge was 5 mm. The welding sample was set and aligned in 1G (down-hand) welding position and a total of four passes were made to fill the groove. Figure 5-2 shows the welding parameter used for this structural alloy.

Cranfield UNIVERSITY

Welding process	Tandem GMAW DC +ve
Welding position	1G
Material Grade	S275 structural steel plate
Thickness	12 mm
Electrode Wire	ϕ = 1 mm
Brand	Union MoNi
Preparation	Saw cut
Backing System	S275 Backing Strip
Cleaning Method	Wire Brush or Grinding
Shielding Gas	92%Ar - 8%CO_2
Flow rate	30 L/min

Designer: Jibrin Sule

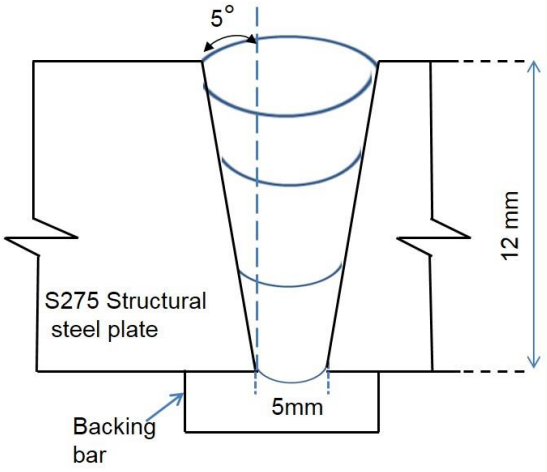

Pass	Travel Speed (m/min)	Lead			Trail			Oscillation		CTWD (mm)
		WFS (m/min)	Amps (I)	Volts (V)	WFS (m/min)	Amps (I)	Volts (V)	Freq. (HZ)	Osc. width	
Root pass	0.9	11	190.7	21.1	11	179.8	20.6	350	90	14
Fill 1	0.9	12	201.4	21.9	13	190.7	20.9	350	135	14
Fill 2	0.9	13	210.9	21.5	12	192.3	21.7	350	190	14
Cap pass	0.7	11	221.3	22.2	11	212.1	21.7	21.7	400	14

Figure 5-2: Welding parameter for the S275JR Structural Steel

5.6.2 Hardness and Tensile Strength Distribution

Figure 5-3 shows the hardness measurement across the cap pass of weld and through the thickness of weld for the four processing conditions while Figure 5-4 shows graphically the tensile strength profile.

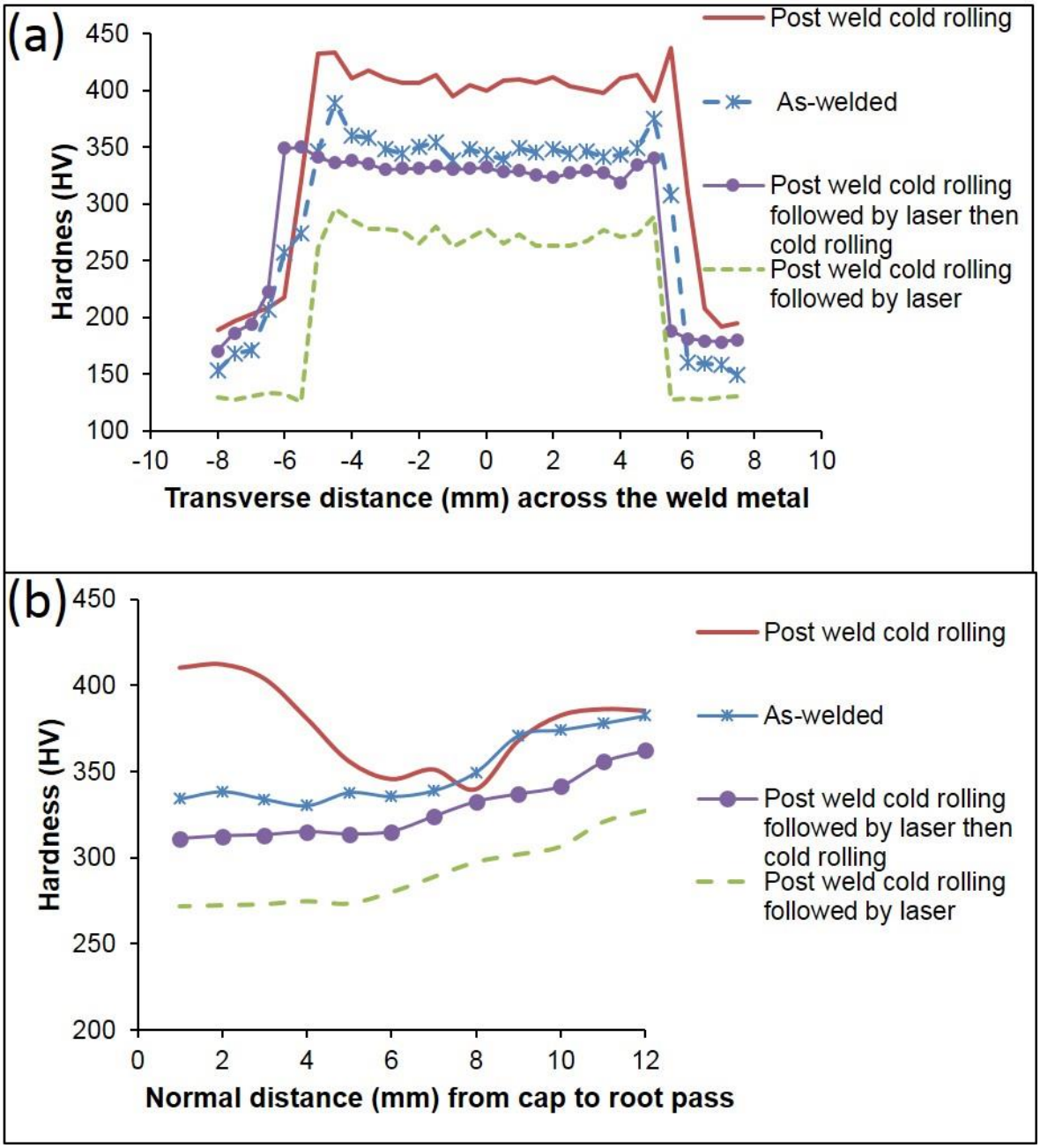

Figure 5-3: Hardness profile (a) capping pass across the weld metal (b) through thickness of weld

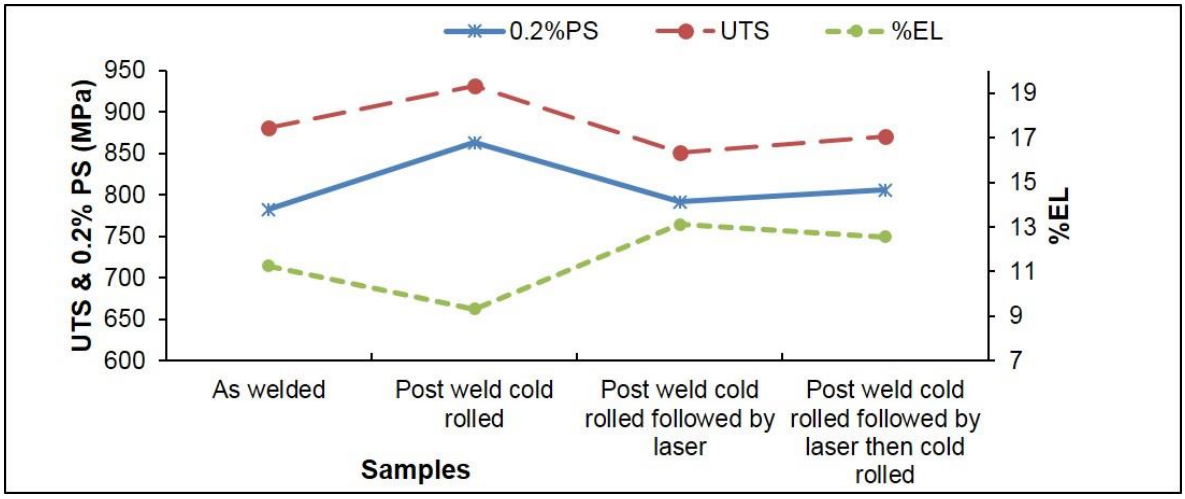

Figure 5-4: Tensile test of the S275 structural steel (cap pass)

5.6.2.1 Hardness on As-Welded Sample

Figure 5-3 shows the hardness measurement across the cap pass of weld and through the thickness of weld for the four processing conditions (as-welded and post weld cold rolling, post weld cold rolling followed by laser, and cold rolling after post weld cold rolling followed by laser). Figure 5-3 (a) shows a maximum hardness occurring at the heat affected zone, followed by the weld metal. The parent metal has the minimum hardness values. This high hardness at the HAZ is caused by the presence of martensite in the microstructure. The presence of martensite was as a result of the high cooling rate experienced at the zone.

However, the hardness recorded at weld metal of the as-welded sample was 3% higher than that obtained in the API 5L X100 pipeline steel plate. This could be attributed to high percentage of carbon content in this structural alloy (0.14%C) as compare to 0.06%C in the API 5L X100 pipeline steel plate shown in chapter 3 of this thesis. Small amount of carbon content (for example, say 0.1% or more) significantly increases the strength and hardness level of steel. Increase in hardness is attributed to interstitial solid solution hardening alongside, metastable phases (e. g. Fe_3C) being formed above 0.008% carbon at room temperature.

The Hardness scan along the weld metal (Figure 5-3 (b)) shows an increase in hardness value from the cap to the root pass of the weld metal, indicating that the root pass, is harder than the cap pass. The higher hardness in the root pass

is as a result of thermal straining since the filler wire is enriched with other solid solution strengthening elements.

5.6.2.2 Effect of Post Weld Cold Rolling on Hardness and Tensile Strength Distribution

Post weld cold rolling increases the hardness value from 341 HV to 400 HV at the weld metal. This is due to effect of cold working which tends to strengthen the material due dislocation movements and dislocation generation within the crystal structure. Figure 5-3 (b) shows a hardness scan that was performed from the reinforcement bead (cap pass) to the root pass. The effect of cold working was also observed throughout the entire thickness. However, up to about 4 mm the effect is more pronounced, after that, from 4-10 mm the effect is less pronounced. However, between 10 – 12 mm the hardness is slightly higher than the middle part of the weld which could be attributed to reaction from the backing bar. The effect of rolling load here is similar to the effect of rolling load observed in 20 mm thick API 5L pipeline steel where the effect of same rolling load (150kN) reaches up to 12 mm below the capping pass (Figure 3-29).

Post weld cold rolling increases the ultimate tensile strength by 6% (881 MPa – 932 MPa) and proof strength also increase by 10% (783 MPa – 863.3 MPa), with corresponding reduction in percentage elongation (11% - 9%) as shown in Figure 5-4. One of the ways in which plastic deformation occurs is the movement of dislocations. The post weld cold rolling increases dislocation density, which restricts the slipping of dislocations which in turn results in increased the strength and reduces the ductility of the weld metal. In this research, it is shown that post weld cold rolling lead to increases in proof strength as well as increase in hardness (Figure 5-3) in the fusion zone (cap pass).

5.6.2.3 Effect of Post Weld Cold Rolling Followed by Laser Processing on Hardness and Tensile Strength Distribution

Figure 5-3 shows the hardness measurement across the cap pass of weld and through the thickness of weld for different processing routes. The laser processing resulted in softening of the weld metal throughout the entire thickness. At the weld centreline, the hardness values drop from 400 HV to 278 HV at the

cap pass. This resulted in nucleation of strain-free grains from the cold-worked metal matrix at points of high lattice strain energy. As a consequence, the hardness also decreases.

Post weld cold rolling followed by laser processing brought about a 9% decrease in UTS (932 MPa – 851 MPa) and 8% decrease in PS 863 MPa – 791 MPa) and slight increase in percentage elongation (9% to 13%), (see Figure 5-4). This change in strength and ductility which is influenced by microstructure could be explained based on the fact that some of the stored internal strain energy was relieved as a result of enhanced atomic diffusion at higher temperature. It was reported by Avner, S. H [139] that an effective indication of recrystallization can be a drop in proof strength due to releasing of internal energy.

5.6.2.4 Effect of Post Weld Cold Rolling Followed by Laser Processing then Cold Rolling on Hardness and Tensile Strength Distribution

As shown in Figure 5-3, at the weld centreline of the weld metal, the hardness value increases from 278 HV to 310 HV at the cap pass, indicating the effect of work hardening after laser processing. This cold working lead to hardening of the weld metal and there by relax the residual stress.

Further cold rolling after post weld cold rolling followed by laser processing brought about further increase (2%) in both UTS and PS with corresponding reduction in percentage elongation (13.1% -12.6%). The increase in hardness and strength is less in cold rolling after laser process because, the matrix was very tough and have high plasticity. This indicates that, this novel technique is effective in improving the strength and microstructure of the weld.

5.6.3 Metallographic Examination

The welds macrostructure and microstructure of the samples are presented below. In this section, the as-welded, post weld cold rolling, post weld cold rolling followed by laser processing and cold rolling after post weld cold rolled followed by laser processing are presented.

5.6.3.1 Macrostructure

Figure 5-5 shows macrographs of the three samples, that is, as-welded, post weld cold rolled and post weld cold rolled followed by laser processing. The profile of the weld bead, the root penetration and weld bead reinforcement are clearly shown. As shown, defects, for example lack of side wall fusion, porosity, solid inclusion etc., are not observed.

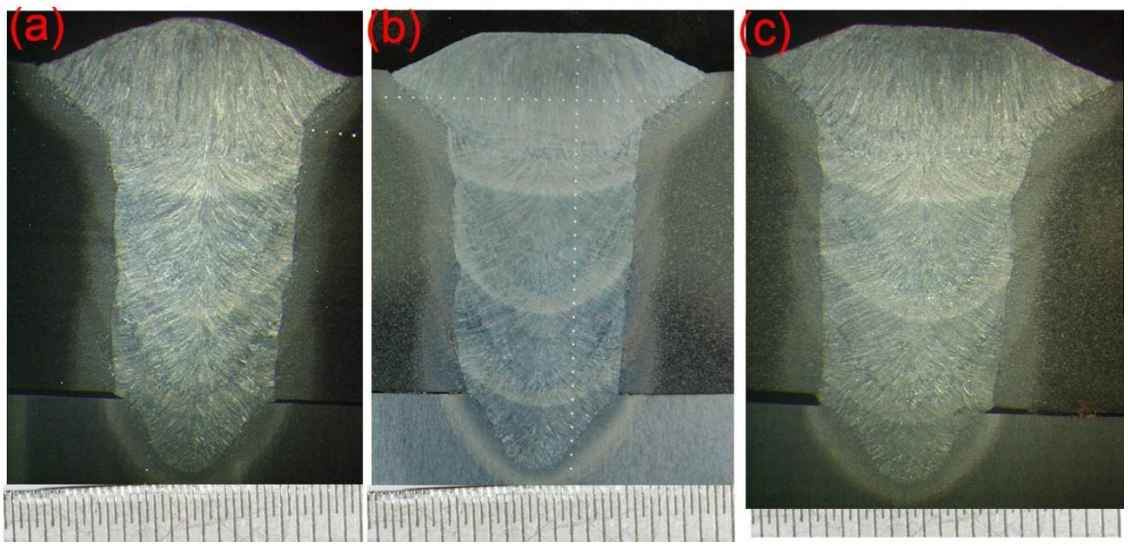

Figure 5-5: Macrographs of weld deposit layers and weld bead profiles of S275 structural steel (a) as-welded (b) post weld cold rolling (c) post weld cold rolling followed by laser processing

Macrographs assessments show an excellent weld with good penetration, good side wall fusion and porosity free welds (Figure 5-5). It was reported by Norrish, J [93] that, the addition of up to 8% CO_2 to argon gives a slightly improved bead shape, with the “wine glass” penetration which was confirmed in this research since the shielding gas used was 8% CO_2 and 92% Argon. Another possible reason for the good profile is the maintenance of the correct CTWD which was vital in ensuring a stable metal transfer.

5.6.3.2 Optical Microstructure

Figure 5-6 shows optical micrographs of both as-welded and post weld cold rolled samples, which consist of martensitic microstructures due enriched solid solution strengthening element in both the parent metal and the filler wire. For

example, silicon (high percentage in the weld metal) which is a powerful ferrite strengthener when compared with other alloying elements promotes considerable hardness through solid solution.

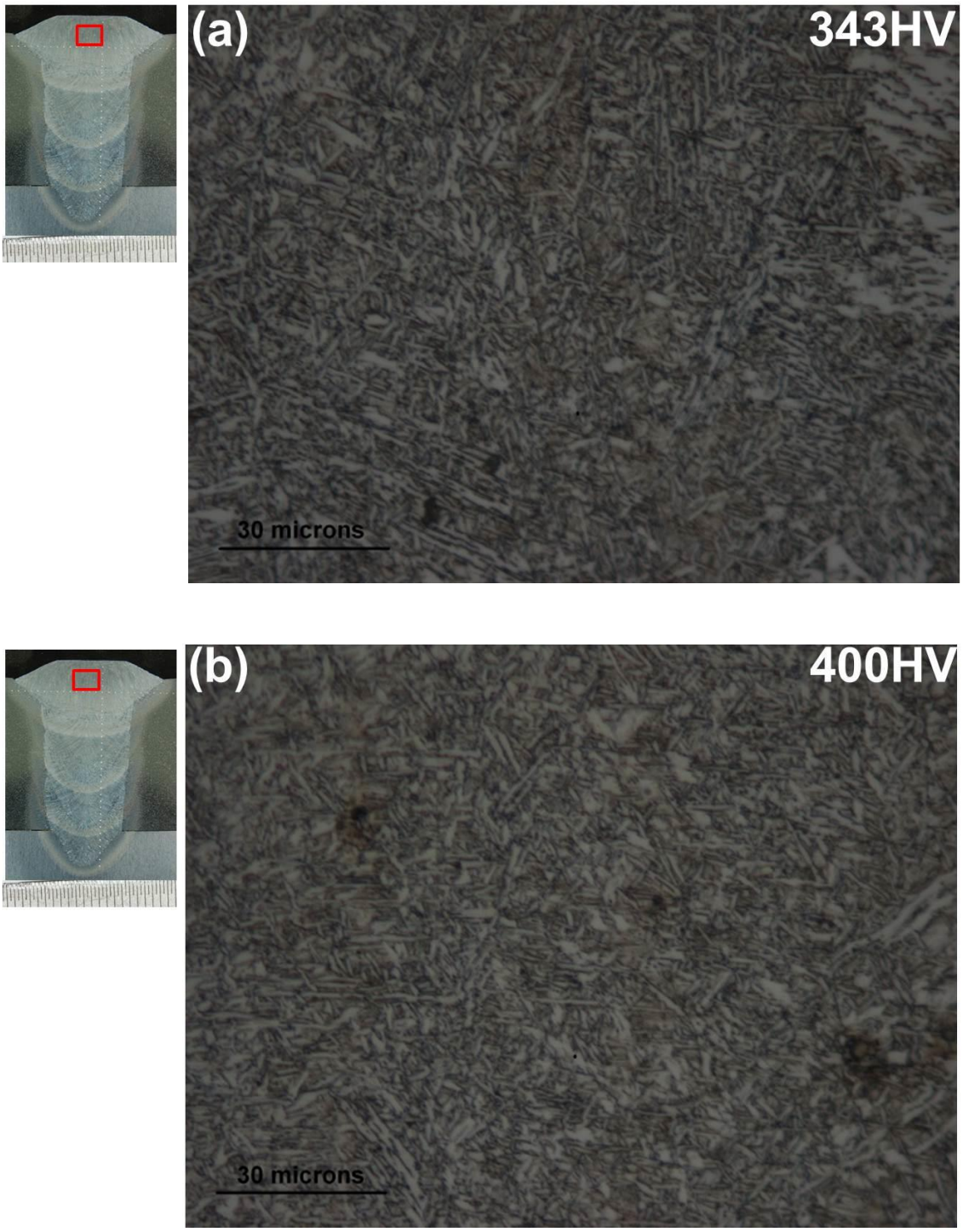

Figure 5-6: Optical micrographs at cap pass (a) as-welded (b) post weld cold rolling

Figure 5-7 shows optical micrographs of post weld cold rolled followed by laser processing as well as post weld cold rolling followed by laser processing then further cold rolling. As shown, both structures are are predominately ferrite (F) structure while pearlite (P) is evenly distributed.

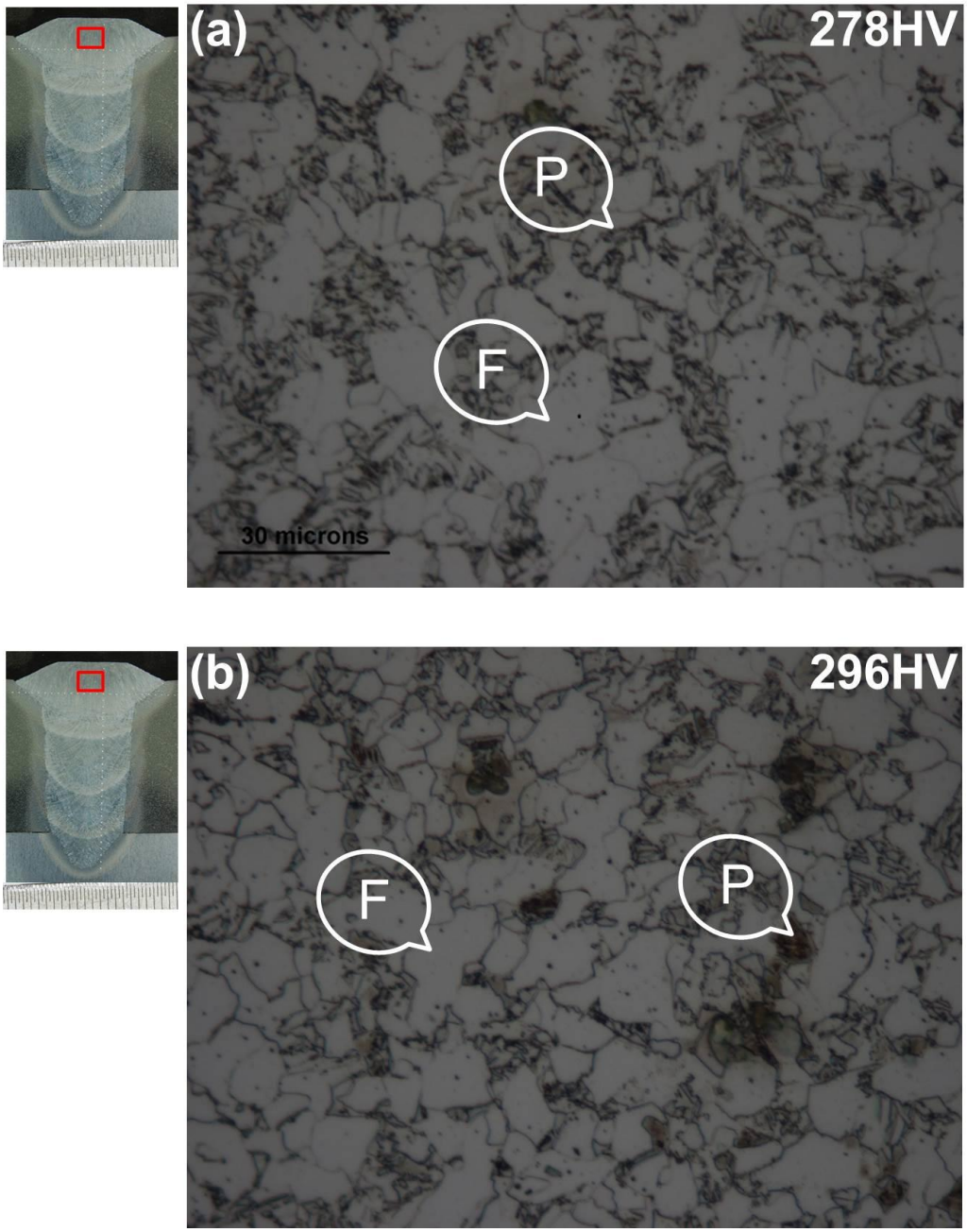

Figure 5-7: Optical micrographs at cap pass (a) post weld cold rolling followed by laser processing (b) post weld cold rolling followed by laser processing then cold rolling

5.6.3.3 Micrographs by Electron Backscatter Diffraction (EBSD)

EBSD techniques were used for further analysis. Figure 5-8 shows the crystallographic texture of the cap pass of both as-welded and post weld cold rolling samples obtained from EBSD. These micrographs were obtained from data collected over an area of 538 µm x 401 µm with step size 0.437 µm.

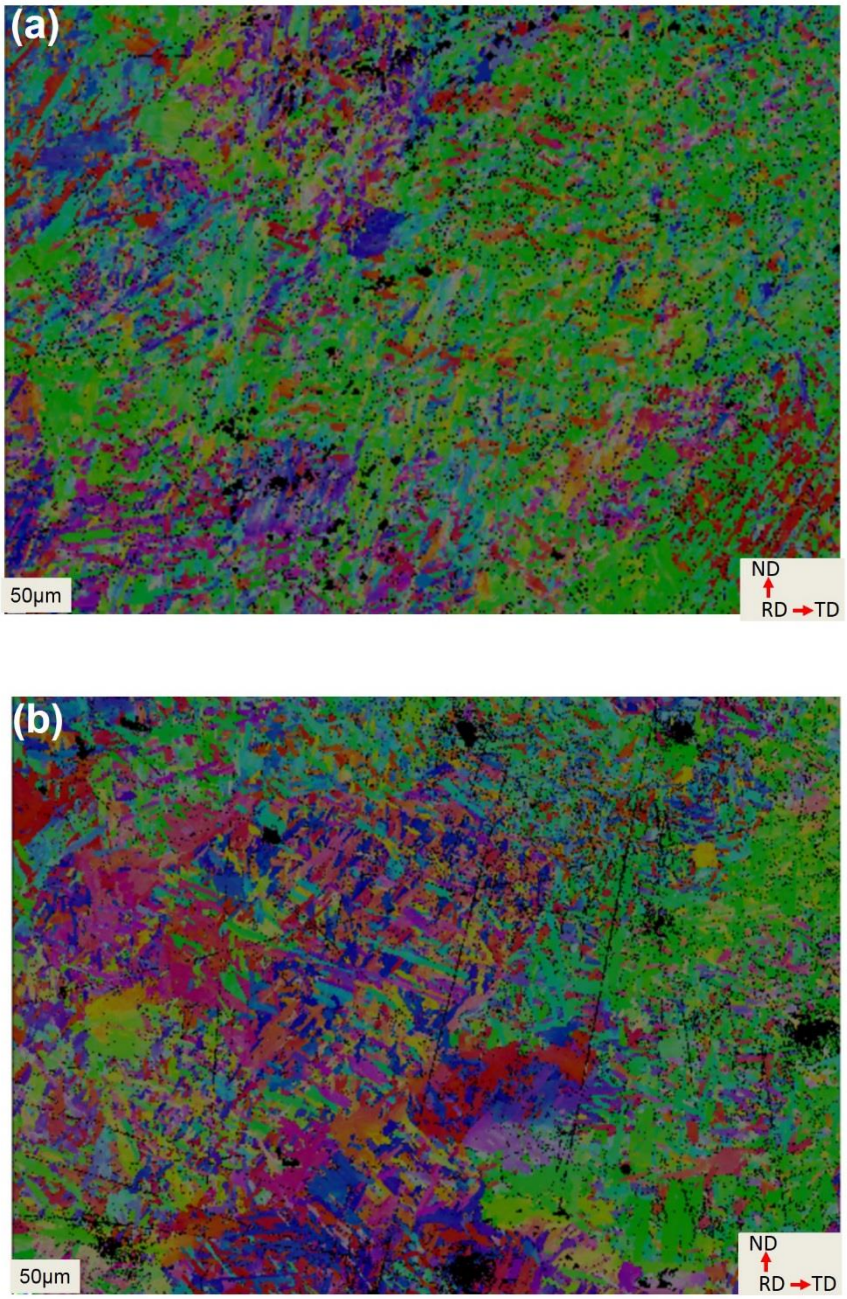

Figure 5-8: Micrograph obtained from EBSD of S275 structural steel at the cap pass (a) as-welded (b) post weld cold rolled

Figure 5-9 shows a clear grains with different orientations after laser treatment and then cold rolled.

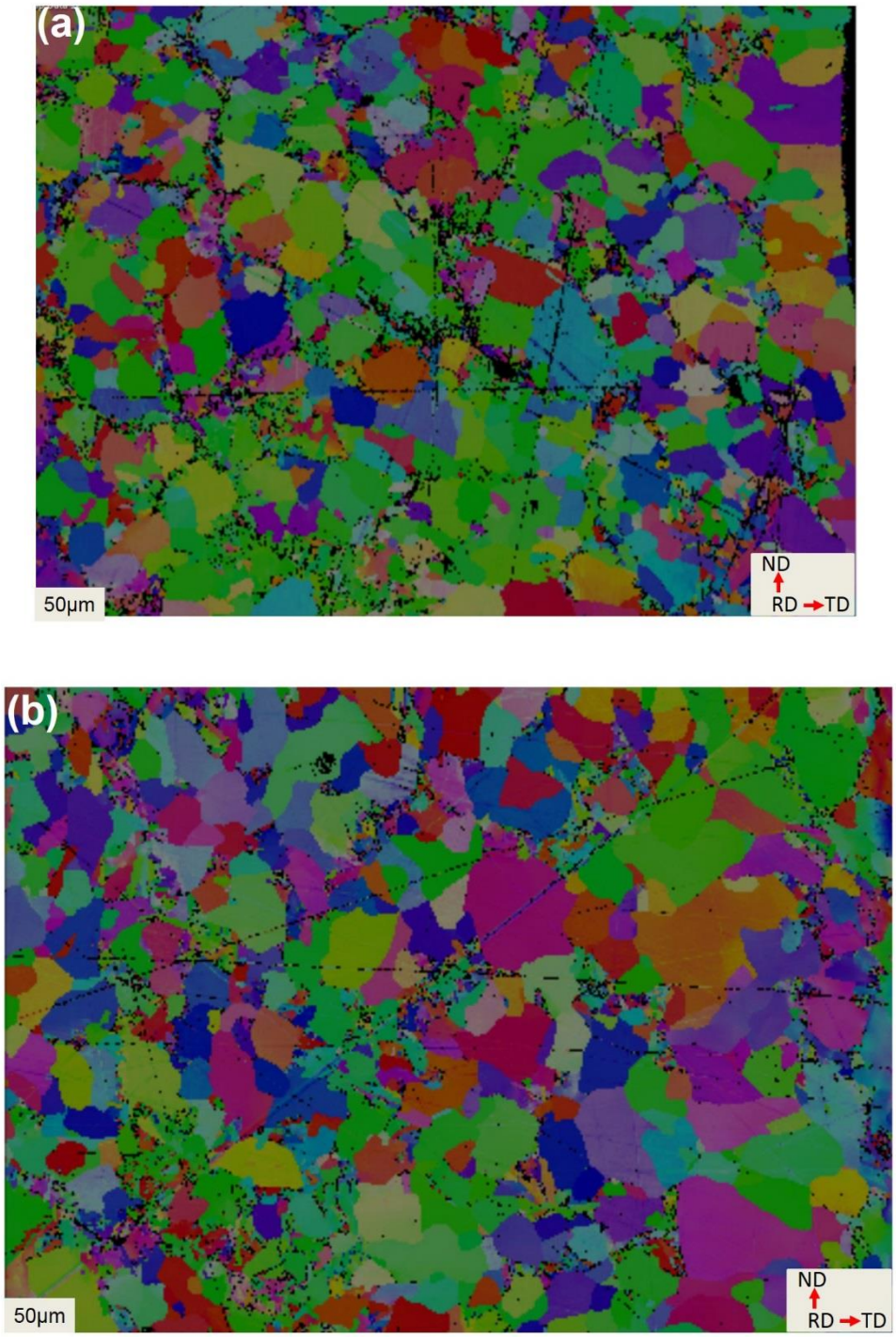

Figure 5-9: Micrograph obtained from EBSD of S275 structural steel at the cap pass of (a) post weld cold rolled followed by laser processing (b) cold rolled after post weld cold rolled followed by laser processing

Grain size is well known to be most significant metallographic measurement of microstructural feature. This is due to the fact that grain sizes are directly related to the mechanical properties of the material. These micrographs were obtained from data collected over an area of 538 µm x 401 µm with step size 0.437 µm. The as-welded and post weld cold rolled samples have dendritic grains structure with low angle grain boundary. The post weld cold rolling followed by laser processing and the cold rolling after post weld cold rolling followed by laser processing have refine grains and high angle grain boundaries. However, based on the step size used, the average grain size of 4.81 µm was found when post cold rolling followed by laser processing was applied on the sample. The post weld cold rolling followed by laser processing then, cold rolling shows a slight change in average grain size of 4.93 µm. Although this changes are very minimal, it could still influence the mechanical properties of the weld metal.

5.6.4 Residual Stress Measurement

In residual stress determination by neutron diffraction, the precise measurement of a stress-free reference lattice parameter is vital. It was reported by Rogante M [234] that, even a small error of 0.1% in stress-free reference lattice parameter (d_0) can cause a significant error in calculation of the strain which in turn affects the successive stress analysis. In order to obtain accurate measurement of the d_0, the stress-free reference should reflect any change of lattice parameter owing to thermal processing history of the component. In fusion-welded material for example, the compositional and microstructural variation across the weld caused by the thermal cycle of welding should be taken into account when determining the residual stress. It was reported [234] that a local change in solute content of the parent alloy can cause significant changes in the stress-free lattice parameter. Therefore, it is necessary to correct the measured strain point-by-point by a stress-free reference for each spatial location across the weld. For example, HAZ of plate is corrected by HAZ of a d_0 sample machined from the plate.

The reference parameter variation as measured in the comb samples, for the longitudinal directions as observed by monochromatic neutrons at the ILL in France is shown in Figure 5-10 and Figure 5-11 respectively.

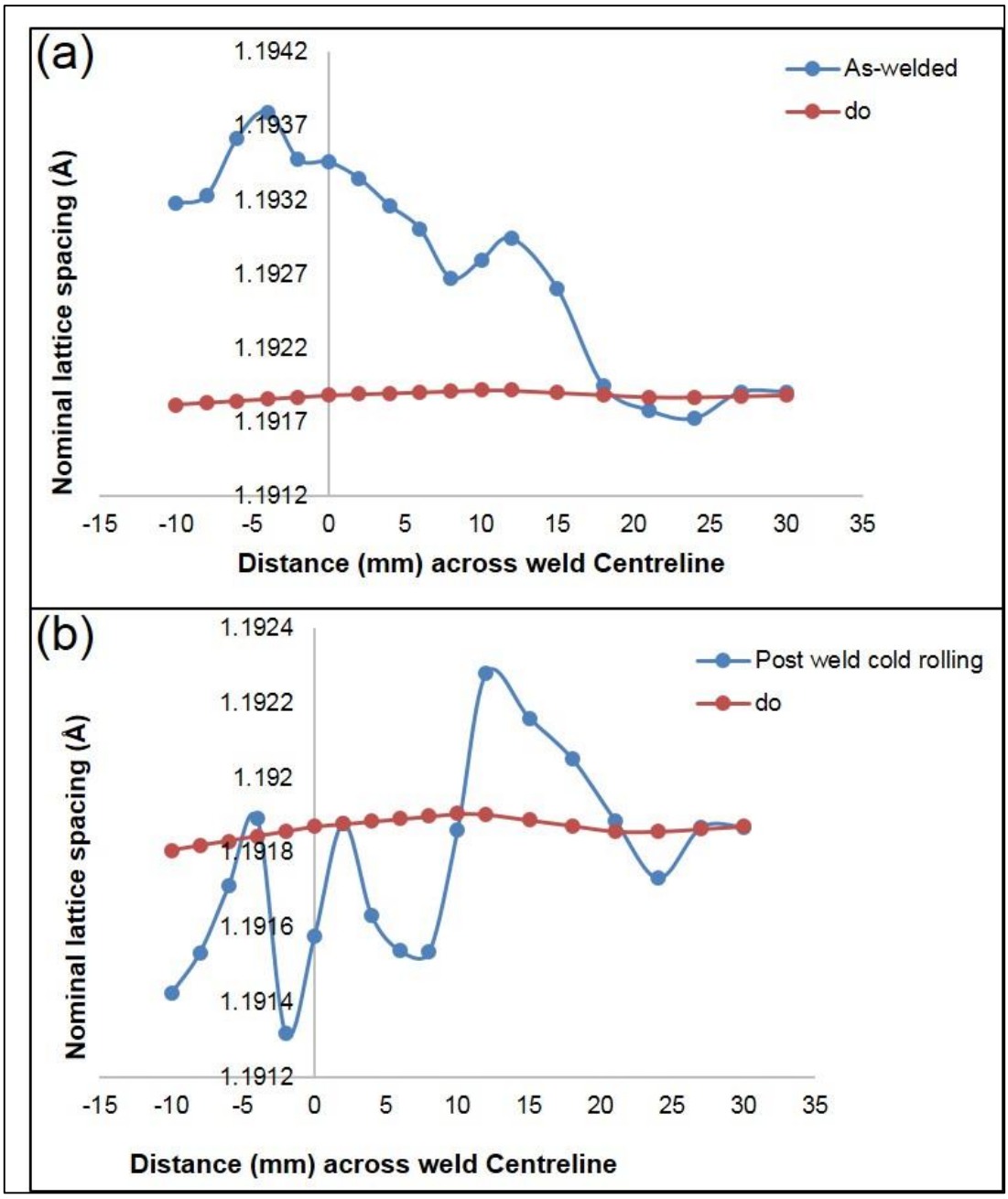

Figure 5-10 : Variation in the unstressed αFe {211} lattice spacing d_0 measured. Measurement taken at 2.5 mm below weld surface (a) as welded (b) post weld cold rolling

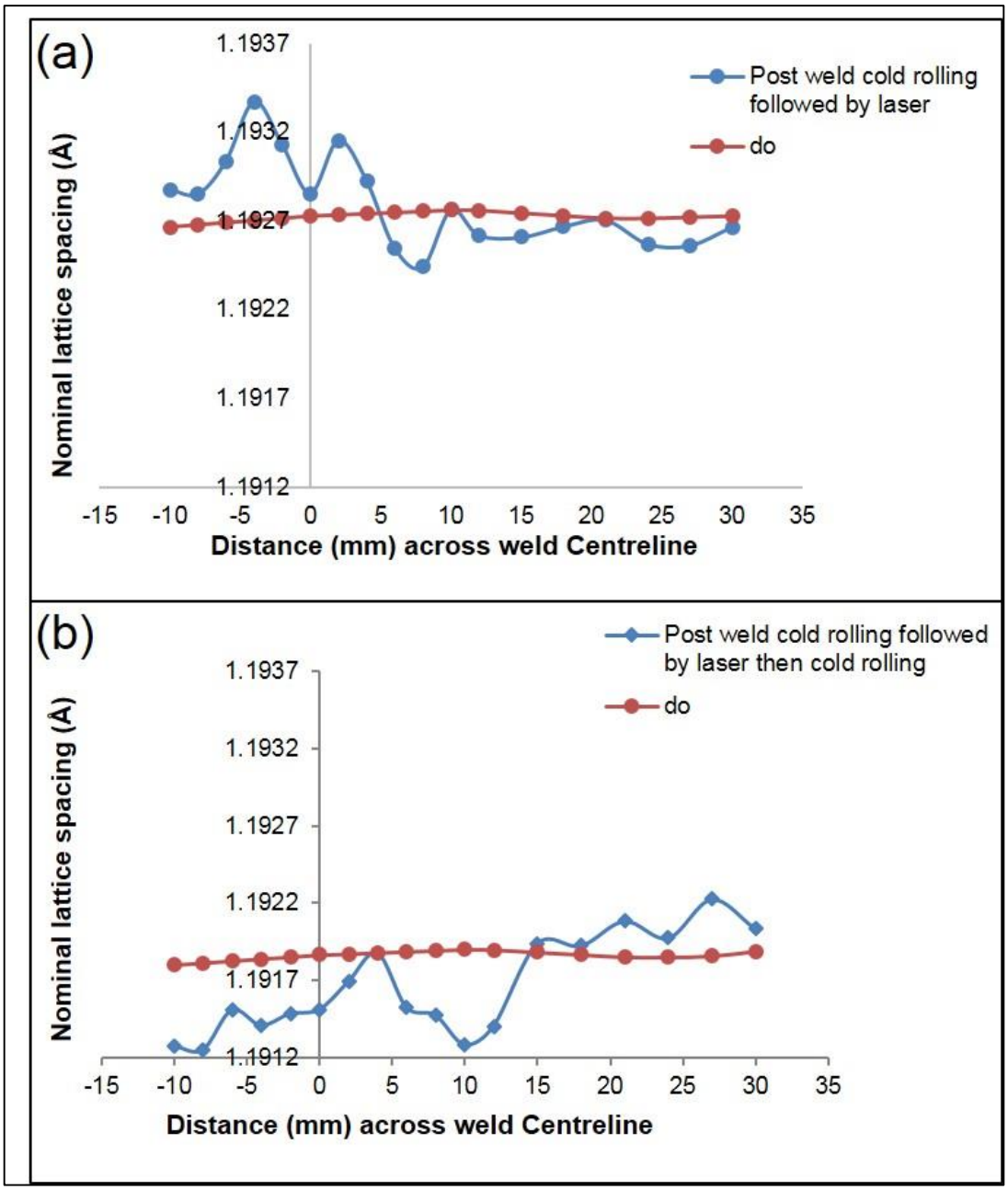

Figure 5-11 : Variation in the unstressed αFe {211} lattice spacing d_0 measured. Measurement taken at 2.5 mm below weld surface (a) post weld cold rolling followed by laser (b) post weld cold rolling followed by laser than cold rolling

Figure 5-12 shows the distribution of the longitudinal residual stress distribution profile. The measurement was taken at 6.5 mm below the weld surface. As shown, both the weld zone and HAZ show mainly tensile stress (as-welded). This stress, with a maximum value of 488 MPa at the weld metal centreline, was produced by longitudinal compressive plastic flow.

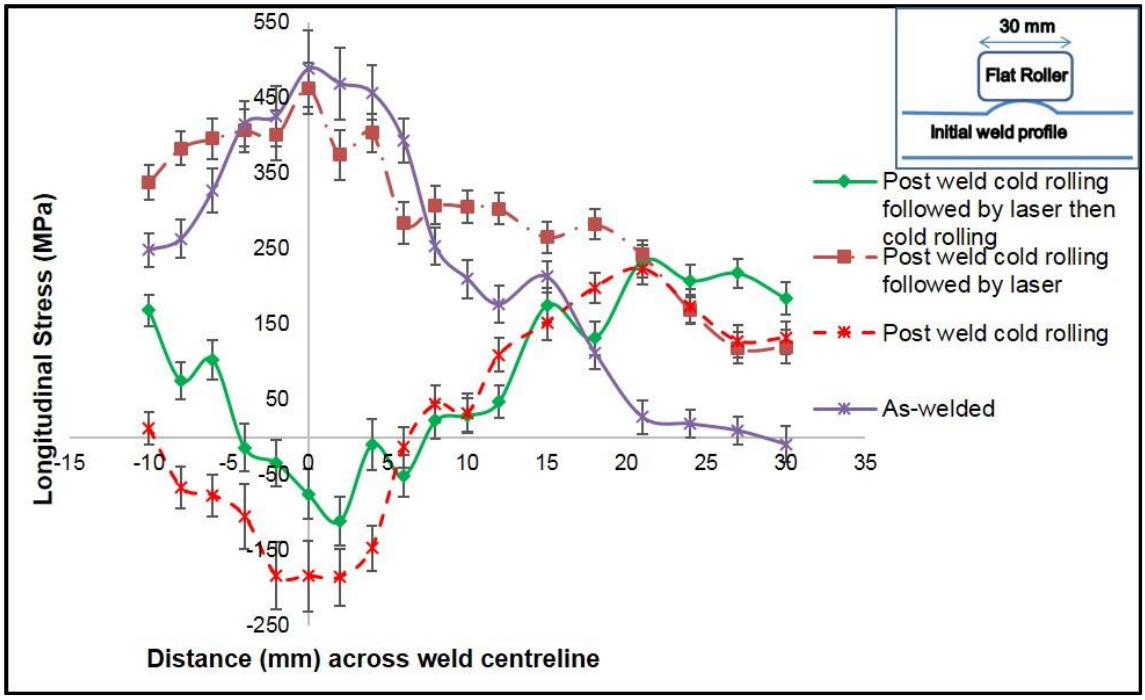

Figure 5-12 :Stress distribution across the weld metal of the samples with different processing conditions (measured 6.5 mm below the weld surface)

5.6.4.1 Effect of Post Weld Cold Rolling on Residual Stress Distribution

In this section, the discussion is focussed on the longitudinal stress direction. This is because, the large magnitude of tensile residual stresses are formed parallel to the welding direction.

Post weld cold rolling as shown in Figure 5-12 has modified the longitudinal residual stress state by modifying the tensile stress formed around the weld metal (from peak tensile stress of 488 MPa to peak compressive tensile stress of 184 MPa). The post weld cold rolling to the welded joints causes yielding of material in the weld region. This cold rolling resulted in hardening of the weld metal and thereby relax the residual stress. Since any stress field applied by external

loading is superimposed upon the distribution of residual stress, the modification of this residual stress from tensile to compressive stress component would likely prevent crack propagation that may be present across the weld under longitudinal fatigue loading.

5.6.4.2 Effect of Post Weld Cold Rolling Followed by Laser Processing on Residual Stress Distribution

Post weld cold rolling followed laser processing has shown an increase in the longitudinal residual stress from peak compressive stress of 184 MPa to peak tensile stress of 462 MPa at the weld centreline (Figure 5-12). This was observed in the previous experiment (section 3.5.6.4 and section 4.5.6.2 of this thesis). However, what is not immediately clear is the tensile stress which did not balance out with compressive stress anywhere in the profile. This can be attributed to large laser beam diameter (110 mm) used since the measured area is entirely within the heated zone. Another possible reason could be that the post weld cold rolling samples was heated for a long period of time, as a result it gives room for expansion during cooling, thus, resulted in reduced tensile stress profile.

5.6.4.3 Effect of Cold Rolled After Post Weld Cold Rolling Followed by Laser Processing on Residual Stress Distribution

Post weld cold rolling followed by laser processing then cold rolling, has modified the longitudinal residual stress state once again, by modifying the tensile stress in the weld metal (from peak tensile stress of 462 MPa to peak compressive stress of 184 MPa as shown in Figure 5-12. This further cold rolling after laser processing has demonstrated that a complete a compressive state of stress can be formed using these techniques.

5.6.4.4 Full Width at Half Maximum (FWHM)

FWHM in diffraction profiles is used to characterize different material properties. For example, it is used to indicate the plastic strain history of a component. Figure 5-13 shows the effect of FWHM at cap pass of the different processing conditions. As shown in the figure, post weld cold rolling sample (FWHM at 2.5 mm below the weld surface), was higher because of the direct contact between local mechanical tensioning (roller) and cap pass indicating more plastic deformation

at that area. This shows that FWHM is influenced by the work hardening effect of the rolling process. Post weld cold rolling followed by laser has reduced the FWHM peak indicating softening of the material by laser processing.

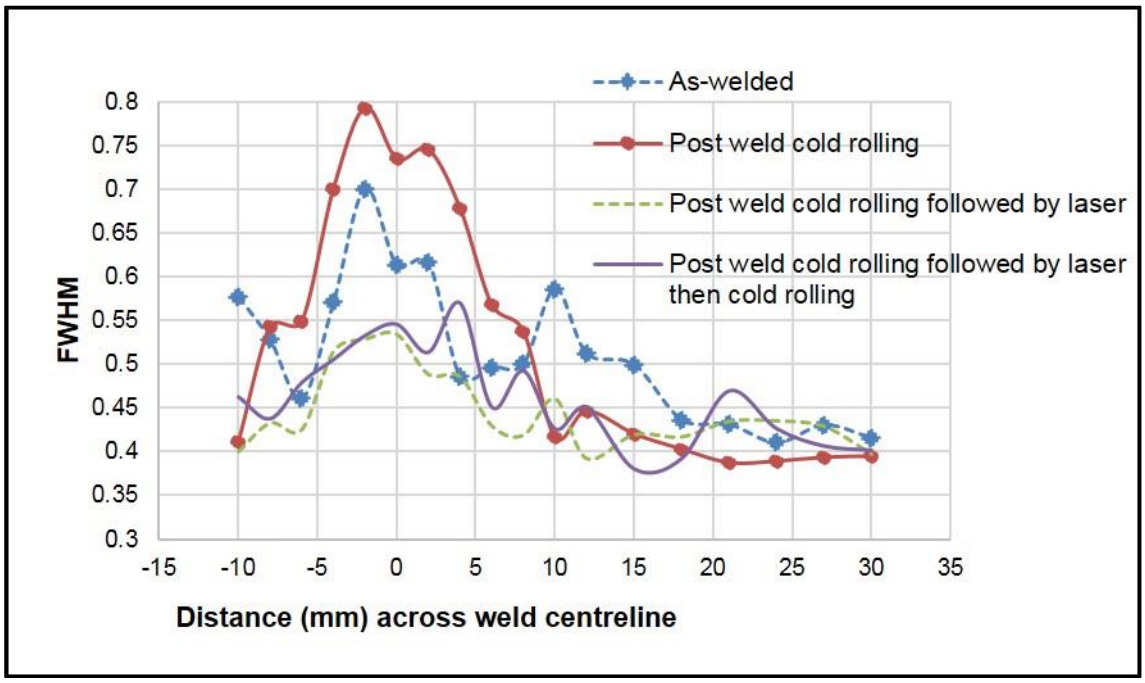

Figure 5-13: Effect of FWHM on the four processing condition at s 2.5 mm below the weld surface of the weld

5.6.5 Conclusion

Significant grain refinement was observed at the cap pass of multi-pass welds when post weld cold rolling followed by new laser processing was applied to the sample. These refined grains would, therefore, have the potential of improving the strength and toughness of the weld metal.

Although the laser processing reinstated the as-welded residual stress state profile with even higher magnitudes of peak stress, cold rolling after laser processing has modified the tensile residual stress state, and a compressive residual stress was formed below the weld metal.

As the modification of stress state is achieved by plastic deformation, 31% increase in ultimate tensile strength and 36% increases in proof strength with

corresponding reduction in percentage elongation (50.5% to 37.5%) in the fusion zone was observed.

It was shown that FWHM increase with increase in plastic deformation in this research.

6 Comparison Between the Three Structural Alloys Studied

This chapter compared the effect of the different processing condition (as-welded, post weld cold rolling, post weld cold rolling followed by laser and cold rolling after post weld cold rolling followed by laser) used in the structural alloys studied in this research.

6.1 Residual Stress Distribution

6.1.1 Effect of Post Weld Cold Rolling on Residual Stress

The effects of the applied rolling load through the thickness of the three structural alloys are presented below.

In the three structural alloys (measurement at 2 mm below the weld surface) post weld cold rolling modify the residual stress from tensile to compressive. For example, in API 5L X100 pipeline steel, the effect modified the peak tensile stress of 522 MPa to compressive stress of 205 MPa. In 304L austenitic stainless steel, measured in the same position, post weld cold rolling also modify the residual stress from tensile to compressive (Peak tensile stress of 395 MPa to compressive stress of 80 MPa). The similar behaviours were observed in S275 Structural steel.

At 6 mm below the weld surface, there was no measurement taken for API 5L X100 pipeline steel. However, in 304L austenitic stainless steel and S275 Structural steel, the effect of post weld cold rolling were observed. It modify the tensile residual stress from 319 MPa to 50 MPa in 304L austenitic stainless steel while in S275 Structural steel, the effect modify residual stress from tensile stress of 488 MPa to compressive stress of 184 MPa.

Measurement at 10 mm below the weld surface, the effect modified the tensile stress from 505 MPa to 405 MPa for API 5L X100 pipeline steel while minimal effect was observed in both 304L austenitic stainless steel and S275 Structural steel.

At 18 mm below the weld surface, there was no significant effect of rolling to modify the stress in API 5L X100 pipeline steel.

6.1.2 Effect of Post Weld Cold Rolling Followed by Laser Processing on Residual Stress

The effect of post weld cold rolling followed by laser processing was carried out in two phases. The first phase was on transient heating mode and it effect through the thickness is shown below.

In the three structural alloys (measurement at 2 mm below the weld surface) post weld cold rolling followed by laser processing, reinstated as-welded residual stress state profile with even higher magnitude of peak stress. In API 5L X100 pipeline steel, post weld cold rolling followed by laser processing change the peak compressive stress of 205 MPa to tensile stress of 770 MPa while in 304L austenitic stainless, the effect change the peak compressive stress of 80 MPa to tensile stress of 479 MPa. Similarly, in S275 Structural steel, the effect modify the compressive stress to tensile stress.

At 6 and 10 mm below the weld surface, only minimal effect were observed in all the structural alloys.

However, in the second phase of post weld cold rolling followed by laser processing (measurement at 3 mm below the weld surface), the effect reinstated as-welded residual stress state profile in all the structural alloys studied.

6.1.3 Effect of Cold Rolling After Post Weld Cold Rolling Followed by Laser Processing on Residual Stress

Further cold rolling after laser processing has redistributed and eliminated the tensile residual stress state formed during laser processing in all the three structural alloys. Generation of this compressive stress state is beneficial in improving the structural integrity of a component as most of the in-service deterioration starts with a surface flaw.

6.2 Hardness Distribution

6.2.1 Effect of Post Weld Cold Rolling on Hardness Profile

The effect of post weld cold rolling on hardness distribution through the thickness of the three structural alloys are presented below.

At distance between 0 – 4 mm below the weld surface, a significant effect of cold working was observed in all the structural alloys. In API 5L X100 pipeline steel hardness values increase from 332 HV – 388 HV, while in 304L austenitic stainless, the hardness values increase from 224 HV – 292 HV. Similarly, in S275 Structural steel the hardness values increase from 343 HV – 400 HV.

At distance between 4 – 12 mm below the weld surface minimal effect of cold working was observed in the three structural alloys.

At distance between 12– 20 mm below the weld surface, no effect of cold working was observed in API 5L X100 pipeline steel.

6.2.2 Effect of Post Weld Cold Rolling Followed by Laser Processing on Hardness Profile

The effect of post weld cold rolling followed by laser processing was carried out in two phases.

The effect of laser in the first phase (transient mode) at a distance between 0 – 4 mm below the weld surface, reduces hardness values from 388 HV – 313 HV in API 5L X100 pipeline steel while in 304L austenitic stainless, the hardness values reduces from 292 HV – 281 HV. The hardness values of S275 Structural steel was not studied in this first phase.

At distance between 4 – 12 mm below the weld surface minimal of the laser processing was observed in the three structural alloys.

Distance between 12– 20 mm below the weld surface no effect of laser processing was observed in API 5L X100 pipeline steel.

In the second phase of the laser processing, a significant effect of laser processing was observed in all the three structural alloys. In API 5L X100 pipeline

steel, the effect reduces the hardness values from 388 HV – 258 HV while in 304L austenitic stainless, the hardness values reduces from 292 HV – 245 HV in the same position (0 – 4 mm below the weld surface). Similarly, in S275 Structural steel the hardness values reduces from 400 HV – 278 HV in the same range below the weld surface.

In all cases, post weld cold rolling followed by laser processing have resulted in refining of cold worked grains which will relax the strains and also allow diffusion of interlocked carbon atoms making a more tempered structure.

At distance between 4 – 12 mm below the weld surface, minimal effect of the laser processing were observed in the three structural alloys. The hardness values of API 5L X100 pipeline steel reduces from 366 HV – 342 HV while in 304L austenitic stainless, the hardness values reduces from 250 HV – 221 HV. At the same position, hardness values of S275 Structural steel reduces from 382 HV – 320 HV.

At a distance between 12– 20 mm below the weld surface, a minimal effect of laser processing was observed reducing the hardness values of API 5L X100 pipeline steel from 390 HV – 386 HV.

6.3 Microstructure

6.3.1 Effect of Post Weld Cold Rolling on Microstructure

Dendritic and columnar grains structures were observed at the cap pass of the three structural alloys when the samples were cold rolled.

6.3.2 Effect of Post Weld Cold Rolling Followed by Laser Processing on Microstructure

The effect of post weld cold rolling followed by laser processing was carried out in two phases. The first phase which was on transient heating mode, minor grain refinement was observed at the cap pass of all the structural alloys. This indicates that recrystallization is not complete because the transient thermal cycle is not sufficient to supply enough energy to sustain the complete kinetics.

In the second phase of the laser processing, significant grain refinement was observed at the cap pass of all the structural alloys. This recrystallized microstructure with large proportion of high angle grain boundaries would increase the strength and toughness of the material which is lower in as-welded dendritic grain structure state.

7 Conclusion and Future Recommendation

This chapter is divided into two part. General conclusion and future recommendation for further research.

7.1 General Conclusion

In this research, redistribution of residual stress magnitude and profile and the microstructural characterisation were studied and compared in three multi-pass welded structural alloys after cold rolling and laser processing. These three alloys are; API 5L X100 pipeline steel plate (20 mm thick), S275JR structural steel plate (12 mm thick) and 304L austenitic stainless steel plate (12 mm thick).

In order to achieve the research aim and objectives; after post weld cold rolling, the laser processing was carried out in two phases. The laser processing in the first phase was in transient heating mode. While, in the second phase, laser processing involves applying thermal energy for a prolonged period. Also in the second phase, further cold rolling after laser processing was applied. From this experiment, it can be concluded that;

- In residual stress analysis of all the structural alloys studied, the stress variation in as-welded state, showed diminishing longitudinal peak stress magnitude through the thickness from cap to root pass.
- Post weld cold rolling was effective in redistributing the stress field. Up to 4 mm below the capping pass in API 5L X100 pipeline steel plate, post weld cold rolling modifies the stress state from tensile to compressive across the weld centre line. While in 304L austenitic stainless steel, post weld cold rolling was effective in modifying the residual stress distribution throughout the entire thickness. Up to 6.5 mm below the capping pass in S275JR structural steel, post weld cold rolling modifies the stress state from tensile to compressive across the weld centre line.
- Post weld cold rolling followed by laser processing in both transient heating mode and prolonged period, in all the three structural alloys reinstated the as-welded residual stress magnitude and distribution.

- Further cold rolling after laser processing has redistributed and eliminated the tensile residual stress state formed during laser processing. Generation of this compressive stress state is beneficial in improving the structural integrity of a component as most of the in-service deterioration starts with a surface flaw.
- Microstructural characterization in the first phase (transient heating mode) showed minor grain refinement near the capping pass for all the structural alloys. While the microstructural characterization in the second phase (prolonged period of heating) shows a full recrystallization of the grain structure and formation of new set of strain free grains at the capping pass of all the three structural alloys. The generation of the recrystallized microstructure with large proportion of high angle grain boundaries would increase the strength and toughness of the material which is lower in as-welded dendritic grain structure state.
- The recrystallized grain structure is particularly important in the 304L austenitic stainless steel. This is because the change in dendritic structure to a kind of equiaxed grains structure will limit the Cr segregation in the welds which would have resulted in formation of corrosion microcells as well as reduction in overall corrosion prevention due to depletion of alloying elements.
- With respect to mechanical properties, in the post weld cold rolling condition, hardness distribution in all the structural alloys showed a significant evidence of plastic deformation at the cap pass of the weld metal.
- The post weld cold rolling results in an increase in ultimate tensile strength and proof strength with corresponding reduction in elongation in the fusion zone of all the alloys. Laser processing after cold rolling reverted back the as-welded conditions with reduction of the ultimate tensile strength and proof strength and corresponding increase in elongation.
- In summary, this novel processing clearly demonstrates the improvement of structural features that can be obtained in traditional welded structural alloys. However, optimisation of the post weld cold rolling and laser

processing would be required for different alloy systems. It would be advisable to consider the material's work hardening characteristics, and the effects of deformation on metallurgical and constitutive properties, if post weld cold rolling is to be applied.

7.2 Recommendations for Further Work

- Modelling of thermal fields will be required to find the effect of post weld cold rolling followed by laser processing on residual stress distribution through the thickness of multi-pass welds. This will give a comprehensive understanding of this novel processing.
- Experiment should be conducted on ferritic and austenitic steel pipe so as to determine the effect of this novel processing on the hoop stresses as well as axial stresses of the pipe.
- Further experimental study should be carried out in other materials e.g., titanium.
- Modelling should be carried out in the way the thermocouples are been attached to the sample. This will give accurate determination of the temperature through the thickness of the multi-pass welds.
- Beam shaping of the laser beam diameter will be recommended to ensure that the heating is within the weld metal.
- Compared thermal – mechanical finite element model of this novel processing.

REFERENCES

[1] Sandrea, R. and Sandrea, I. (2010), "Deepwater crude oil output: How large will the uptick be?", *Oil and Gas Journal,* vol. 108, no. 41, pp. 48-53.

[2] Yapp, D. and Blackman, S. A. (2004), "Recent Developments in High Productivity Pipeline Welding", *Journal of the Brazilian Society of Mechanical Sciences and Engineering,* vol. 26, no. 1, pp. 89-97.

[3] Demofonti, G. and Mannucci, G. (2008), "A critical revue of the developed and available know how devoted to a safe use of X100 grade steel in large diameter pipelines", *New Developments on Metallurgy and Applications of High Strength Steels, Buenos Aires 2008 - Proc. Int. Conf. New Developments on Metallurgy and Applications of High Strength Steels,* Vol. 1 Plenary Lectures Automotive Applications High Temperature Applications Oils and Gas Applications, pp. 625.

[4] Spinelli, C. M., Demofonti, G., Lucci, A., Di Biagio, M. and Ahmad, M. (2014), "CO_2 pipeline transportation new needs", *Proceedings of the International Offshore and Polar Engineering Conference,* pp. 9.

[5] Liessem, A., Schröder, J., Pant, M., Erdelen-Peppler, M., Liedtke, M., Höhler, S. and Stallybrass, C. (2008), "Manufacturing challenges of high strength line pipes", *New Developments on Metallurgy and Applications of High Strength Steels, Buenos Aires 2008 - Proc. Int. Conf. New Developments on Metallurgy and Applications of High Strength Steels,* Vol. 1 Plenary Lectures Automotive Applications High Temperature Applications Oils and Gas Applications, pp. 543.

[6] Honeycombe, R. W. K. and Bhadeshia, H. K. D. H. (1995), “Steels: microstructure and properties*”,* 2nd ed, Butterworth-Heinemann, Oxford.

[7] Jibrin, S. (2010), “Pigging requirements for deepwater pipelines as part of integrity management routine” (MSc thesis), Cranfield University, Cranfield University, UK.

[8] Gowrisankar, I., Bhaduri, A. K., Seetharaman, V., Verma, D. D. N. and Achar, D. R. G. (1987), “Effect of the number of passes on the structure and properties of Submerged Arc welds of AISI Type 316L stainless steel”, available at: http://www.aws.org/wj/supplement/WJ_1987_05_s147.pdf (accessed 09/18/2014).

[9] Park, M. J., Yang, H. N., Jang, D. Y., Kim, J. S. and Jin, T. E. (2004), "Residual stress measurement on welded specimen by neutron diffraction", *Journal of Materials Processing Technology,* vol. 155-156, no. 1-3, pp. 1171-1177.

[10] Kou, S. (2003), *Welding Metellury,* 2nd ed, John Wiley & Sons, Inc., Hoboken, New Jersey., Canada.

[11] Coules, H. E., Cozzolino, L. D., Colegrove, P., Ganguly, S., Wen, S. W. and Pirling, T. (2012), "Neutron Diffraction Analysis of Complete Residual Stress Tensors in Conventional and Rolled Gas Metal Arc Welds", *Experimental Mechanics,* vol. 53, no. 2, pp. 195-204.

[12] Mullins, J. and Gunnars, J., (2011), *Deformation histories relevant to multipass girth welds: Temperature, stress and plastic strain histories*, Riva del Garda, Trento ed.

[13] Francis, J. A., Bhadeshia, H. K. D. H. and Withers, P. J. (2007), "Welding residual stresses in ferritic power plant steels", *Materials Science and Technology,* vol. 23, no. 9, pp. 1009-1020.

[14] Palanichamy, P., Vasudevan, M. and Jayakumar, T. (2009), "Measurement of residual stresses in austenitic stainless steel weld joints using ultrasonic technique", *Science and Technology of Welding and Joining,* vol. 14, no. 2, pp. 166-171.

[15] Yanagida, N. and Koide, H. (2006), "Residual stress improvement in multi-layer welding of austenitic stainless steel plates by using water-shower cooling during welding process", Vol. 2006, .

[16] Monin, V. I., Gurova, T., Castello, X. and Estefen, S. F. (2009), "Analysis of residual stress state in welded steel plates by X-ray diffraction method", *Reviews on Advanced Materials Science,* vol. 20, no. 2, pp. 172-175.

[17] Withers, P. J. (2007), "Residual stress and its role in failure", *Reports on Progress in Physics,* vol. 70, no. 12, pp. 2211-2264.

[18] Albertini, G., Bruno, G., Carradò, A., Fiori, F., Rogante, M. and Rustichelli, F. (1999), "Determination of residual stresses in materials and industrial components by neutron diffraction", *Measurement Science and Technology,* vol. 10, no. 3, pp. R56-R73.

[19] Pirling, T., Bruno, G. and Withers, P. J. (2006), "SALSA-A new instrument for strain imaging in engineering materials and components", *Materials Science and Engineering A,* vol. 437, no. 1, pp. 139-144.

[20] Smith, D. J. and Garwood, S. J. (1992), "Influence of postweld heat treatment on the variation of residual stresses in 50 mm thick welded ferritic steel plates", *International Journal of Pressure Vessels and Piping,* vol. 51, no. 2, pp. 241-256.

[21] Porowski, J. S., O'Donnell, W. J., Badlani, M. L. and Hampton, E. J. (1990), "Use of the mechanical stress improvement process to mitigate stress corrosion cracking in BWR piping systems", *Nuclear Engineering and Design,* vol. 124, no. 1-2, pp. 91-100.

[22] Richards, D. G., Prangnell, P. B., Williams, S. W. and Withers, P. J. (2008), "Global mechanical tensioning for the management of residual stresses in welds", *Materials Science and Engineering A,* vol. 489, no. 1-2, pp. 351-362.

[23] Jurcius, A. and Valiulis, A. V. (2008), "Reduce of material residual stresses using vibration energy", *VIBROENGINEERING 2008 - Proceedings of 7th International Conference,* pp. 50.

[24] Rao, D., Chen, L. and Ni, C. (2006), "Vibratory stress relief of welded structure in China", *Materials at High Temperatures,* vol. 23, no. 3-4, pp. 245-250.

[25] Kurkin, S. A. and Anufriev, V. I. (1984), "Preventing distortion of welded thin-walled members of AMg6 1201 Aluminium alloys by rolling the weld with a roller behind the welding arc.", *Welding Production (English translation of Svarochnoe Proizvodstvo),* vol. 31, no. 10, pp. 52-55.

[26] Kurkin, S. A. and Anufriev V.I. Milekhin, E. S. (1980), "Improving the mechanical properties of welded joints in the AMg6 alloy by plastic deformation during arc welding, svarochnoe proizvodstvo,", vol. 27, pp. 20 - 24.

[27] Liu, W., Tian, X. and Zhang, X. (1996), "Preventing weld hot cracking by synchronous rolling during welding", *Welding Journal (Miami, Fla),* vol. 75, no. 9, pp. 297-s.

[28] Coules, H. E., Colegrove, P., Cozzolino, L. D., Wen, S. W., Ganguly, S. and Pirling, T. (2012), "Effect of high pressure rolling on weld-induced residual stresses", *Science and Technology of Welding and Joining,* vol. 17, no. 5, pp. 394-401.

[29] Altenkirch, J., Steuwer, A., Withers, P. J., Williams, S. W., Poad, M. and Wen, S. W. (2009), "Residual stress engineering in friction stir welds by roller tensioning", *Science and Technology of Welding and Joining,* vol. 14, no. 2, pp. 185-192.

[30] Flemings, M. C. (1974), *Solidification processing,* McGraw-Hill, New York.

[31] Feest, E. A. and Doherty, R. D. (1973), "Dendritic solidification of Cu-Ni alloys: Part II. The influence of initial dendrite growth temperature on microsegregation", *Metallurgical Transactions,* vol. 4, no. 1, pp. 125-136.

[32] Staron, P., Koçak, M., Williams, S. and Wescott, A. (2004), "Residual stress in friction stir-welded A1 sheets", *Physica B: Condensed Matter,* vol. 350, no. 1-3 SUPPL. 1, pp. e491-e493.

[33] Price, D. A., Williams, S. W., Wescott, A., Harrison, C. J. C., Rezai, A., Steuwer, A., Peel, M., Staron, P. and Koçak, M. (2007), "Distortion control in welding by mechanical tensioning", *Science and Technology of Welding and Joining,* vol. 12, no. 7, pp. 620-633.

[34] Kondakov, G. F. and Martynov, A. N. (1986), "Effect of methods of local deformation on residual stresses and properties of welded joints.", *Welding Production (English translation of Svarochnoe Proizvodstvo),* vol. 33, no. 5, pp. 28-30.

[35] Klas, W. and Gunnar, L. (eds.) (2006), *MIG welding guide,* 1st ed, Woodhead Publishing Limited and CRC Press LLC, England.

[36] Palani, P. K. and Murugan, N. (2006), "Selection of parameters of pulsed current gas metal arc welding", *Journal of Materials Processing Technology,* vol. 172, no. 1, pp. 1-10.

[37] Sven, G. (2001)*, Tandem MIG/Mag Welding*, available at: www.esabindo.co.id/global/en/products/upload/tandem.pdf (accessed 06/12/2011).

[38] Theocharis, L. (2007), “Tandem Gas Metal Arc Pipeline Welding (PhD. thesis)”, Cranfield University, Cranfield University, UK.

[39] Lassaline, E., Zajaczkowski, B. and North, T. H. (1989), "Narrow groove twin-wire GMAW of high-strength steel", *Welding Journal (Miami, Fla),* vol. 68, no. 9, pp. 53-58.

[40] Michie, K. (1998), “Twin-wire GMAW of pipeline girth welds (unpublished MSc. thesis)”, Cranfield Uinversity, Cranfield University, UK.

[41] Hudson, M. G. (2004), “Welding of X100 Linepipe (PhD. thesis)”, Cranfield University, Cranfield University, UK.

[42] International Institute of welding (1974), “Development and application of narrow gap arc welding processes in Japan”, IIW/Doc-XII-584-74, Japan Institute of welding, Japan.

[43] Malin, V. (1987), "Monograph on narrow-Gap Welding Technology", *Welding Research Council,* vol. 323, pp. 1-52.

[44] Meister, R. P. and Martin, D. C. (1966), "narrow-gap welding process", *British Welding Journal,* vol. 13, no. 5, pp. 252-257.

[45] Malin, V. Y. (1983), "State-of-the-art of Narrow Gap Welding- Part II", *Welding Journal (Miami, Fla),* vol. 62, no. 6, pp. 37-46.

[46] Westing (2011), “Narrow-groove welding system”, available at: http://www.westinghousenuclear.com/products_&_Services/docs/flysheets/NS-IMS-0035.pdf (accessed 06/08/2012).

[47] Baxter, C. F. G. (1979), “Narrow gap MIG welding- a review of the literature”, WI-104/1979, The welding Institute, Abington, Cambridge.

[48] Michael, N. (2008), “Experimental tandem GMAW in narrow gap X100 pipe material.(unpublished Msc. thesis)”, Cranfield University, Cranfield, Cranfield, UK.

[49] Hutt, G. A. (1984), "Narrow Gap Welding.", *Metal construction,* vol. 16, no. 6, pp. 355-361.

[50] Modenesi, P. J. (1990), *Statistical Modelling of the Narrow Gap Gas Metal Arc Welding Process* (PhD thesis), Cranfield University, Cranfield University.

[51] Bel'chuk, G. A. and Titov, N. Y. (1970), "Effects of automatic welding conditions with a narrow gap on weld shape", *Automatic Welding,* vol. 23, no. 12, pp. 48-51.

[52] Kurokawa, T., Nakajima, M., Ishikawa, Y. and Urayama, A. (1966), "The narrow gap MIG welding process for thick steel plates", *International Institute of welding,* vol. 3, no. 3, pp. 1-12.

[53] Lebedev, V. K. and et'al. (1977), "The gas-shielded welding of joints in low-carbon high-alloy steels with a slit preparation", *Automatic Welding,* vol. 30, no. 5, pp. 1-5.

[54] Kimura, S., Ishihara, I. and Nagai, Y. (1979), "Narrow gap gas metal arc welding process in flat position", vol. 58, no. 7, pp. 44-52.

[55] Matsunawa, A. and Nishiguchi, K. (1979), "Arc behaviour, plate melting and pressure balance of molten pool in narrow grooves", *Proceedings, International Conference on Arc Physics and Weld Pool Behavour,* no. Paper 9, pp. 301-310.

[56] Fennel, M. M. (1986), “The process parameters of horizontal-vertical narrow gap welding using CTP MIG welding process (MSc thesis)”, Cranfield University, Cranfield University, UK.

[57] Jackson, J. E. and Sargent, H. B. (1967), "Striaght-Polarity Groove welding of Thick steel plate", *Welding Journal,* vol. 46, pp. 905-914.

[58] Smith, A. A. and British Welding Research Association (1959), “Positional welding of steel with the CO2 process”, Bwra, London.

[59] Akbari, D. and Sattari-Far, I. (2009), "Effect of the welding heat input on residual stresses in butt-welds of dissimilar pipe joints", *International Journal of Pressure Vessels and Piping,* vol. 86, no. 11, pp. 769-776.

[60] Qian, G. (1999), "A survey of develpment in welding stress and distortion controlling in aerospace manufacturing in China", vol. 43 (1), pp. 64 - 74.

[61] Taljat, B., Radhakrishnan, B. and Zacharia, T. (1998), "Numerical analysis of GTA welding process with emphasis on post-solidification phase transformation effects on residual stresses", *Materials Science and Engineering A,* vol. 246, no. 1-2, pp. 45-54.

[62] Ghosh, A., Chattopadhyaya, S. and Das, R. K. (2011), "Effect of heat input on submerged arc welded plates", *11th International Conference on the Mechanical Behavior of Materials, ICM11,* Vol. 10, 5 June 2011 through 9 June 2011, Como, pp. 2791.

[63] Murugan, S., Kumar, P. V., Raj, B. and Bose, M. S. C. (1998), "Temperature distribution during multipass welding of plates", *International Journal of Pressure Vessels and Piping,* vol. 75, no. 12, pp. 891-905.

[64] Howard, B. C. (1998), "Modern welding technology", 4 th edition ed, Prentice-Hall inc, New Jersey.

[65] Funderburk, R. S. (2014), "The important of interpass temperature", available at: http://www.jflf.org/pdfs/papers/keyconcepts3.pdf (accessed 02/22/2014).

[66] Trevisan, R. E., Santos, N. F., Fals, H. C. and Santos, A. A. (2002), "Effect of interpass temperature on morphology, microstructure and microhardness of welded API 5L X65 steel", *Proceedings of the 4th International Pipeline Conference,* Vol. A, 30 September 2002 through 3 October 2002, Calgary, Alta., pp. 327.

[67] Jones, J. E. and Luo, Y. (1990), "Welding: Theory and Practice", Elsevier.

[68] Radaj, D. (1992), "Heat Effects of Welding-temperature field, residual stress, distortion", in Springer-Verlag, USA, pp. 348.

[69] Lord, M. (1999), "Effect of interpass temperature on properties of high-strength weld metals", *Svetsaren, a Welding Review,* vol. 54, no. 1, pp. 53-58.

[70] Lord, M. and Bhadeshia, H. K. D. H. (1998), "Scatter in Steel Weld Metal Tensile Properties due to Variations in the Interpass Temperature", *ASM Proceedings of the International Conference: Trends in Welding Research,* pp. 870.

[71] Lord, M. (1998), "Interpass temperature and the welding of strong steels", *Welding in the World, Le Soudage Dans Le Monde,* vol. 41, no. 5, pp. 452-459.

[72] Anon (1986), "Guidelines for the clasification of ferritic steel weld metal microstructural constituents using the light microscope. ", *Welding in the World, Le Soudage Dans Le Monde,* vol. 24, no. 7-8, pp. 144-149.

[73] Thewlis, G. (2004), "Materials perspective: Classification and quantification of microstructures in steels", *Materials Science and Technology,* vol. 20, no. 2, pp. 143-160.

[74] Narayanan, B. K., Kovarik, L., Quintana, M. A. and Mills, M. J. (2011), "Characterisation of ferritic weld microstructures using various electron microscopy techniques: A review", *Science and Technology of Welding and Joining,* vol. 16, no. 1, pp. 12-22.

[75] Anon (1991), "Guide to the light microscope examination of ferritic steel weld metals", *Welding in the World, Le Soudage Dans Le Monde,* vol. 29, no. 7-8, pp. 160-177.

[76] Tweed, J. H. and Knott, J. F. (1983), "Effect of reheating on microstructure and toughness of C-Mn weld metal", *Metal Science,* vol. 17, pp. 45-54.

[77] Komizo, Y. -. and Terasaki, H. (2010), "In-situ study of phase transformation in steel during welding", *20th International Offshore and Polar Engineering Conference, ISOPE-2010,* Vol. 4, 20 - 25 June 2010, Beijing, pp. 303.

[78] Hamelin, C.J., Muránsky, O., Bendeich, P., Short, K. and Edwards, L., (2012), “Predicting solid-state phase transformations during welding of ferritic steels”, Quebec City, QC ed.

[79] Rojko, D. and Gliha, V. (2005), "The influence of simulated thermal cycle on the formation of microstructures of multi-pass weld metal", *Metalurgija,* vol. 44, no. 1, pp. 19-24.

[80] Shome, M. and Mohanty, O. N. (2006), "Continuous cooling transformation diagrams applicable to the heat-affected zone of HSLA-80 and HSLA-100 steels", *Metallurgical and Materials Transactions A: Physical Metallurgy and Materials Science,* vol. 37, no. 7, pp. 2159-2169.

[81] Babu, S. S. (2004), "The mechanism of acicular ferrite in weld deposits", *Current Opinion in Solid State and Materials Science,* vol. 8, no. 3-4, pp. 267-278.

[82] Babu, S. S., Elmer, J. W., David, S. A. and Quintana, M. A. (2002), "In situ observations of non-equilibrium austenite formation during weld solidification of an Fe-C-Al-Mn low-alloy steel", *Proceedings of the Royal Society A: Mathematical, Physical and Engineering Sciences,* vol. 458, no. 2020, pp. 811-821.

[83] Shanmugam, S., Ramisetti, N. K., Misra, R. D. K., Mannering, T., Panda, D. and Jansto, S. (2007), "Effect of cooling rate on the microstructure and mechanical properties of Nb-microalloyed steels", *Materials Science and Engineering A,* vol. 460-461, pp. 335-343.

[84] Xu, G., Wan, L., Yu, S., Liu, L. and Luo, F. (2008), "A new method for accurate plotting continuous cooling transformation curves", *Materials Letters,* vol. 62, no. 24, pp. 3978-3980.

[85] Zhao, M. -., Yang, K., Xiao, F. -. and Shan, Y. -. (2003), "Continuous cooling transformation of undeformed and deformed low carbon pipeline steels", *Materials Science and Engineering A,* vol. 355, no. 1-2, pp. 126-136.

[86] Offerman, S.E., Strandlund, H., Van Dijk, N.H., Sietsma, J., Lauridsen, E.M., Margulies, L., Poulsen, H.F., Ågren, J. and Van Der Zwaag, S., (2007), “Ferrite formation during slow continuous cooling in steel”, Manchester ed.

[87] Lee, J. -., Hon, M. -. and Cheng, G. -. (1987), "The continuous cooling transformation of carbon-manganese steel", *Scripta Metallurgica,* vol. 21, no. 4, pp. 521-526.

[88] Krauss, G. and Thompson, S. W. (1995), "Ferritic microstructures in continuously cooled low- and ultralow carbon steels", *ISIJ International,* vol. 35, no. 8, pp. 937-945.

[89] Madhusudhan Reddy, G., Mohandas, T. and Sarma, D. S. (2003), "Cold cracking studies on low alloy steel weldments: Effect of filler metal composition", *Science and Technology of Welding and Joining,* vol. 8, no. 6, pp. 407-414.

[90] Hunt, A. C., Kluken, A. O. and Edwards, G. R. (1994), "Heat input and dilution effects in microalloyed steel weld metals", *Welding Journal,* vol. 73, no. 1, pp. 9s-15s.

[91] Salter, G. and Dye, S. (1971), "Selecting gas mixtures for MIG welding", *Metal Constr Brit Weld J,* vol. 3, no. 6, pp. 230-233.

[92] Kah, P. and Martikainen, J. (2012), "Influence of shielding gases in the welding of metals", *International Journal of Advanced Manufacturing Technology,* vol. 64, pp. 1411-1421.

[93] Norrish, J. and Institute of Physics (1992), “Advanced welding processes”, Institute of Physics Publishing, Bristol.

[94] Dillenbeck, V.,R. and Castagno, L. (1987), "The effects of various shielding gases and associated mixtures in GMA welding of mild steel", *Welding Journal,* vol. 66, no. 9, pp. 45-49.

[95] Dixon, K. (1999), "Shielding gas selection for GMAW of steels", *Welding and Metal Fabrication,* vol. 67, no. 4, pp. 8-13.

[96] Uygur, I. and Gulenc, B. (2004), "The effect of shielding gas compositions for MIG welding process in mechanical behavior of low carbon steel", *Metalurgija,* vol. 43, no. 1, pp. 35-40.

[97] Canto, M. A. A. (1992), "MIG/MAG welding: shielding gas effects on weld metal mechanical properties and bead geometry", vol. 2, pp. 895-908.

[98] Kim, K. H., Seo, J. S., Lee, C. and Kim, H. J. (2011), "Grain size of acicular ferrite in ferritic weld metal", *Welding in the World,* vol. 55, no. 9-10, pp. 36-40.

[99] Ricks, R. A., Howell, P. R. and Barritte, G. S. (1982), "The nature of acicular ferrite in HSLA steel weld metals", *Journal of Materials Science,* vol. 17, no. 3, pp. 732-740.

[100] Farrar, R. A. and Harrison, P. L. (1987), "Acicular ferrite in carbon-manganese weld metals: An overview", *Journal of Materials Science,* vol. 22, no. 11, pp. 3812-3820.

[101] Kim, Y. M., Lee, H. and Kim, N. J. (2008), "Transformation behavior and microstructural characteristics of acicular ferrite in linepipe steels", *Materials Science and Engineering A,* vol. 478, no. 1-2, pp. 361-370.

[102] Kim, Y. M., Lee, H., Yoo, J. Y. and Kim, N. J. (2005), "Microstructural characteristics of acicular ferrite in linepipe steels", *15th International Offrshore and Polar Engineering Conference, ISOPE-2005,* Vol. 2005, 19 - 24 June 2005, Seoul, pp. 135.

[103] Yang, J. R., Huang, C. Y., Huang, C. F. and Aoh, J. H. (1995), "Acicular ferrite transformation in deformed austenite of an alloy-steel weld metal", *Journal of Materials Science,* vol. 30, no. 19, pp. 5036-5041.

[104] Zalazar, M., Quesada, H. J. and Asta, E. P. (1998), "Microstructure produced in the welding of steels for wide diameter pipes", *Revista de Metalurgia (Madrid),* vol. 34, no. 6, pp. 469-475.

[105] Mythili, R., Thomas Paul, V., Saroja, S., Vijayalakshmi, M. and Raghunathan, V. S. (2003), "Microstructural modification due to reheating in multipass manual metal arc welds of 9Cr-1Mo steel", *Journal of Nuclear Materials,* vol. 312, no. 2-3, pp. 199-206.

[106] Clyde, M. A. (1958), "Cooling rates and peak temperatures in fusion welding", *Welding Journal,* vol. 37, pp. 210s-215s.

[107] Haze, T. and Aihara, S. (1986), "Metallurgical factors controlling HAZ toughess in HT50 Steels," vol. IIW Doc., no. UK. pp. IX-1423-86.

[108] Easterling, K. (1992), "Phase transformations during cooling of the weld metal", in *Introduction to the physical metallurgy of welding,* 2nd ed, Butterworth-Heinemann, Oxford, pp. 94-97.

[109] Cary, H. B. (1981), "Modern welding technology", in *Modern Welding Technology,* 2nd. ed, Amercian Welding Society, USA, pp. 497-498.

[110] Liao, M. T. and Chen, W. J. (1998), "The influence of shielding gas on notch toughness of stainless steel weld metals", *Materials and Manufacturing Processes,* vol. 13, no. 4, pp. 565-573.

[111] Karci, F., Kaçar, R. and Gündüz, S. (2009), "The effect of process parameter on the properties of spot welded cold deformed AISI304 grade austenitic stainless steel", *Journal of Materials Processing Technology,* vol. 209, no. 8, pp. 4011-4019.

[112] Lippold, J. C. and Kotecki, D. J. (2005), *Welding metallurgy and weldability of stainless steels John C. Lippold and Damian J. Kotecki,* John Wiley & Sons Inc, Hoboken, NJ.

[113] Hunter, A. and Ferry, M. (2002), "Phase formation during solidification of AISI 304 austenitic stainless steel", *Scripta Materialia,* vol. 46, no. 4, pp. 253-258.

[114] Ferrandini, P. L., Rios, C. T., Dutra, A. T., Jaime, M. A., Mei, P. R. and Caram, R. (2006), "Solute segregation and microstructure of directionally solidified austenitic stainless steel", *Materials Science and Engineering A,* vol. 435-436, pp. 139-144.

[115] Ma, J. C., Yang, Y. S., Tong, W. H., Fang, Y., Yu, Y. and Hu, Z. Q. (2007), "Microstructural evolution in AISI 304 stainless steel during directional solidification and subsequent solid-state transformation", *Materials Science and Engineering A,* vol. 444, no. 1-2, pp. 64-68.

[116] Elmer, J. W., Wong, J. and Ressler, T. (2000), "In-situ observations of phase transformations during solidification and cooling of austenitic stainless steel welds using time-resolved X-ray diffraction", *Scripta Materialia,* vol. 43, no. 8, pp. 751-757.

[117] Kotecki, D. J. and Siewert, T. A. (1992), "WRC-1992 constitution diagram for stainless steel weld metal: a modification of the WRC-1988 diagram." *Welding Journal,* vol. 71, no. 5, pp. 171s-178s.

[118] Vasudevan, M., Bhaduri, A. K., Raj, B. and Prasad Rao, K. (2003), "Delta ferrite prediction in stainless steel welds using neural network analysis and comparison with other prediction methods", *Journal of Materials Processing Technology,* vol. 142, no. 1, pp. 20-28.

[119] Raj, B., Shankar, V. and Bhaduri, A. K. (2006), “Welding technology for engineers”, Alpha Science International Ltd, Oxford.

[120] Huang, H. -. (2009), "Effects of shielding gas composition and activating flux on GTAW weldments", *Materials and Design,* vol. 30, no. 7, pp. 2404-2409.

[121] Cui, Y. and Lundin, C. D. (2005), "Evaluation of initial corrosion location in E316L austenitic stainless steel weld metals", *Materials Letters,* vol. 59, no. 12, pp. 1542-1546.

[122] Liao, M. T. and Chen, W. J. (1999), "A comparison of gas metal arc welding with flux-cored wires and solid wires using shielding gas", *International Journal of Advanced Manufacturing Technology,* vol. 15, no. 1, pp. 49-53.

[123] Lin, Y. C. and Chen, P. Y. (2001), "Effect of nitrogen content and retained ferrite on the residual stress in austenitic stainless steel weldments", *Materials Science and Engineering A,* vol. 307, no. 1-2, pp. 165-171.

[124] Silva, C. C., de Miranda, H. C., de Sant'Ana, H. B. and Farias, J. P. (2009), "Microstructure, hardness and petroleum corrosion evaluation of 316L/AWS E309MoL-16 weld metal", *Materials Characterization,* vol. 60, no. 4, pp. 346-352.

[125] Song, Y., Baker, T. N. and McPherson, N. A. (1996), "A study of precipitation in as-welded 316LN plate using 316L/317L weld metal", *Materials Science and Engineering A,* vol. 212, no. 2, pp. 228-234.

[126] Padilha, A. F., Escriba, D. M., Materna-Morris, E., Rieth, M. and Klimenkov, M. (2007), "Precipitation in AISI 316L(N) during creep tests at 550 and 600 °C up to 10 years", *Journal of Nuclear Materials,* vol. 362, no. 1, pp. 132-138.

[127] Sahlaoui, H., Makhlouf, K., Sidhom, H. and Philibert, J. (2004), "Effects of ageing conditions on the precipitates evolution, chromium depletion and intergranular corrosion susceptibility of AISI 316L: Experimental and modeling results", *Materials Science and Engineering A,* vol. 372, no. 1-2, pp. 98-108.

[128] Matula, M., Hyspecka, L., Svoboda, M., Vodarek, V., Dagbert, C., Galland, J., Stonawska, Z. and Tuma, L. (2001), "Intergranular corrosion of AISI 316L steel", *Materials Characterization,* vol. 46, no. 2-3, pp. 203-210.

[129] Tusek, J. and Suban, M. (2000), "Experimental research of the effect of hydrogen in argon as a shielding gas in arc welding of high-alloy stainless steel", *International Journal of Hydrogen Energy,* vol. 25, no. 4, pp. 369-376.

[130] Durgutlu, A. (2004), "Experimental investigation of the effect of hydrogen in argon as a shielding gas on TIG welding of austenitic stainless steel", *Materials and Design,* vol. 25, no. 1, pp. 19-23.

[131] Leggatt, R. H. (2008), "Residual stresses in welded structures", *International Journal of Pressure Vessels and Piping,* vol. 85, no. 3, pp. 144-151.

[132] Kuhlmann-Wilsdorf, D. and Hansen, N. (1991), "Geometrically necessary, incidental and subgrain boundaries", *Scripta Metallurgica et Materiala,* vol. 25, no. 7, pp. 1557-1562.

[133] Liu, Q. and Hansen, N. (1995), "Geometrically necessary boundaries and incidental dislocation boundaries formed during cold deformation", *Scripta Metallurgica et Materiala,* vol. 32, no. 8, pp. 1289-1295.

[134] Jakobsen, B., Poulsen, H. F., Lienert, U., Almer, J., Shastri, S. D., Sørensen, H. O., Gundlach, C. and Pantleon, W. (2006), "Formation and subdivision of deformation structures during plastic deformation", *Science,* vol. 312, no. 5775, pp. 889-892.

[135] Hoffmann, B., Vöhringer, O. and Macherauch, E. (2001), "Effect of compressive plastic deformation on mean lattice strains, dislocation densities and flow stresses of martensitically hardened steels", *Materials Science and Engineering A,* vol. 319-321, pp. 299-303.

[136] Yasnij, P. V., Glad'o, V. B. and Gutsailyuk, V. B. (2003), "Effect of elastic-plastic deformation on dislocation structure of 15Kh2MFA steel", *Problemy Prochnosti,* , no. 6, pp. 30-38.

[137] Pham, M. S., Solenthaler, C., Janssens, K. G. F. and Holdsworth, S. R. (2011), "Dislocation structure evolution and its effects on cyclic deformation response of AISI 316L stainless steel", *Materials Science and Engineering A,* vol. 528, no. 7-8, pp. 3261-3269.

[138] Takaki, S., Tsuchiyama, T., Nakashima, K., Hidaka, H., Kawasaki, K. and Futamura, Y. (2004), "Microstructure development of steel during severe plastic deformation", *Metals and Materials International,* vol. 10, no. 6, pp. 533-539.

[139] Avner, S. H. (1974), “Introduction to physical metallurgy*”,* 2nd ed, McGraw Hill Kogakusha, Tokyo.

[140] L'Uboš, M., Karlsson, L., Ivan, H., Pavol, M. and Miroslav, V., (2010), “Influence of plastic deformation on the residual stress distribution and fatigue behaviour of high strength steels welds”.

[141] William, D. C. (2007), “Material science & engineering; an introduction”, 7th ed, , USA.

[142] Hallberg, H. and Ristinmaa, M. (2013), "Microstructure evolution influenced by dislocation density gradients modeled in a reaction-diffusion system", *Computational Materials Science,* vol. 67, pp. 373-383.

[143] Cotterill P., M. P. R. (1976), “Recrystallization and Grain Growth in metals”, First ed, Surrey University Press, London.

[144] Doherty, R. D., Hughes, D. A., Humphreys, F. J., Jonas, J. J., Juul Jensen, D., Kassner, M. E., King, W. E., McNelley, T. R., McQueen, H. J. and Rollett, A. D. (1997), "Current issues in recrystallization: A review", *Materials Science and Engineering A,* vol. 238, no. 2, pp. 219-274.

[145] Humphreys, F. J. and Hatherly, M. (2004), “Recrystallization and related annealing phenomena”, 2nd ed, Elsevier, Amsterdam; Boston.

[146] Wilkinson, A. J. and Hirsch, P. B. (1997), "Electron diffraction based techniques in scanning electron microscopy of bulk materials", *Micron,* vol. 28, no. 4, pp. 279-308.

[147] Humphreys, F. J. (2001), "Grain and subgrain characterisation by electron backscatter diffraction", *Journal of Materials Science,* vol. 36, no. 16, pp. 3833-3854.

[148] Messler, R. W. (2007), "Fusion welding processes in Principles of Welding”. Wiley, pp. 60-63.

[149] Coule, H. E. (2012), “Characterising the effects of high-pressure rolling on residual stress in structural steels welds (PhD Thesis thesis)”, Cranfield University, Cranfield University, UK.

[150] Withers, P. J. and Bhadeshia, H. K. D. H. (2001), "Residual stress part 1 - Measurement techniques", *Materials Science and Technology,* vol. 17, no. 4, pp. 355-365.

[151] Masubuchi, K. (1980.), “Analysis of Welded Structures”, Pergamon Press, Oxford.

[152] Hallen, K. (1985), “Introduction to fracture mechanics”, McGraw-Hill, New York.

[153] Finch, D. M. and Burdekin, F. M. (1992), "Effects of welding residual stresses on significance of defects in various types of welded joint", *Engineering Fracture Mechanics,* vol. 41, no. 5, pp. 721-735.

[154] Chang, K. -. and Lee, C. -. (2007), "Residual stresses and fracture mechanics analysis of a crack in welds of high strength steels", *Engineering Fracture Mechanics,* vol. 74, no. 6, pp. 980-994.

[155] Mahmoudi, A. H., Truman, C. E. and Smith, D. J. (2008), "Using local out-of-plane compression (LOPC) to study the effects of residual stress on apparent fracture toughness", *Engineering Fracture Mechanics,* vol. 75, no. 6, pp. 1516-1534.

[156] Ainsworth, R. A., Sharples, J. K. and Smith, S. D. (2000), "Effects of residual stresses on fracture behaviour - experimental results and assessment methods", *Journal of Strain Analysis for Engineering Design,* vol. 35, no. 4, pp. 307-316.

[157] Anderson, T. L. (2005), “Fracture mechanics: fundamentals and applications”, CRC Press, Boca Raton, FL.

[158] McClung, R. C. (2007), "A literature survey on the stability and significance of residual stresses during fatigue", *Fatigue and Fracture of Engineering Materials and Structures,* vol. 30, no. 3, pp. 173-205.

[159] Dong, P. (2008), "Length scale of secondary stresses in fracture and fatigue", *International Journal of Pressure Vessels and Piping,* vol. 85, no. 3, pp. 128-143.

[160] Fricke, S., Keim, E. and Schmidt, J. (2001), "Numerical weld modeling - A method for calculating weld-induced residual stresses", *Nuclear Engineering and Design,* vol. 206, no. 2-3, pp. 139-150.

[161] Horn, R. M., Gordon, G. M., Ford, F. P. and Cowan, R. L. (1997), "Experience and assessment of stress corrosion cracking in L-grade stainless steel BWR internals", *Nuclear Engineering and Design,* vol. 174, no. 3, pp. 313-325.

[162] Leis, B. N. and Parkins, R. N. (1998), "Mechanics and material aspects in predicting serviceability limited by stress-corrosion cracking", *Fatigue and Fracture of Engineering Materials and Structures,* vol. 21, no. 5, pp. 583-601.

[163] Korsunsky, A. M. and Regino, G. M. (2007), "Residual elastic strains in autofrettaged tubes: Variational analysis by the eigenstrain finite element method", *Journal of Applied Mechanics, Transactions ASME,* vol. 74, no. 4, pp. 717-722.

[164] Dong, P. (2005), "Residual stresses and distortions in welded structures: A perspective for engineering applications", *Science and Technology of Welding and Joining,* vol. 10, no. 4, pp. 389-398.

[165] Masubuchi, K. (1997), "Prediction and control of residual stresses and distortion in welded structures", *Welding Research Abroad,* vol. 43, no. 6-7, pp. 2-16.

[166] Michael, A. W. (2013), "Effect of different loading conditions on the accumulation of residual strain in a creep resistant 1%CrMoV steel, A neutron and X-ray diffraction study", available at: http://infoscience.epfl.ch/record/186305/files/EPFL_TH5722.pdf (accessed 06/16/2013).

[167] Schajer, G. S. (2010), "Relaxation methods for measuring residual stresses: Techniques and opportunities", *Proceedings of the Society for Experimental Mechanics, Inc.,* vol. 67, pp. 1117-1127.

[168] Withers, P. J., Turski, M., Edwards, L., Bouchard, P. J. and Buttle, D. J. (2008), "Recent advances in residual stress measurement", *International Journal of Pressure Vessels and Piping,* vol. 85, no. 3, pp. 118-127.

[169] Prime, M. B. (2001), "Cross-sectional mapping of residual stresses by measuring the surface contour after a cut", *Journal of Engineering Materials and Technology, Transactions of the ASME,* vol. 123, no. 2, pp. 162-168.

[170] Schajer, G. S. (2010), "Hole-drilling residual stress measurements at 75: Origins, advances, opportunities", *Experimental Mechanics,* vol. 50, no. 2, pp. 245-253.

[171] Withers, P. J. (2007), "Mapping residual and internal stress in materials by neutron diffraction", *Comptes Rendus Physique,* vol. 8, no. 7-8, pp. 806-820.

[172] Hutchings, M.T., Withers P.J., Holden T.M., and Lorentzen T., (2005), “Introduction to the characterization of residual stress by neutron diffraction”, CRC Press, Boca Raton, FL.

[173] Krawitz, A. D. (2011), "Neutron strain measurement", *Materials Science and Technology,* vol. 27, no. 3, pp. 589-603.

[174] Reimers, W., Broda, M., Brusch, G., Dantz, D., Liss, K. -., Pyzalla, A., Schmackers, T. and Tschentscher, T. (1998), "Evaluation of residual stresses in the bulk of materials by high energy synchrotron diffraction", *Journal of Nondestructive Evaluation,* vol. 17, no. 3, pp. 129-140.

[175] Joseph, A., Palanichamy, P., Rai, S. K., Jayakumar, T. and Raj, B. (1998), "Non-destructive measurement of residual stresses in carbon steel

weld joints", *Science and Technology of Welding and Joining,* vol. 3, no. 6, pp. 267-271.

[176] Jang, J. -., Son, D., Lee, Y. -., Choi, Y. and Kwon, D. (2003), "Assessing welding residual stress in A335 P12 steel welds before and after stress-relaxation annealing through instrumented indentation technique", *Scripta Materialia,* vol. 48, no. 6, pp. 743-748.

[177] Cho, J. R., Lee, B. Y., Moon, Y. H. and Van Tyne, C. J. (2004), "Investigation of residual stress and post weld heat treatment of multi-pass welds by finite element method and experiments", *Journal of Materials Processing Technology,* vol. 155-156, no. 1-3, pp. 1690-1695.

[178] Smith, D. J., Bouchard, P. J. and George, D. (2000), "Measurement and prediction of residual stresses in thick-section steel welds", *Journal of Strain Analysis for Engineering Design,* vol. 35, no. 4, pp. 287-305.

[179] Şedek, P., Bŕozda, J., Wang, L. and Withers, P. J. (2003), "Residual stress relief in MAG welded joints of dissimilar steels", *International Journal of Pressure Vessels and Piping,* vol. 80, no. 10, pp. 705-713.

[180] Dhooge, A. and Vinckier, A. (1987), "Reheat cracking-A review of recent studies", *International Journal of Pressure Vessels and Piping,* vol. 27, no. 4, pp. 239-269.

[181] Gery, D., Long, H. and Maropoulos, P. (2005), "Effects of welding speed, energy input and heat source distribution on temperature variations in butt joint welding", *Journal of Materials Processing Technology,* vol. 167, no. 2-3, pp. 393-401.

[182] Colegrove, P., Ikeagu, C., Thistlethwaite, A., Williams, S., Nagy, T., Suder, W., Steuwer, A. and Pirling, T. (2009), "Welding process impact on residual stress and distortion", *Science and Technology of Welding and Joining,* vol. 14, no. 8, pp. 717-725.

[183] Lombard, H., Hattingh, D. G., Steuwer, A. and James, M. N. (2009), "Effect of process parameters on the residual stresses in AA5083-H321 friction stir welds", *Materials Science and Engineering A,* vol. 501, no. 1-2, pp. 119-124.

[184] Lin, Y. C. and Lee, K. H. (1997), "Effect of preheating on the residual stress in type 304 stainless steel weldment", *Journal of Materials Processing Technology,* vol. 63, no. 1-3, pp. 797-801.

[185] Dan, S. and Chandra, U. (2003), "Handbook of Aluminium: Physical metallurgy and process,", vol. 1, pp. 305 - 345.

[186] Maddox, S. J. (1985), "Improving the fatigue strength of welded joints by peening.", *Metal construction,* vol. 17, no. 4, pp. 220-224.

[187] Hacini, L., Van Lê, N. and Bocher, P. (2008), "Effect of impact energy on residual stresses induced by hammer peening of 304L plates", *Journal of Materials Processing Technology,* vol. 208, no. 1-3, pp. 542-548.

[188] Lah, N. A. C., Ali, A., Ismail, N., Chai, L. P. and Mohamed, A. A. (2010), "The effect of controlled shot peening on fusion welded joints", *Materials and Design,* vol. 31, no. 1, pp. 312-324.

[189] Gnirss, G. (1988), "Vibration and vibratory stress relief: Historical development, theory and practical application", *Welding in the World, Le Soudage Dans Le Monde,* vol. 26, no. 11-12, pp. 284-291.

[190] Sonsino, C. M., Müller, F., De Back, J. and Gresnigt, A. M. (1996), "Influence of stress relieving by vibration on the fatigue behaviour of welded joints in comparison to post-weld heat treatment", *Fatigue and Fracture of Engineering Materials and Structures,* vol. 19, no. 6, pp. 703-708.

[191] Walker, C. A., Waddell, A. J. and Johnston, D. J. (1995), "Vibratory stress relief - an investigation of the underlying processes", *Proceedings of*

the Institution of Mechanical Engineers, Part E: Journal of Process Mechanical Engineering, vol. 209, no. E1, pp. 51-58.

[192] Kwofie, S. (2009), "Plasticity model for simulation, description and evaluation of vibratory stress relief", *Materials Science and Engineering A,* vol. 516, no. 1-2, pp. 154-161.

[193] Yang, Y. P. (2009), "Understanding of vibration stress relief with computation modeling", *Journal of Materials Engineering and Performance,* vol. 18, no. 7, pp. 856-862.

[194] Yang, Y. P., Dong, P., Zhang, J. and Tian, X. (2000), "Hot-cracking mitigation technique for welding high-strength aluminum alloy", *Welding Journal (Miami, Fla),* vol. 79, no. 1, pp. 9s-17s.

[195] Van Der Aa, E. M., Hermans, M. J. M. and Richardson, I. M. (2006), "Conceptual model for stress and strain development during welding with trailing heat sink", *Science and Technology of Welding and Joining,* vol. 11, no. 4, pp. 488-495.

[196] Li, J., Guan, Q., Shi, Y. W. and Guo, D. L. (2004), "Stress and distortion mitigation technique for welding titanium alloy thin sheet", *Science and Technology of Welding and Joining,* vol. 9, no. 5, pp. 451-458.

[197] Soul, F., Ateeg, M., Beshay, S. and Senfier, M. (2010), "Residual stress correlation in two different mitigation techniques using FEA", *Advanced Materials Research,* vol. 83-86, pp. 1254-1261.

[198] Richards, D. G., Prangnell, P. B., Withers, P. J., Williams, S. W., Nagy, T. and Morgan, S. (2010), "Efficacy of active cooling for controlling residual stresses in friction stir welds", *Science and Technology of Welding and Joining,* vol. 15, no. 2, pp. 156-165.

[199] Wen, S. W., Colegrove, P. A., Williams, S. W., Morgan, S. A., Wescott, A. and Poad, M. (2010), "Rolling to control residual stress and distortion in

friction stir welds", *Science and Technology of Welding and Joining,* vol. 15, no. 6, pp. 440-447.

[200] Sun, Y. -., Zang, Y. and Shi, Q. -. (2010), "Numerical simulations of friction stir welding process and subsequent post weld cold rolling process", *Key Engineering Materials,* vol. 419-420, pp. 433-436.

[201] Neeraj, T., Gnäupel-Herold, T., Prask, H. J. and Ayer, R. (2011), "Residual stresses in girth welds of carbon steel pipes: Neutron diffraction analysis", *Science and Technology of Welding and Joining,* vol. 16, no. 3, pp. 249-253.

[202] Demofonti, G., Mannucci, G., Hillenbrand, H. G. and Harris, D. (2003), *"*Suitability Evaluation of X100 Steel Pipes for High Pressure Gas Transportation Pipelines by full Scale Tests", available at: http://www.europipe.com/files/ep_tp51_03en.pdf (accessed 06/25/2013).

[203] DNV - OS - F101 (2012),*"* Submarine Pipeline Systems", available at: https://www.google.co.uk/?gws_rd=ssl#q=offshore+standard+dnv-os-f101 (accessed 06/25/2012).

[204] Katsina, I. N. (2012), "Effect of welding thermal cycles on the heat affected zone microstructure and toughness of multi-pass welded pipeline steels (PhD thesis)", Cranfield University, Cranfield University, UK

[205] Girbo, A., A. (2011), "Study on the effect of oxygen content on the impact toughness of weld metal (unpublished MSc. thesis)", Cranfield University, Cranfield University, UK.

[206] IPG Photonics (2014), IPG Photonics Fiber Lasers YLR Series, available at: www.ipgphotonics.com/apps_materials_multi_ylr.htm (accessed 06/23/2014).

[207] Usani Unoh Ofem. (2013), “Laser Assisted Arc Welding Process for Dry Hyperbaric Deep water Application (unpublished PhD Thesis thesis)”, Cranfield University, Cranfield University, UK

[208] Nadzam, J. (2002), "Tandem GMAW: The Flexibilty of Pulsed Spray Transfer", *Welding innovation,* vol. 19, no. 2, pp. 12-15.

[209] Lincoln Electric: (2004), "Power Wave 455M Operators Manual.", in , pp. 5-13.

[210] Withers, P. J., Turski, M., Edwards, L., Bouchard, P. J. and Buttle, D. J. (2008), "Recent advances in residual stress measurement", *International Journal of Pressure Vessels and Piping,* vol. 85, no. 3, pp. 118-127.

[211] Kim, J. -. and Chung, H. -. (2003), "Electrochemical characteristics of orthorhombic LiMnO2 with different degrees of stacking faults", *Journal of Power Sources,* vol. 115, no. 1, pp. 125-130.

[212] Tung, H. -., Huang, J. -., Tsai, D. -., Ai, C. -. and Yu, G. -. (2009), "Hardness and residual stress in nanocrystalline ZrN films: Effect of bias voltage and heat treatment", *Materials Science and Engineering A,* vol. 500, no. 1-2, pp. 104-108.

[213] Rai, S., Choudhary, B. K., Jayakumar, T., Rao, K. B. S. and Raj, B. (1999), "Characterization of low cycle fatigue damage in 9Cr-1Mo ferritic steel using X-ray diffraction technique", *International Journal of Pressure Vessels and Piping,* vol. 76, no. 5, pp. 275-281.

[214] Quesnel, D.J., Meshii, M. and Cohen, J.B., (1978), “Residual stresses in high strength low alloy steel during low cycle fatigue”.

[215] Eroglu, M., Aksoy, M. and Orhan, N. (1999), "Effect of coarse initial grain size on microstructure and mechanical properties of weld metal and HAZ of a low carbon steel", *Materials Science and Engineering A,* vol. 269, no. 1-2, pp. 59-66.

[216] Khodabakhshi, F., Kazeminezhad, M. and Kokabi, A. H. (2011), "Mechanical properties and microstructure of resistance spot welded severely deformed low carbon steel", *Materials Science and Engineering A,* vol. 529, no. 1, pp. 237-245.

[217] Krauss, G. and Thompson, S. W. (1995), "Ferritic microstructures in continuously cooled low- and ultralow carbon steels", *ISIJ International,* vol. 35, no. 8, pp. 937-945.

[218] Li, K. H., Zhang, Y. M., Xu, P. and Yang, F. Q. (2008), "High-strength steel welding with consumable double-electrode gas metal arc welding", *Welding Journal (Miami, Fla),* vol. 87, no. 3, pp. 57-s-64-s.

[219] Pisarski, H. G., Tkach, Y. and Quintana, M. (2004), "Evaluation of weld metal strength mismatch in X100 pipeline girth welds", *Proceedings of the Biennial International Pipeline Conference, IPC,* Vol. 2, pp. 1589.

[220] British Steel. (1999), "Structural Interity Assement Procedures for European Industry", available at: http://www.eurofitnet.org/sintap_BRITISH_STEEL_BS-25.pdf (accessed 04/03/2015).

[221] Chung, B. G., Rhee, S. and Lee, C. H. (1999), "The effect of shielding gas types on CO2 laser tailored blank weldability of low carbon automotive galvanized steel", *Materials Science and Engineering A,* vol. 272, no. 2, pp. 357-362.

[222] Jones, S. J. and Bhadeshia, H. K. D. H. (1997), "Competitive formation of inter- and intragranularly nucleated ferrite", *Metallurgical and Materials Transactions A: Physical Metallurgy and Materials Science,* vol. 28, no. 10, pp. 2005-2013.

[223] Bhadeshia, H. K. D. H. (2001), "Bainite in steels", 2nd ed, IOM Communications ltd, London, UK.

[224] Lee, C. H., Bhadeshia, H. K. D. H. and Lee, H. -. (2003), "Effect of plastic deformation on the formation of acicular ferrite", *Materials Science and Engineering A,* vol. 360, no. 1-2, pp. 249-257.

[225] Acevedo, C., Evans, A. and Nussbaumer, A. (2012), "Neutron diffraction investigations on residual stresses contributing to the fatigue crack growth in ferritic steel tubular bridges", *International Journal of Pressure Vessels and Piping,* vol. 95, pp. 31-38.

[226] Kumar, S. and Shahi, A. S. (2011), "Effect of heat input on the microstructure and mechanical properties of gas tungsten arc welded AISI 304 stainless steel joints", *Materials and Design,* vol. 32, no. 6, pp. 3617-3623.

[227] Yilmaz, R. and Uzun, H. (2002), "Mechanical Properties of Austenitic Stainless Steels Welded by GMAW and GTAW", *Journal of Marmara for Pure and Applied Science,* no. 18, pp. 97 - 113.

[228] Krawitz, A. D. (1990), "Residual stress analysis with neutrons", *Mater. Res. Soc.,* vol. 166, pp. 281-292.

[229] ASM Aerospace Specification Metals, Inc. (2015), *"*AISI Type 304 Stainless Steel -ASM Material Data Sheet", available at: http://asm.matweb.com/search/SpecificMaterial.asp?bassnum=MQ304A (accessed 01/06/2015).

[230] Mitra, A., Srivastava, P. K., De, P. K., Bhattacharya, D. K. and Jiles, D. C. (2004), "Ferromagnetic properties of deformation-induced martensite transformation in AISI 304 stainless steel", *Metallurgical and Materials Transactions A: Physical Metallurgy and Materials Science,* vol. 35 A, no. 2, pp. 599-605.

[231] Peguet, L., Malki, B. and Baroux, B. (2007), "Influence of cold working on the pitting corrosion resistance of stainless steels", *Corrosion Science,* vol. 49, no. 4, pp. 1933-1948.

[232] Garda, C. (2000), "Effect of prior cold work on intergranular and transgranular corrosion in type 304 stainless steels: Quantitative discrimination by image analysis", *Corrosion,* vol. 56, no. 3, pp. 243-255.

[233] Bannistera, A. C., Ruiz Ocejo, J. and Gutierrez-Solana, F. (2000), "Implications of the yield stress/tensile stress ratio to the SINTAP failure assessment diagrams for homogeneous materials", *Engineering Fracture Mechanics,* vol. 67, no. 6, pp. 547-562.

[234] Rogante, M. (2000), "Stress-free reference sample: The problem of the determination of the interplanar distance d0", *Physica B: Condensed Matter,* vol. 276-278, pp. 202-203.

[235] J. Gauthier, T. W. Krause, and D. L. Atherton (1998). Measurement of residual stress in steel using the magnetic Barkhausen noise technique. NDT and E International, 31(1):23–31.

APPENDICES

Appendix A : API 5L X100 Pipeline Steel Plate (20 mm thick)

A.1 Appendix: Welding Thermal Cycles of the Six Passes

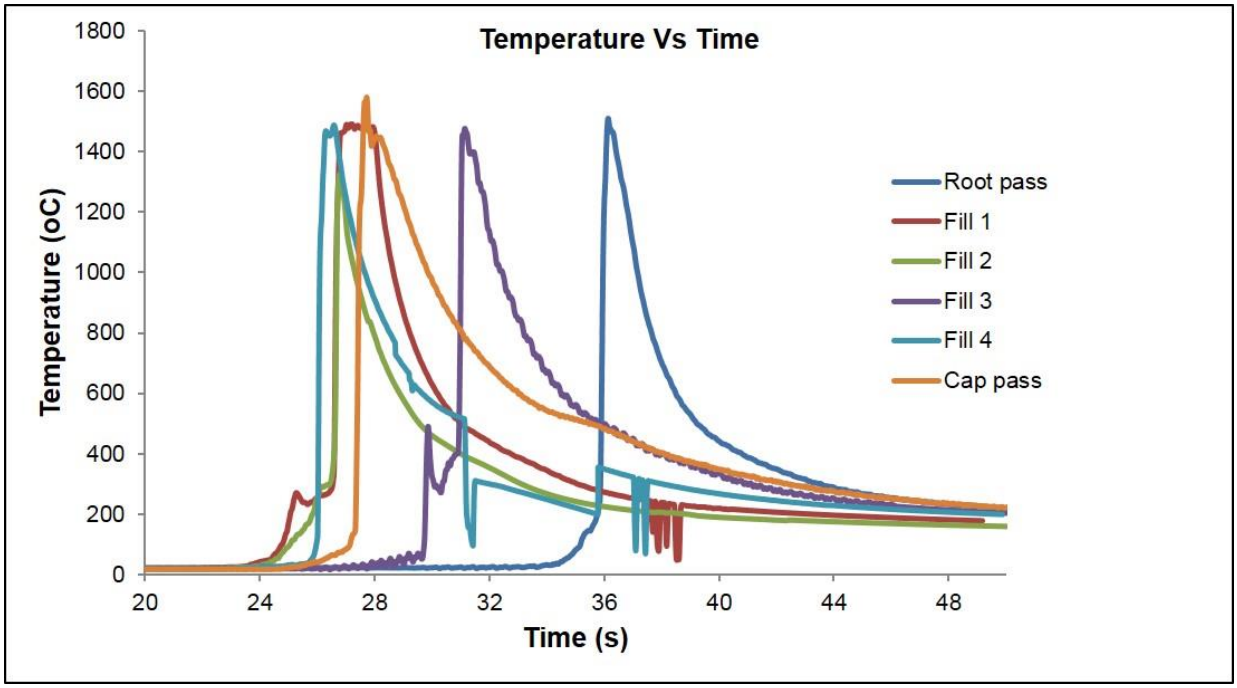

A.1.1 **:** Welding thermal cycles of the six deposited layers

A.2 Appendix: Laser Thermal Cycles and Welds Appearance

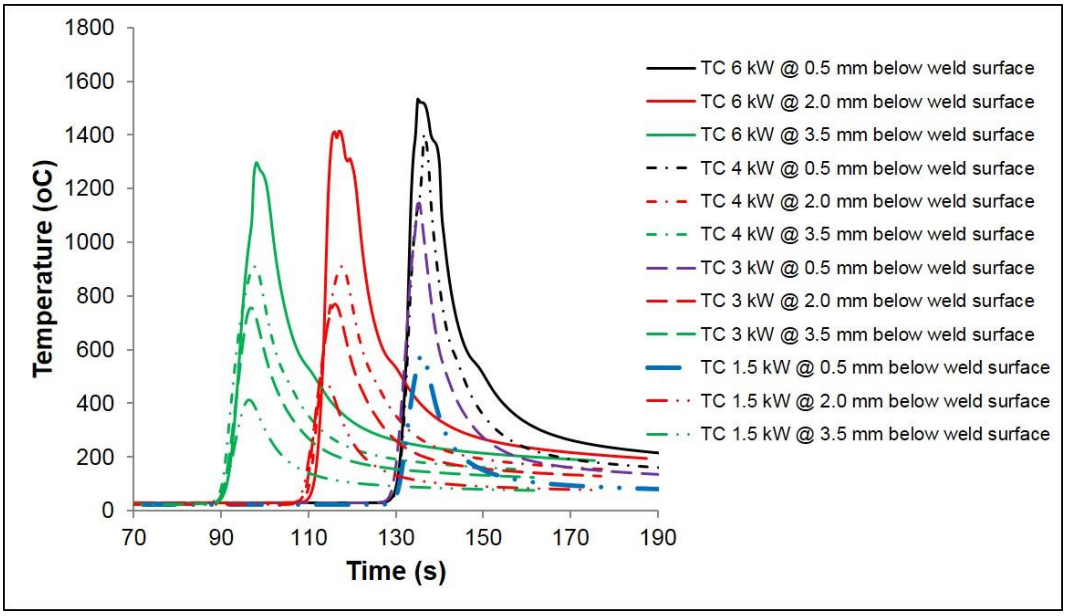

A.2.1 **:** Thermal cycles of laser powers of 1.5 kW, 3 kW, 4 kW and 6 kW with travel speed of 0.2 m.min^{-1} at constant beam diameter of 20 mm

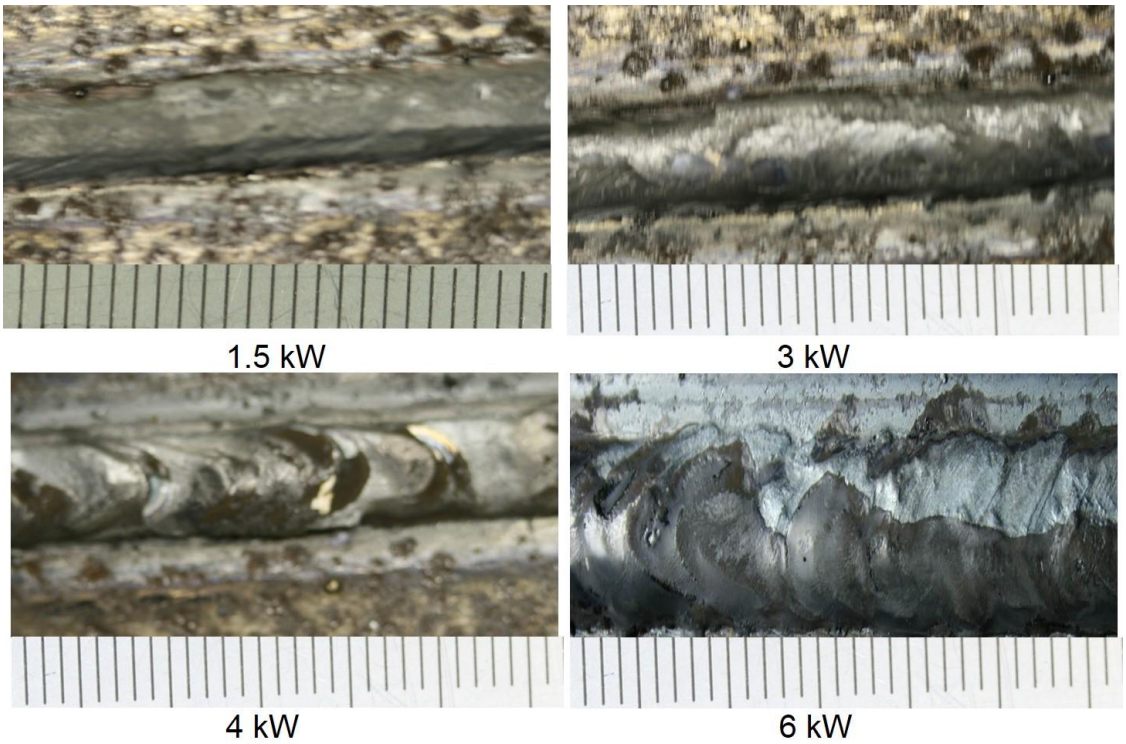

A.2.2 : Physical weld appearance of using different laser power with travelled speed of 0.2 m.min^{-1} at constant beam diameter (20 mm)

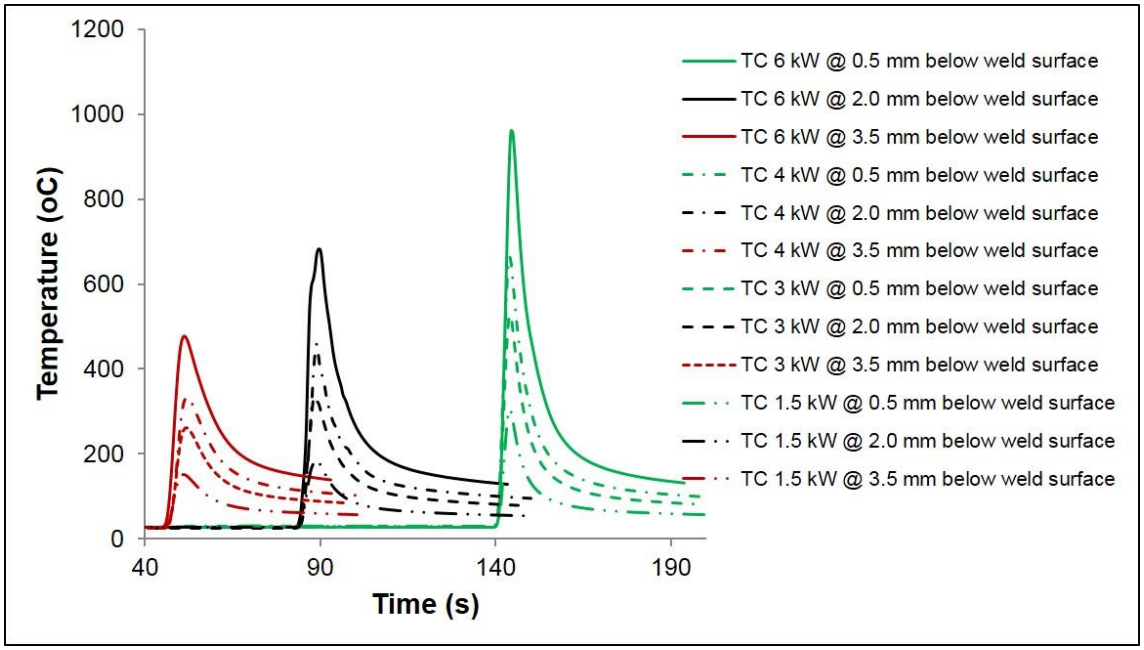

A.2.3 : Thermal cycles of laser powers of 1.5 kW, 3 kW, 4 kW and 6 kW with travel speed of 0.4 m.min^{-1} at constant beam diameter of 20 mm

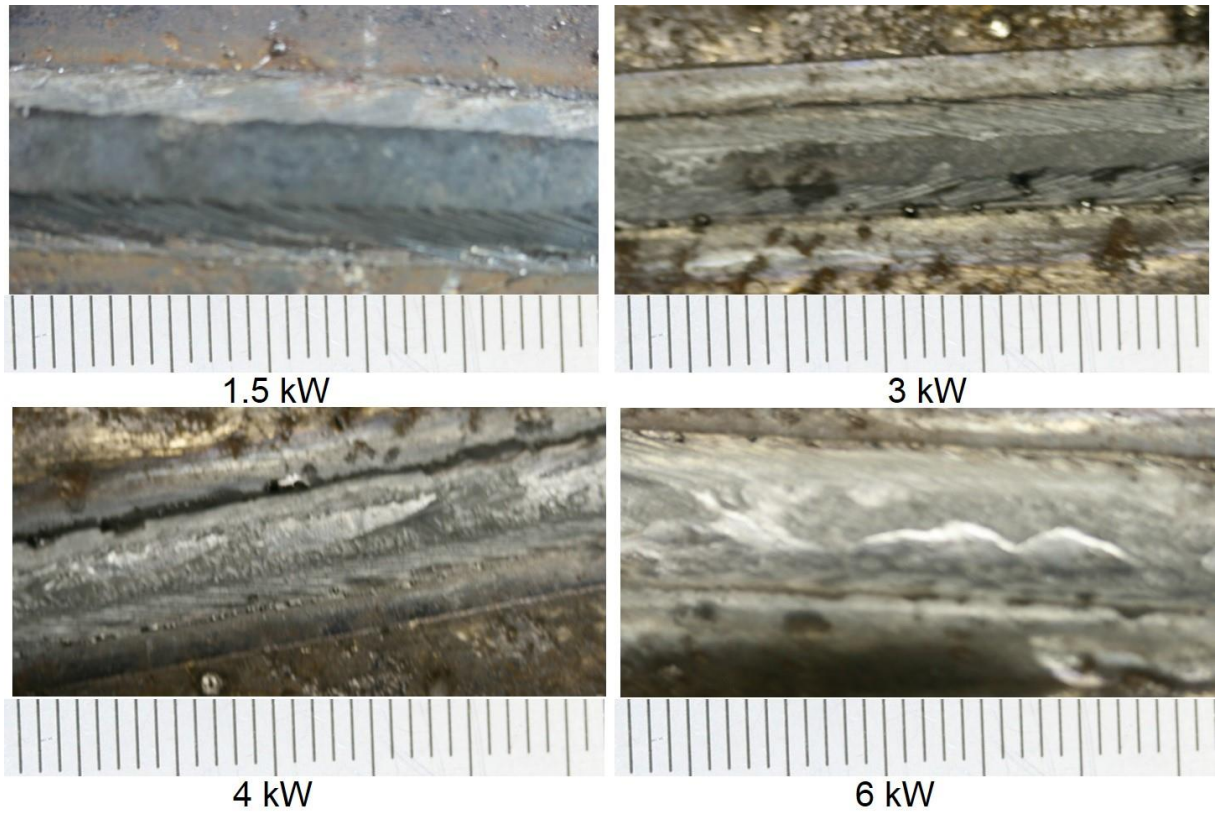

A.2.4 : Physical weld appearance (top view) of using different laser power with travelled speed of 0.4 m.min^{-1} at constant beam diameter (20 mm)

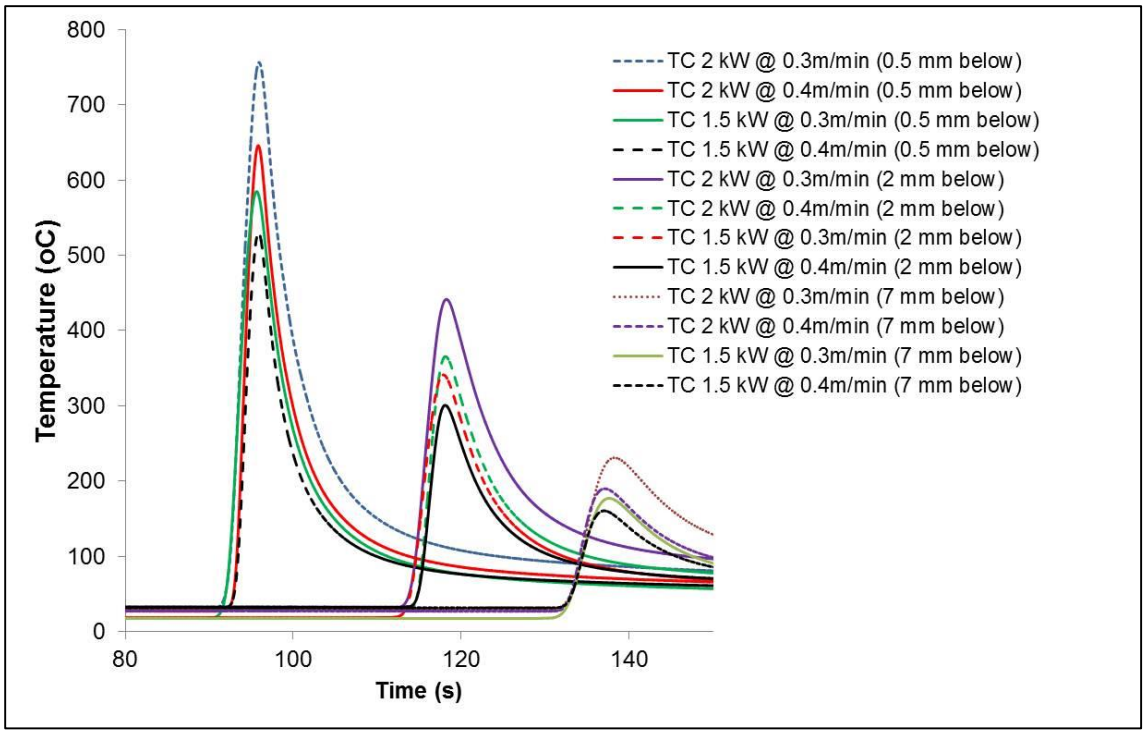

A.2.5 : Thermal cycles of laser powers of 1.5 kW and 2.0 kW with travel speed of 0.3 m.min^{-1} and 0.4 m.min^{-1} at constant beam diameter of 20 mm

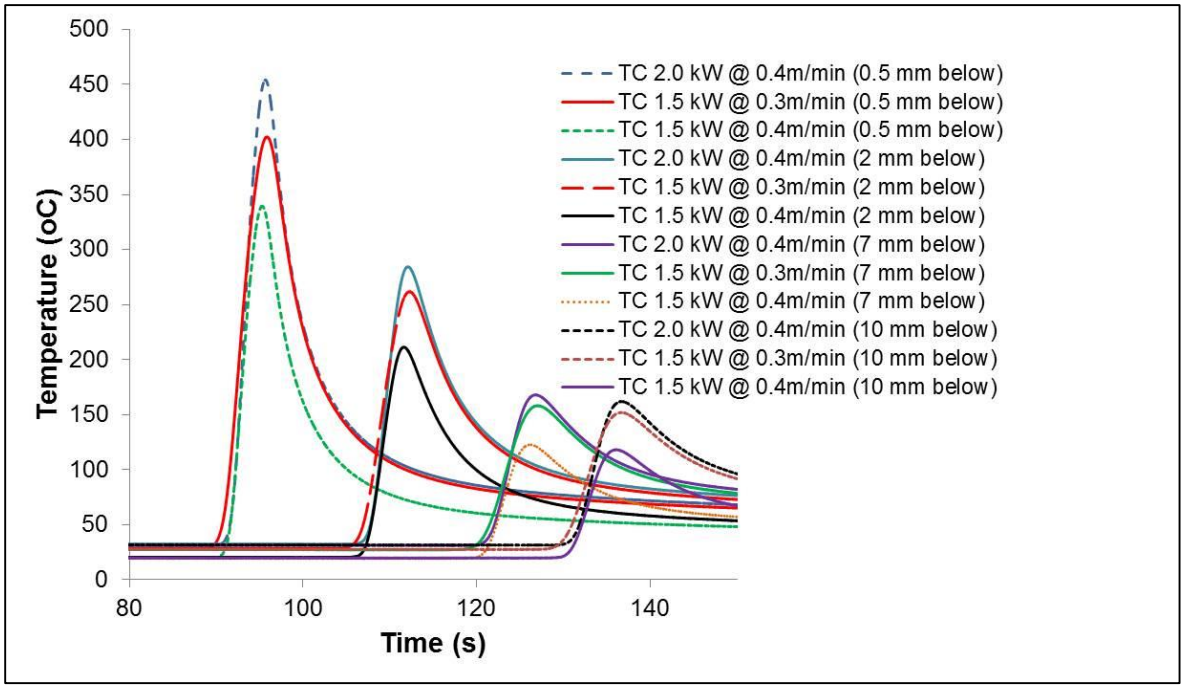

A.2.6 Thermal cycles of laser powers of 1.5 kW and 2.0 kW with travel speed of 0.3 m.min^{-1} and 0.4 m.min^{-1} at constant beam diameter of 30 mm

A.3 Appendix: Effect of Laser Power Through the Thickness

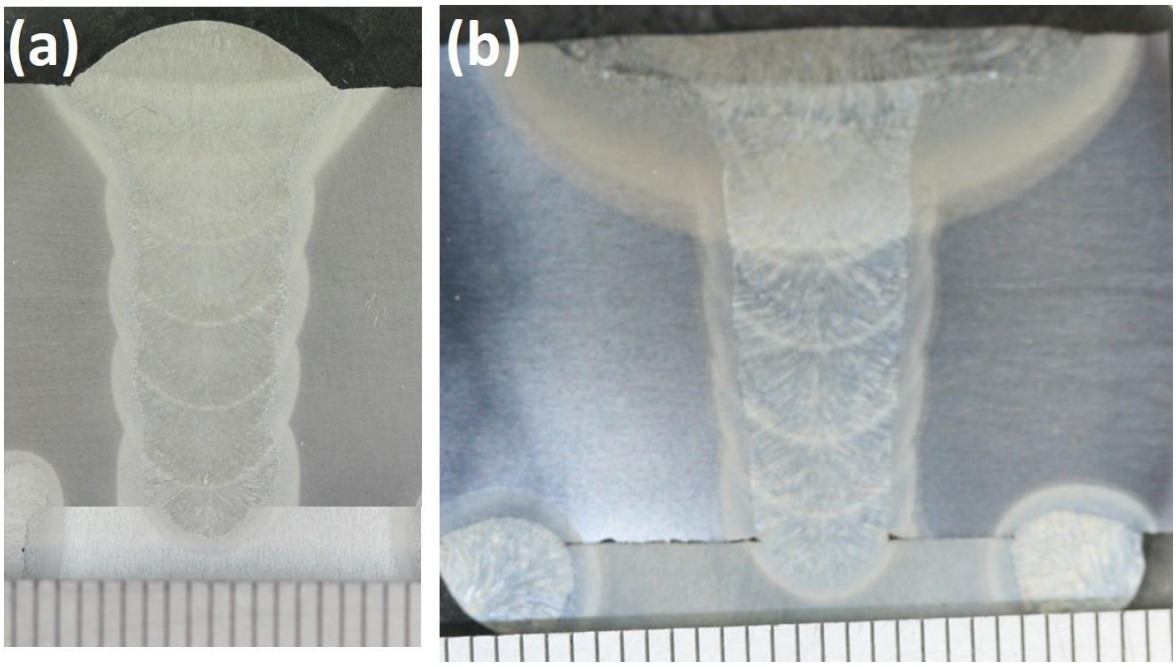

A.3.1 (a) As welded (b) showing the effect of laser powers of 6kW with travel speed of 0.3 m min^{-1} at constant beam diameter of 20 mm

A.4 Appendix: Effect of Laser Power on Residual Stress

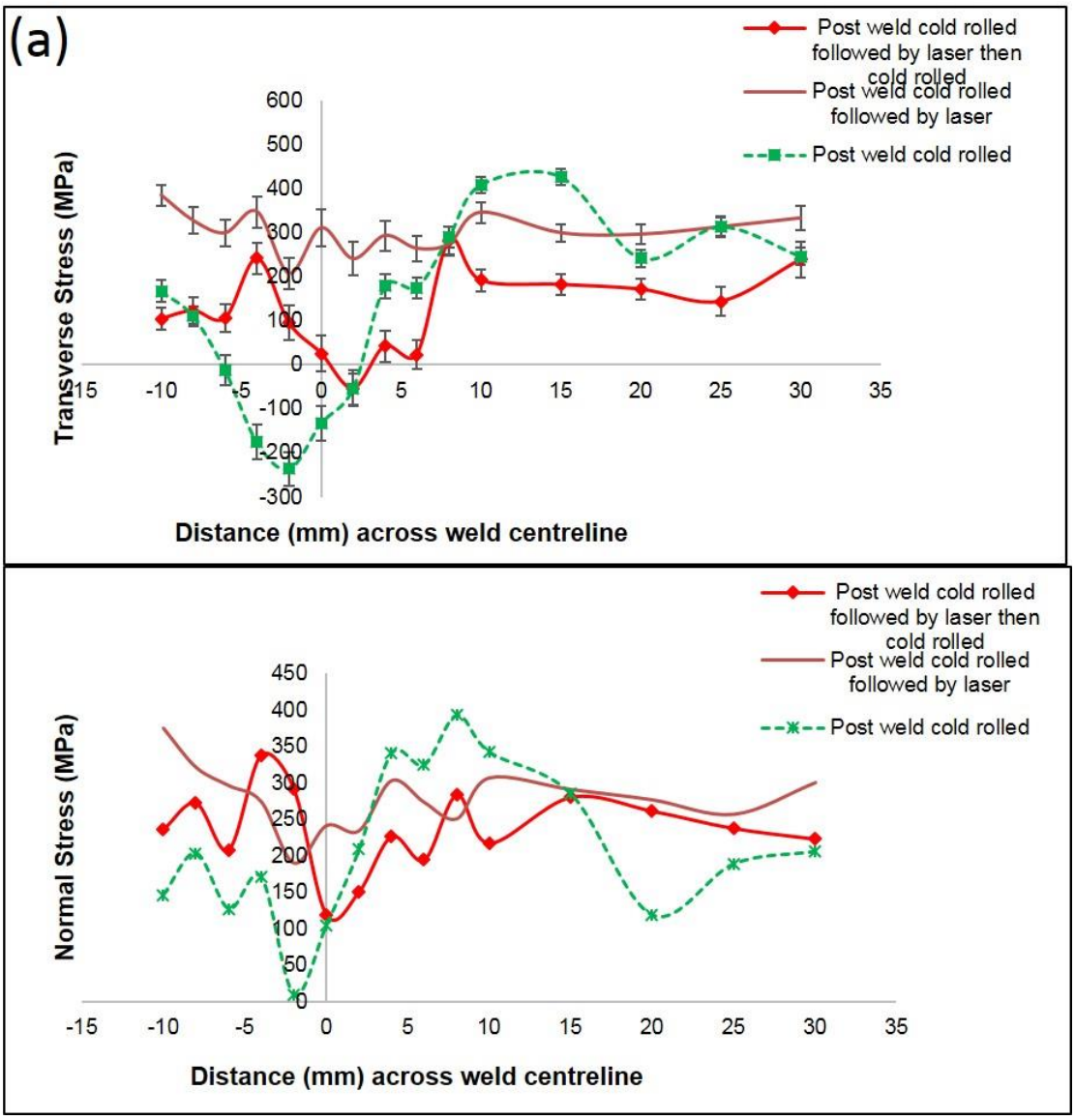

A.4.1 Residual stress profile across the weld in specimen (measured 3.5 mm below the top surface), (a) Transverse (b) Normal direction

Appendix B : AISI 304L Austenitic Stainless Steel Plate (12 mm thick)

B.1 : Welding Thermal Cycles

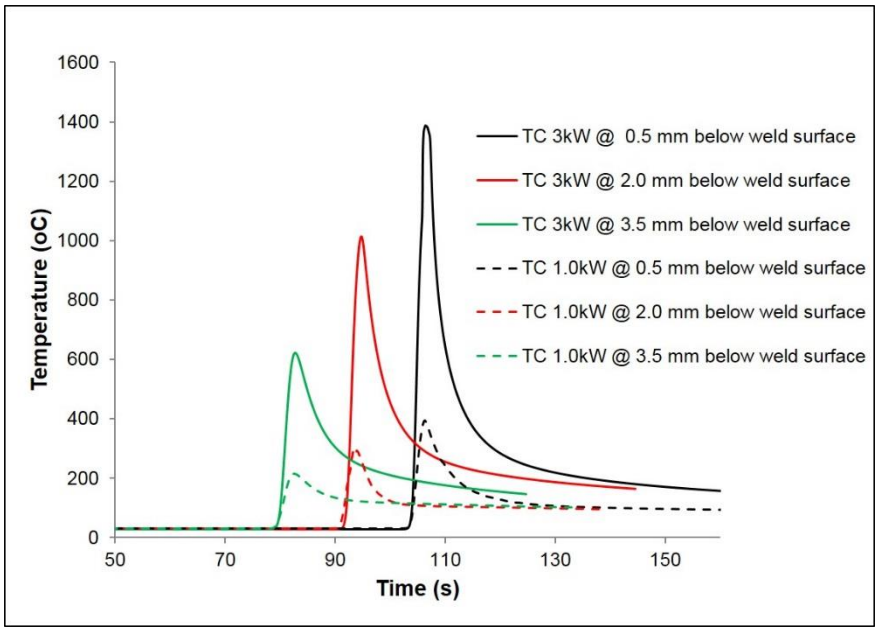

B.1.1 Thermal cycles of laser powers of 1.0 kW and 3.0 kW with travel speed of 0.4 m min^{-1} at constant beam diameter of 20 mm

B.2 : Optical Micrograph

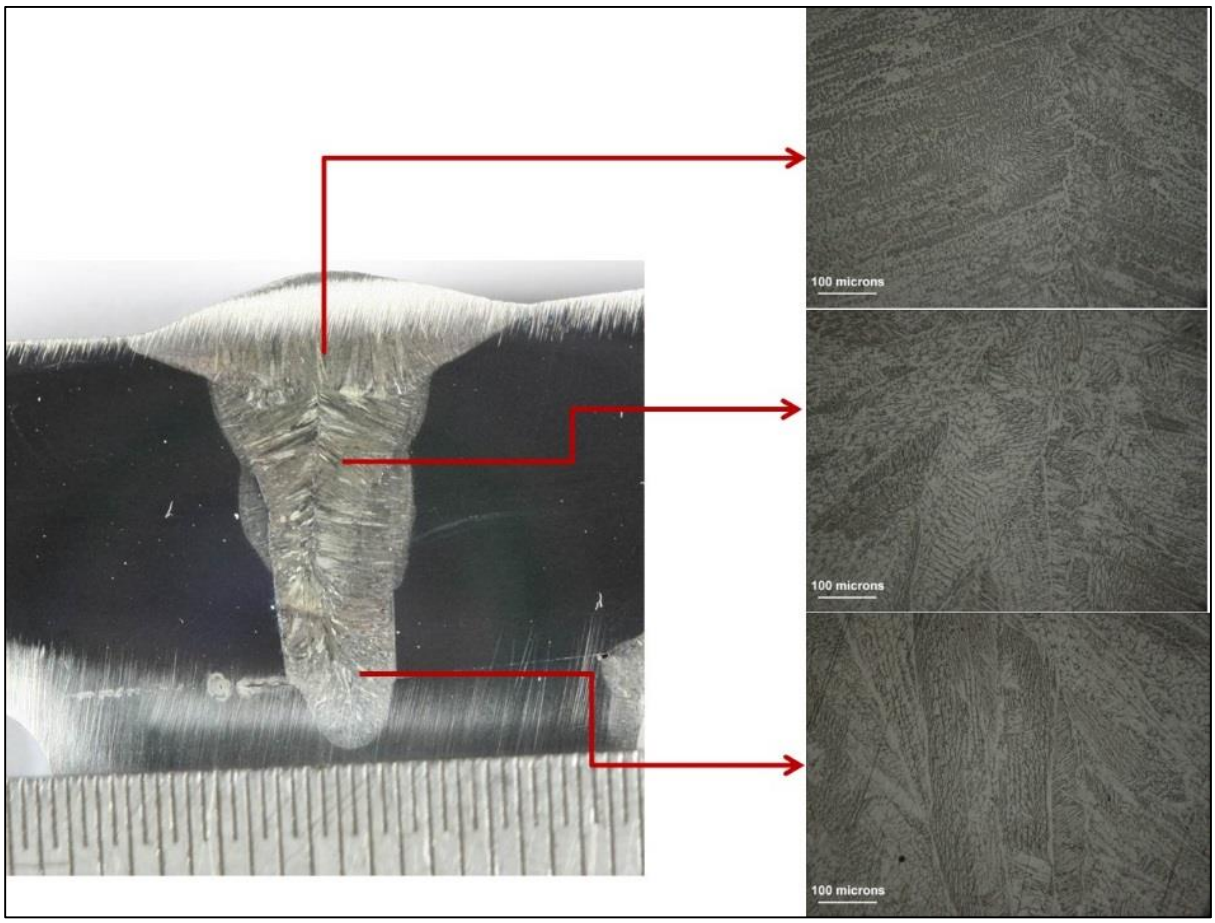

B.2.1 Optical micrograph of 304L stainless steel of the three pass in as-welded

B.3 Effect of New Laser Power on Residual Stress of 304L Stainless Steel

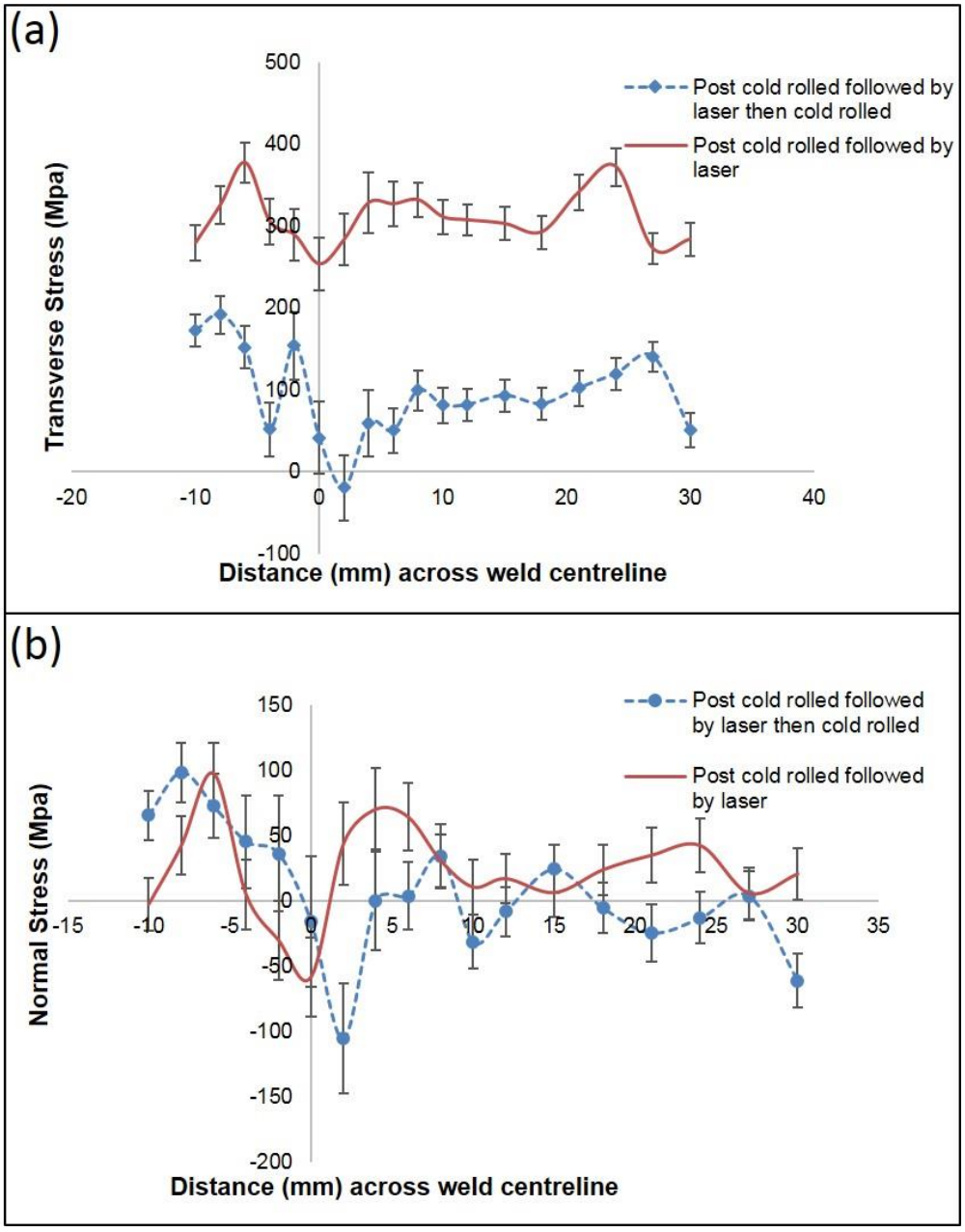

B.3.1 : Residual stress profile across the weld in sample with different processing conditions (measured 3 mm below the top surface)

The behaviour of the residual stress profile is due to the fact that, the measurement are within the heated zone. The laser beam diameter was 110 mm hence the stress could not balance to zero.

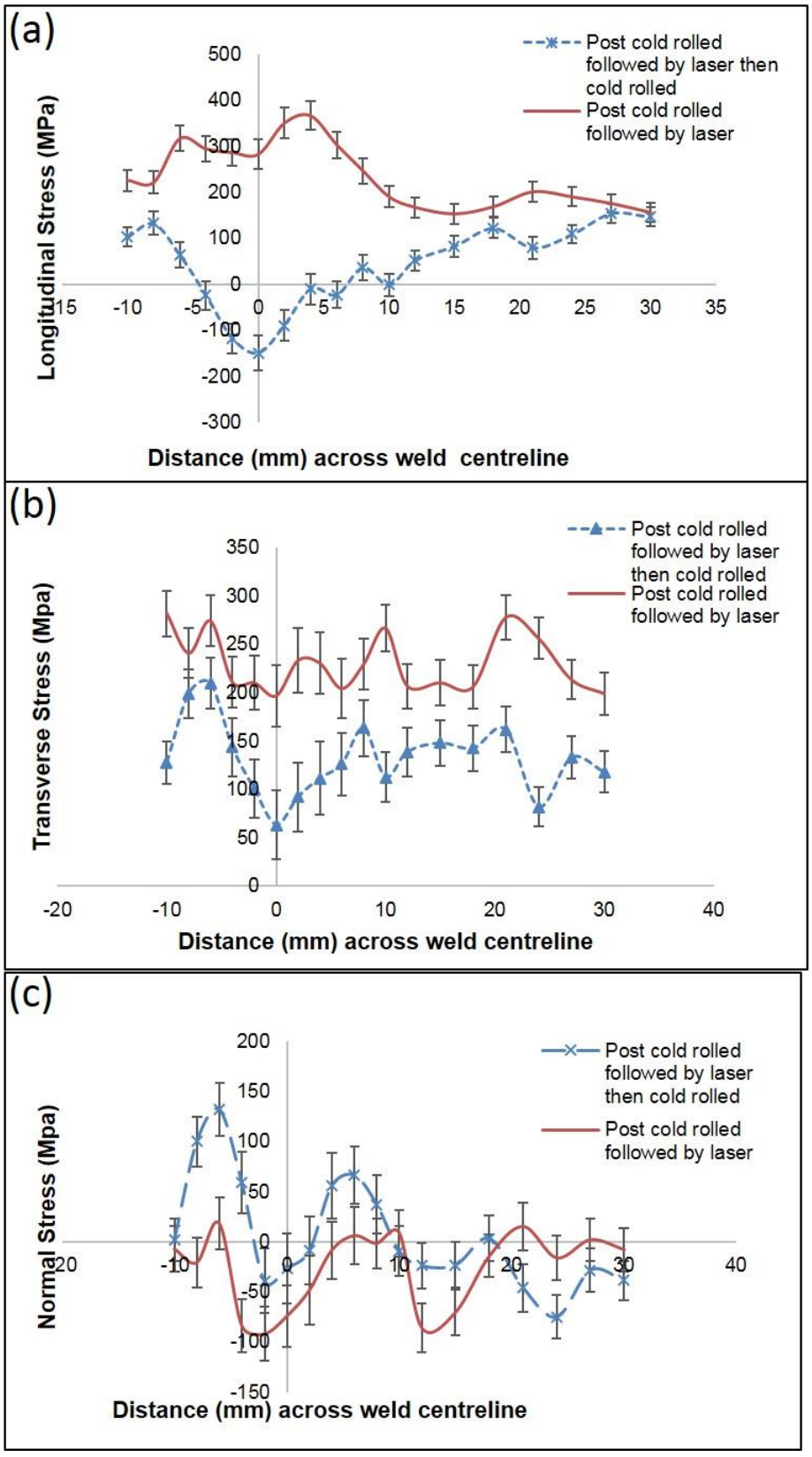

B.3.2 Residual stress profile across the weld in sample with different processing conditions (measured 7 mm below the top surface)

Appendix C : S275JR Structural Steel (12 mm thick)

C.1 Effect of Processing Condition on Residual Stress of S275 Structural Steel

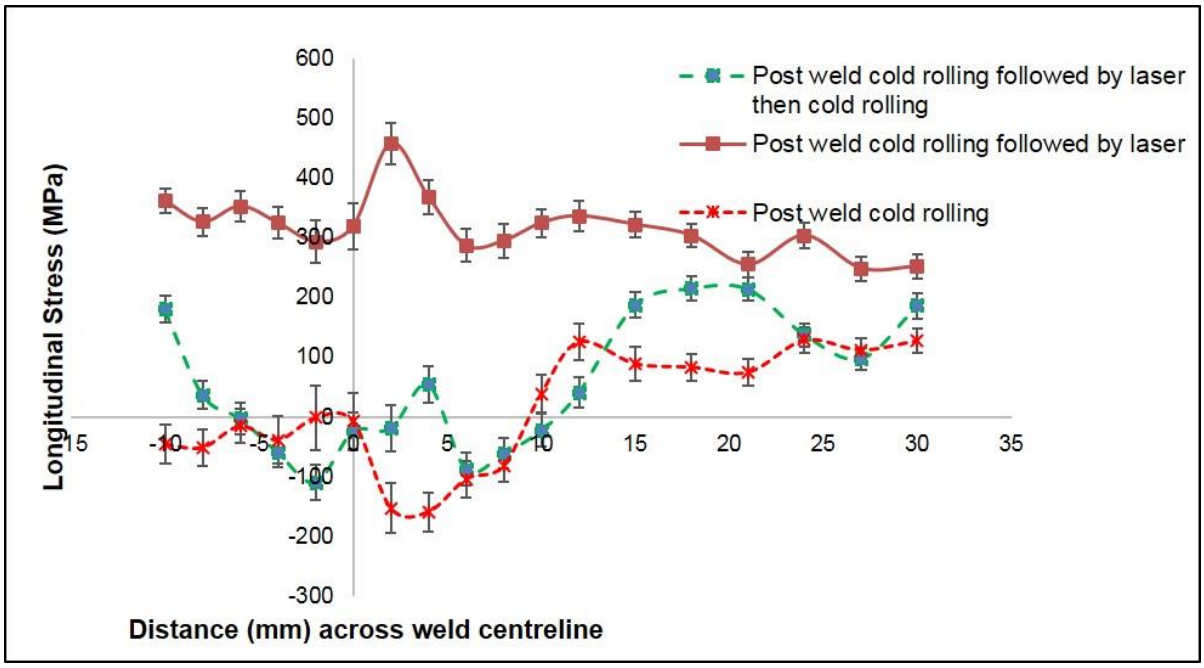

C.1.1 Residual stress profile across the weld in sample with different processing conditions (measured 10.5 mm below the top surface)